NASA CONTRACTOR REPORT

NASA CR-1098

NASA CR-1098

FULL-SCALE GROUND PROXIMITY INVESTIGATION OF A VTOL FIGHTER MODEL AIRCRAFT

by Rabim Lavi, Gordon R. Hall, and Wilbur W. Stark

Prepared by
NORTHROP CORPORATION
Hawthorne, Calif.
for Ames Research Center

NATIONAL AERONAUTICS AND SPACE ADMINISTRATION • WASHINGTON, D. C. • JUNE 1968

NASA CR-1098

FULL-SCALE GROUND PROXIMITY INVESTIGATION OF A VTOL FIGHTER MODEL AIRCRAFT

By Rahim Lavi, Gordon R. Hall, and Wilbur W. Stark

Issued by Originator as Report No. NOR 67-221

Prepared under Contract No. NAS 2-4287 by
NORTHROP CORPORATION
Hawthorne, Calif.

for Ames Research Center

NATIONAL AERONAUTICS AND SPACE ADMINISTRATION

For sale by the Clearinghouse for Federal Scientific and Technical Information
Springfield, Virginia 22151 – CFSTI price $3.00

FULL-SCALE GROUND PROXIMITY INVESTIGATION OF A VTOL FIGHTER MODEL AIRCRAFT

By Rahim Lavi, Gordon R. Hall, and Wilbur W. Stark

SUMMARY

An experimental investigation was conducted to determine the exhaust gas ingestion characteristics and induced aerodynamics for a large-scale VTOL lift engine fighter model operating in ground proximity. The model was powered by as many as seven J-85 turbojet engines. The investigation was conducted at Ames Research Center Static Test Facility.

Ingestion of hot exhaust gases by the engines proved to be strongly configuration dependent. The flow field created by a split arrangement of lift or lift-plus-lift/cruise engines caused intermittent localized ingestion of exhaust gases by the engine inlets which often resulted in large temperature gradients and distortion at the compressor face. The inlet thermal environment frequently caused engine stall, with the internal hot gases expelled from the stalled engine occasionally causing stall of adjacent engines. The test results showed that transient measurements with rapid-response thermocouples and recording equipment are needed for realistic assessment of the VTOL ground proximity thermal effects.

Jet induced vertical forces and pitching moments were dependent on model height, wing location, engine grouping, number of engines, and model pitch attitude. Induced lift can be either positive or negative, depending on configuration and model height above ground.

Sound pressure levels were primarily dependent on the height of the vehicle above the ground plane. Close to the ground, the far field sound levels diminished, but at all model heights sound levels in the proximity of the test model exceeded the tolerance of the unprotected human ear.

INTRODUCTION

When jet-powered VTOL aircraft operate in ground proximity, the engine inlets are exposed to an environment contaminated by the engines' own exhaust gases. If these hot gases are ingested, thrust is reduced; and if the ingestion is excessive, engine stall can occur. In addition, the jet-induced flow on the lower surfaces of the vehicle may create forces that adversely affect vehicle lift and stability. Knowledge of these ground proximity effects is needed for reliable preliminary design of VTOL aircraft, and to permit advanced assessment of potential lift losses and trouble areas. Historically, this kind of information has been developed for conventional aircraft configurations by means of small-scale tests. For VTOL configurations, however, simulation of full-scale effects by small-scale testing has not been demonstrated. In view of the lack of proven modeling techniques and applicable small-scale data in the area of hot gas recirculation, a test program employing a large-scale test model (Figure 1) was undertaken to explore ground proximity effects. A number of potential VTOL configurations employing various arrangements of lift and lift-plus-lift/cruise engines in combination with various locations of wing and lift/cruise engine inlets were tested. The objectives were to determine: (1) engine inlet thermal environment caused by hot gas ingestion and the influence of the environment on engine performance and operating characteristics; and (2) jet-induced lift effects in ground proximity.

SYMBOLS

$\bar{c}$	Mean aerodynamic chord, ft
D	Nozzle diameter, ft
H	Model height above ground, ft
ΔL	Jet-induced lift, lb
L_∞	Lift out of ground effect, lb
M	Pitching moment, ft-lb
N	Engine speed, rpm
P_s	Static pressure, psia
P_∞	Ambient pressure, psia
P_{t8}	Exhaust gas pressure, psia
P_3/P_2	Compressor pressure ratio
T	Local temperature, ^oF
T_j	Exhaust gas temperature, ^oF

T_∞	Ambient temperature, ^oF
δ	$P_\infty/14.7$
θ	$T_\infty/518.7$

MODEL DESCRIPTION AND STATIC TEST FACILITY

The NASA-Ames Research Center Static Test Facility is an outdoor complex designed to support powered models and aircraft in hover tests at varying heights above ground and different angles of attack. Within this complex Ames maintains a VTO Thrust Stand (Figure 2) incorporating a fixed ground plane test site, a towable trailer containing the motorized model support struts, and an office-type instrumentation trailer. The support trailer and ground plane form a flat 78- by 80-foot area. During the tests reported here, the model was mounted on the thrust stand by three beams, two extending from opposite sides of the fuselage just forward of the wing, and the third extending below the nose to take out pitch loads via a toggle mechanism. The engines exhausted aft of the primary mounting struts, minimizing flow interference. Two-axis load cells (Figure 3) were located on each side of the main support beam, and a third attached at the nose. All power and instrumentation to and from the vehicle were routed either under the ground plane or along the top of one of these support arms.

A small office trailer fifty feet from the stand served as a control room containing all data-recording equipment and two engine-run consoles, one of which controlled the five lift engines and the other the two lift/cruise engines. All engine instrumentation (rpm, exhaust gas temperature, throttle position indicator, etc.) as well as throttle actuator control switches and controls for starter, ignition, deflector doors, and hydraulics were installed in this trailer. Electrical and hydraulic power, cooling water, fuel, and compressed air were externally supplied to the test stand.

The configuration of the VTOL test model (Figure 1) allowed representation of direct lift and composite (lift plus lift/cruise engines) supersonic fighter configurations. A Northrop T-38 wing and horizontal stabilizer were mounted on the 42-foot-long fuselage. In this installation the wing span was 23 feet, the leading edge sweep angle 24 degrees, and the projected area 156 square feet. Six wing locations were provided: high, mid, or low position, either forward or aft (37-inch longitudinal variation - see Figure 7).

The center fuselage section was the NASA-Ames VTOL lift engine test pod. This pod had been used previously for wind tunnel investigations of lift engine inlet flow systems (Reference 1). Five General Electric YJ85 engines without afterburners were installed in the center fuselage at an angle of 10 degrees from the vertical on 30.5-inch centers (a spacing ratio of 1.9, based on compressor inlet diameter). The engines were equipped with bellmouth inlets integrated into the fuselage.

Two General Electric YJ85 engines representing lift/cruise engines, also without afterburners, were mounted horizontally in the aft fuselage (Figure 4) with fixed 90-degree elbow tailpipes directed downward. The centerline of the exhausts of these engines was 16 feet aft of the rear lift engine.

Remotely controlled exhaust vectoring doors were used to direct the exhaust gases of all engines in a rearward direction from vertical to 50 degrees from vertical. Because of the ten-degree inclination of the lift engines, however, secondary vectoring doors (Figure 5) were incorporated to deflect the engine thrusts to vertical. The secondary vectoring doors were smaller than the primary vectoring doors, and produced nominally vertical thrust when installed at an angle of "minus" 25 degrees (bottom edge forward). They were linked to the primary doors, and automatically rotated to the -25 degree position when the primary doors were fully rotated.

The particular configurations and test conditions shown in Table 1 were selected for reporting from a more comprehensive test program defined in References 2 and 3. These configurations include three operating engine arrangements: (l) four lift engines forward of the wing box, two lift/cruise engines, wing in the aft position, (2) three lift engines forward and one lift engine aft of the wing box, two lift/cruise engines, wing in the forward position, and (3) three lift engines immediately adjacent to the wing, lift/cruise engines not operating, wing in the forward position. The lift/cruise engines were provided with the three alternate inlet locations shown in Figure 6.

INSTRUMENTATION

Engine Performance Parameters

During each test the exhaust nozzle total pressure (P_{t8}) and exhaust nozzle temperature (EGT) of all engines were recorded on oscillographs. Continuous recordings were also made of the rpm of Engine No. 3 (lift only) and Engine No. 7 (lift/cruise). Speed and exhaust gas temperature of all engines were monitored at the engine control console.

Engine Inlet Temperature and Pressures

Eight iron-constantan 0.01 inch diameter (30-gage) thermocouples were installed in the inlets of all engines except Engine No. 6. The standard installation consisted of two rakes of three thermocouples each, located on the forward and left side radii, and single thermocouples near the outer wall on the aft and right side. The inlet of Engine No. 6 was instrumented with four single thermocouples located near the wall. The rake thermocouples were spaced to define inlet temperatures over approximately equal flow areas. The time constant for the thermocouple-recording system combination was of the order of 100 milliseconds. A detailed evaluation of thermocouple response characteristics is presented in Appendix A.

Vehicle Surface Pressures

Surface static pressures on the undersides of the wings, horizontal tailplane, and fuselage were measured in order to assess the vertical forces and pitching moments caused by jet-induced effects. These measurements were recorded on manometer boards. Eight pressure pickups were installed on the right wing (Figure 7), three on the left wing, three on the right tailplane, and thirteen on the fuselage.

Ground Plane Temperatures

Ground plane temperatures were measured at eight locations (Figure 8). At one of these locations, a four-probe rake was installed to define the vertical temperature gradient, and during the program the locations were varied to obtain a survey. All temperatures were continuously recorded on an oscillograph.

Force Data

During each test the vertical and axial loads at the two main attachment points, and the vertical load at the nose mount, were continuously recorded (Figure 3). The three load cells were calibrated before installation and at the conclusion of the test program.

Sound Pressure Levels

At seven locations on the test vehicle (Figure 9), sound pressure levels under selected test conditions were recorded by means of Bruel and Kjaer Model 4316 microphones fitted with four-millimeter probes terminating flush with the vehicle surfaces. Sound pressure levels at three farfield locations were recorded by means of Bruel and Kjaer Model 4134 microphones fitted with Model UA 0052 nose cones, to reduce wind noise. All data were recorded on FM tape.

TEST PROCEDURES

The test procedures were designed to yield meaningful data representative of an operational VTOL aircraft. For operational VTOL aircraft, quick thrust-vectoring techniques may be employed in conjunction with engine acceleration to lift-off power in order to prevent rapid inlet-temperature rise at takeoff. This technique was therefore employed in all test runs. The normal test procedure was to stabilize all engines at a representative idle condition (70 percent rpm) with the exhausts vectored rearward by the vectoring doors. A vectoring angle of 50 degrees from the vertical was selected as operationally representative. On signal, full military power was applied to all test engines and the vectoring doors simultaneously rotated downward. With the model mounted in the low position (closest to the ground plane), full power was held for approximately 5 seconds; in the highest position full power was held for 10 to 15 seconds. These time intervals were selected to be at least twice the exposure time experienced by a vehicle undergoing an upward acceleration of 0.02 g from the ground plane to the particular test height. The initial engine speed of 70 percent maximum rpm was greater than normal idle for the YJ85 engine, but was selected to permit rapid acceleration to full power, which was attained in about one second.

With minor exceptions, each configuration of the test program documented in Reference 3 was tested at five vehicle heights. In terms of height-to-exhaust-diameter ratios (H/D) these heights were 2.4, 3.0, 4.5, 6.5 and 8.7. (Actual measured values between the ground plane and the bottom surface of the test vehicle ranged from 2.75 feet to 10 feet.)

Data recording was started at engine idle and continued to completion of each test.

RESULTS

Hot Gas Ingestion

Basically two types of inlet-temperature rise were observed: (1) relatively flat temperature traces with very little distortion, associated with configurations having little or no ingestion and (2) temperature traces of a highly transient character, associated with ingestion-prone configurations. The lift-engine inlet temperature rise for ingestion-prone configurations was often localized and sporadic, and occurred over time intervals ranging from a few milliseconds to several seconds. The lift/cruise engines exhibited the same transient characteristics, but the temperature rise was uniform over the compressor face, resulting in a minimum distortion level. This was due to thorough mixing of the ingested gases in the long ducts before reaching the thermal instrumentation immediately ahead of the compressor face.

To provide an accurate assessment of the inlet thermal environment for a highly transient inlet temperature field, it was decided to present inlet temperature-time histories rather than assigning a steady-state mean inlet temperature level. Steady-state values resulting from similar tests are given in Reference 4. The inlet time-histories for each engine, obtained directly from oscillograph traces, are presented in Figures 10 through 23. The thermocouple locations for each inlet are shown at the top of each graph. The results for a configuration with four adjacent lift engines operating are shown in Figures 10 through 15, and three adjacent engines in Figures 22 and 23. Figures 16 through 21 show the results of configurations with four operating engines, three of which were adjacent and the fourth separated from the adjacent three by 3.8 inlet diameters. The effect of change of height above the ground plane is shown in Figures 11 and 13. Exhaust gas temperature and pressure time histories, time-correlated to the inlet thermal data, are also presented on each plot to permit assessment of the engine performance with respect to inlet temperature rise.

Time histories of Figures 10 through 23 show the values of the various parameters between the time the vectoring doors were rotated (time = 0) and approximately 8-1/2 seconds of the run duration. The time at which engines reached 100 percent rpm and the time of engine stall (when applicable) are also identified on each graph. It should be noted that the loss of an operating engine because of stall creates an altered configuration, and the test data subsequent to stall are no longer meaningful in terms of the original configuration.

Certain combinations of engine arrangement, wing position, and engine inlet location proved effective from the standpoint of minimizing ingestion. Of the three basic arrangements of engines (see Table 1), the configuration having four lift engines closely spaced in combination with the wing in the low, aft position and the lift/cruise engine inlets in either the top or rear position were least ingestion-prone. Configurations in which the wings did not shield the lift/cruise engine inlets from the hot exhaust gases experienced moderate to high ingestion. The split-lift engine arrangement (three engines forward and one engine aft of the wing box) developed moderate ingestion in combination with low wing position and lift/cruise engine inlet on top of the fuselage. All other wing positions and lift/cruise engine inlet locations caused excessive ingestion.

In general the split-lift engine arrangement caused more severe ingestion than other arrangements at various vehicle heights above ground plane. The arrangement of three lift engines closely spaced did not experience ingestion of any consequence at any wing position or vehicle height above ground plane.

Hot gas ingestion generally increased as model height was reduced from H/D = 8.7 to H/D = 3. However, when the model height was further reduced from H/D = 3.0 to H/D = 2.4 the ingestion was usually less severe. The majority of compressor stalls occurred at H/D = 3.0.

Jet-Induced Effects

Jet-induced lift forces were measured by two methods: (1) two-axis load cells attached to the three main support beams; and (2) integration of static pressures on the undersides of the wings, horizontal tailplane, and fuselage. The load cells would normally have provided more dependable data, but during these tests the cantilever mounting of the vehicle on the test stand caused oscillation of the vehicle about the main support beam. The load cell traces reflected these oscillations, and consequently were not accurate enough to permit separation of jet-induced effects from overall force levels. Jet-induced lift forces were therefore calculated by integration of the surface static pressures. The induced moment parameter $M/L_\infty \bar{c}$ was also based on fuselage and wing static pressures. Lift out of ground L_∞ was based on calibrated engine thrust. The thrust calibration for each engine was obtained with the engines installed in the model. Reference thrusts of 2000 lbs and 2200 lbs were used for lift and lift/cruise engines, respectively, to determine induced lift effects ($\Delta L/L_\infty$).

Trends of jet-induced lift and pitching moments at various heights above ground plane are shown in Figure 24 for Configuration F, with the wing mounted in the low, aft position and the lift/cruise inlets in the front location. With the test vehicle positioned 10 feet above ground plane, lift loss amounted to 6 percent. As the model was lowered, the lift loss decreased. This trend was typical of configurations employing an arrangement of lift-plus-lift/cruise engines. Figure 25 shows jet-induced lift and moment for configurations mounting the wing in the low or high, forward position and the lift/cruise engine inlet in the top location. The trend of jet-induced lift is the same as for Configuration F (Figure 24), but negative induced force level in ground proximity is minimized. A breakdown of jet-induced forces (Figure 25b, c) shows the respective contributions of wing and fuselage to the overall force level. The positive force contributed by the fuselage is primarily due to the high-pressure field developed under the fuselage by the fountain effect resulting from interaction of exhaust gases from lift and lift/cruise engines. When the vehicle was positioned closer to the ground plane, a strong fountain formed between the lift/cruise engines because the reduced distance to the ground plane prevented jets from merging.

All evaluated configurations experienced 6 to 7 percent loss of lift with the model positioned at the maximum test height (H/D = 8.7). Close to the ground plane, however, two distinct lift trends developed. Composite configurations (lift plus lift/cruise engines) produced induced lift effects resulting in net lift from 5 to 9 percent higher than the lift experienced at the maximum test height, regardless of the wing location. Configuration M employing only lift engines suffered increasing lift loss as the vehicle was positioned closer to the ground. For the same engine arrangement but the wing at high position (Configuration N), the induced lift losses decreased as model was positioned closer to the ground plane. For the upper wing position, induced forces on the wing did not change with model height above the ground plane.

Acoustic Measurements

Acoustic measurements were obtained on the exposed surfaces of the vehicle and in the surrounding area. Sound pressure levels for two basic engine arrangements are presented in Figure 26 at various vehicle heights above ground. These data represent the maximum sound pressure level for a given configuration, microphone location, and H/D during a test run. No significant differences between the sound levels of the two configurations were observed except at microphone location 3 (microphone installed in the side panel of Engine No. 5) where the 5 to 6 db difference is attributed to the combined effect of wing position (fore and aft) and engine arrangement.

The data of Figure 26 and other configurations showed that, in general, highest near-field sound levels on vehicle surfaces occurred at H/D = 2.4, where the vehicle was nearest to the ground reflecting plane and decreased with increasing H/D.

On the other hand, the far-field maximum sound levels occurred when the model was raised high enough above the ground plane for the full acoustic power of the jet to be developed. Figure 27 shows 125-db sound pressure levels obtained for high and low wing locations at various heights above ground. The inverse square law and sound measurements obtained at microphone locations 8, 9, and 10 (see Figure 9) were used to develop these curves. It is shown that with increased height above ground, the constant 125 db lines move outward as a result of the increased acoustic power developed by the increasing length of the uninterrupted jet exhaust flow.

Engine Characteristics

Ingestion of hot exhaust gases resulted in engine thrust loss which amounted to about one percent loss for every 3 to 4° F average inlet temperature rise. The engine performance degradation due to ingestion is presented in terms of exhaust gas temperature and pressure-time histories on Figures 10 through 23. In addition to thrust degradation, severe inlet temperature environment occasionally resulted in engine stall. Figure 28 shows several cases where stall occurred, reflected by a sharp drop in exhaust pressure. As discussed in more detail in the Appendix, the inlet thermocouples had a time constant of about 100 milliseconds and a 99 percent rise time of 500 milliseconds. Therefore, rapid changes in temperature are subject to attenuation. The relation between the magnitude of the attenuations and the frequency of the temperature oscillation is given in the Appendix.

Field Temperature Environment

Ground-plane temperature data for two configurations employing lift and lift plus lift/cruise engines are presented in Figures 29 and 30. The local temperature data are referenced to the difference between the engine exhaust gas temperature and the ambient temperature.

DISCUSSION

Hot Gas Ingestion

The test results show that hot gas ingestion is highly configuration dependent and governed by either the "buoyancy effect" or the "fountain effect." The buoyancy effect is characterized by the exhaust gases of a single engine extending along the ground for an appreciable distance, mixing with the ambient air, then rising as a result of the density being less than the ambient air, with subsequent ingestion by the engine. Two or more engines closely spaced, so that the exhaust gases merge before reaching the ground plane, create near-ground flow-field characteristics and ingestion tendencies similar to a single engine. The buoyancy effect is presented schematically in Figure 31(a) for a pod containing 5 lift engines closely spaced. Ingestion associated with the buoyancy effect produced an inlet temperature rise generally of the order of 10°F, which developed an appreciable time after the initial downward flow of hot exhaust gases. The time between the initial impingement of hot exhaust gases on the ground plane and subsequent engine ingestion is strongly influenced by the exhaust gas velocity, temperature, and prevailing winds in the proximity of the model.

Hot gas ingestion due to buoyancy should not seriously affect an operating aircraft during takeoff, since the vehicle should gain enough altitude in 2 to 5 seconds to rise above the exhaust-contaminated environment. For the vertical landing mode, however, ingestion due to buoyancy effects could be an important consideration as the vehicle is exposed to the hot gas environment for considerably longer times during descent.

For the case of two or more engines widely spaced (the jets do not merge before reaching the ground plane), the hot exhaust gases impinge on the ground plane and spread radially, encountering each other and creating an upward flow. Schematic representation of this "fountain effect" for two engines widely spaced is shown in Figure 31(b). The ingestion associated with fountain effect cannot, in general, be tolerated, because it creates excessive thrust loss and moment imbalance and may result in engine stall.

Wing position can have a strong influence on hot gas recirculation and ingestion. Comparisons of ingestion levels for Configurations A and B (Figures 10 and 11), B and D (Figures 11 and 13), and G, H, and I (Figures 16, 17, and 18), showing the influence of wing location in combination with various engine arrangements, indicate that a low wing position reduces ingestion most effectively. In general, the aft positioned wing with the closely spaced lift engine arrangement, at all wing heights, reduced the tendency to ingestion, by comparison with the forward position with the split lift engine configuration. This was particularly true when the wing was mounted low on the fuselage. In the region where the lift engine exhaust gases interacted with the lift/cruise engine exhaust gases, the low aft-mounted wing provided an effective shield in deflecting the upward-directed high velocity gases away from the engine inlet. In contrast, higher wing positions were not as effective in deflecting the lower velocity exhaust gases which were able to flow around the high wing and enter the engine inlets.

Ingestion resulting from engine arrangements that produced the effect of single-jet flow ("buoyancy effect") was affected very little by wing location. Both configurations M and N, employing three closely-spaced lift engines, show very little ingestion, and disclose no significant effect attributable to wing position. Wing influence thus appears to depend on engine arrangement; a low wing, for example, reduces ingestion effectively

only when it is properly positioned with respect to the propulsion system arrangement employed. If the interrelationship between wing position and engine arrangement is not taken into consideration, deflection of exhaust gases and shielding of the inlets may not be accomplished.

The top location of the lift/cruise engine inlet was least ingestion-prone for all configurations. The rear lift/cruise engine inlet also experienced very little ingestion when protected by the wing (the inlet was located on top of the wing when the wing was in the low position). When no protection was provided (such as front location) extreme ingestion was experienced. In general, ingestion may be reduced or eliminated by proper shielding of the inlet by wings or auxiliary deflectors.

Jet-Induced Effects

Jet-induced lift forces were strongly configuration-dependent and resulted in either negative or positive induced lift depending primarily on engine arrangement and vehicle height above ground (Figures 24 and 25). Negative induced lift was experienced by all configurations during operation out of ground effect. In close ground proximity, positive lift was in general associated with propulsion arrangements creating an upward flow of hot exhaust gases under the fuselage and wing while negative induced lift resulted from operation of single engine or several engines closely spaced. The positive lift created during close ground proximity diminishes very rapidly with increased height above ground. Also, induced lift effects cause adverse pitching moment during near-ground operation requiring additional control power beyond normal requirements of a VTOL aircraft.

Jet-induced forces and moments appear to be unaffected by the location of lift/cruise engine inlets. The wing location, on the other hand, has a significant effect on the overall level of induced force and moments. The influence of the wing is closely tied to its relative location with respect to the propulsion system and height of the wing on the fuselage. Greater induced-force levels were generally experienced at lower wing locations compared with high wing position. Induced-force levels on the wing were appreciably greater at vehicle heights closer to ground.

The major portion of the total induced force was developed on the fuselage lower surfaces mainly in the area near the engine exhaust nozzles. The trend was from negative lift force out of ground proximity to positive lift force near the ground caused by the impingement of the upward directed exhaust gases on the lower surfaces of the fuselage.

Engine Stall Analysis

Compressor stall phenomena - High speed compressor stall is of primary concern, and the following discussion consequently pertains to stall occurring at or near 100 percent rpm. Rapid inlet temperature rise appears to be an important factor in inducing compressor stall. The inlet temperature rise causes a reduction of corrected airflow and corrected rpm, shifting the engine operating point in the direction of the quasi-steady stall line. At high engine speeds, the opening of the interstage bleed valves, in response to quasi-steady increases in inlet temperature, retards the degradation of the stall margin. Figure 32 illustrates the effect of interstage bleed on improving the compressor stall margin. The stall margin for the case with no bleed

is shown in Figure 32(a) while Figure 32(b) shows improved stall margin for a typical compressor bleed schedule. Interstage bleed corrects the matching of the compressor and turbine and the matching of the compressor stages. This improves the lower speed stall characteristics by providing higher weight flow through the forward stages of the compressor without increasing the compressor pressure ratio to the stall condition. For very rapid changes in inlet temperature, however, the steady state bleed valve schedule is not achievable due to relatively slow response of the bleed valve system (e.g., approximately 8 seconds for J-85 engines). As a result, the engine stall margin will decrease as the corrected airflow decreases as indicated in Figure 32(a).

Figure 33 (based on test data of Reference 5) illustrates the effect of rate of temperature rise on engine stall. The transient excursion of the operating point is shown for three different rates. For rates of rise on the order of 2000 degrees/second, for example, the compressor may be able to adjust to the change without stall, as shown by point 1. The effect of higher temperature rise rate is also shown in Figure 33(a). The compressor pressure ratio drops rapidly but recovers at the end of temperature rise and returns to near-normal operating line (point 2) at lower corrected speed corresponding to the elevated inlet temperature. At considerably higher rates of temperature rise (on the order of 6000 degrees/second), the operating point crosses the stall line and leads to compressor stall as shown by point 3 of Figure 33(b). Stall may occur on either side of the stall line, however, depending on the severity of ingestion and propagation of stall in the compressor stages. The front and back stages of the compressor may be operating under different thermal conditions due to hot gas ingestion, resulting in a considerable mismatch among the stages. Stall usually develops in the last stages of the compressor because of the lower tolerance of these stages to temperature rise. A very high temperature rise rate can stall the forward compressor stage before any change has occurred in the last stages.

Analyses conducted to determine the excursion of the operating point during a temperature transient have indicated that, for a J-85 engine, the stall line is crossed when temperature rates approaching 6000 degrees/second with a temperature rise of 60 to 80^{o}F exist at the compressor face.

Test data - Figure 28 illustrates selected inlet temperature-time histories used for stall analysis. Evaluation of data indicates that inlet temperature distortion has a definite effect on engine stall; if distortion results from localized high temperatures over very small areas of the inlet, the compressor is more likely to adjust to distortion without stall. The shift in corrected flow and corrected rpm caused by small localized "hot spots" is small enough to allow the compressor to adjust to the stage mismatch. Thus high temperature transients with high but localized distortion may be tolerated without stall. On the other hand, distortion levels occurring over a larger portion of the compressor face appear to induce compressor stall more readily. Figure 28(c) shows the inlet temperature-time history for the case of localized high temperature distortion (on the order of 200-300^{o}F and 4000 degrees/second) which did not induce engine stall. Figure 28(f) shows the temperature transient for the case where approximately a full quadrant of the inlet experiences a large temperature rise which nearly causes stall, as shown by the sharp drop and subsequent recovery of exhaust gas pressure transient. Here the temperature rise is of the order of 200^{o}F, and the rate less than 3000 degrees/sec. For cases in which stall occurred the initial rate of temperature rise and distortion level is not generally discernible because the temperature rise resulting from backflow of hot exhaust gases cannot be distinctly separated from temperature rise caused by ingestion.

The influence of distortion is further illustrated in Figures 28(g) and 28(h), where highly distorted but localized temperature rise, shown during the initial part of the run, did not induce engine stall, although the engine stalled following reduction of distortion level. These effects are also shown in Figures 28(i) and 28(j). For uniform inlet temperature rise, such as that experienced by the lift/cruise engines, stall occurred less frequently.

This analysis indicates the probability of compressor stall when an inlet temperature rise of 100-150 degrees is experienced over a large portion of the compressor face at rates in excess of 3000 degrees/second. The likelihood of stall is reduced if the temperature increase is confined to a small area.

CONCLUDING REMARKS

Tests of a large-scale VTOL fighter model aircraft have been conducted to obtain design data on hot gas ingestion and jet-induced effects in ground proximity. It was found that induced effects and ingestion are strongly configuration dependent, and for certain arrangements of engine and wing location the degree of ingestion may result in excessive thrust degradation and loss of stability.

The severity of the near-field temperature environment is strongly influenced by the engine arrangement and to a lesser degree by a number of operating engines. Single engine or engine groupings which behave similarly to a single engine (jets merge before reaching the ground plane) do not significantly alter the temperature environment in the vicinity of the inlets (for duration of operation near the ground required by a representative operational VTOL aircraft) and thus pose no serious problem. By contrast, engine arrangements or groupings which cause a "fountain" effect (widely spaced engines) create a severe temperature environment in the proximity of the vehicle which, if permitted to reach the vicinity of the inlet, will create an unacceptable inlet temperature environment.

The geometry effects are interdependent and their influence on ingestion cannot often be isolated. Lower wing location, for example, appears to be more effective in reducing ingestion only if it is properly located with respect to the propulsion system arrangement to permit effective deflection and shielding of the hot exhaust gases. Pitch attitude effects are closely tied to the shift in local stagnation point of the ground jets and may reduce or aggravate ingestion depending on other geometrical variations such as wing location, size, geometry and lift/cruise engine-inlet location.

Composite configurations (lift-plus-lift/cruise engines) produced induced lift effects resulting in net lift gain from 5 to 9 percent over the lift experienced at the maximum test height. Configurations employing only lift engines and low wing position suffered increasing lift loss as the vehicle was positioned closer to the ground plane.

Sound pressure levels were dependent on the height of the vehicle above the ground plane and relatively independent of the number of operating engines. Close to the ground, the far field decibel values diminished, but at all model heights the sound pressure levels in the proximity of test model exceeded the tolerance of the unprotected human ear.

It appears that large temperature rise occurring over a very small area of the compressor face may be tolerated without stall. However, a less severe thermal environment distributed over a larger portion of the compressor face is more likely to induce stall. Internal hot gases expelled from one engine subsequent to stall may stall adjacent engines.

Northrop Corporation, Norair Division
Hawthorne, California
October 31, 1967

APPENDIX A

RESPONSE OF BARE WIRE THERMOCOUPLES TO TEMPERATURE VARIATIONS IN A JET ENGINE INTAKE

INTRODUCTION

Recent full-scale VTOL exhaust gas ingestion tests have indicated engine inlet air temperature histories of a highly transient character for many of the configurations tested. Considering the transient character of these data, highly responsive thermocouples are required to reproduce the actual temperature transients experienced within the inlets. In general, however, thermocouples of small enough thermal mass to follow the actual temperature transients may not withstand the hostile vibration and acoustic environment within an engine inlet. Considering these practical factors, along with the generally large number of thermocouples required to define the inlet temperature fields for multijet configurations, it may be necessary to accept a temperature pick-up which sacrifices thermal response.

Depending upon the particular objective of the investigation, damped thermal response may or may not represent a serious compromise in the test objective. For instance, in determining the thrust degradation resulting from exhaust gas ingestion for a particular airplane configuration, measurements of short duration temperature pulses of the order of a few milliseconds are not required due to the relatively slow response of the engine to changes in inlet temperature. For evaluations of this type, some damping of the instantaneous temperature field is acceptable; in fact, there is some merit to matching the response of the temperature read-out circuit to the response of the engines for experimental correlations of this type.

On the other hand, for configurations in which exhaust gas ingestion is severe enough to result in engine stall caused by sharp localized temperature pulses within the engine inlet, then undamped measurements of these temperature pulses are obviously important. This means selection of a highly responsive temperature pick-up and a recorder with response equal to or greater than that of the temperature pick-up.

Although an example is pointed out above for a case in which instantaneous temperature determination is not important and for an example in which instantaneous temperature determination is important, it is not the purpose of this note to discuss what one should be measuring since there is no unique answer to this question. Rather, the purpose of this note is to aid one in the selection of a particular temperature pick-up once the desired response is established, or, if the desired response results in wire gage too fine to withstand the environment, to provide data from which the actual response may be determined so that the data may be interpreted accordingly. If in following the latter course, one feels that the instantaneous temperature is highly

important, it is still possible to reconstruct the actual input temperature history, given the output temperature history and temperature pick-up response characteristics. This can be accomplished by use of compensating amplifiers either directly in the instrumentation circuit or through various data playback techniques, or by manual reconstruction of the true temperature input through step-by-step calculations based on the differential equation governing the thermal response of the temperature pick-up in conjunction with the measured output.

ANALYSIS

Consider a thermocouple wire oriented normal to an approaching airflow. Neglecting radiation, heat loss from the ends of the wire by conduction, and assuming the radial temperature gradient through the wire is negligible, the following heat balance may be written

$$\dot{q} = hA\,(T_g - T_w) = wc\,\frac{dT_w}{dt} \tag{1}$$

where
- h = convection coefficient
- A = wire surface area
- T_g = recovery temperature of the air
- T_w = wire temperature
- w = weight of the wire
- c = heat capacity of the wire
- t = time

For typical bare thermocouple wire sizes projected approximately 1/8" - 1/4" beyond the supporting probe, and whose temperature is within a few hundred degrees of ambient temperature, the assumptions stated above, namely, (1) neglecting radiation, (2) neglecting conduction heat loss from the ends of the wire and (3) neglecting the radial thermal gradient, have been checked by numerical calculations and were found to be good engineering approximations for an analysis of the thermal response of the thermocouple junction.

CASE I: Step Input - Consider the case for which T_w is in equilibrium with the air temperature at $t < 0$ ($T_w = T_{g_1}$). At $t = 0$, the air temperature is suddenly changed to the value T_{g_2} and remains constant for $t > 0$. The solution to equation (1) is then given by

$$\frac{T_w - T_{g_1}}{T_{g_2} - T_{g_1}} = 1 - e^{-\lambda t} \tag{2}$$

where

$$\lambda = \frac{hA}{wc}$$

CASE II: Sine Wave Input - Consider the case in which the air temperature varies sinusoidally with time. That is, let T_g of equation (1) be given by

$$T_g = T_o + A_o \text{ SIN } \omega t$$

For this case the particular solution to equation (1) may be shown to be given by

$$\frac{T_w - T_o}{A_o} = \frac{1}{\sqrt{1 + \left(\frac{\omega}{\lambda}\right)^2}} \text{ SIN}\left(\omega t + \text{SIN}^{-1} \frac{-\omega/\lambda}{\sqrt{1 + \left(\frac{\omega}{\lambda}\right)^2}}\right) \tag{3}$$

The amplitude ratio is then given by

$$\frac{A_w}{A_o} = \frac{1}{\sqrt{1 + \left(\frac{\omega}{\lambda}\right)^2}} \tag{4}$$

where

$$A_w \equiv \left(T_w - T_o\right) \text{MAX}$$

and the phase lag angle φ is

$$\varphi = \text{SIN}^{-1} \frac{-\omega/\lambda}{\sqrt{1 + \left(\frac{\omega}{\lambda}\right)^2}} \tag{5}$$

For the purpose of evaluating λ in equations (2) through (5), the convection coefficient, h, may be determined from experimental data of Reference 6 which gives $Nu = f(Re_d)$ for flow across wires. For the iron-constantan thermocouple response results presented in Figures 34 through 35, values of $\rho = 486$ lb/ft^3 and $c = 0.12$ BTU/lb$^\circ$F were used. It is seen from equation (2) that the thermocouple time constant is simply the inverse of λ.

RESULTS

The results of the analysis were compared to experimental data obtained for the response of a 30-gage (d = 0.010" diameter) iron-constantan thermocouple subjected to a step change in air temperature. The step change in air temperature was achieved by thrusting the thermocouple, which was initially in thermal equilibrium with the

ambient environment, into a uniform stream of hot gas at 230°F issuing from a 4- by-4-inch-square duct. The output of the thermocouple was monitored on an oscilloscope and the thermal response was documented with an oscilloscope camera. Data were obtained for hot air flow velocities of V = 100, 200, and 300 feet/second.

Figure 34 shows the comparison of the theoretical calculations with the experimental data for a step change in air temperature from T_{g_1} to T_{g_2} at t = 0. The curve is the theoretical calculation as given by equation (2) with the numerical value of λ calculated for the actual conditions of the experiment. The experimental data are represented by the symbols, each of which is an average of duplicate data which were within 2 percent of each other for all data points measured. Although continuous traces of the experimental data were obtained, the agreement between the experimental data and the theoretical calculations is too close to allow definition of two discrete curves. As a result, points were measured from the continuous trace experimental data at 100 m.s. time intervals for the comparison shown in Figure 34.

The near perfect agreement of the calculated curves and the experimental data must be considered somewhat fortuitous. In reviewing the various inputs to the analysis in detail, one may have expected disagreement between the analysis and the experimental data in the neighborhood of 10-20 percent if the anticipated differences between the analysis and the experiment had accumulated in a more unfavorable way. Even with an unfavorable accumulation of differences, however, the analysis must be considered as a good indication of the actual thermocouple response.

Figures 35 through 37 show some numerical results of the analysis which are of particular interest for the response of thermocouples within the inlet to a jet engine. The results given are for iron-constantan thermocouples of various wire gage sizes oriented normal to an airstream with a velocity of 400 feet/second at standard pressure and temperature. The curves are also considered indicative of the response for other wire orientations and indicative of the response for chromel-alumel thermocouples since the response depends only upon the value of λ, which for chromel-alumel thermocouples is within a few percent of the value for iron-constantan thermocouples for the same wire size and flow conditions. The data of Fig. 35, which give the response to a step change in air temperature, indicate a time constant to approximately 100 m.s. and a 99 percent rise time of approximately one-half second for the 30 gage (d = 0.010" diameter) thermocouple wire used in recent exhaust gas ingestion tests performed by Norair and others.

Figures 36 and 37 show, respectively, the amplitude ratio, A_w/A_o (equation 4) and the phase lag angle, φ (equation 5) as a function of frequency for a gas temperature which varies sinusoidally with time. From Figure 36, it is seen that flat response for the 30 gage (0.010" wire) is limited to frequencies of less than a few tenths of a cycle/second while at 15 cps the input signal is attenuated 90 percent.

REFERENCES

1. Rahim Lavi, "An Experimental Investigation of VTOL Lift-Engine Inlet," AIAA Journal of Aircraft, March-April 1967.

2. W. W. Watson, R. Lavi, H. Asdurian, "Design and Instrumentation of a Large-Scale VTOL Test Bed for Investigation of Ground Proximity Effects," AIAA Paper No. 67-181 presented at the AIAA 5th Aerospace Sciences Meeting, New York, January 23-26, 1967.

3. W. Stark, R. F. Carmichael, "Results of a Hot-Gas Ingestion and Jet Effects Test Program with a Large-Scale VTOL Test Vehicle in Ground Proximity," Northrop Report number NOR 66-246, 1966.

4. Rahim Lavi, "Parametric Investigations of VTOL Ground Proximity," AIAA Paper No. 67-440, July 1967.

5. Lewis E. Wallner, James W. Useller, and Martin J. Saari, "A Study of Temperature Transients at the Inlet of a Turbojet Engine," NACA RME57C22, 1957.

6. "Physical Measurements in Gas Dynamics and Combustion," Volume IX of High Speed Aerodynamics and Jet Propulsion, Princeton University Press, 1954.

TABLE 1. CONFIGURATION LIST

CONFIGURATION	CRUISE INLET LOCATION	WING POSITION	ENGINE NUMBER (FIGURE 6)	MODEL HEIGHT H/D	SEE FIGURE NUMBER
A	Top	Mid/Aft	1, 2, 3, 4, 6, 7	3.0	10
B		Low/Aft		2.4	11(a) - 11(f)
				3.0	11(g) - 11(l)
				4.5	11(m) - 11(r)
				6.5	11(s) - 11(x)
				8.7	11(y) - 11(ad)
C	Rear	Low/Aft		3.0	12
D		High/Aft		4.5	13(a) - 13(f)
				6.5	13(g) - 13(l)
				8.7	13(m) - 13(r)
E	Front	High/Aft		3.0	14
F		Low/Aft		3.0	15, 24, 26
G	Top	High/Fwd	1, 2, 3, 5, 6, 7	3.0	16, 25
H		Mid/Fwd		3.0	17
I		Low/Fwd			18, 25
J	Rear				19
K	Front				20, 26
L		High/Fwd			21
M	Top	Low/Fwd	3, 4, 5	3.0	22
N		High/Fwd			23

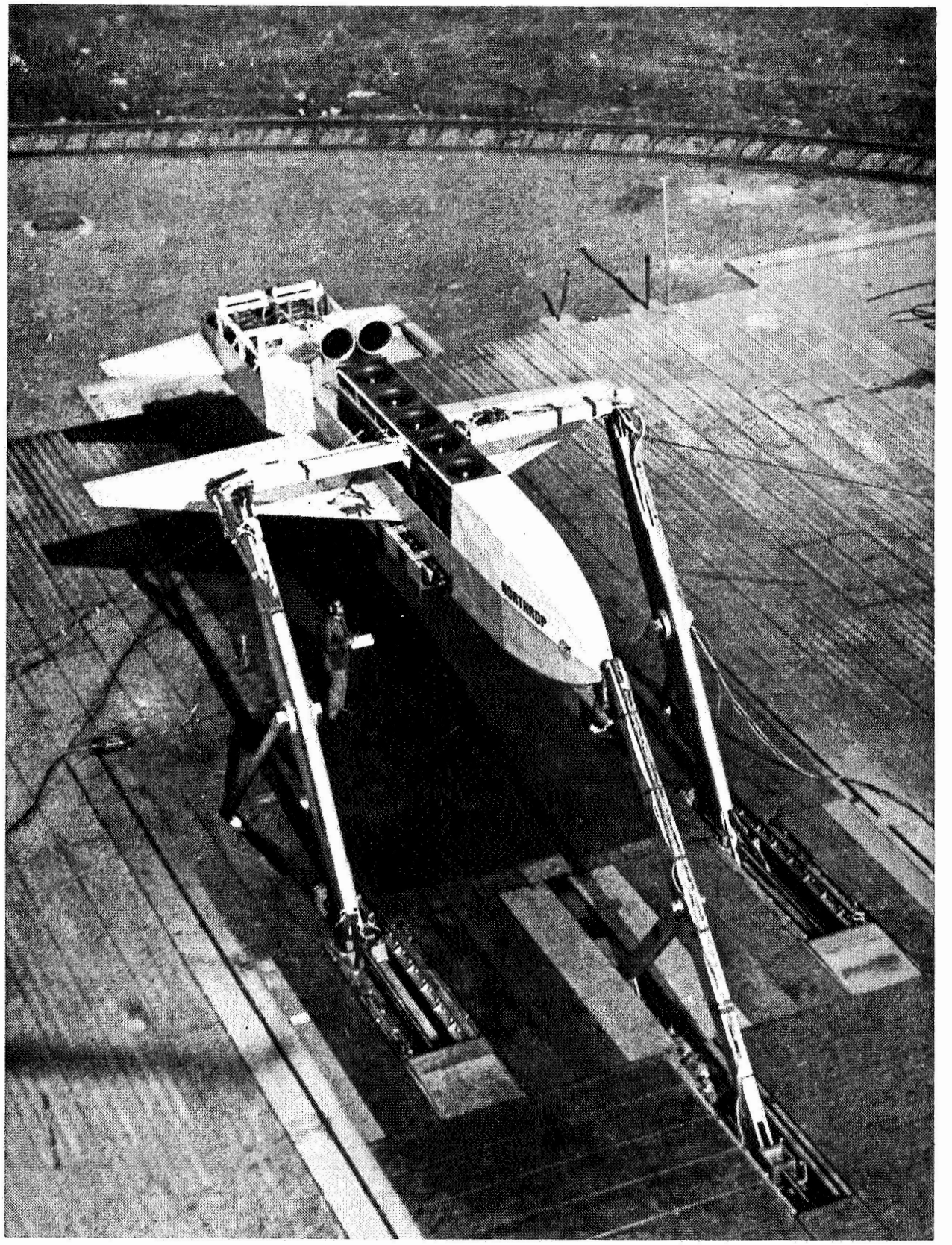

FIGURE 1. TEST VEHICLE MOUNTED ON NASA-AMES STATIC TEST STAND (CONFIGURATION B)

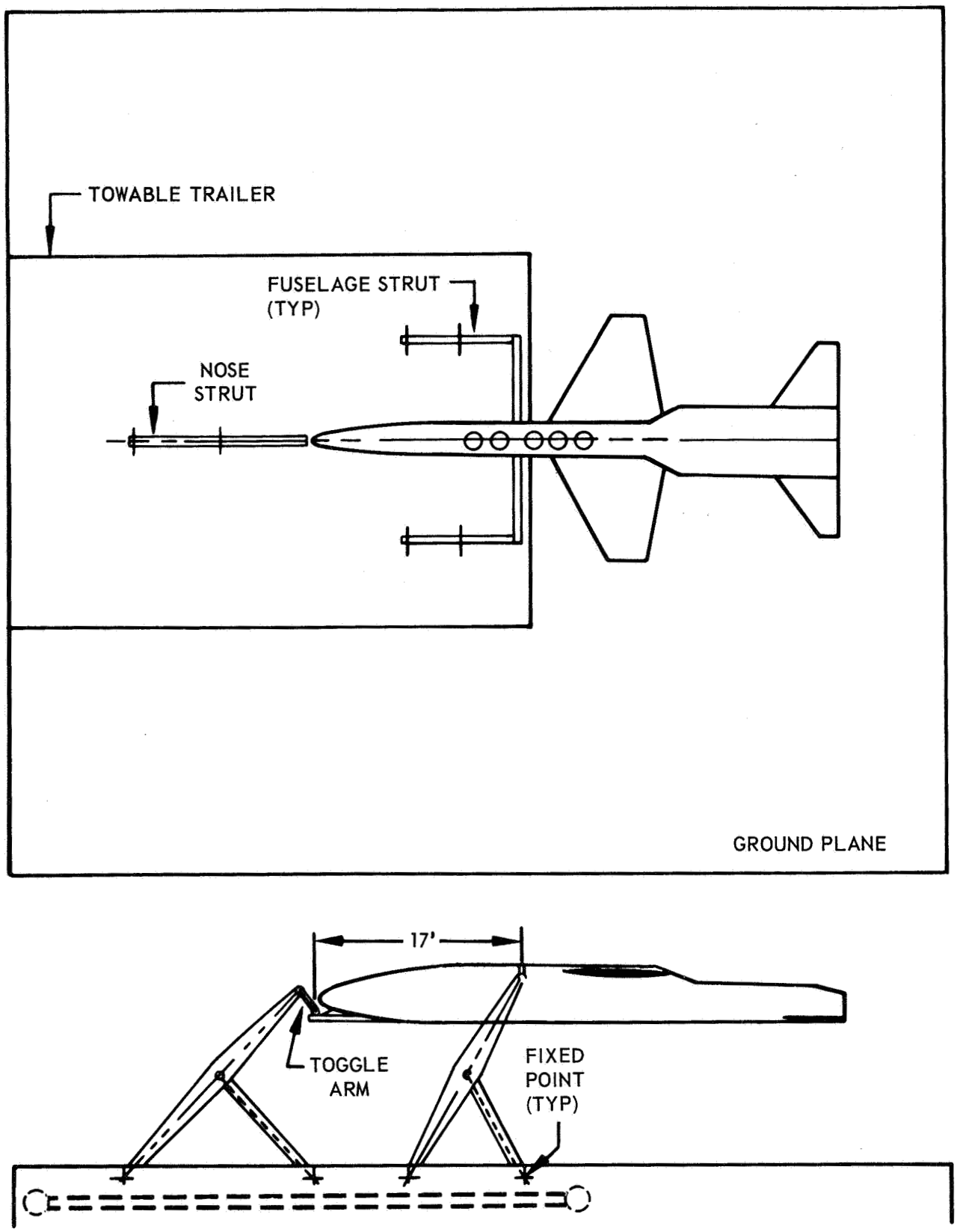

FIGURE 2. AMES VTO THRUST STAND GENERAL ARRANGEMENT

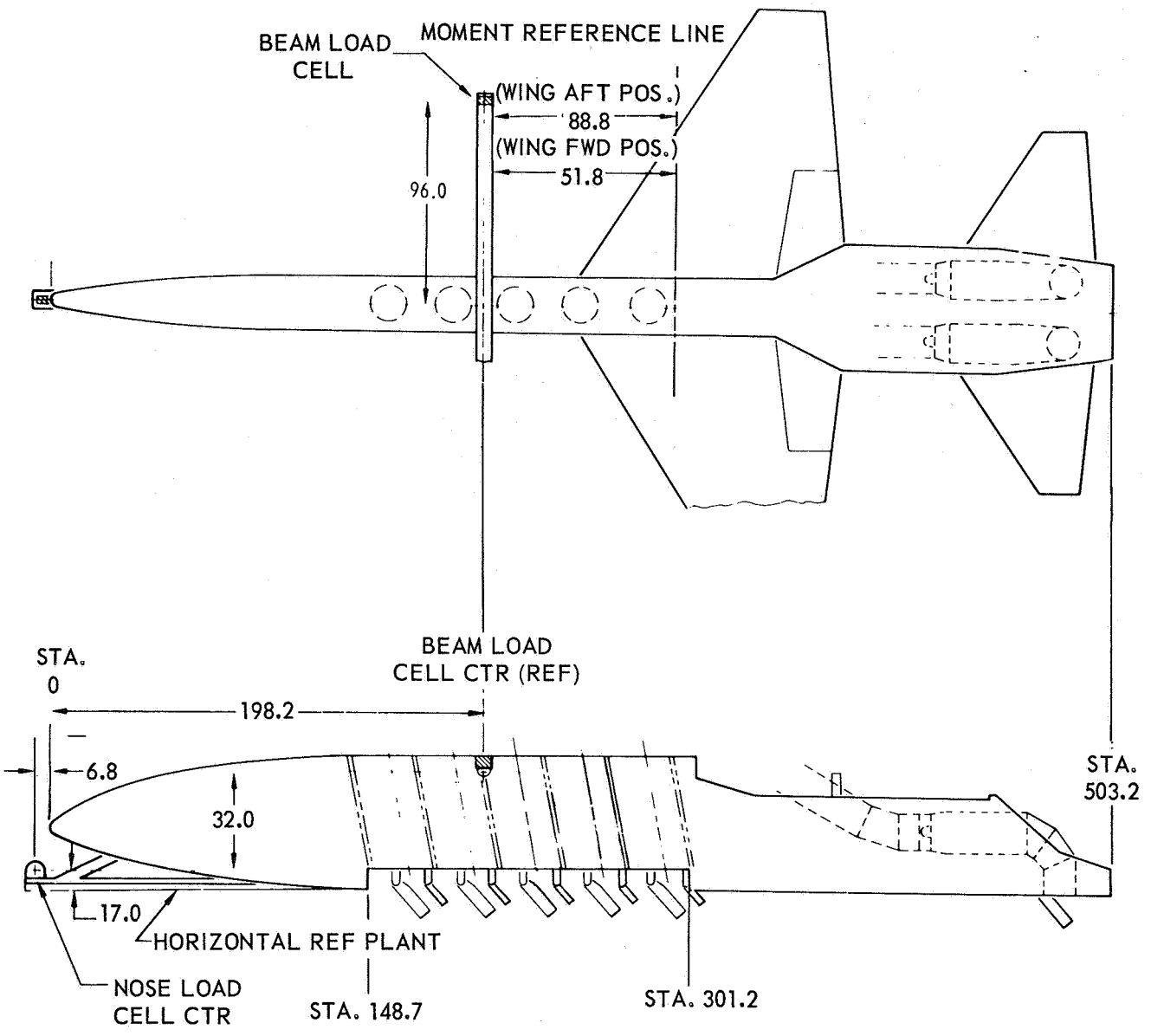

FIGURE 3. LOAD CELL LOCATION

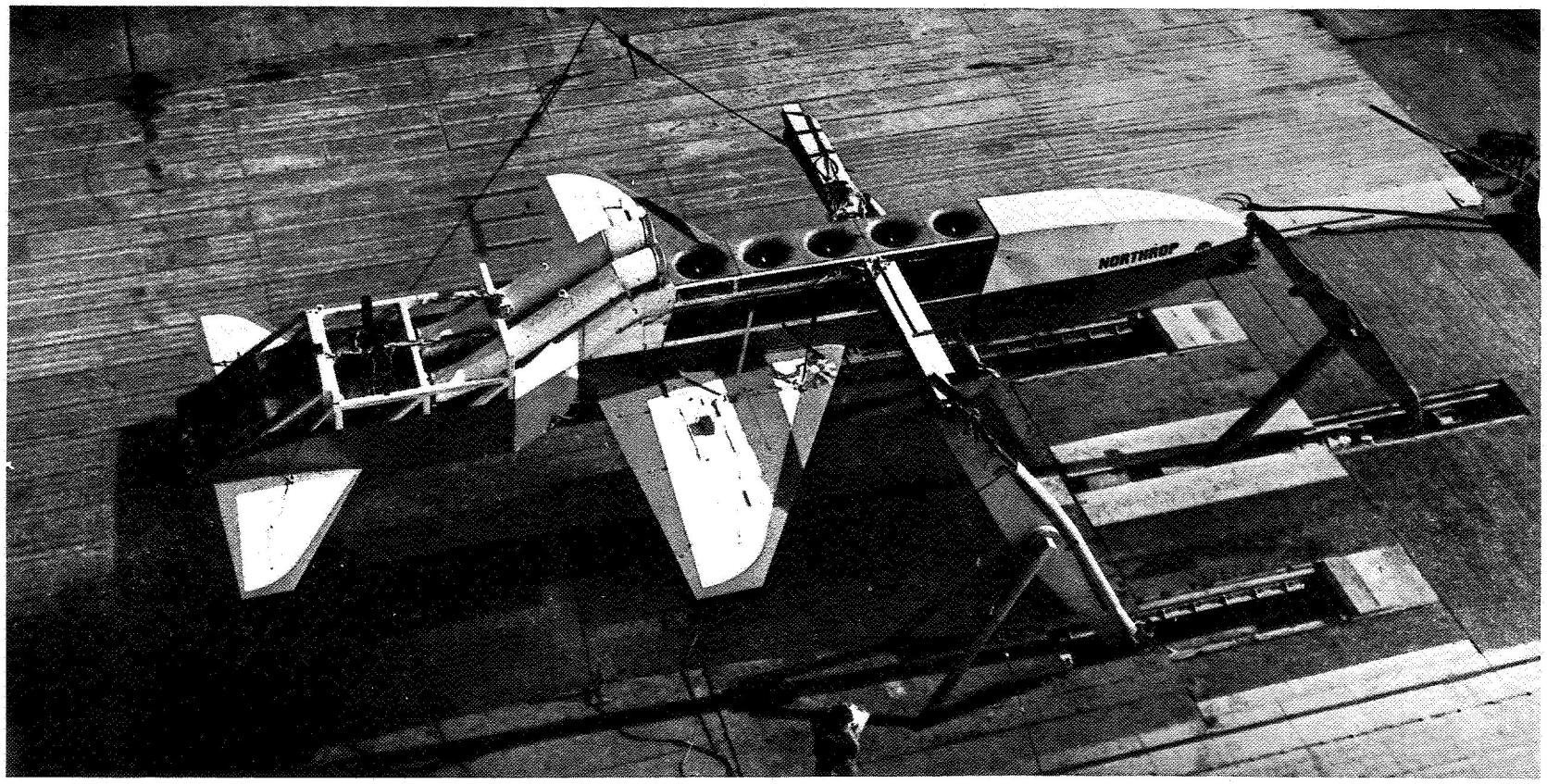

FIGURE 4. TEST MODEL GENERAL ARRANGEMENT (CONFIGURATION B)

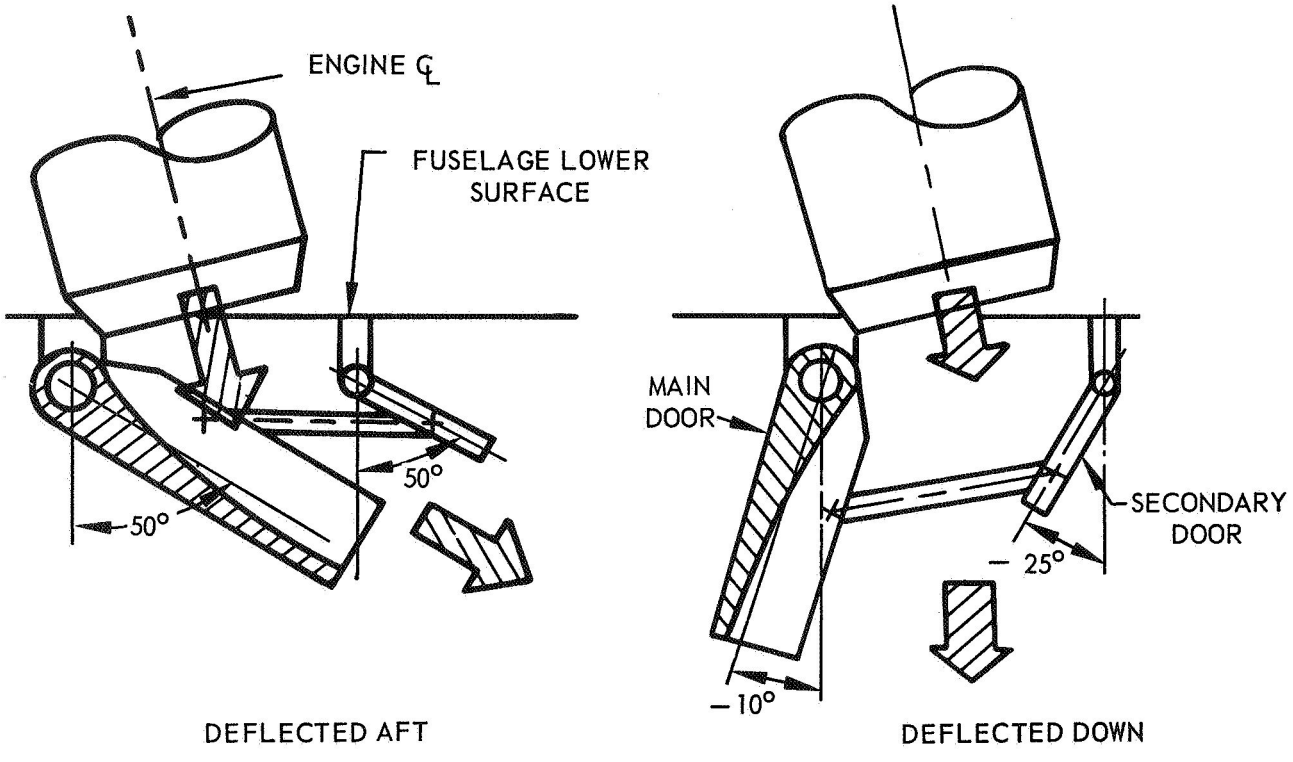

FIGURE 5. DEFLECTOR DOOR ARRANGEMENT

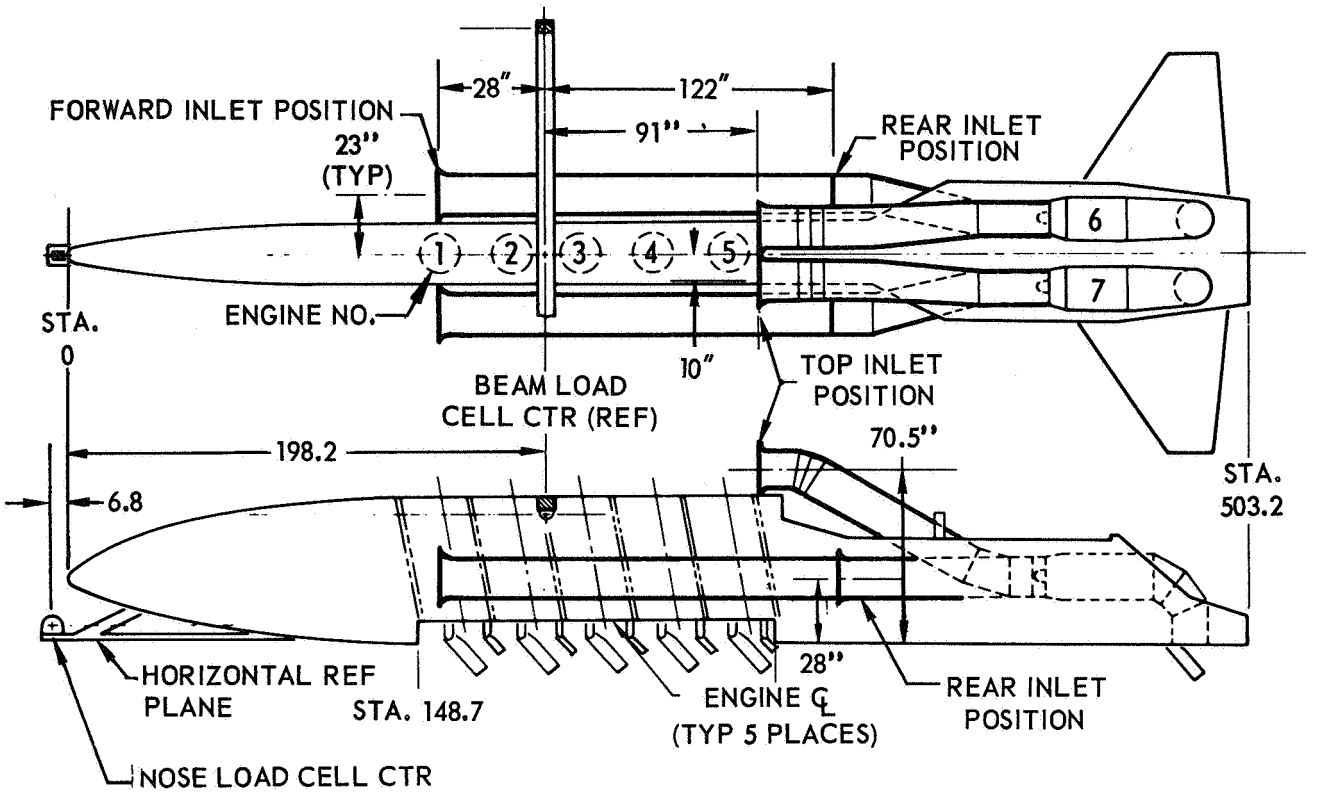

(a) LIFT CRUISE INLET LOCATIONS

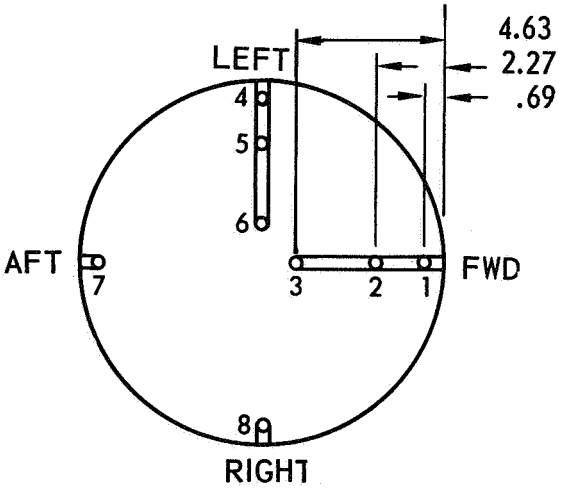

(b) INLET THERMOCOUPLE LOCATIONS

FIGURE 6. TEST MODEL GENERAL ARRANGEMENT AND INLET INSTRUMENTATION

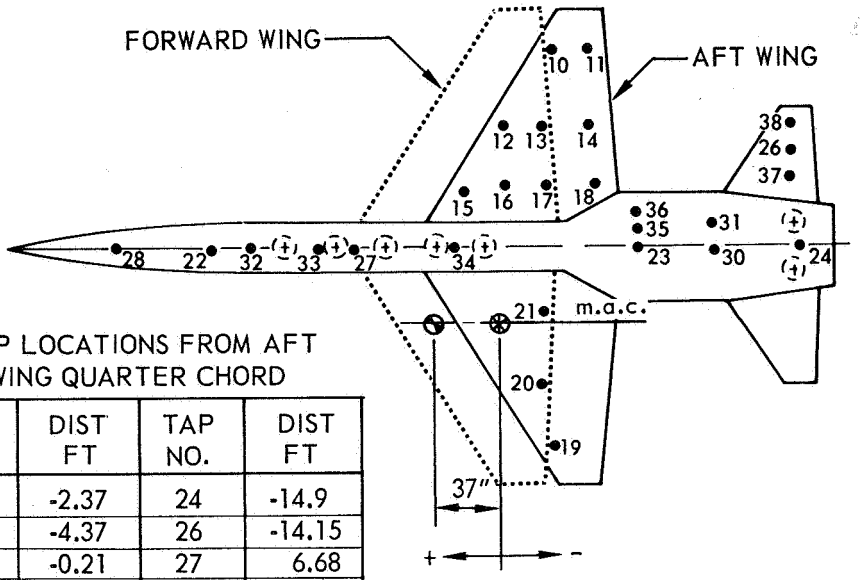

TAP LOCATIONS FROM AFT WING QUARTER CHORD

TAP NO.	DIST FT	TAP NO.	DIST FT
10	-2.37	24	-14.9
11	-4.37	26	-14.15
12	-0.21	27	6.68
13	-2.5	28	19.7
14	-4.5	29	-3.02
15	2.0	30	-10.8
16	-0.25	31	-10.8
17	-2.5	32	12.4
18	-4.58	33	9.8
19	-2.37	34	2.08
20	-2.5	35	-7.0
21	-2.5	36	-7.0
22	15.4	37	-13.85
23	-7.0	38	-14.6

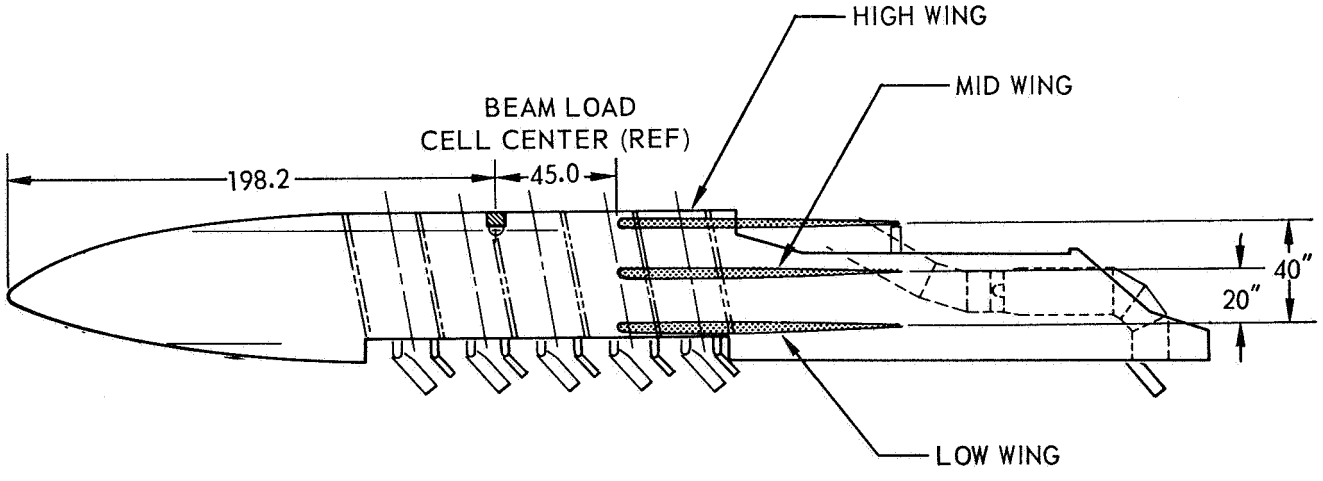

FIGURE 7. MODEL WING POSITIONS AND STATIC PRESSURE TAP LOCATIONS

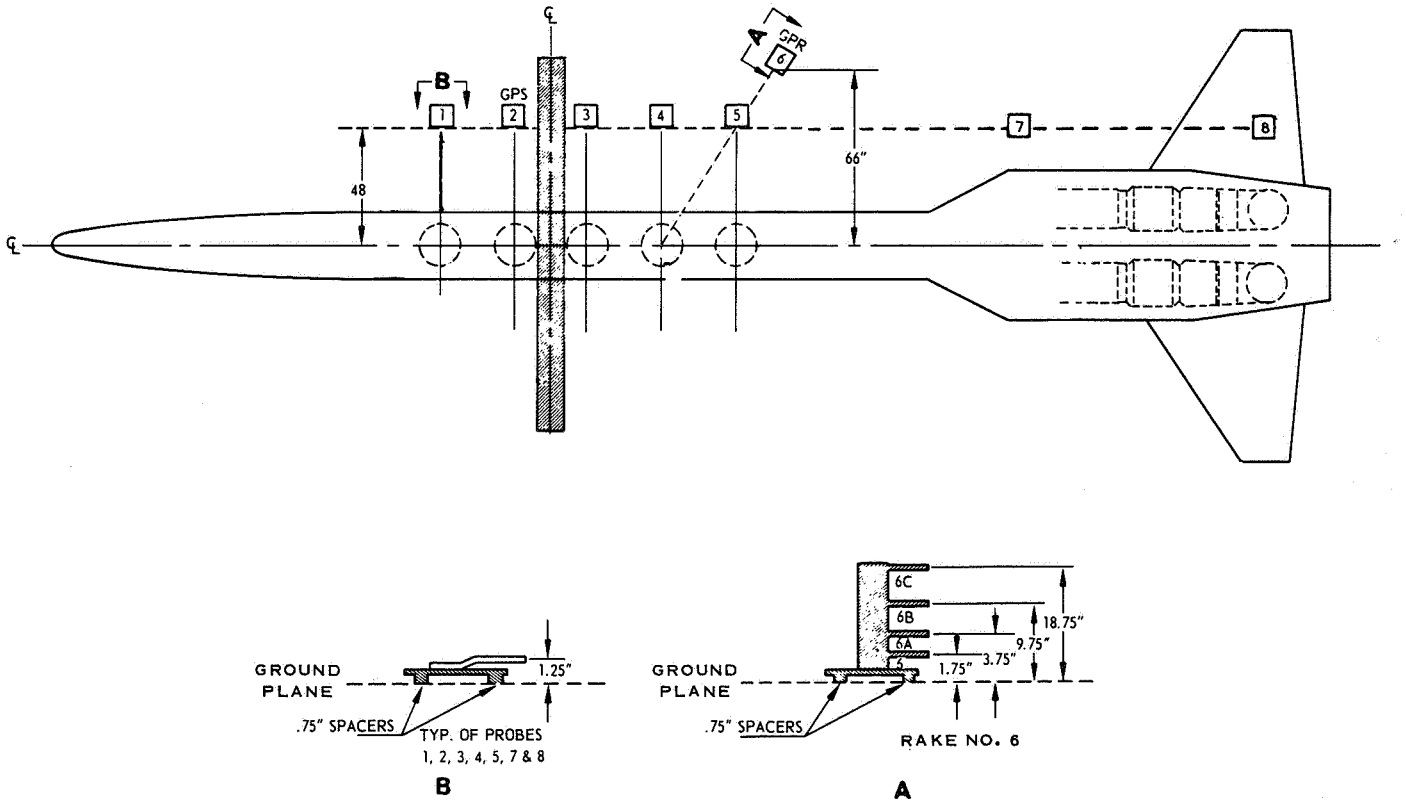

FIGURE 8. GROUND PLANE TEMPERATURE PROBES

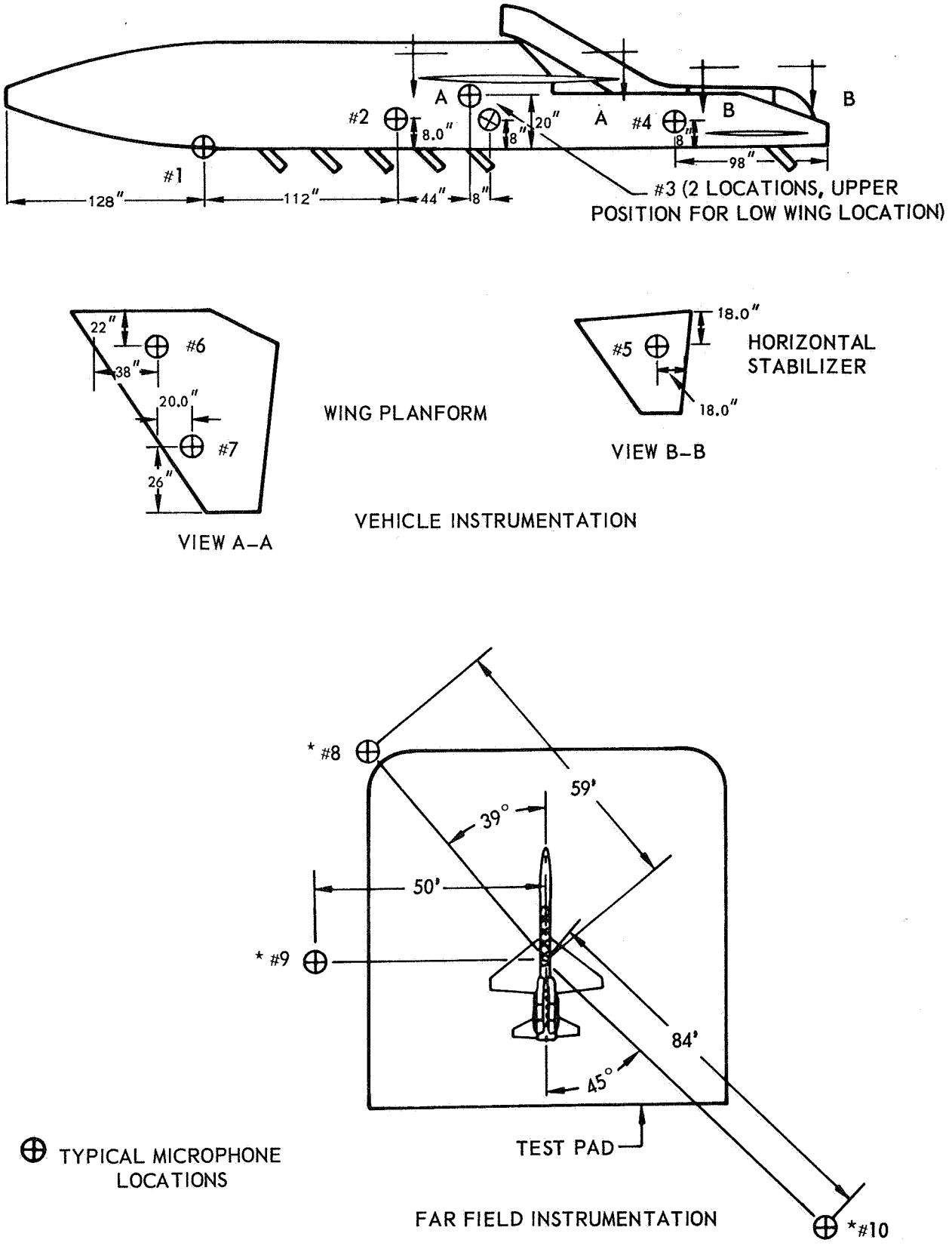

FIGURE 9. ACOUSTIC INSTRUMENTATION LOCATION

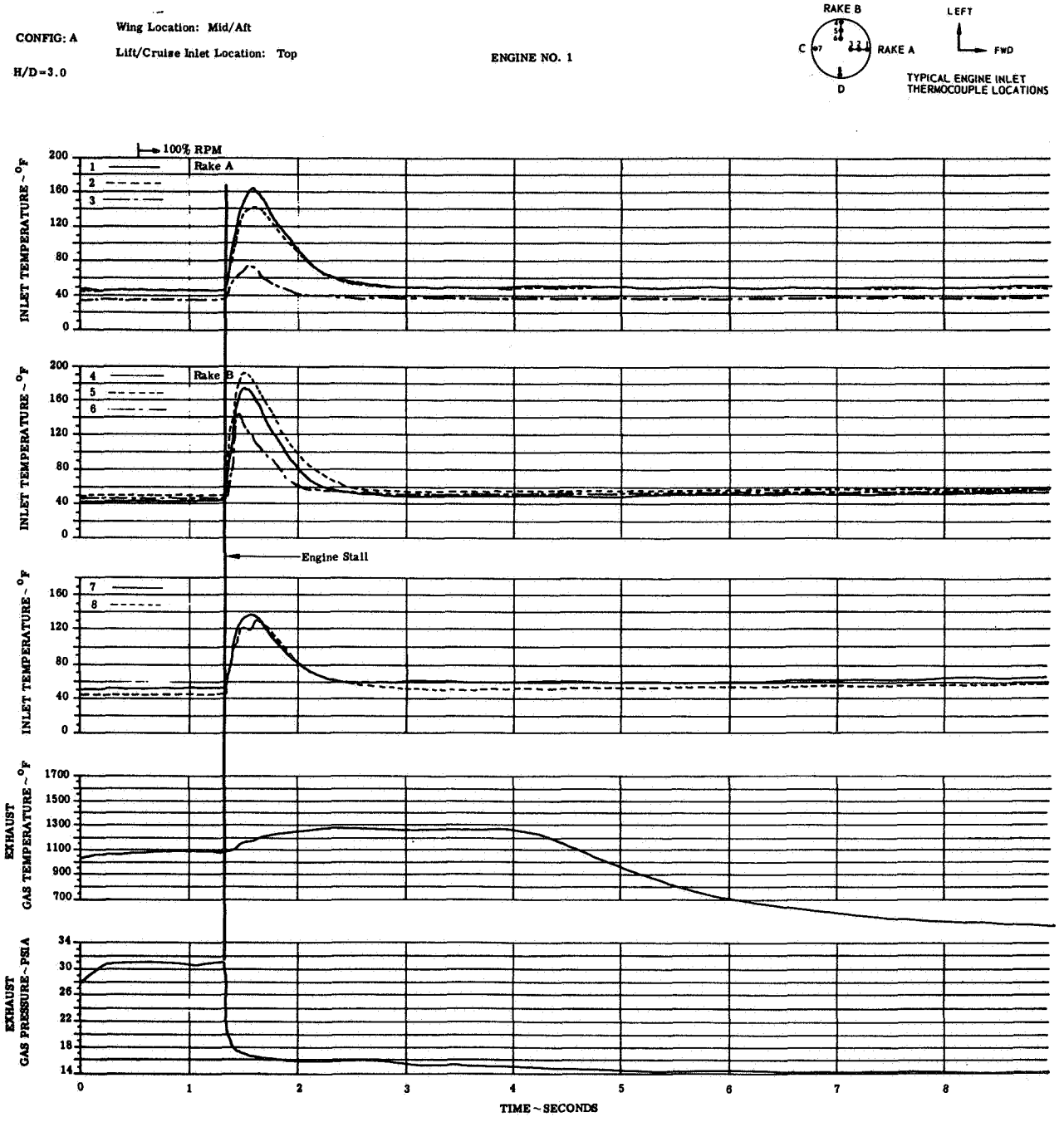

FIGURE 10(a). ENGINE TEMPERATURE AND PRESSURE TRANSIENTS

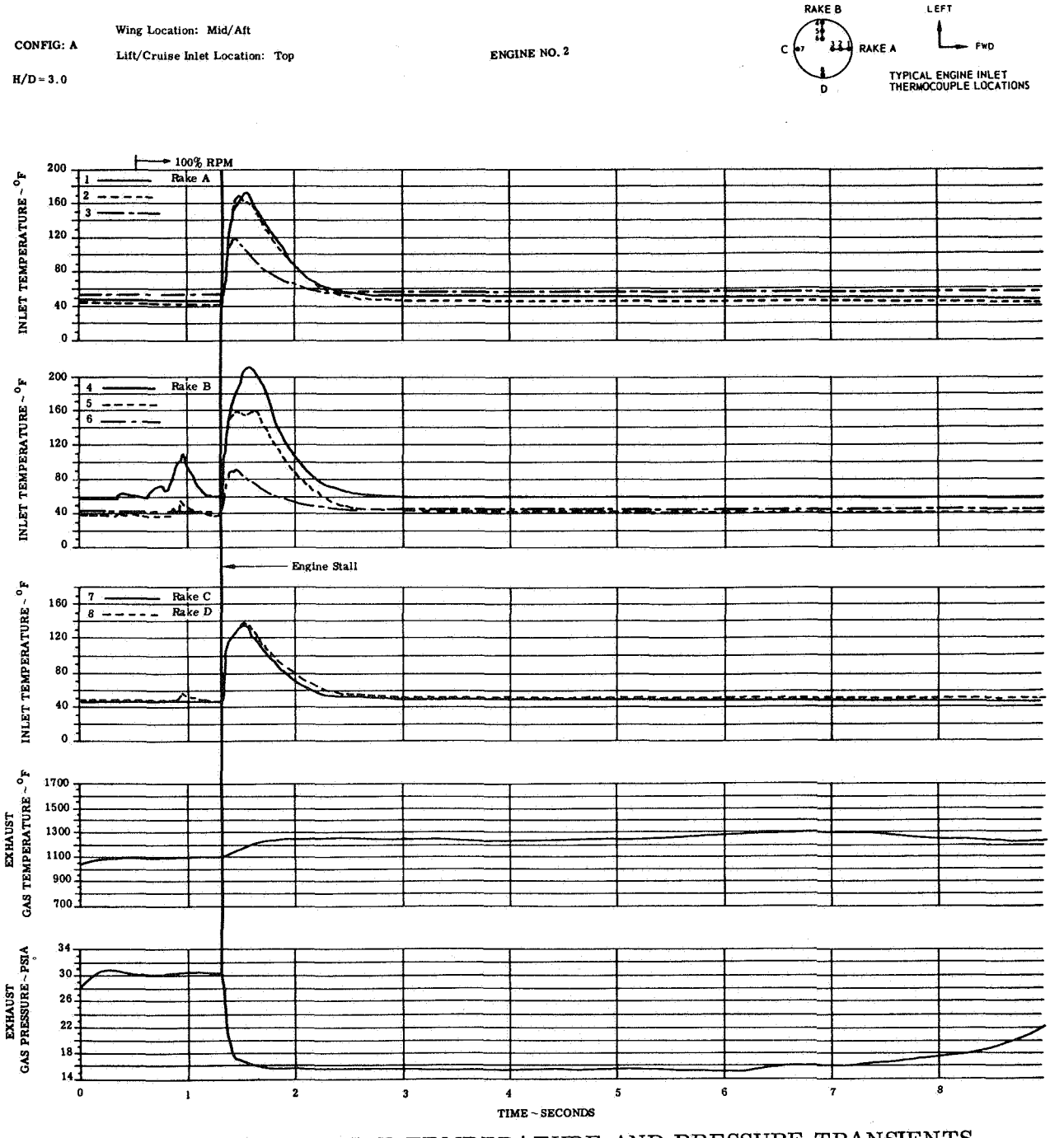

FIGURE 10(b). ENGINE TEMPERATURE AND PRESSURE TRANSIENTS

CONFIG: A

Wing Location: Mid/Aft

Lift/Cruise Inlet Location: Top

H/D - 3.0

ENGINE NO. 3

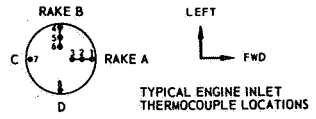

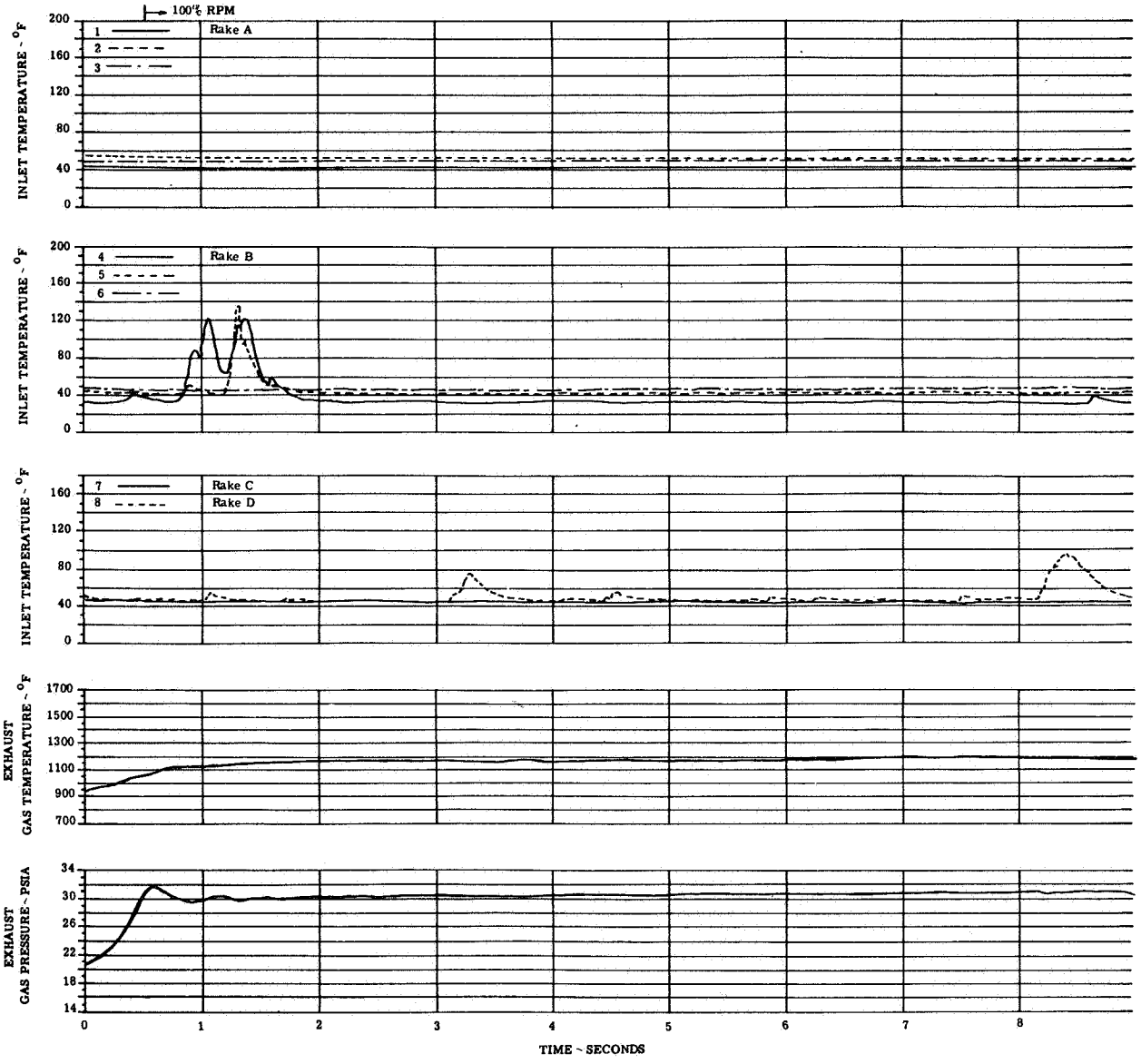

FIGURE 10(c). ENGINE TEMPERATURE AND PRESSURE TRANSIENTS

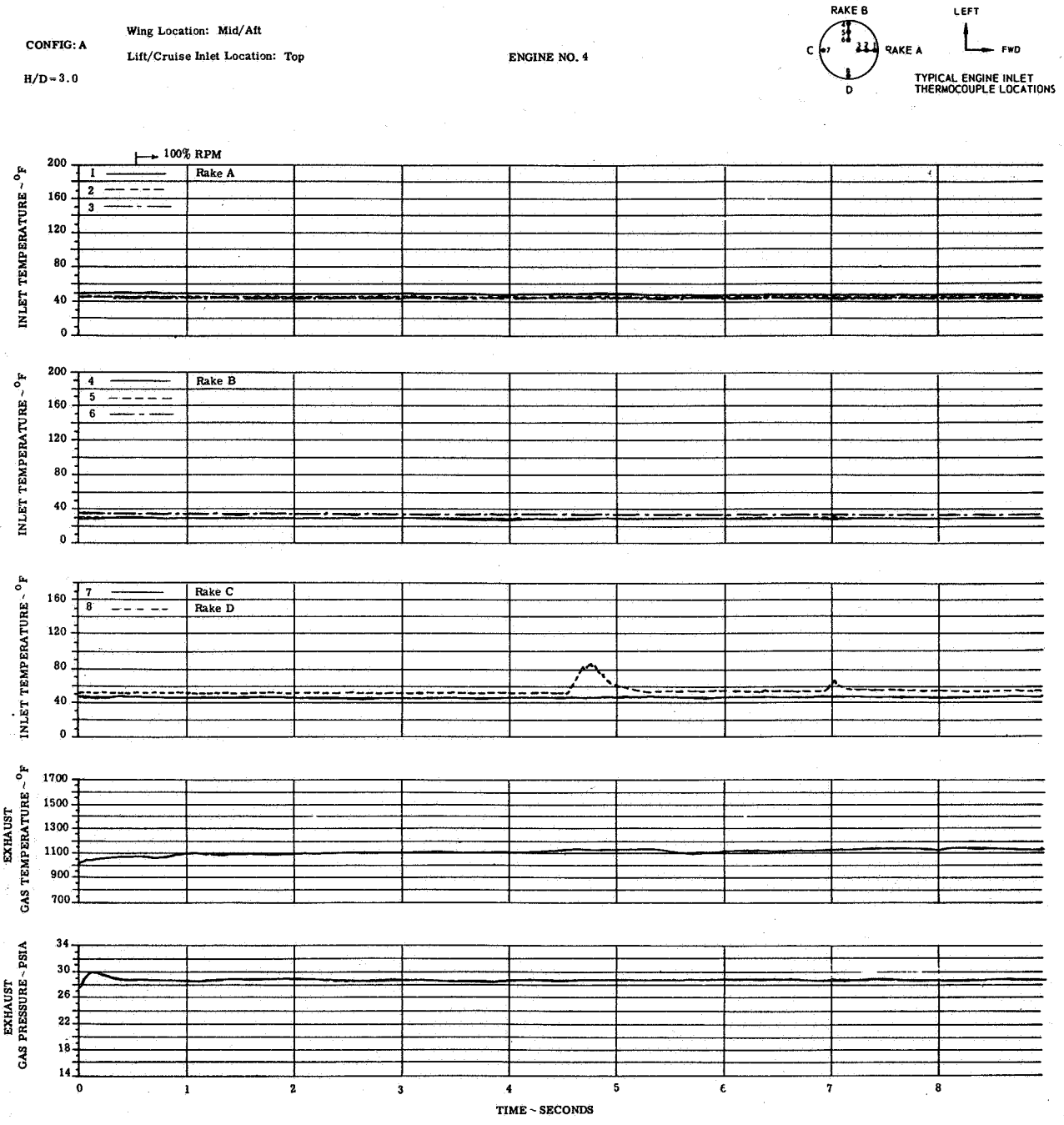

FIGURE 10(d). ENGINE TEMPERATURE AND PRESSURE TRANSIENTS

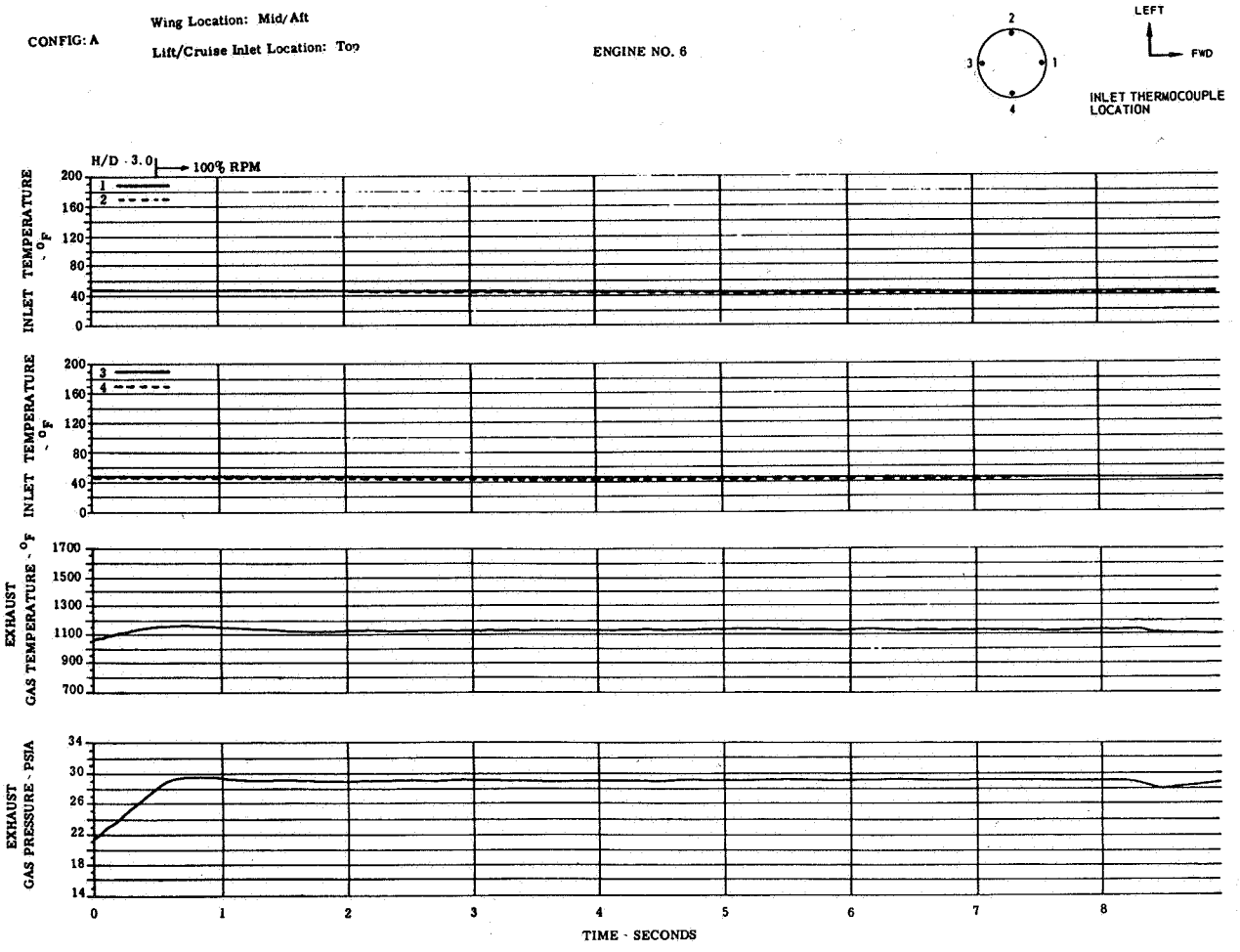

FIGURE 10(e). ENGINE TEMPERATURE AND PRESSURE TRANSIENTS

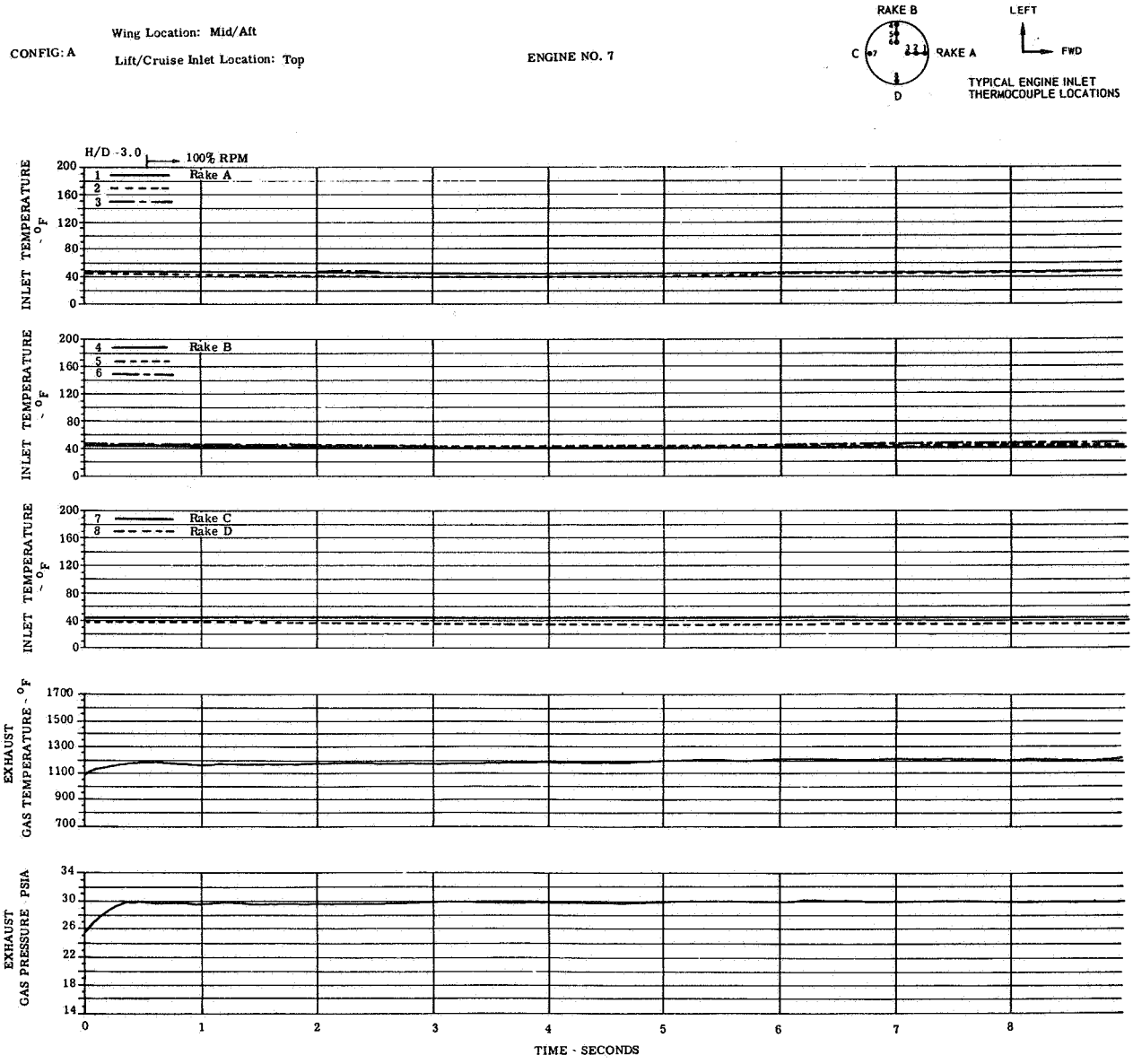

FIGURE 10(f). ENGINE TEMPERATURE AND PRESSURE TRANSIENTS

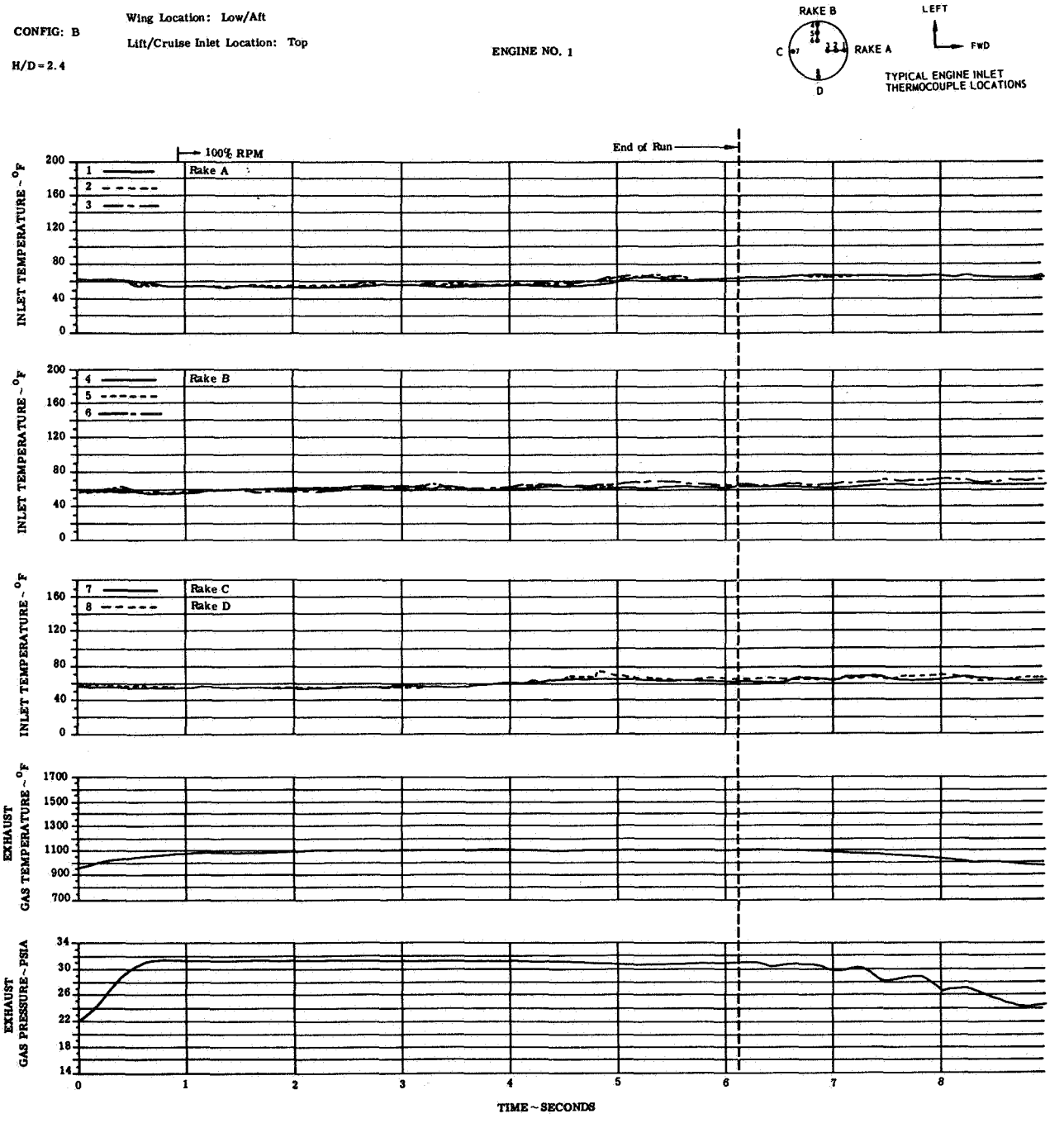

FIGURE 11(a). ENGINE TEMPERATURE AND PRESSURE TRANSIENTS

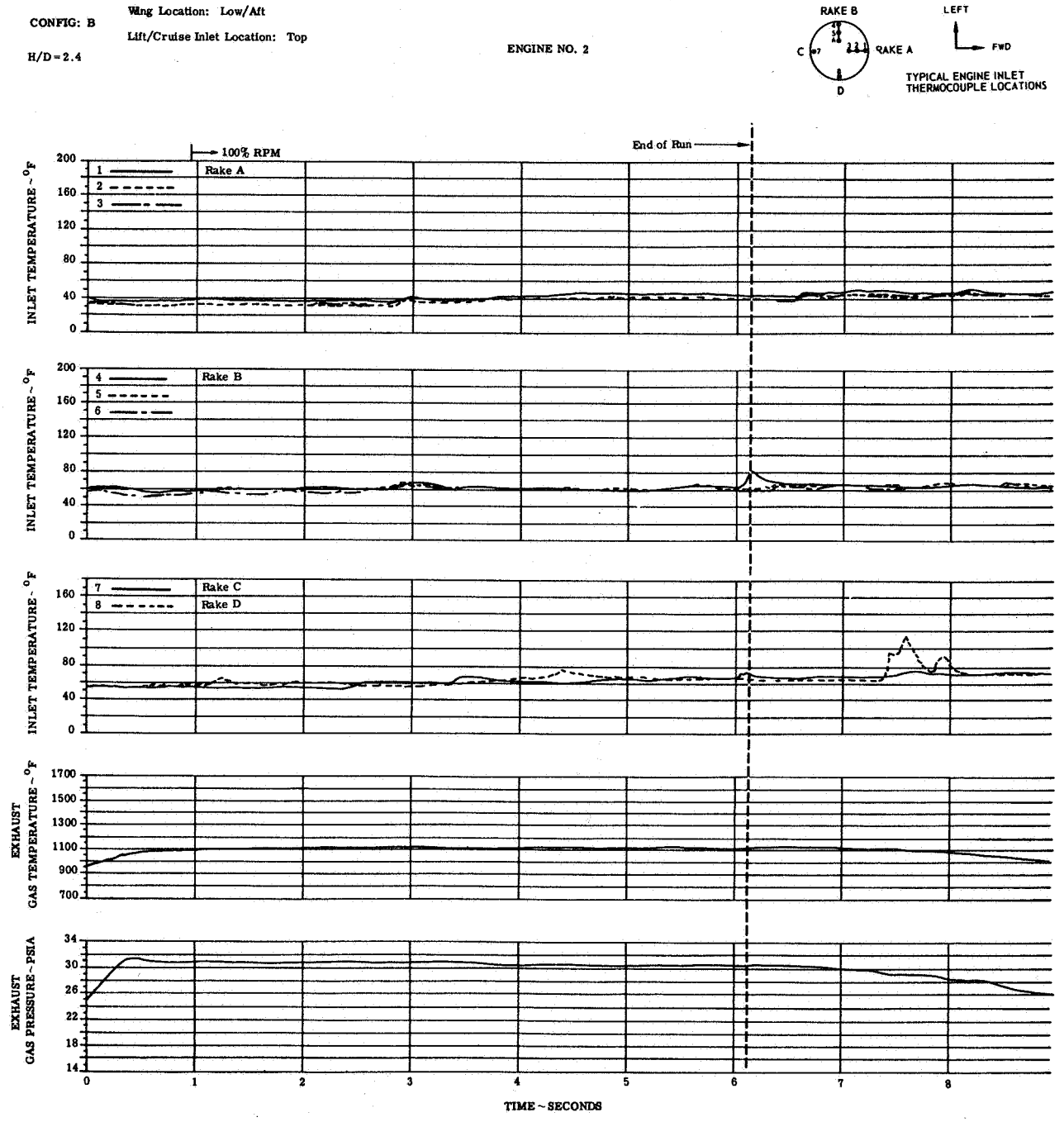

FIGURE 11(b). ENGINE TEMPERATURE AND PRESSURE TRANSIENTS

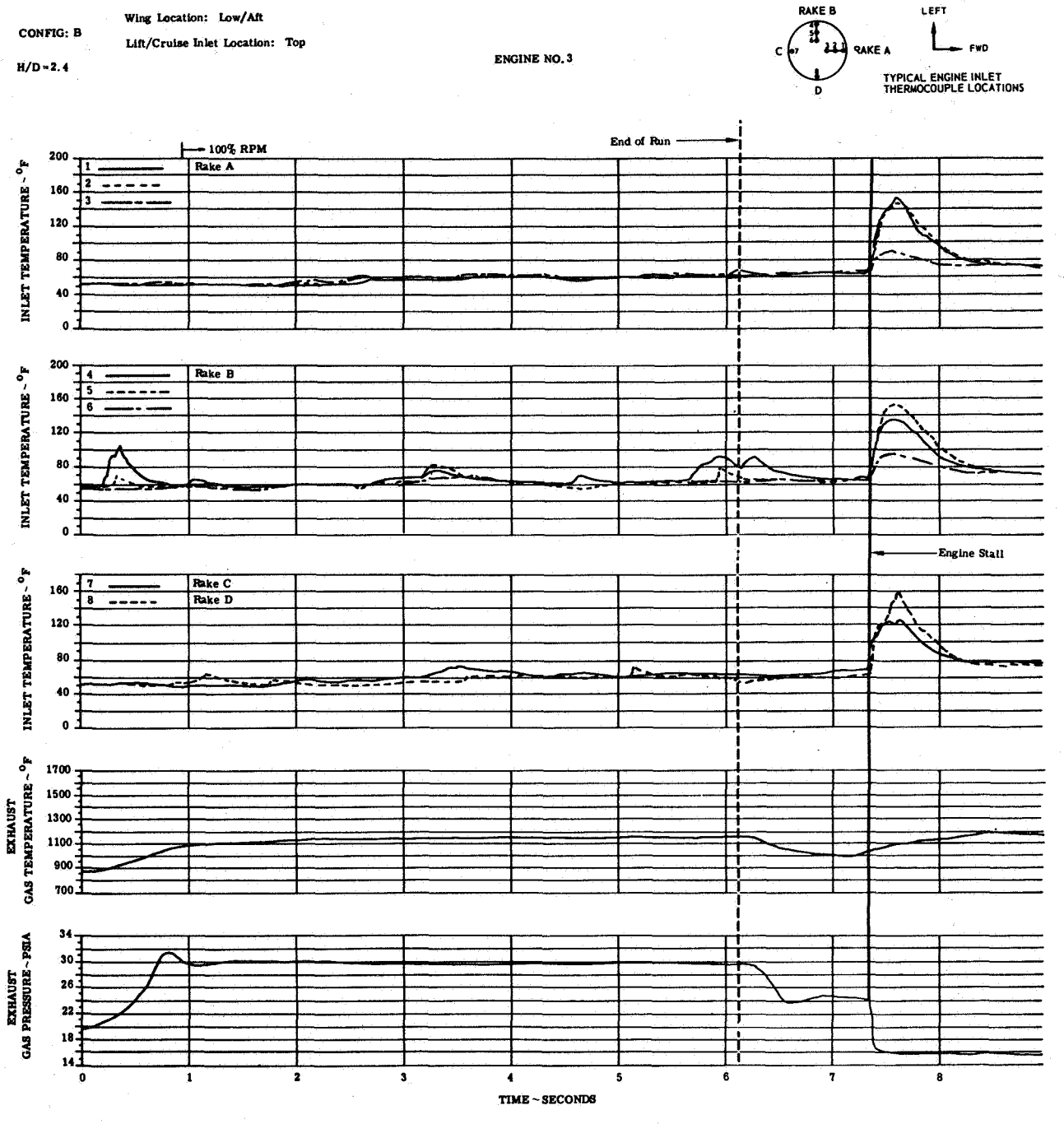

FIGURE 11(c). ENGINE TEMPERATURE AND PRESSURE TRANSIENTS

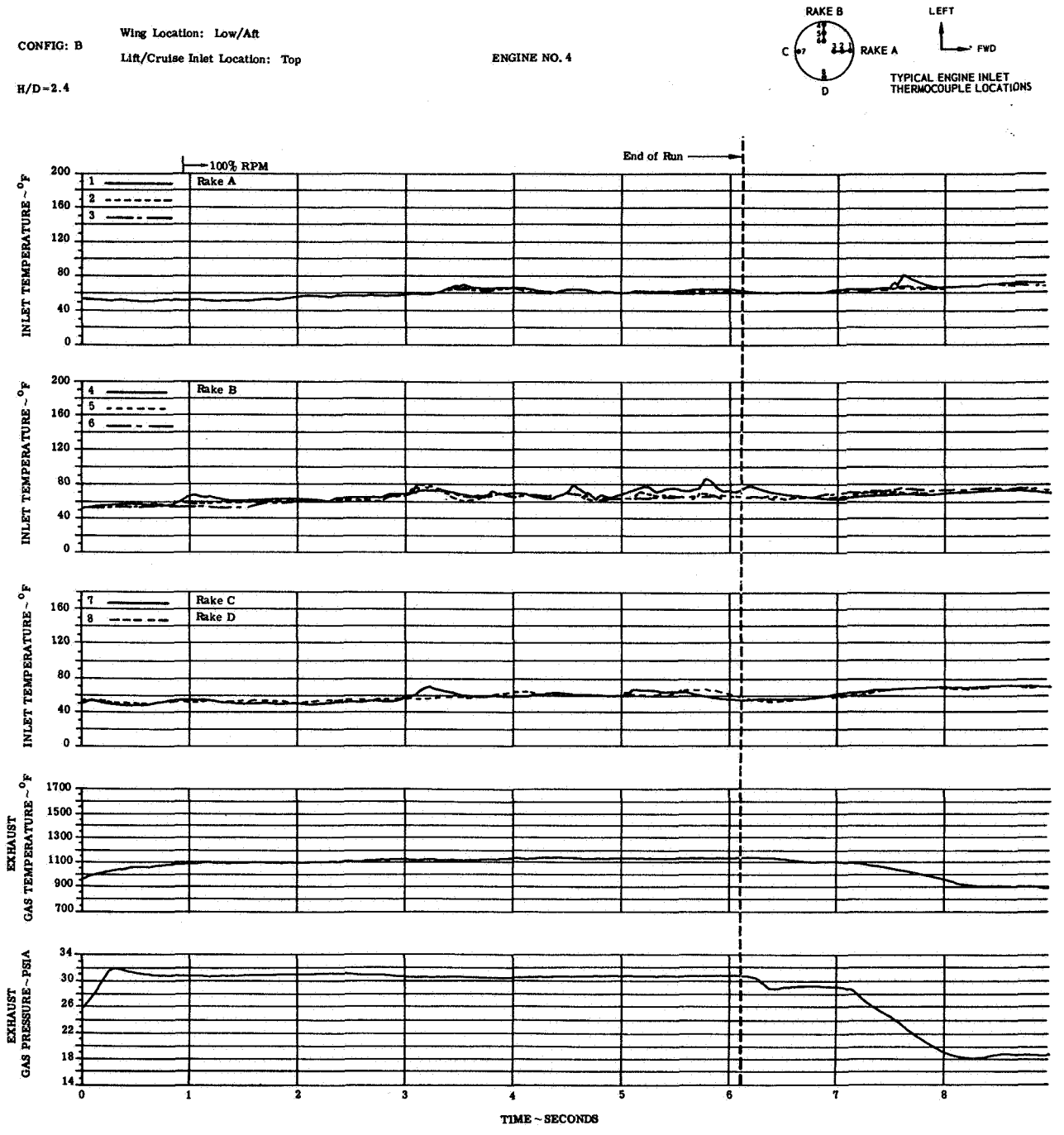

FIGURE 11(d). ENGINE TEMPERATURE AND PRESSURE TRANSIENTS

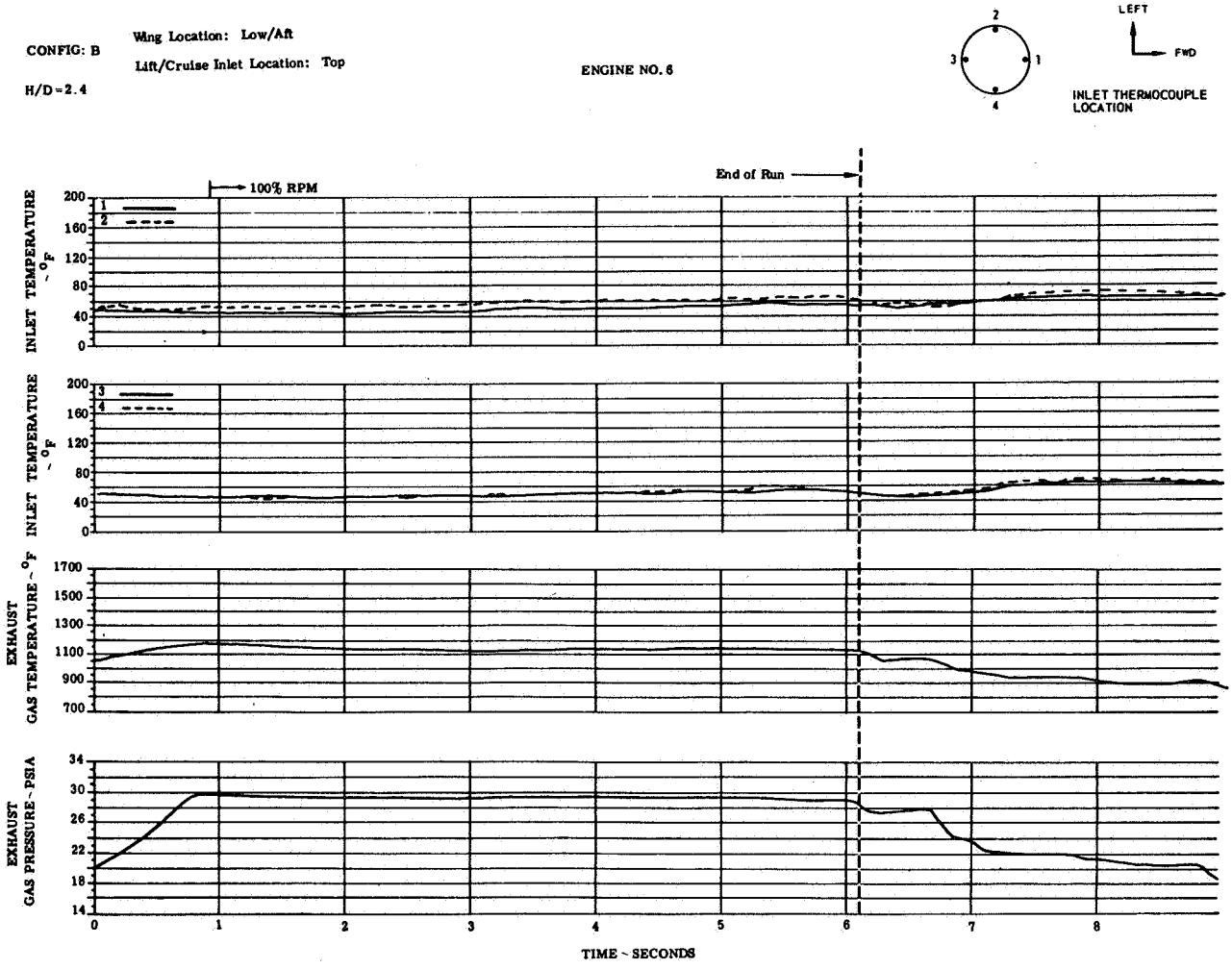

FIGURE 11(e). ENGINE TEMPERATURE AND PRESSURE TRANSIENTS

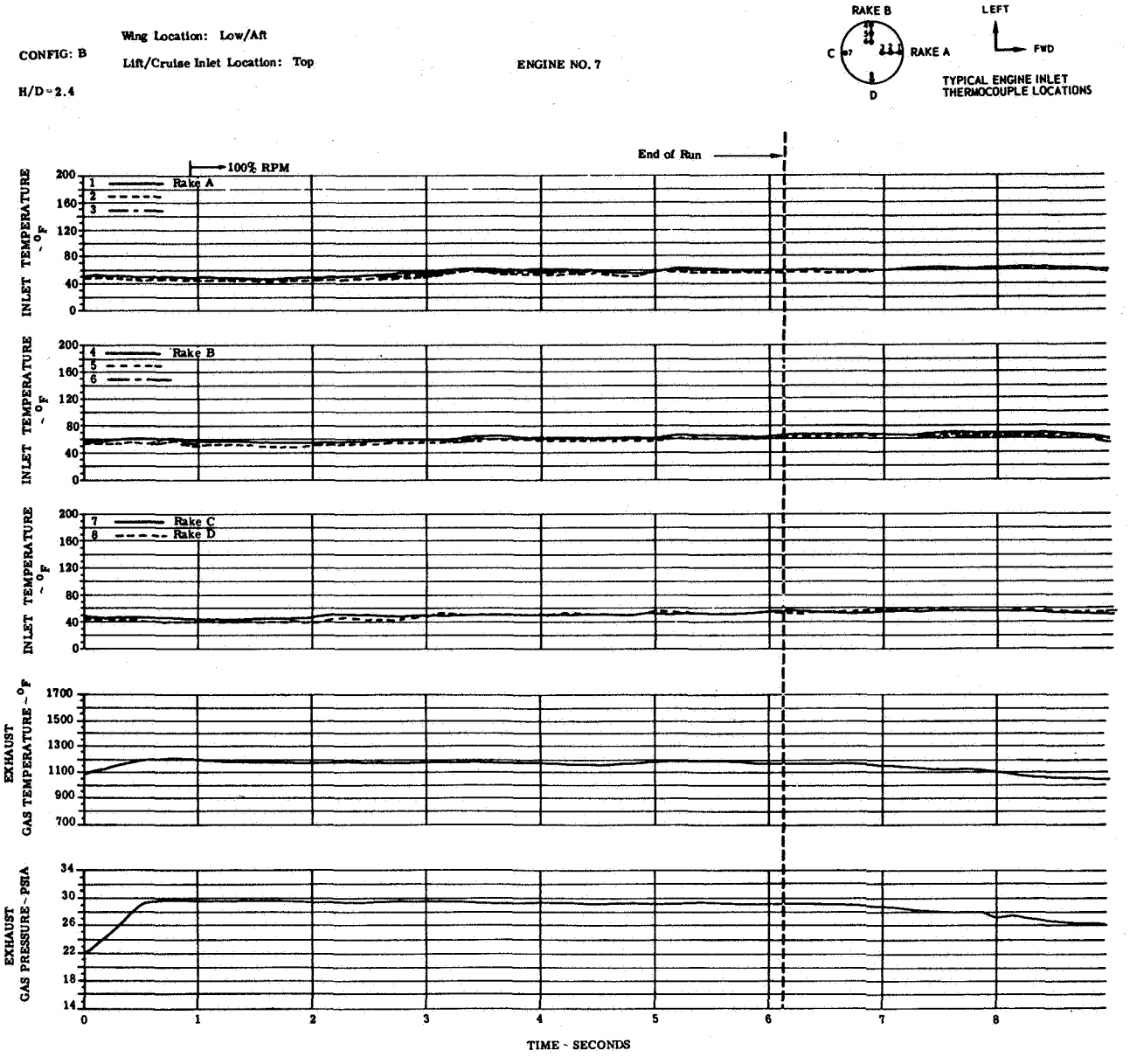

FIGURE 11(f). ENGINE TEMPERATURE AND PRESSURE TRANSIENTS

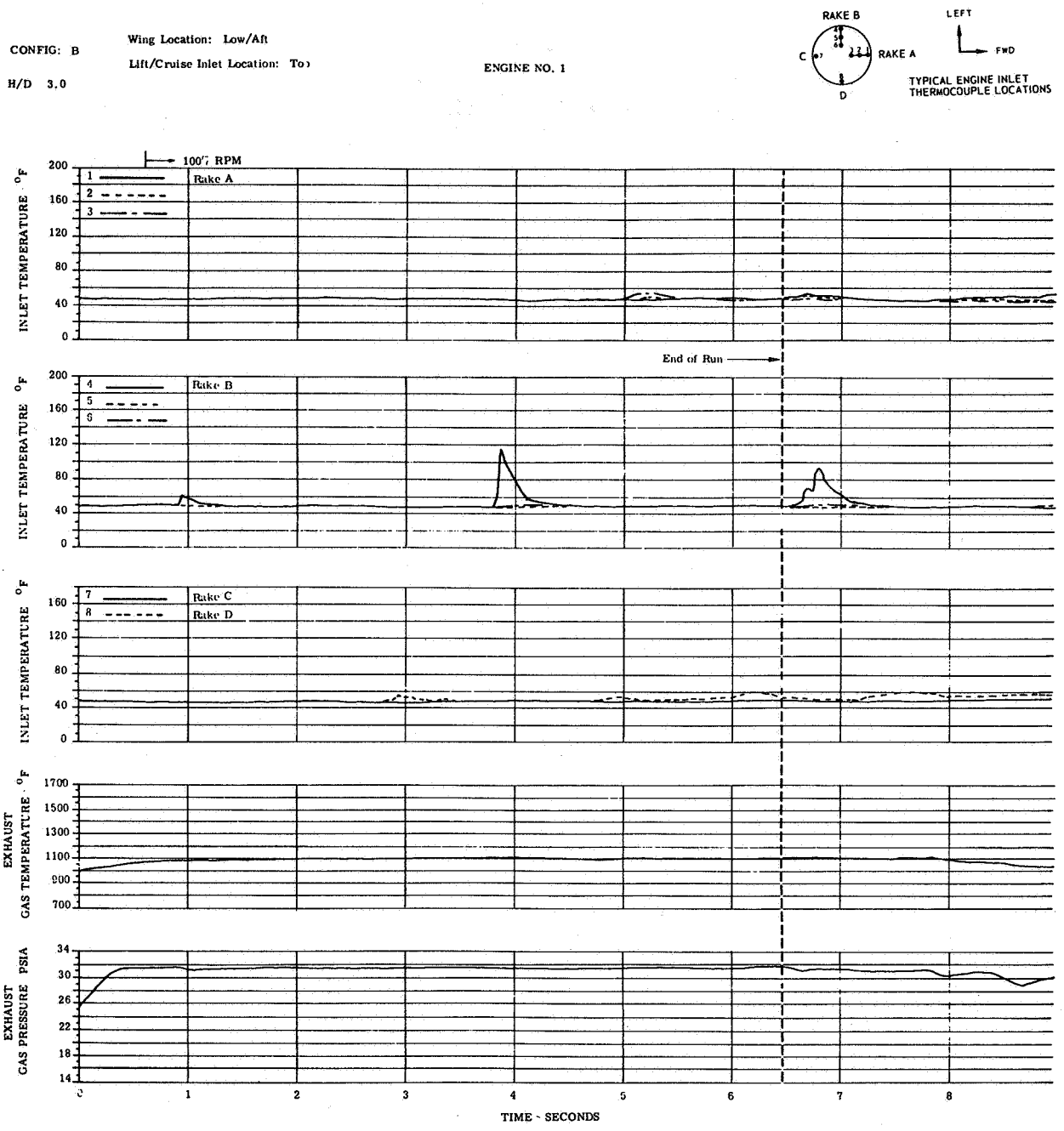

FIGURE 11(g). ENGINE TEMPERATURE AND PRESSURE TRANSIENTS

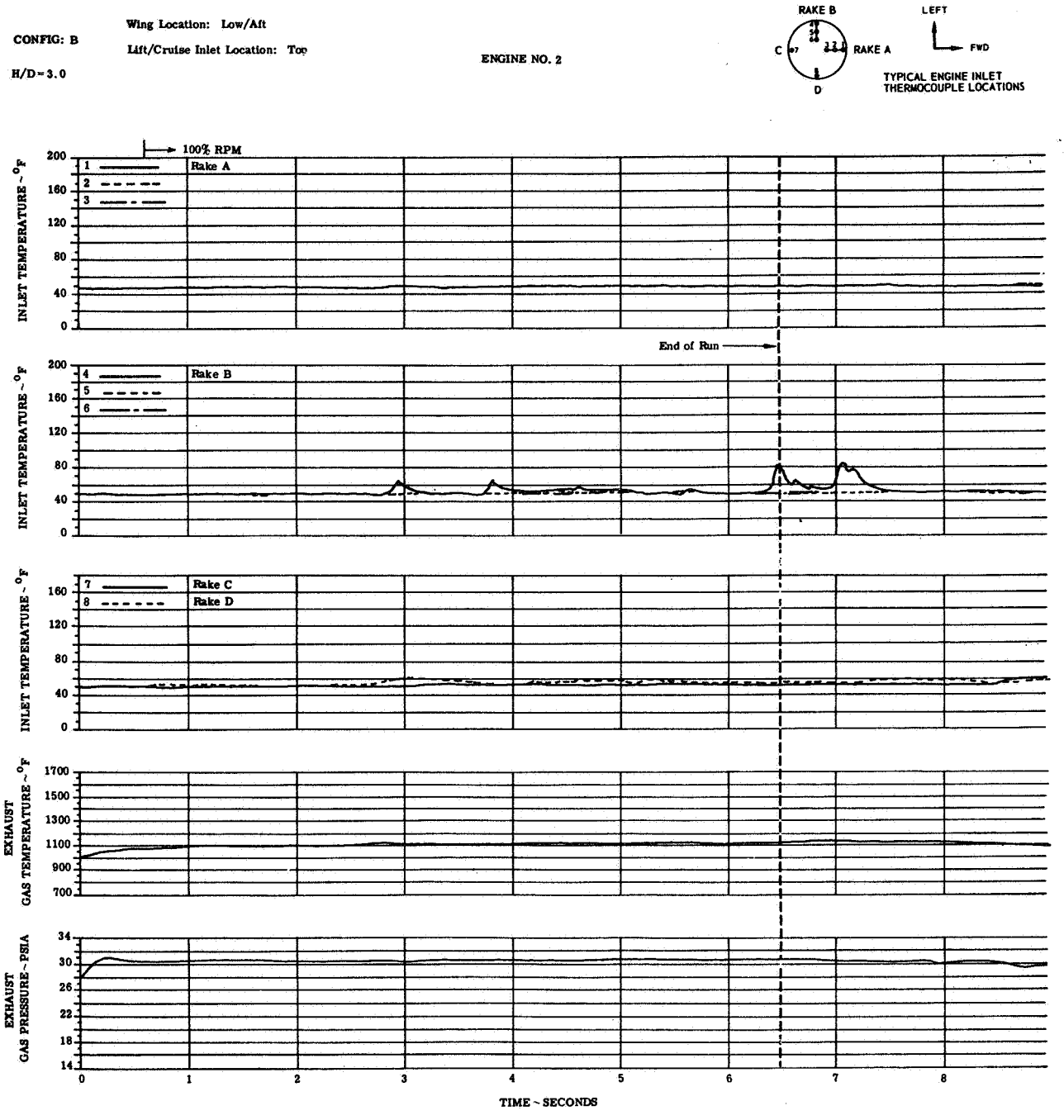

FIGURE 11(h). ENGINE TEMPERATURE AND PRESSURE TRANSIENTS

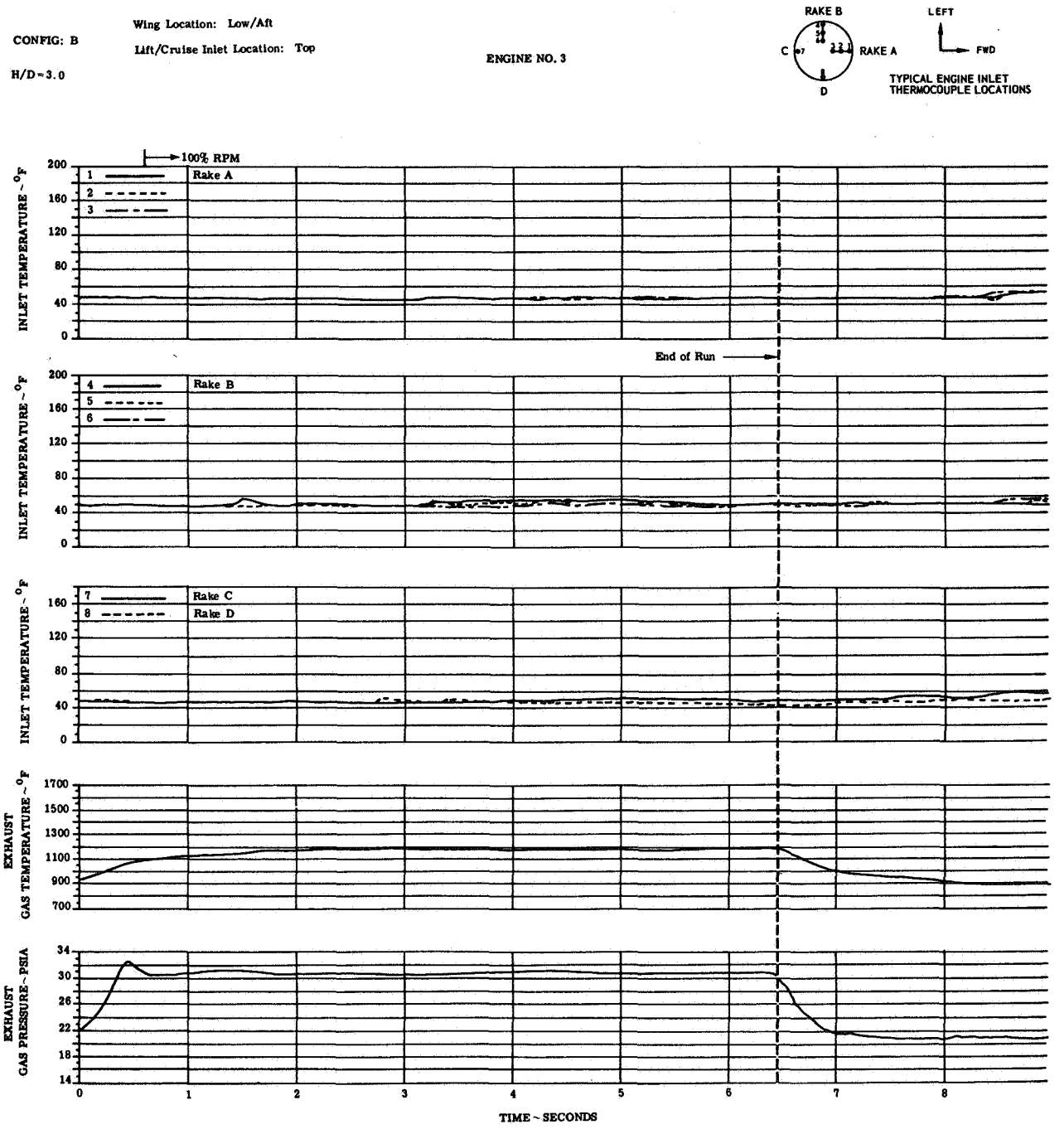

FIGURE 11(i). ENGINE TEMPERATURE AND PRESSURE TRANSIENTS

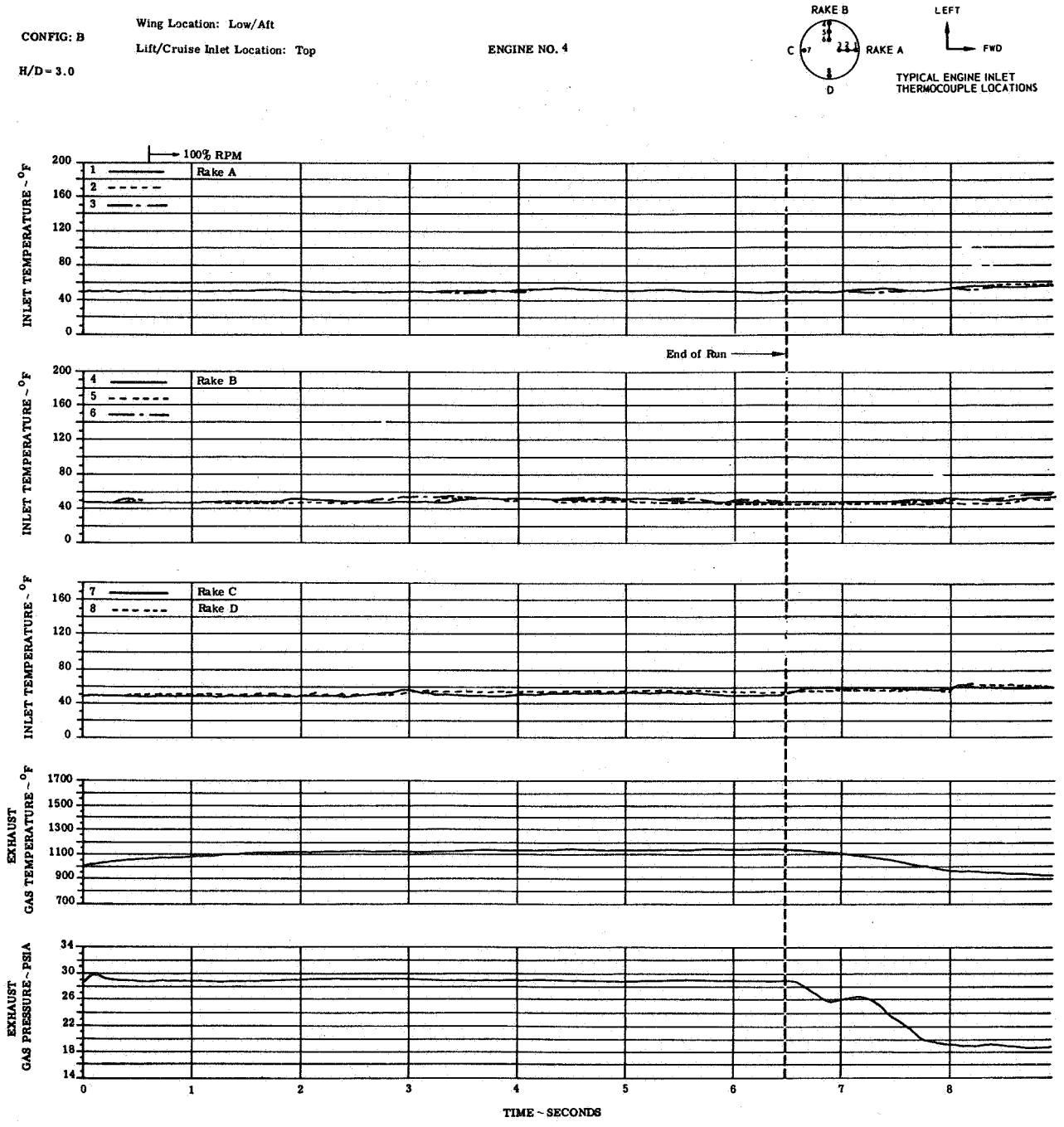

FIGURE 11(j). ENGINE TEMPERATURE AND PRESSURE TRANSIENTS

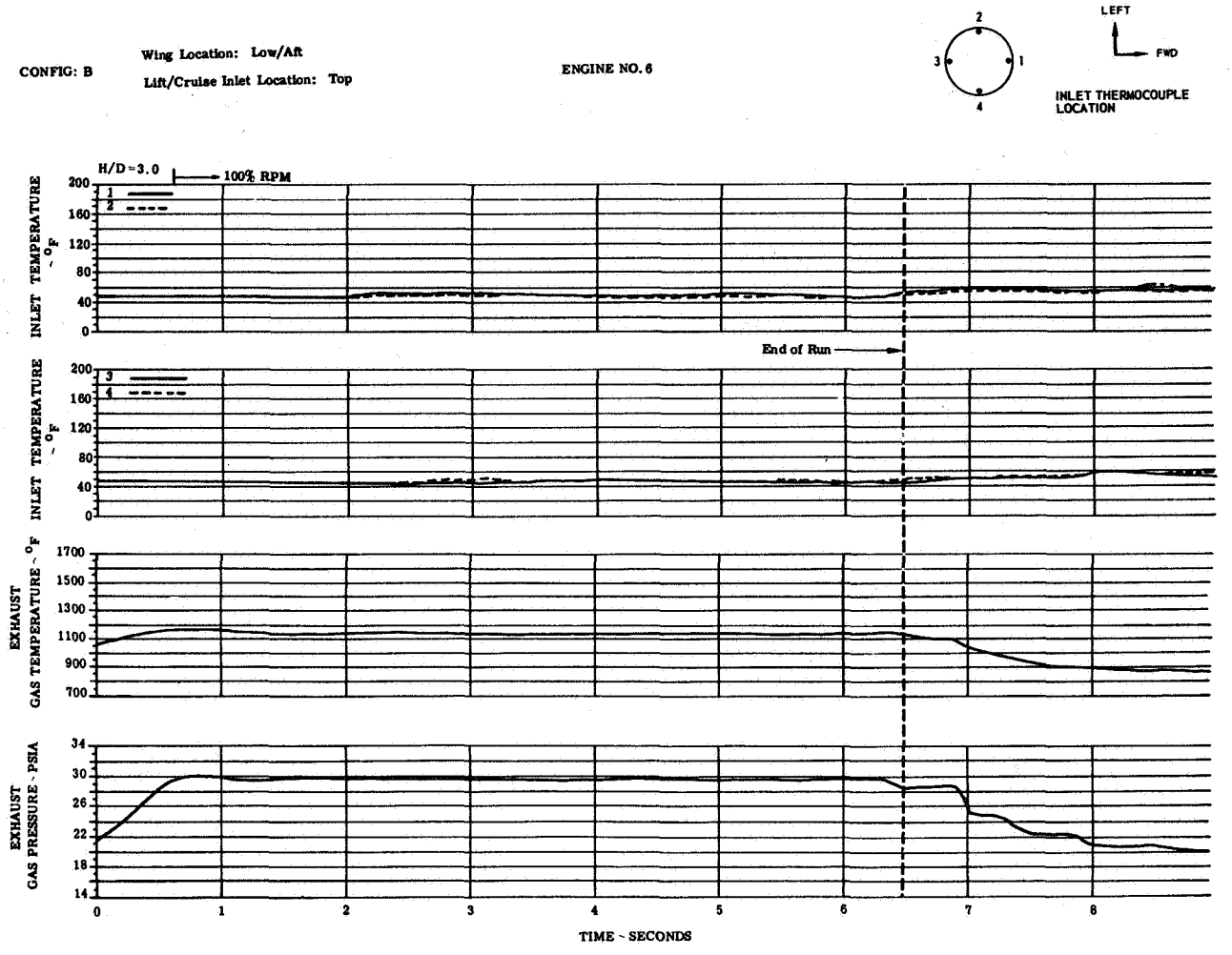

FIGURE 11(k). ENGINE TEMPERATURE AND PRESSURE TRANSIENTS

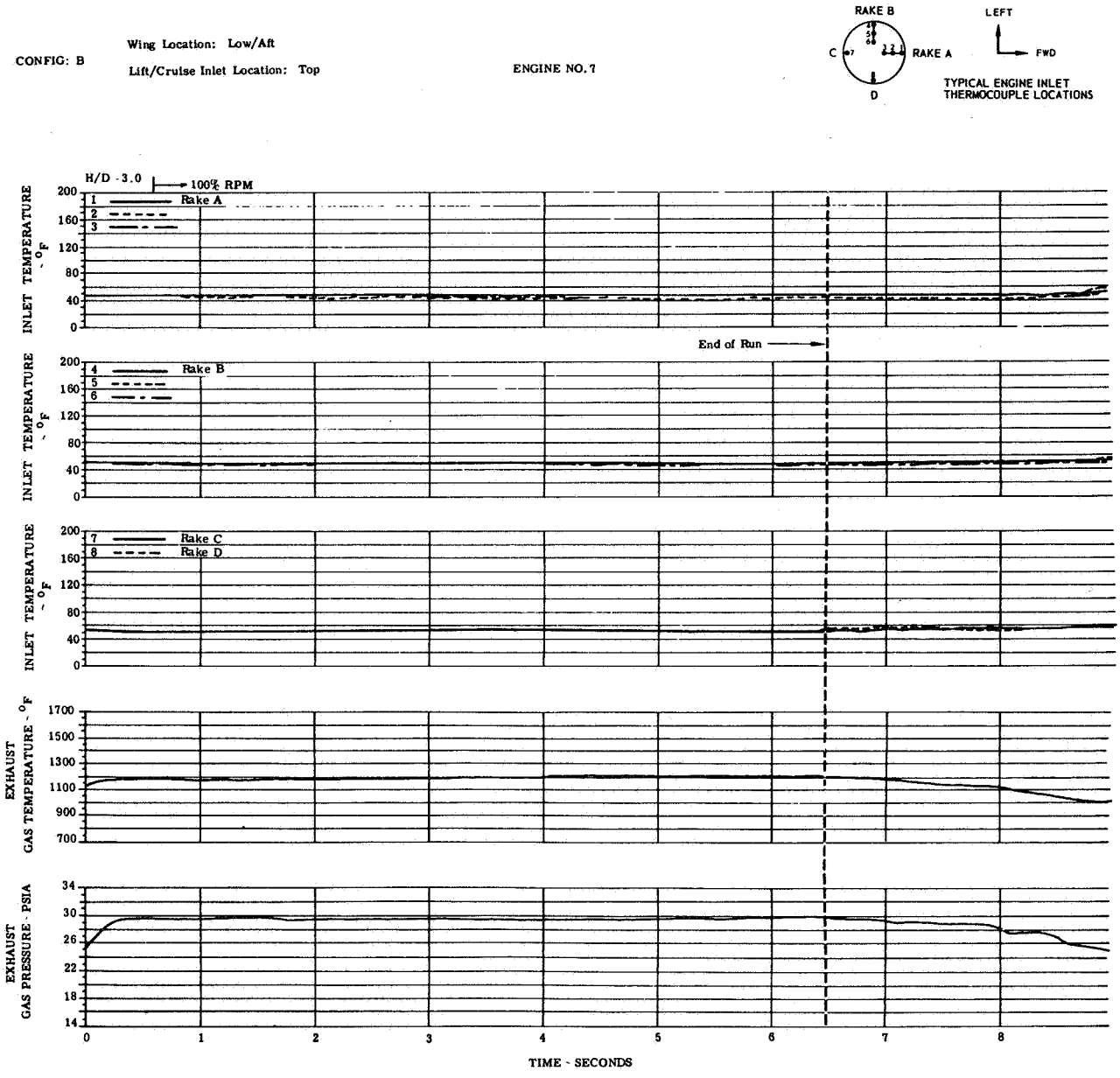

FIGURE 11(l). ENGINE TEMPERATURE AND PRESSURE TRANSIENTS

CONFIG: B

Wing Location: Low/Aft

Lift/Cruise Inlet Location: Top

H/D 4.5

ENGINE NO. 1

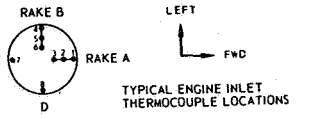

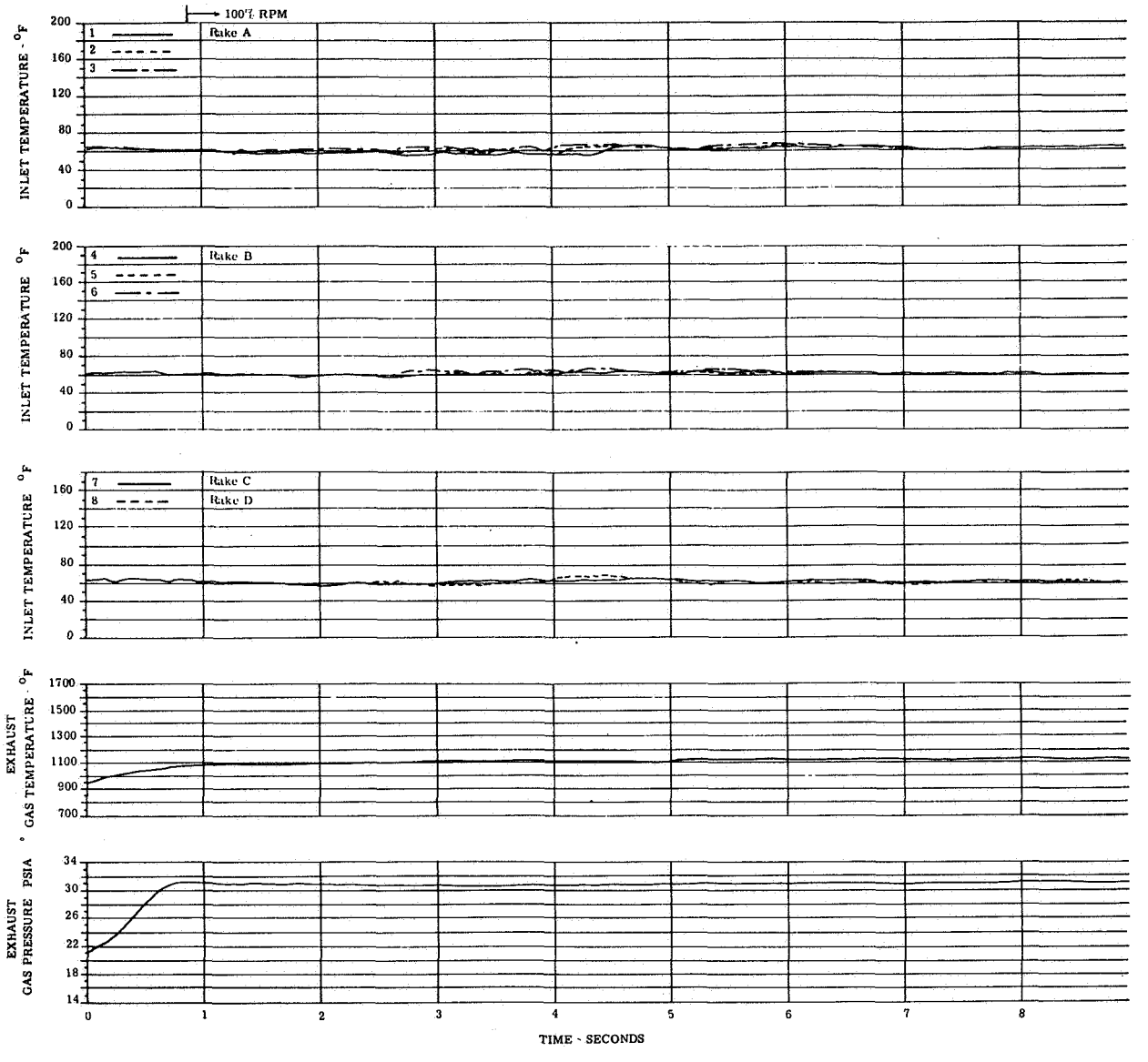

FIGURE 11(m). ENGINE TEMPERATURE AND PRESSURE TRANSIENTS

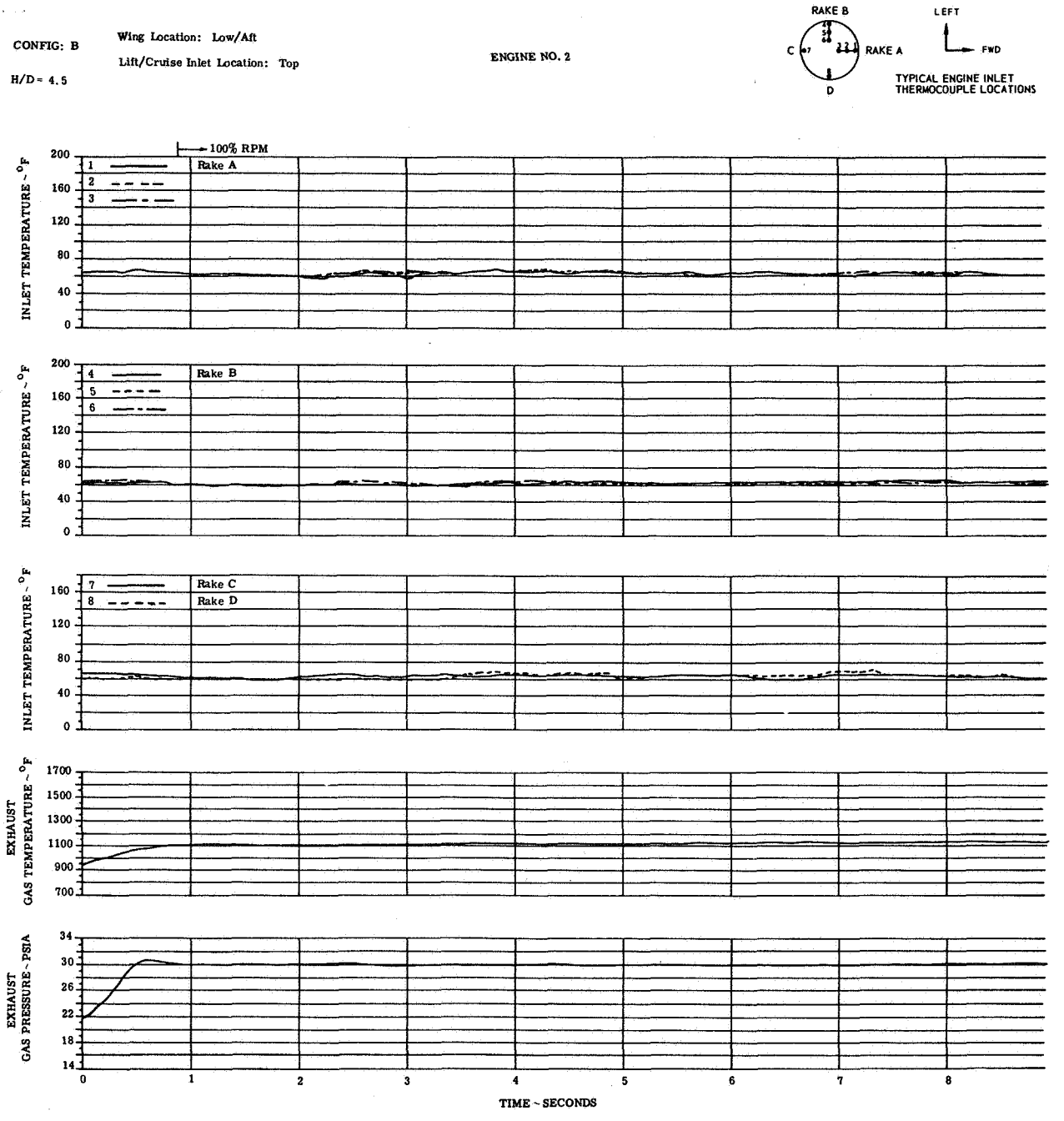

FIGURE 11(n). ENGINE TEMPERATURE AND PRESSURE TRANSIENTS

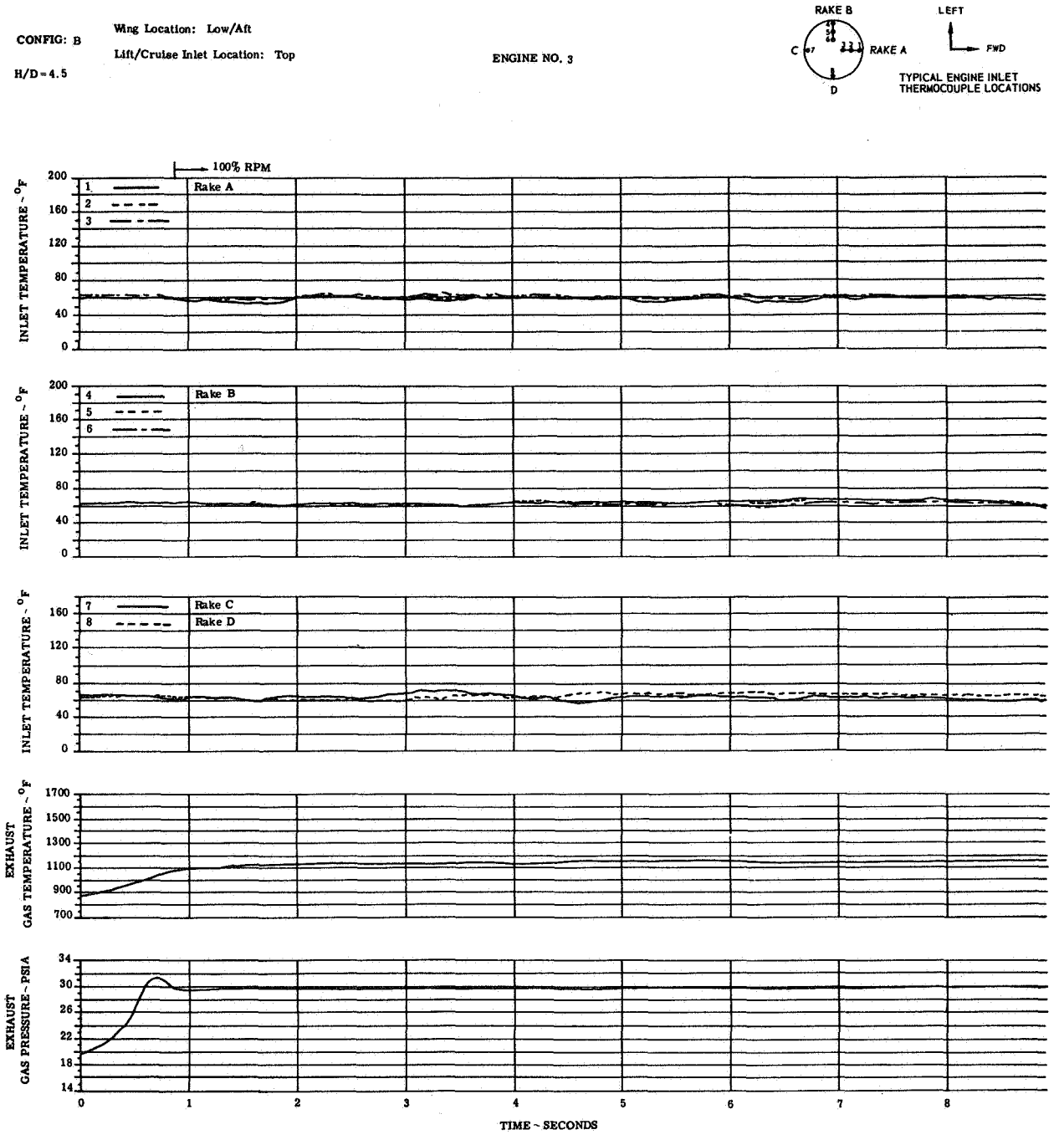

FIGURE 11(o). ENGINE TEMPERATURE AND PRESSURE TRANSIENTS

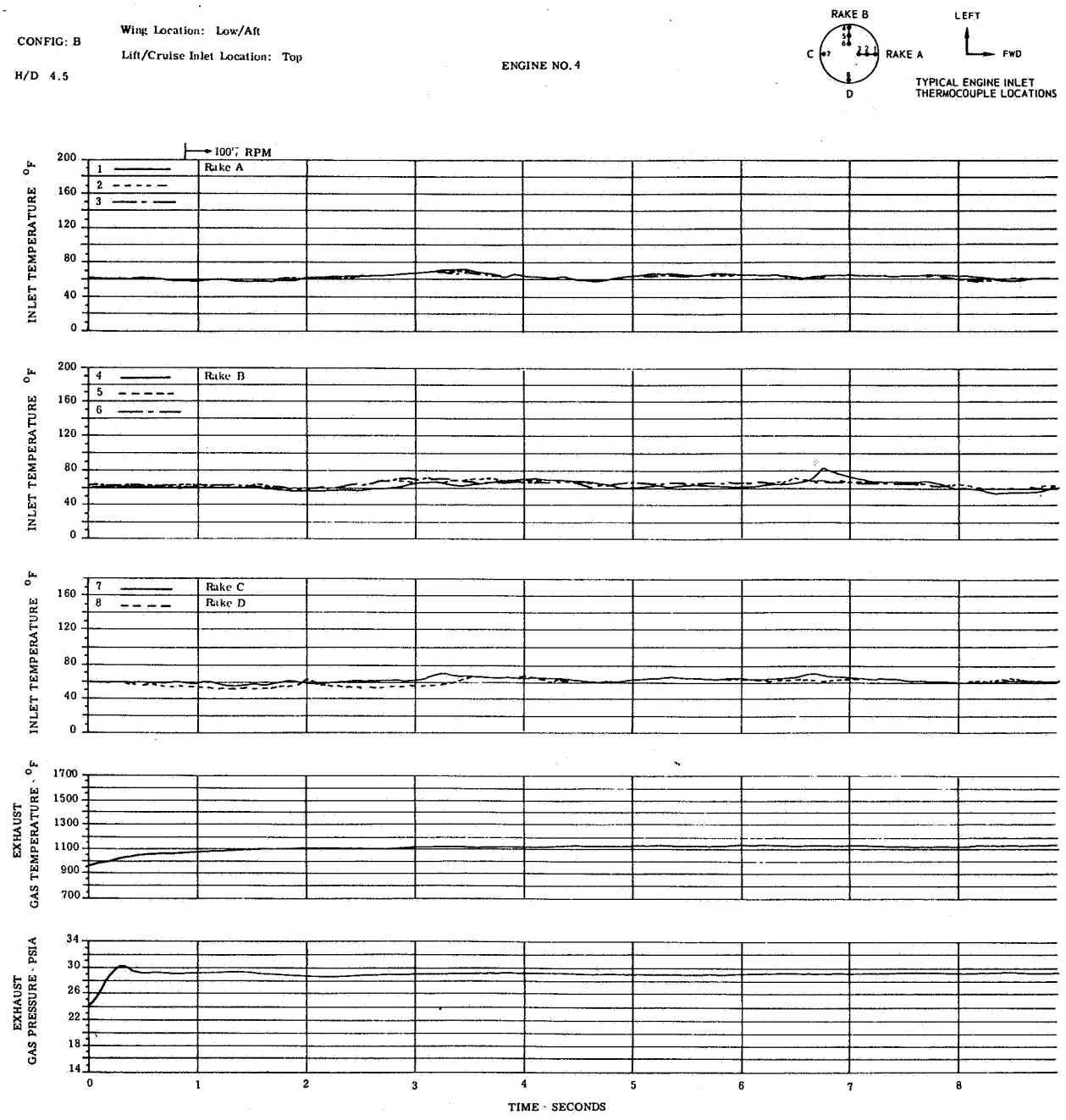

FIGURE 11(p). ENGINE TEMPERATURE AND PRESSURE TRANSIENTS

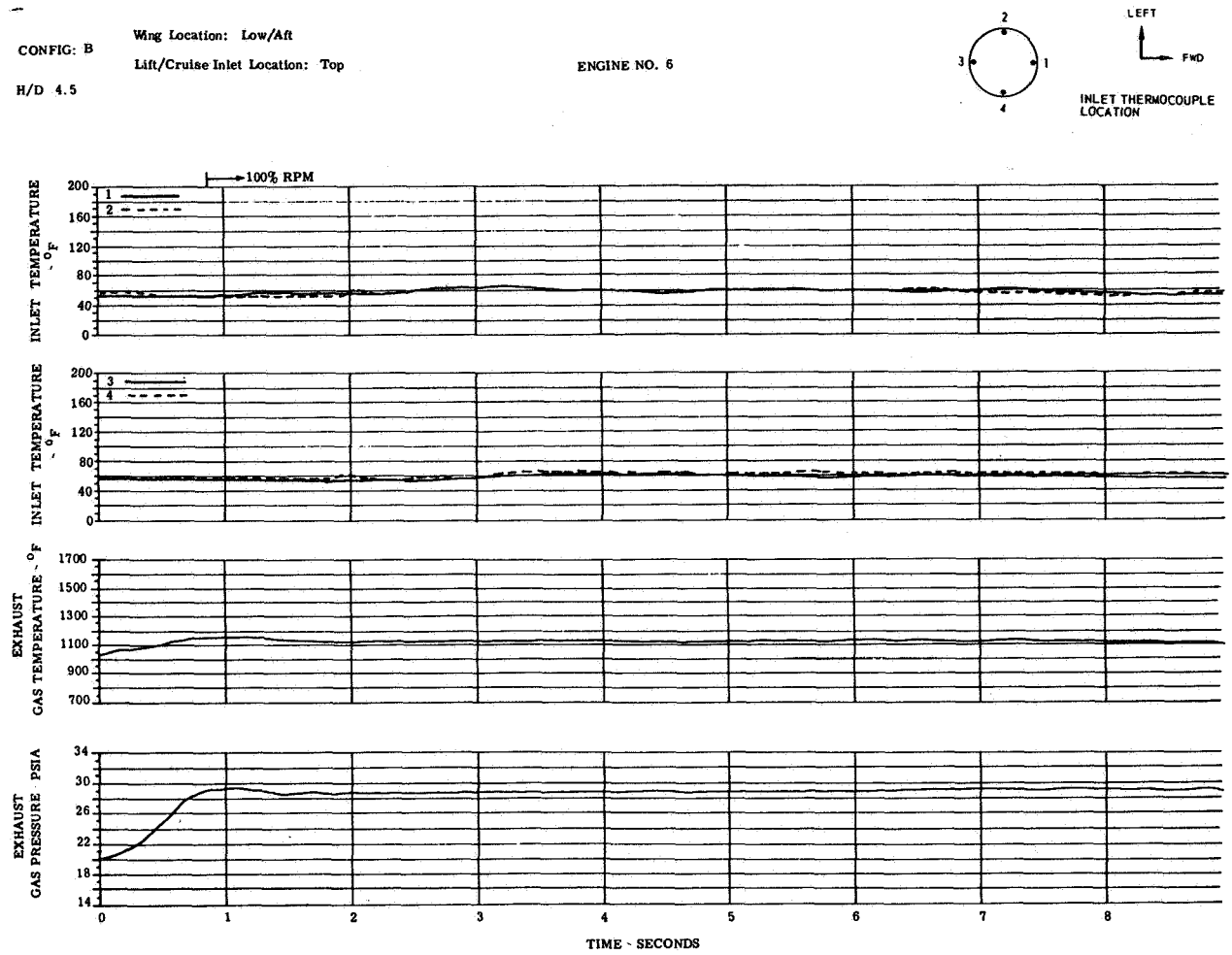

FIGURE 11(q). ENGINE TEMPERATURE AND PRESSURE TRANSIENTS

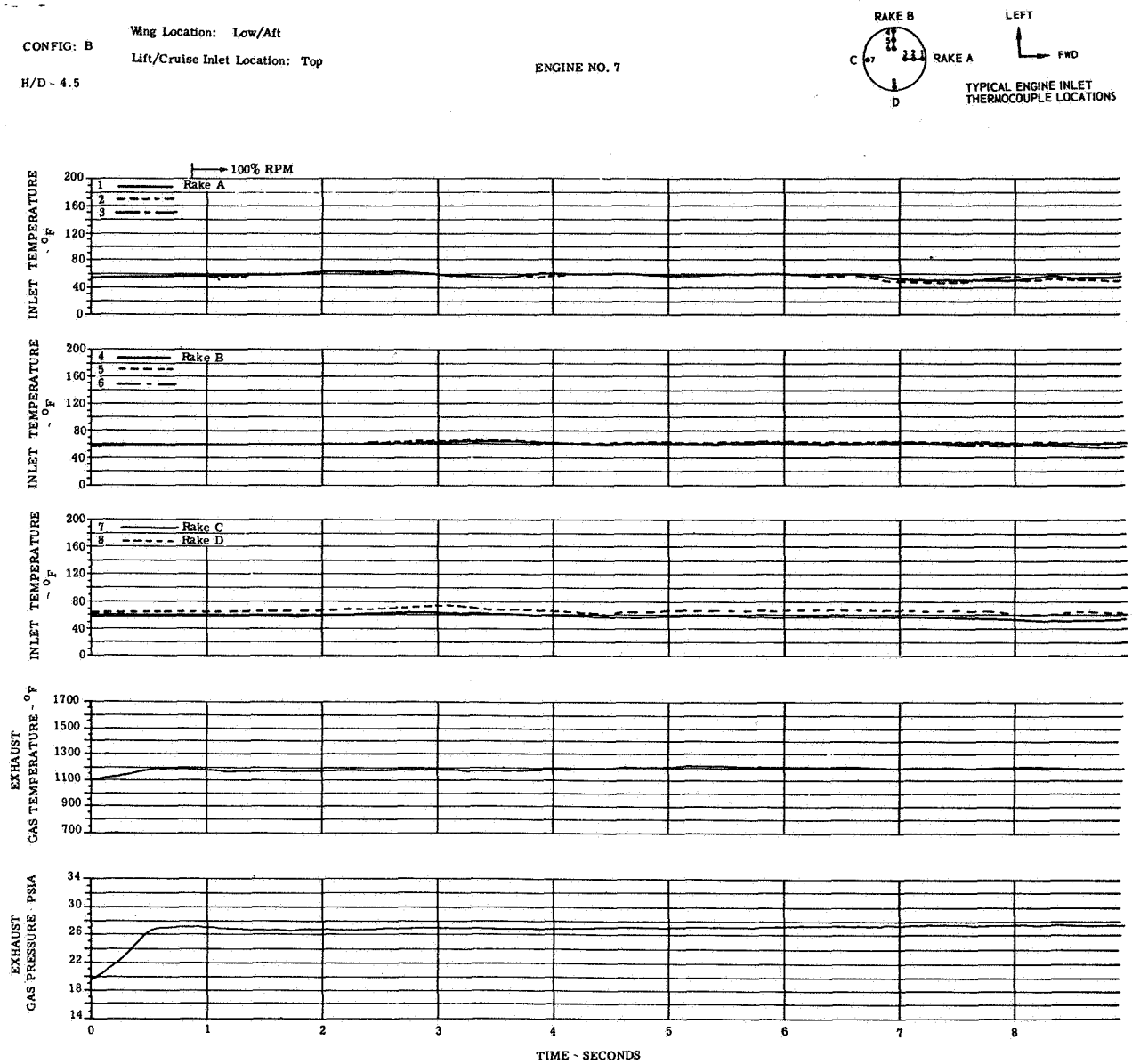

FIGURE 11(r). ENGINE TEMPERATURE AND PRESSURE TRANSIENTS

CONFIG: B

Wing Location: Low/Aft

Lift/Cruise Inlet Location: Top

H/D=6.5

ENGINE NO. 1

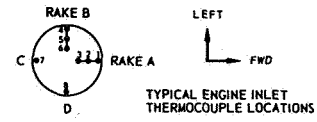

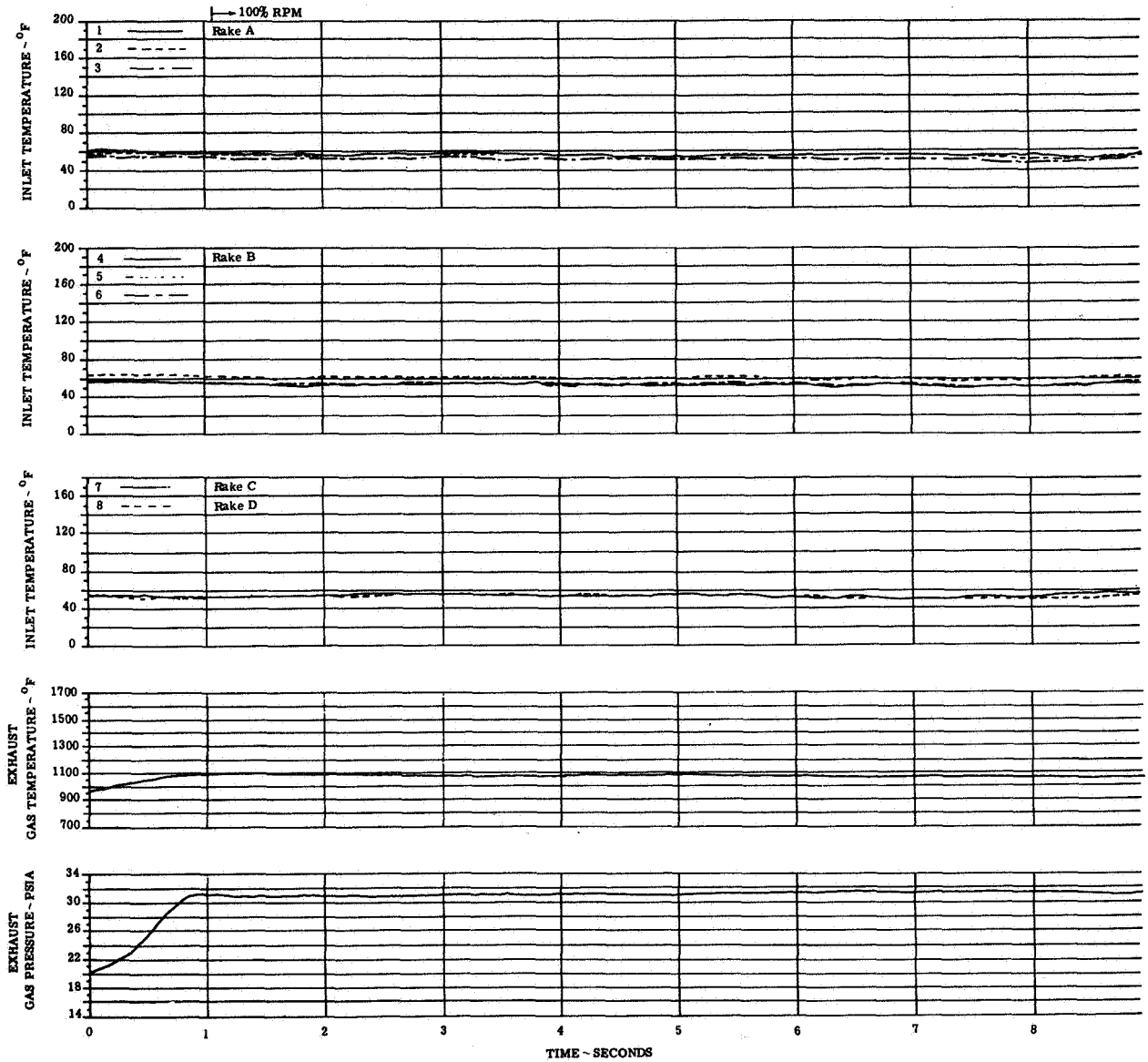

FIGURE 11(s). ENGINE TEMPERATURE AND PRESSURE TRANSIENTS

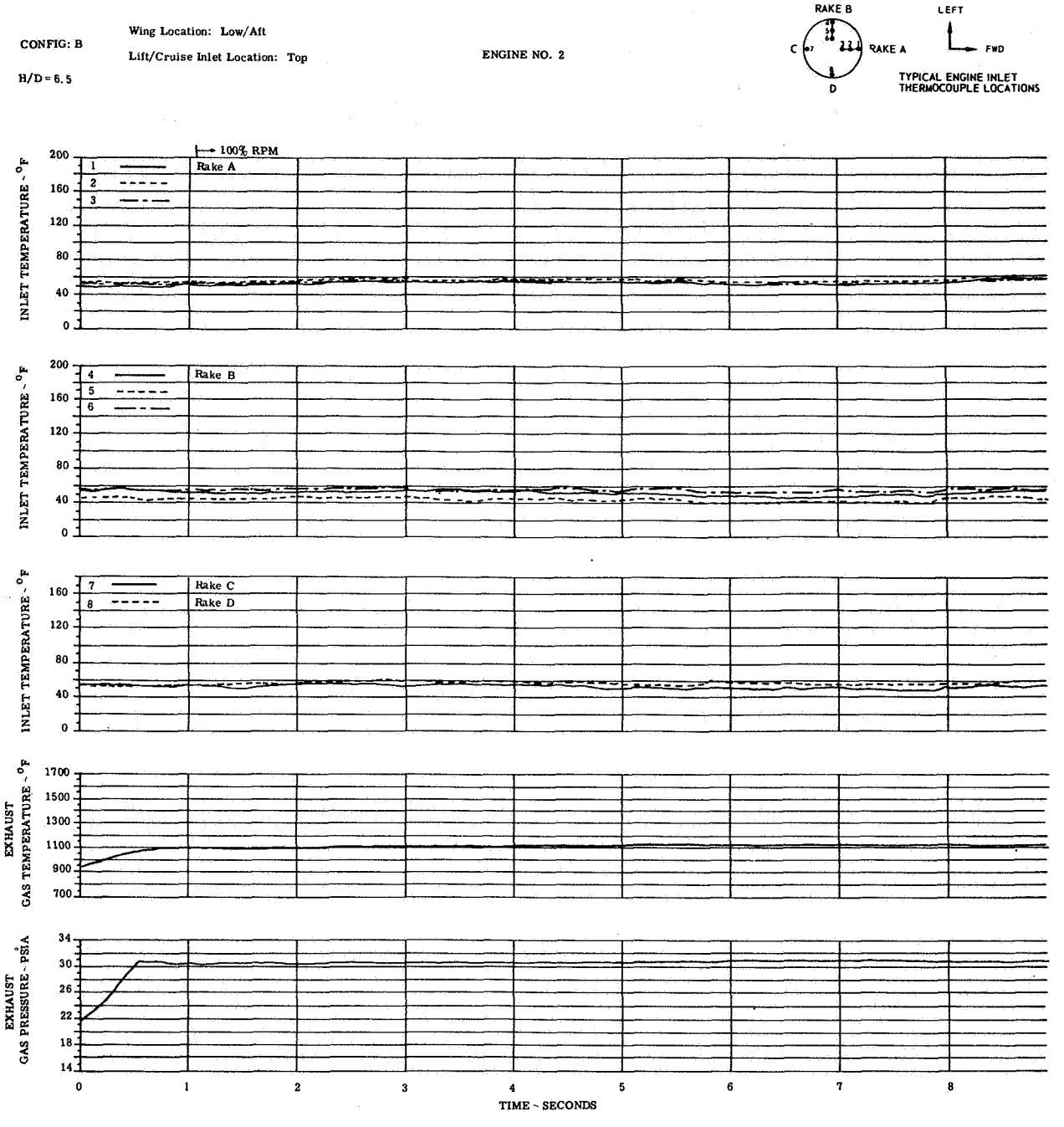

FIGURE 11(t). ENGINE TEMPERATURE AND PRESSURE TRANSIENTS

CONFIG: B

Wing Location: Low/Aft

Lift/Cruise Inlet Location: Top

ENGINE NO. 3

H/D = 6.5

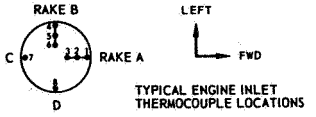

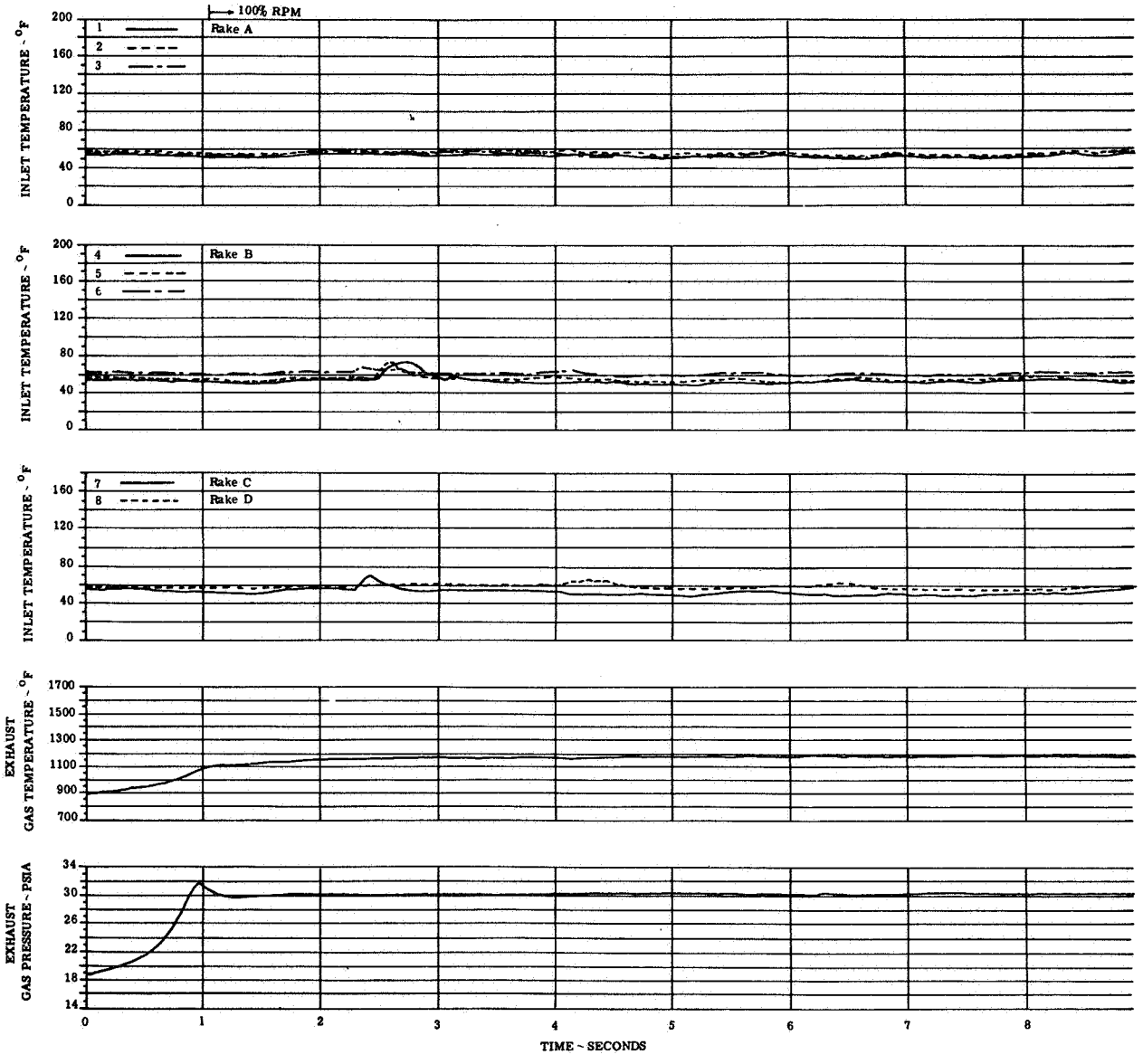

FIGURE 11(u). ENGINE TEMPERATURE AND PRESSURE TRANSIENTS

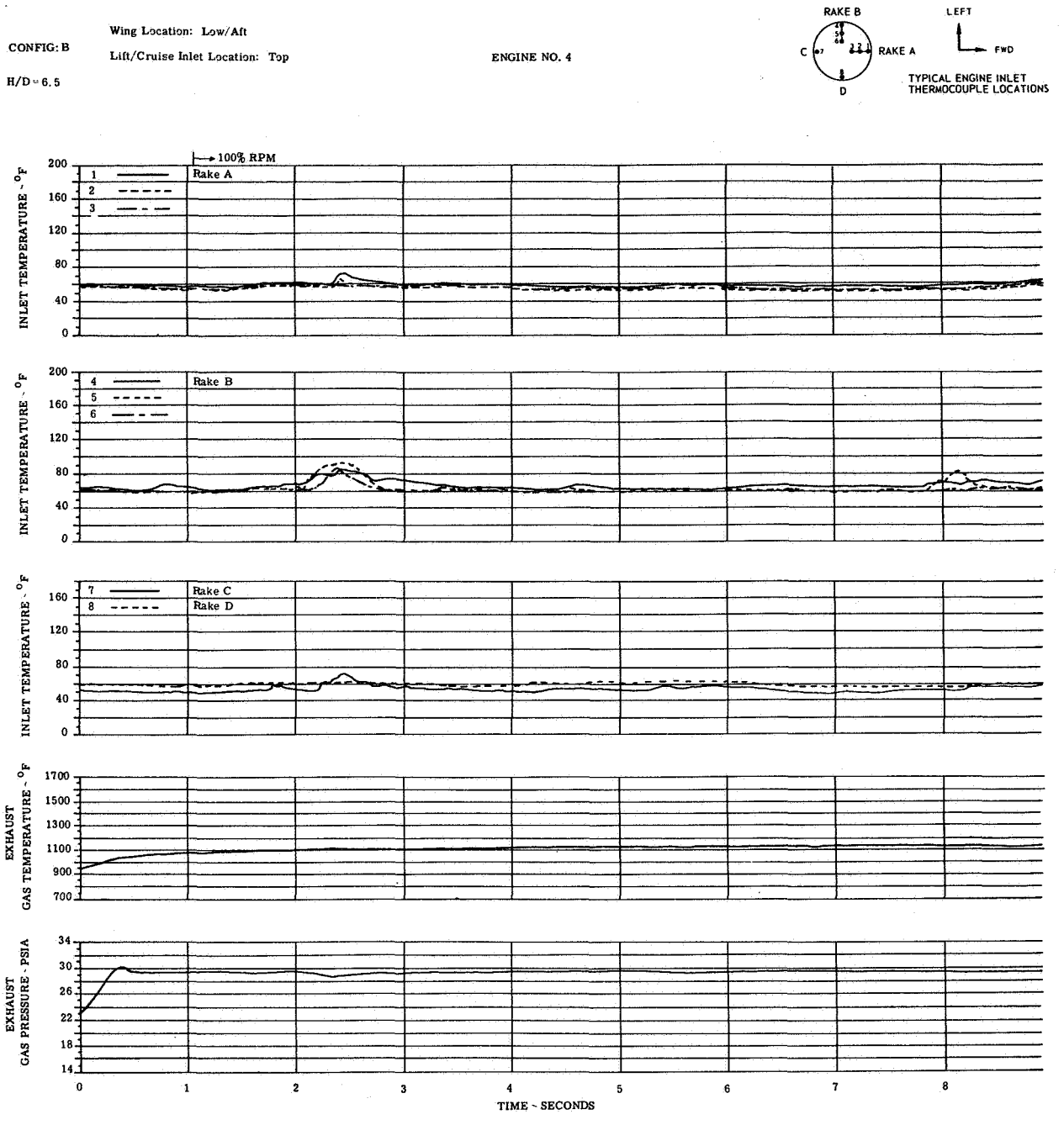

FIGURE 11(v). ENGINE TEMPERATURE AND PRESSURE TRANSIENTS

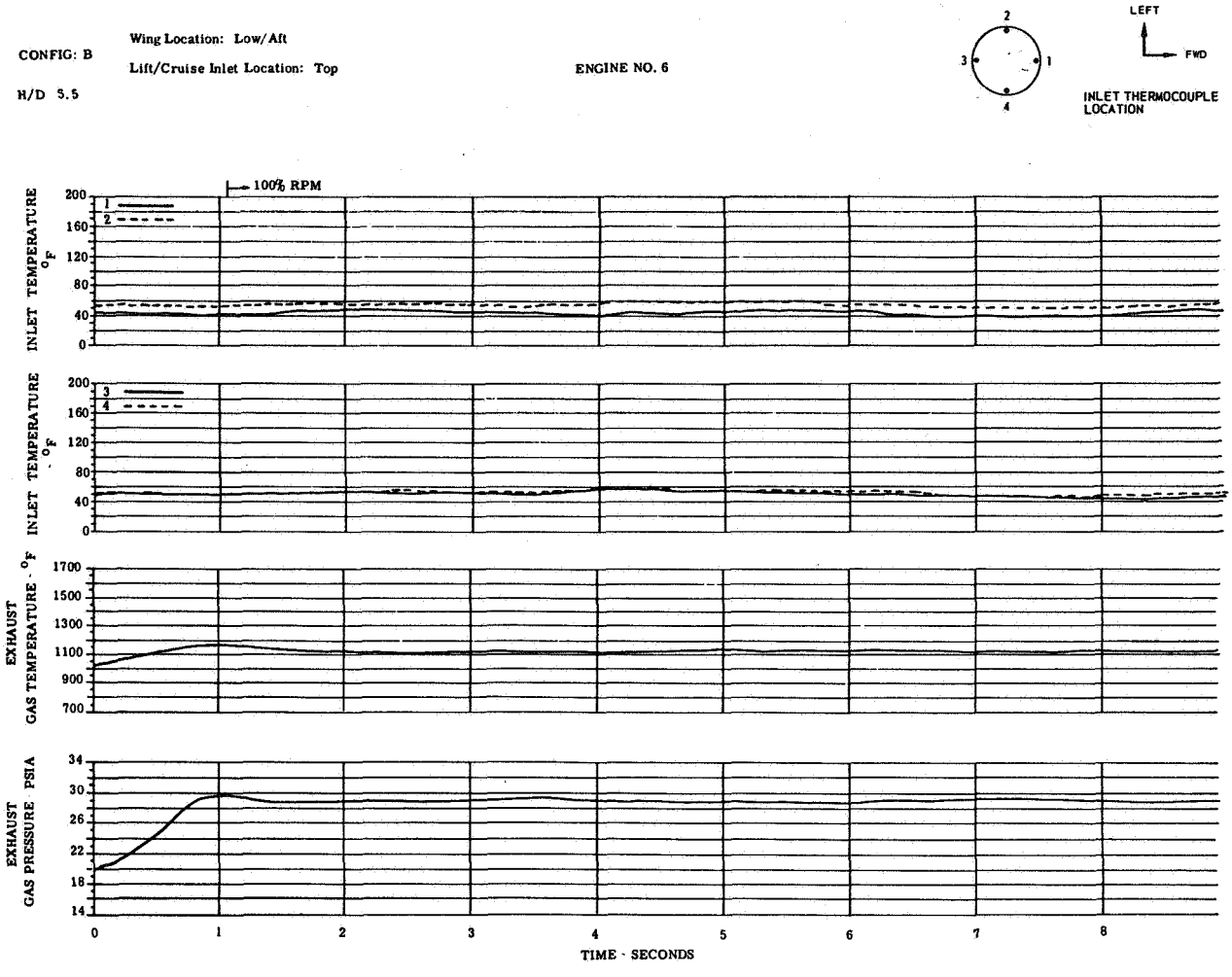

FIGURE 11(w). ENGINE TEMPERATURE AND PRESSURE TRANSIENTS

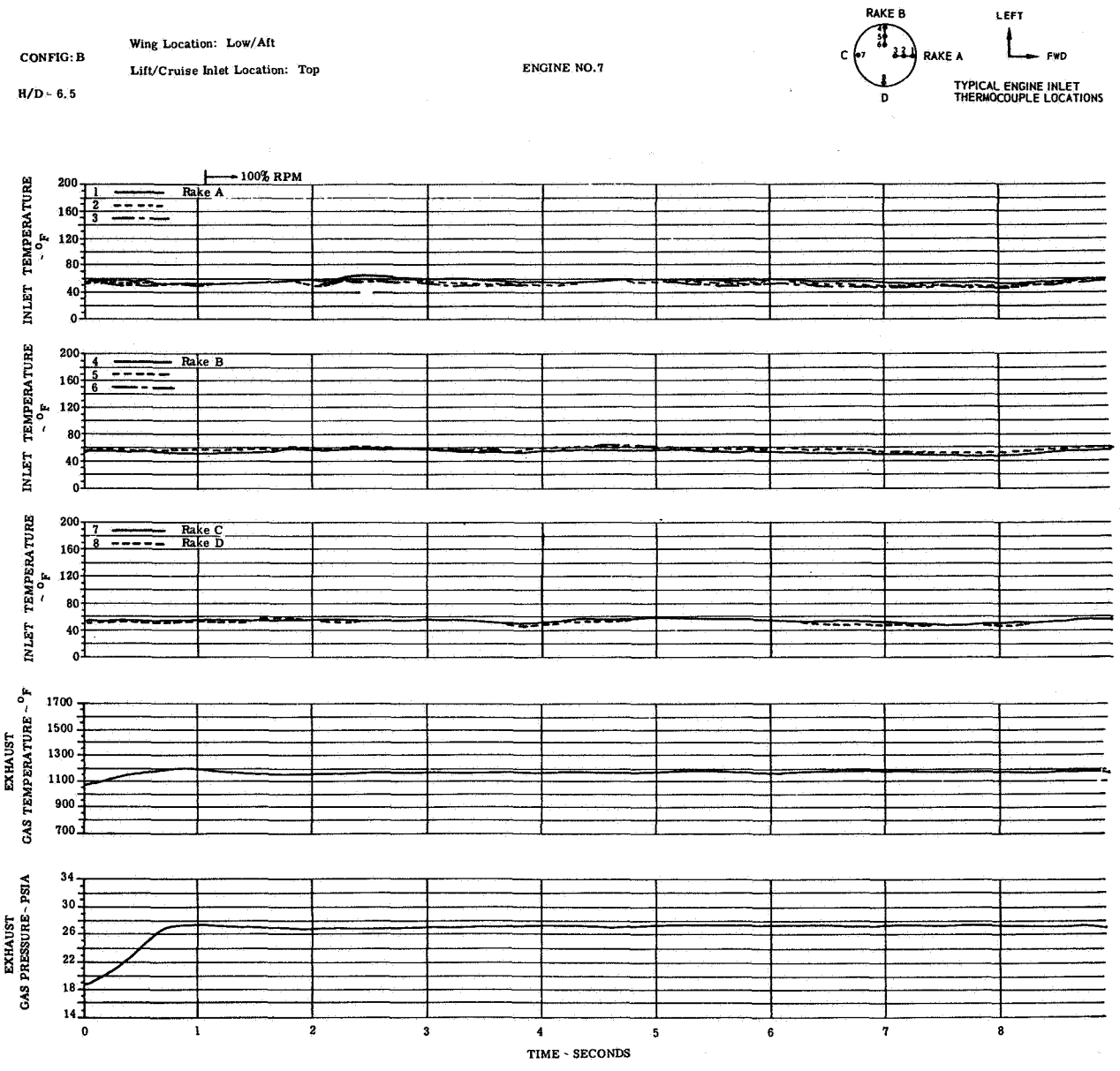

FIGURE 11(x). ENGINE TEMPERATURE AND PRESSURE TRANSIENTS

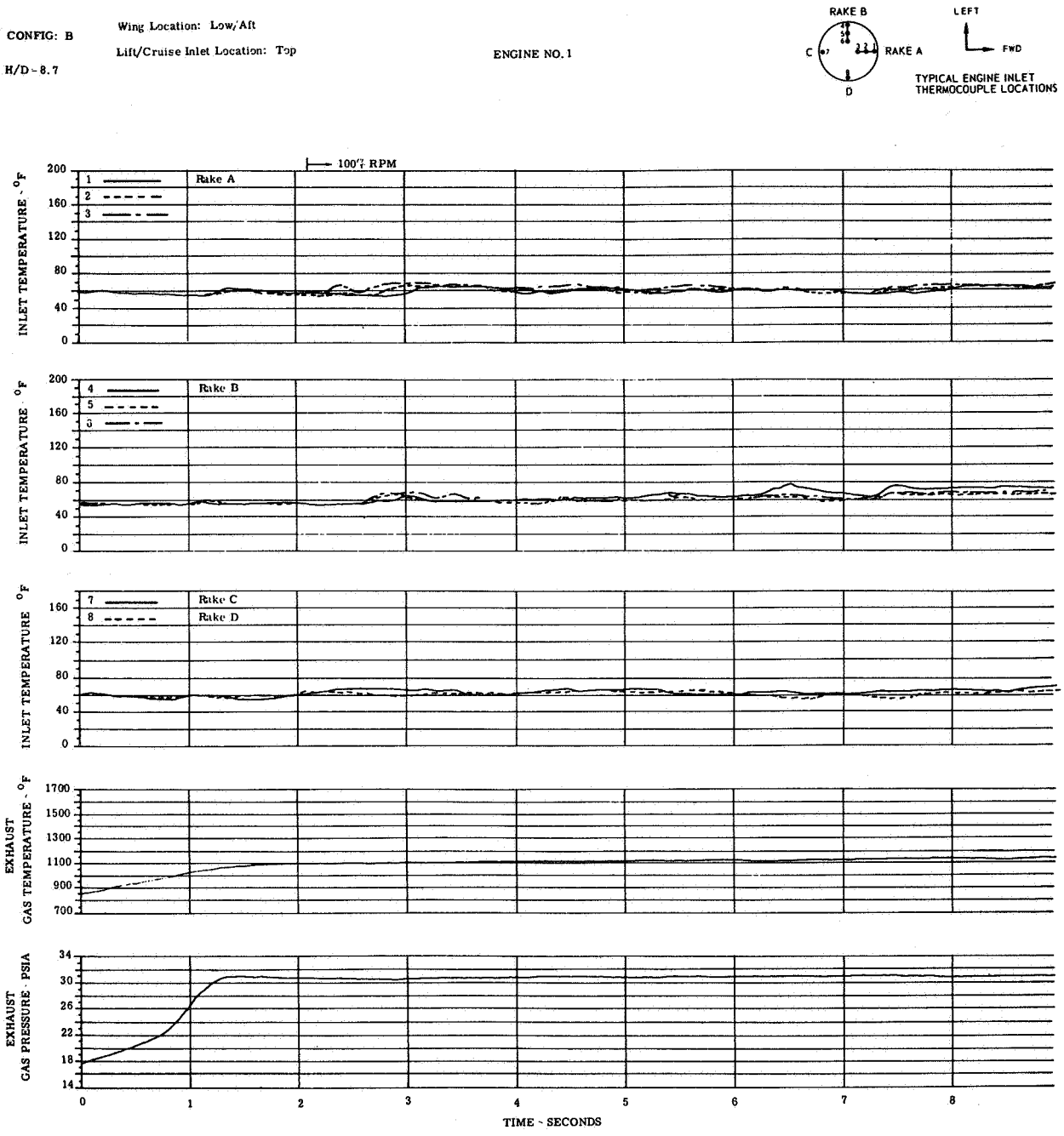

FIGURE 11(y). ENGINE TEMPERATURE AND PRESSURE TRANSIENTS

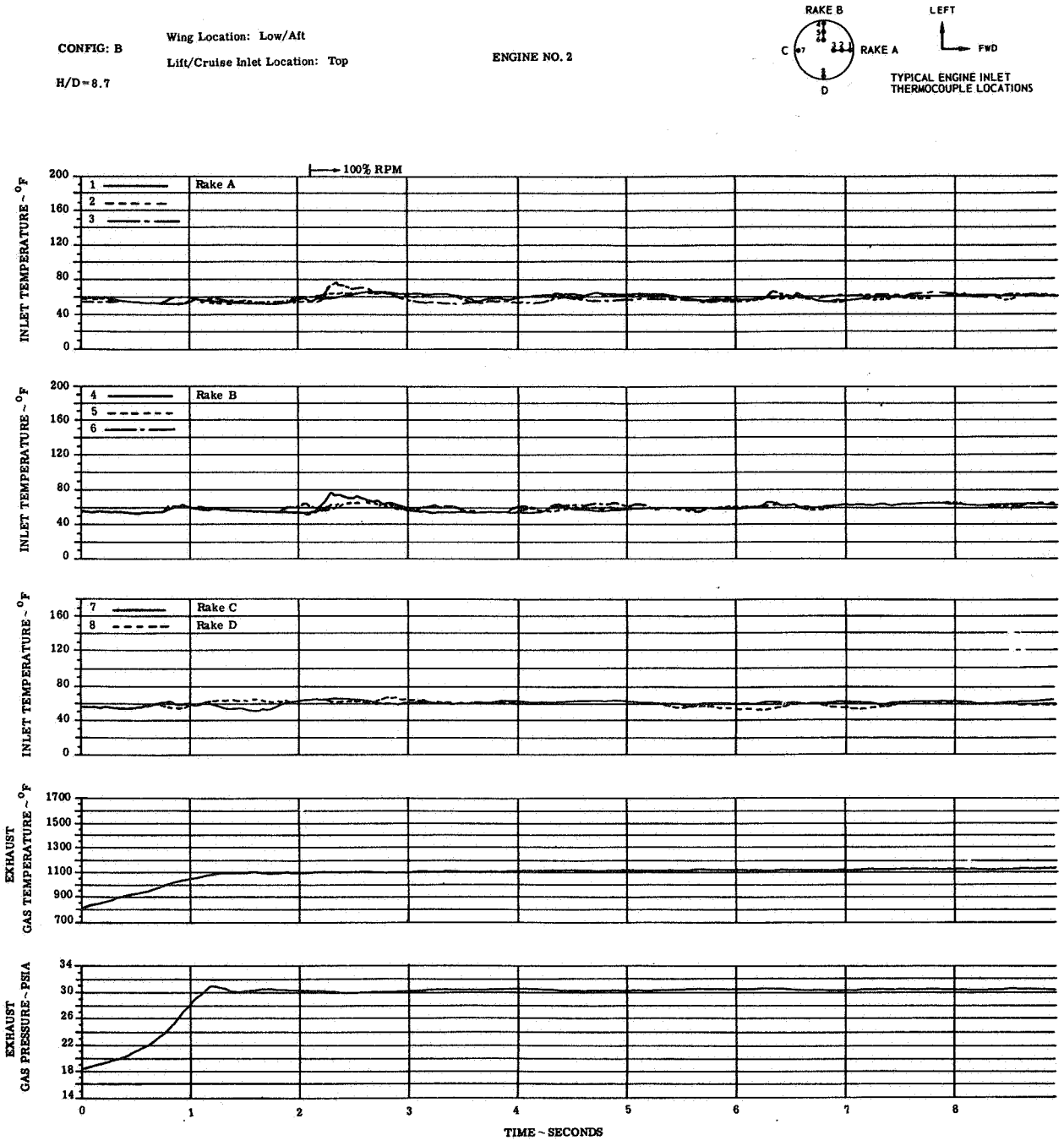

FIGURE 11(z). ENGINE TEMPERATURE AND PRESSURE TRANSIENTS

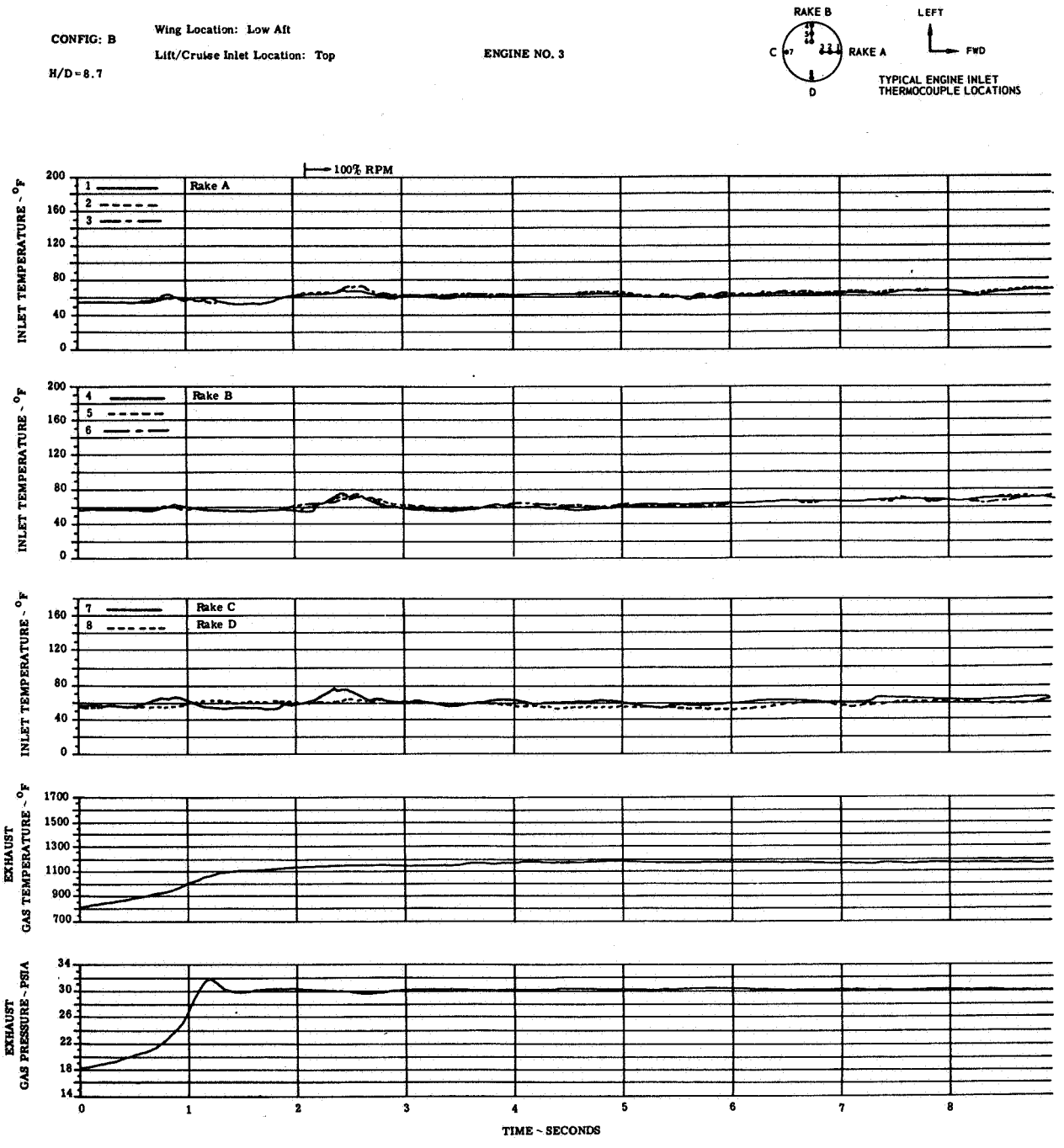

FIGURE 11(aa). ENGINE TEMPERATURE AND PRESSURE TRANSIENTS

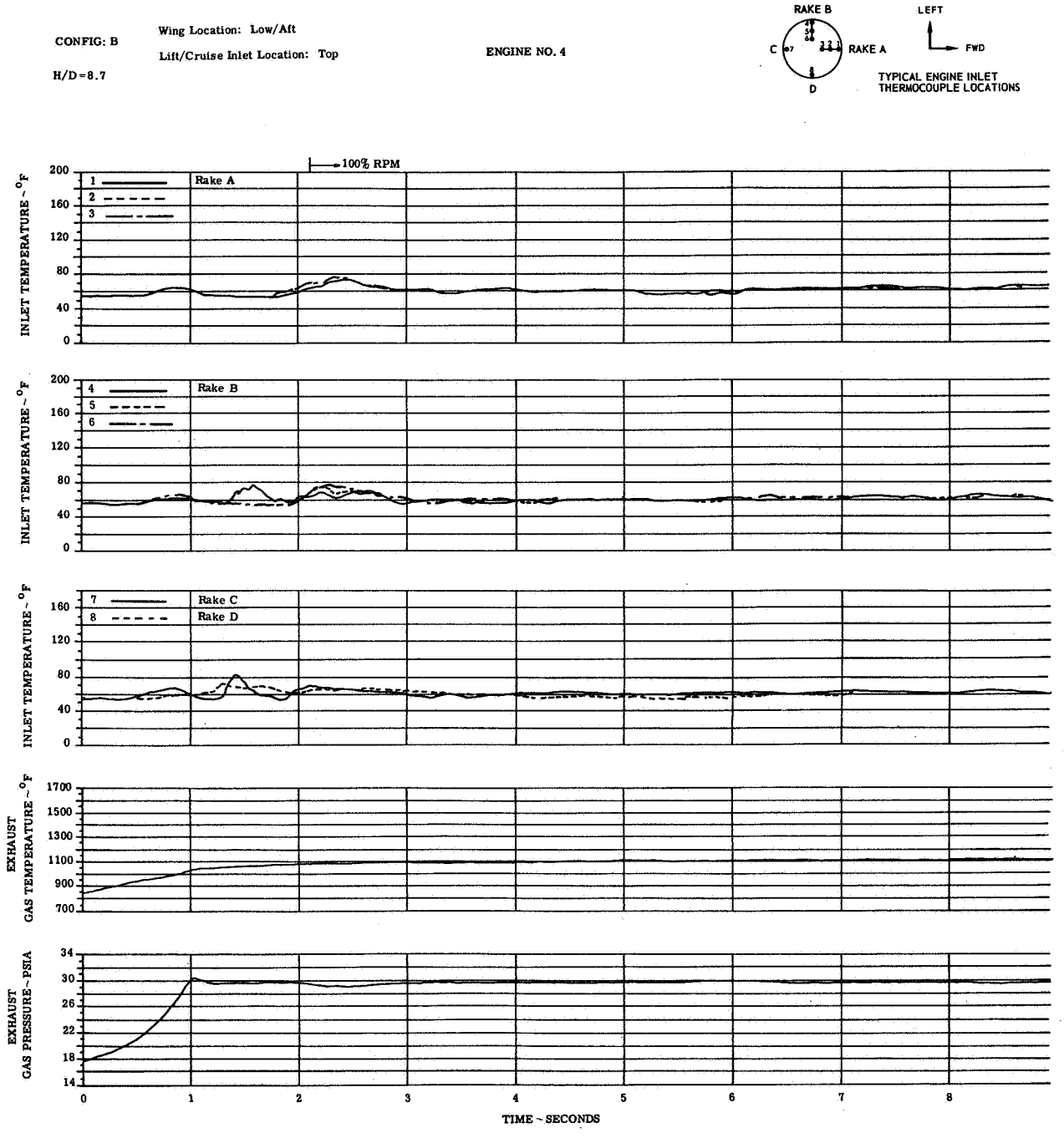

FIGURE 11(ab). ENGINE TEMPERATURE AND PRESSURE TRANSIENTS

CONFIG: B

Wing Location: Low/Aft

Lift/Cruise Inlet Location: Top

H/D - 8.7

ENGINE NO. 6

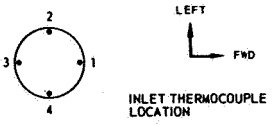

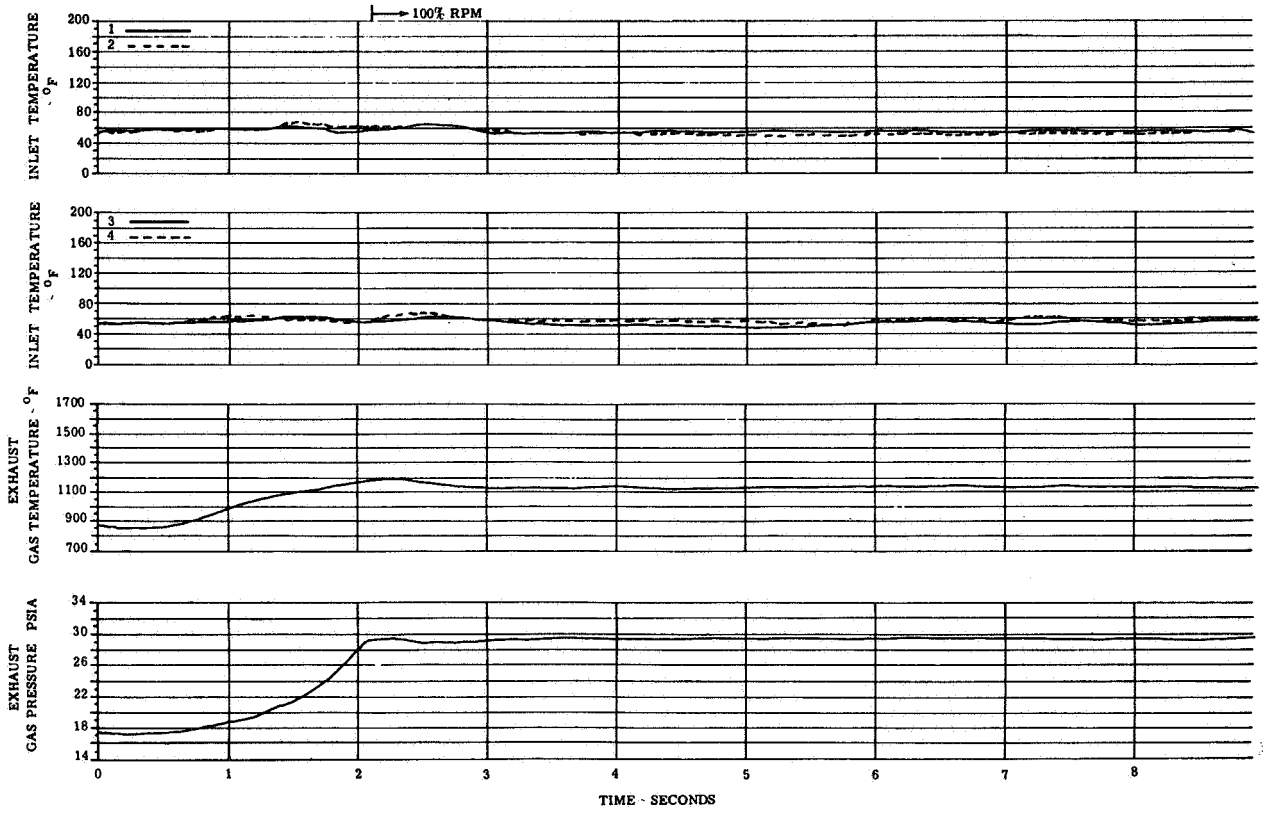

FIGURE 11(ac). ENGINE TEMPERATURE AND PRESSURE TRANSIENTS

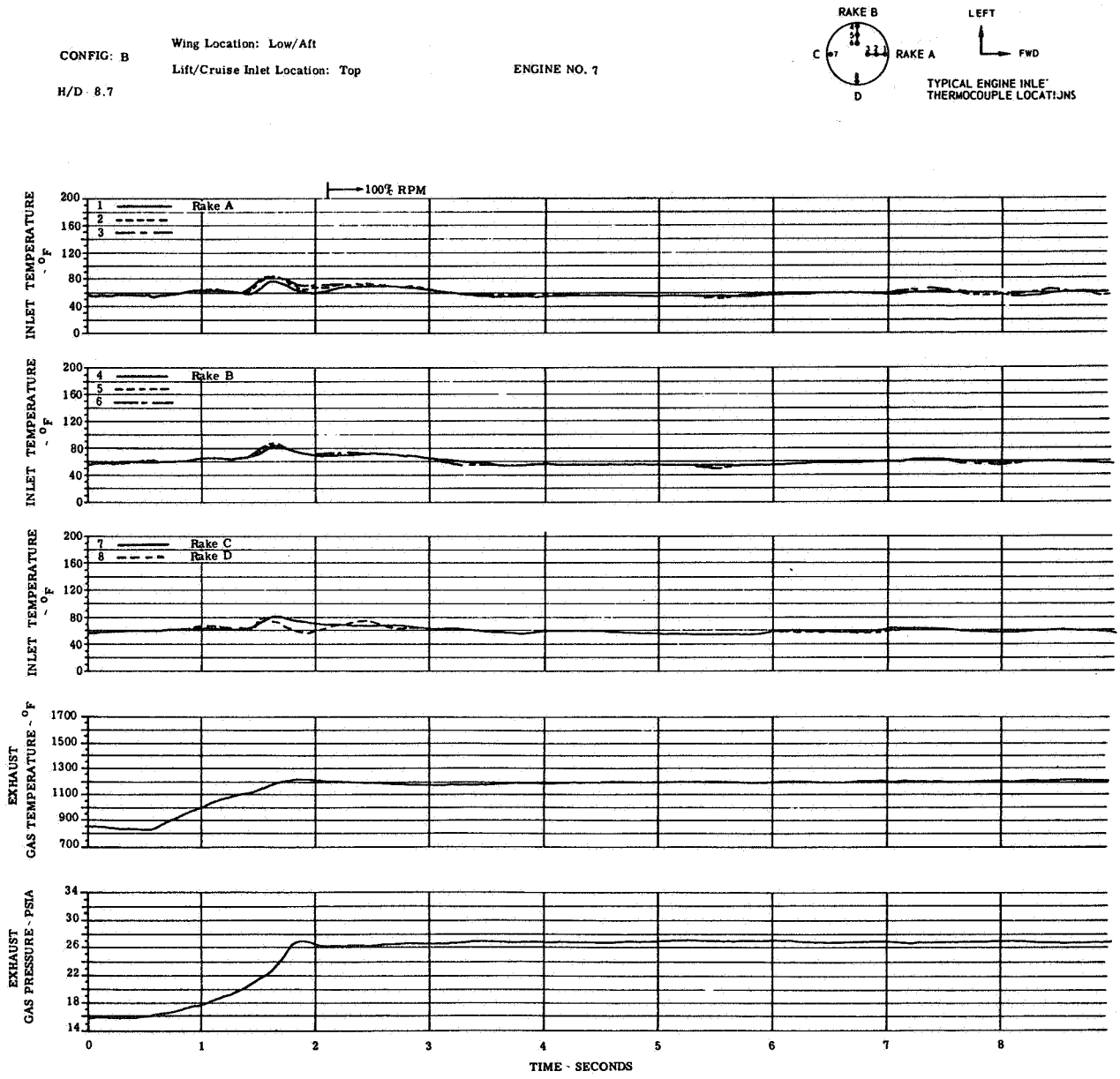

FIGURE 11(ad). ENGINE TEMPERATURE AND PRESSURE TRANSIENTS

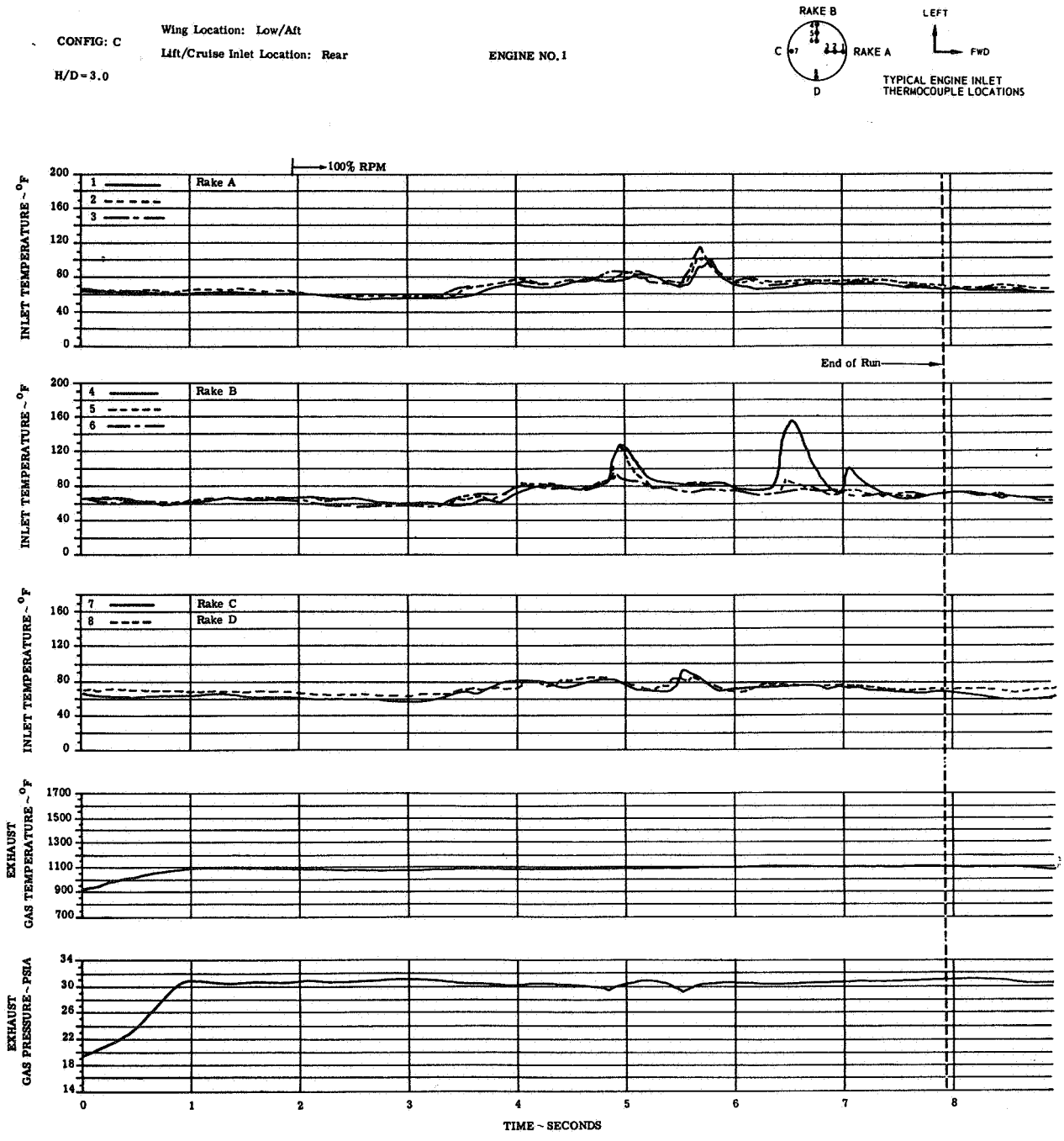

FIGURE 12(a). ENGINE TEMPERATURE AND PRESSURE TRANSIENTS

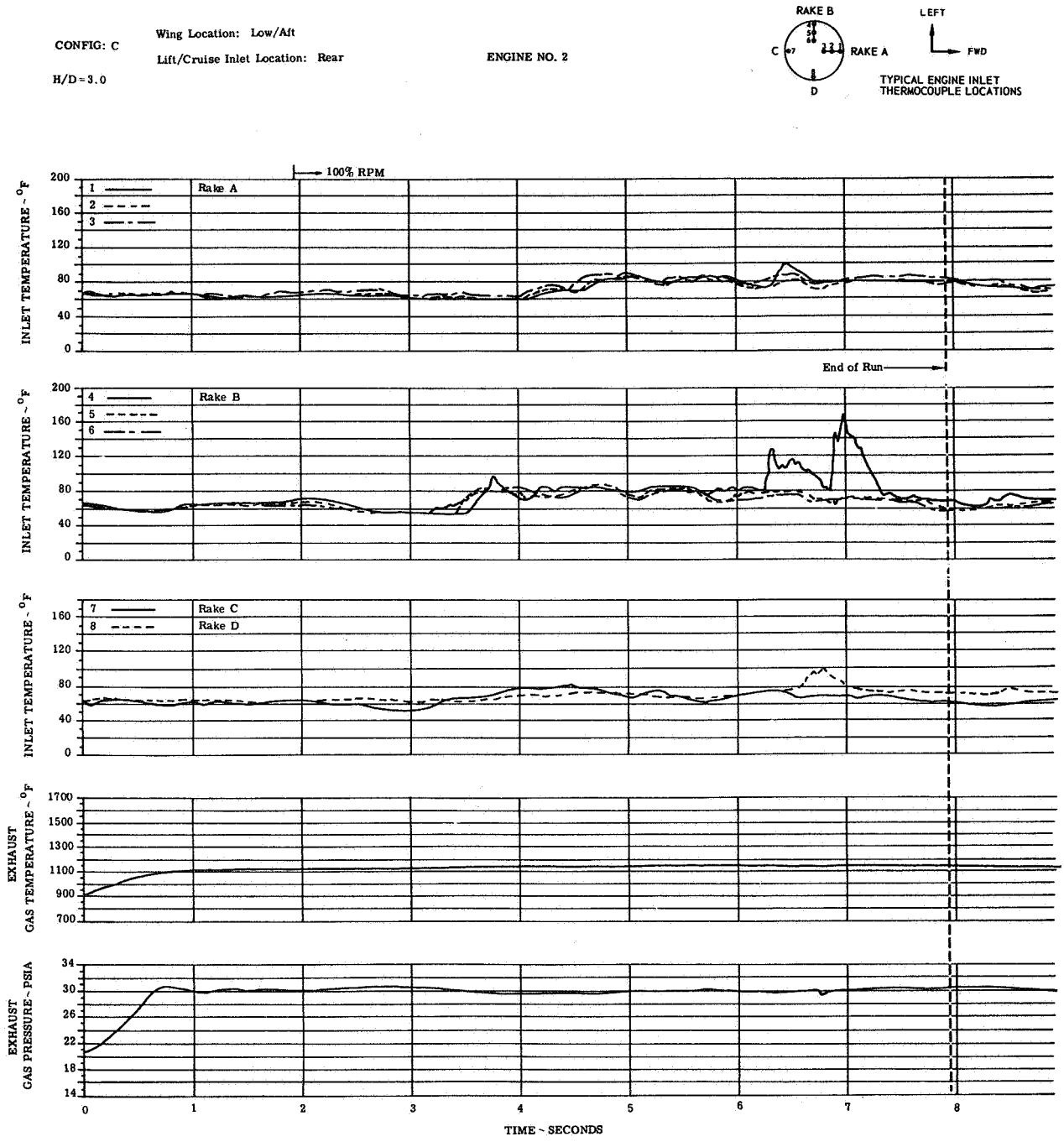

FIGURE 12(b). ENGINE TEMPERATURE AND PRESSURE TRANSIENTS

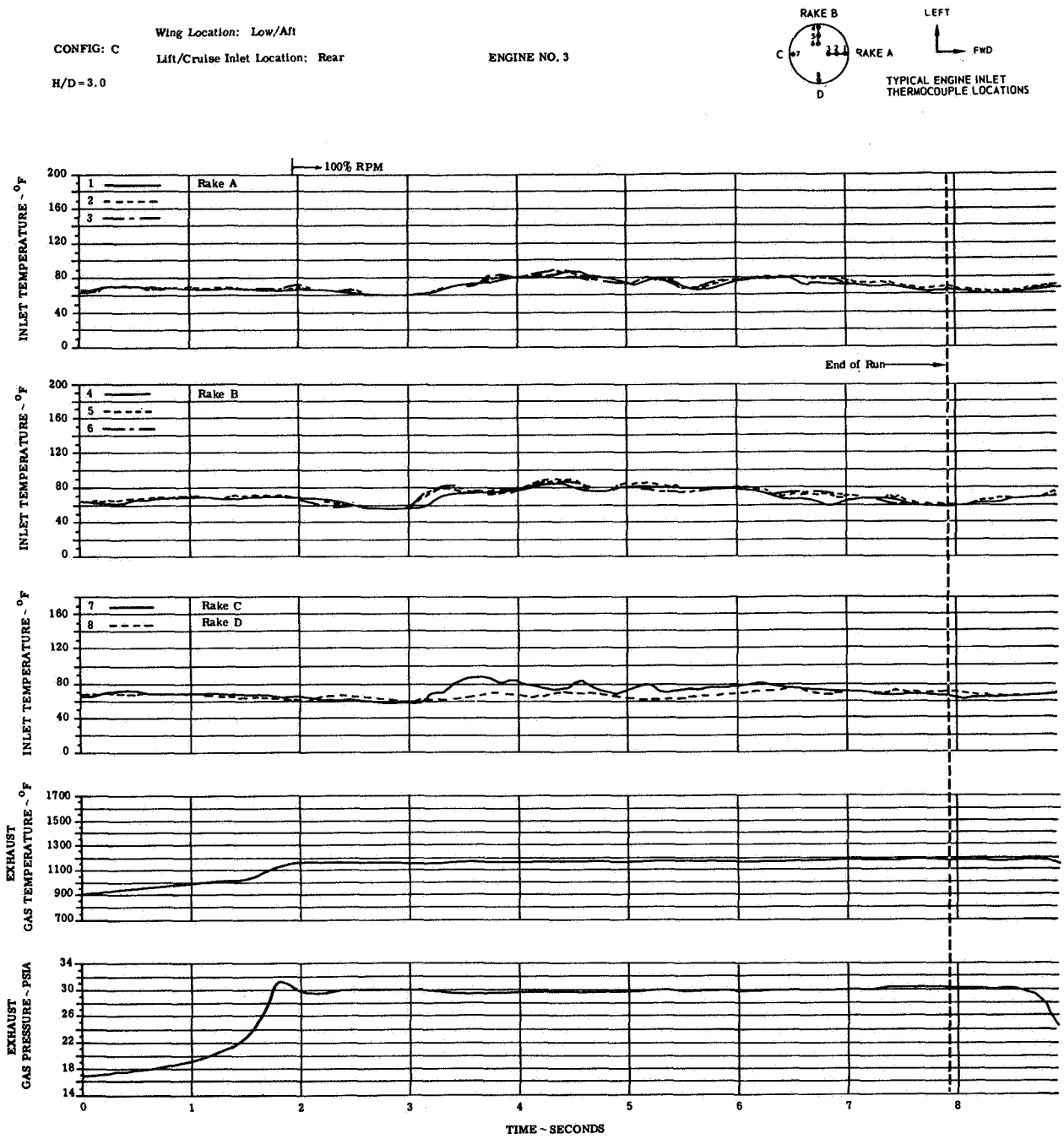

FIGURE 12(c). ENGINE TEMPERATURE AND PRESSURE TRANSIENTS

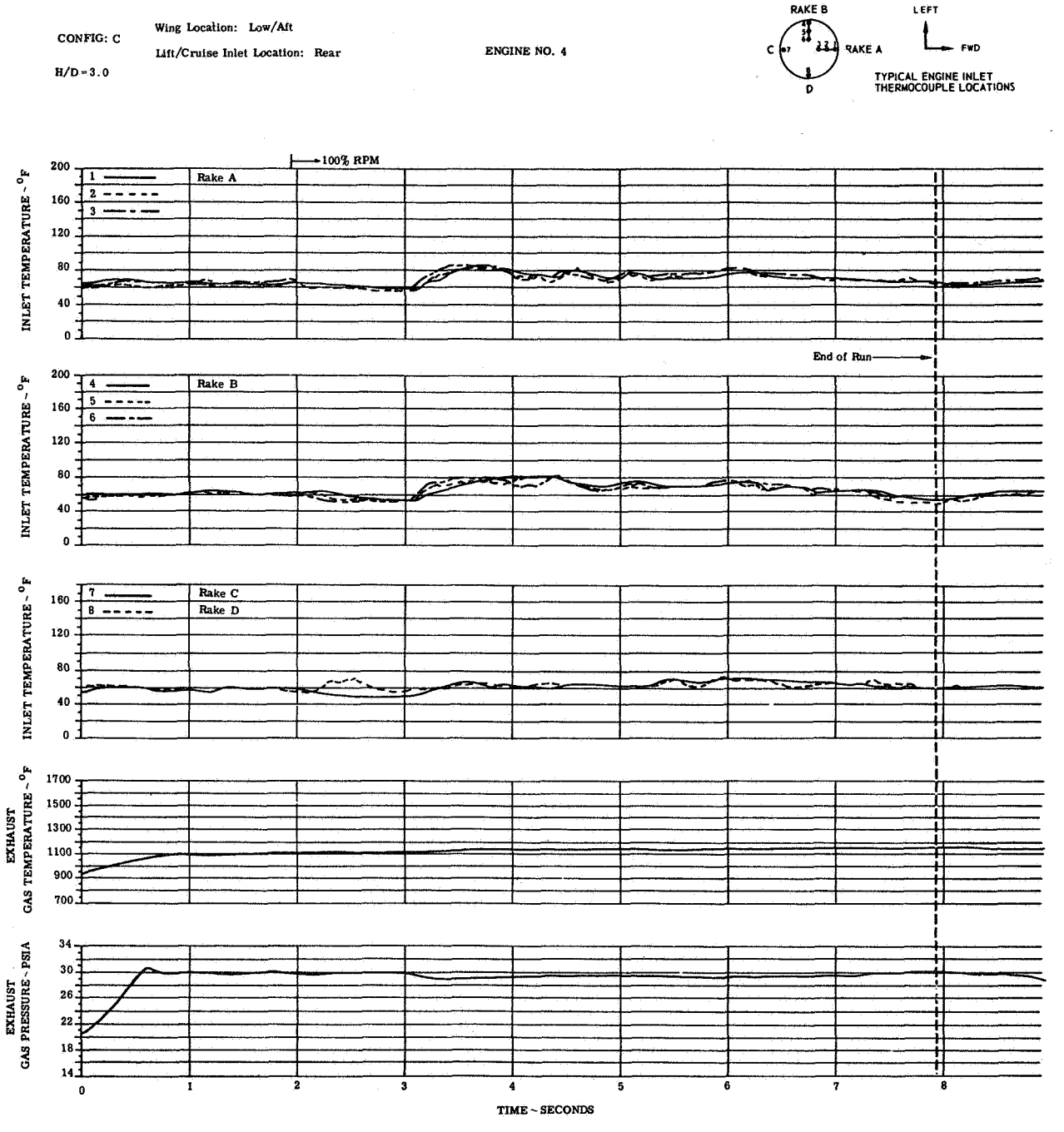

FIGURE 12(d). ENGINE TEMPERATURE AND PRESSURE TRANSIENTS

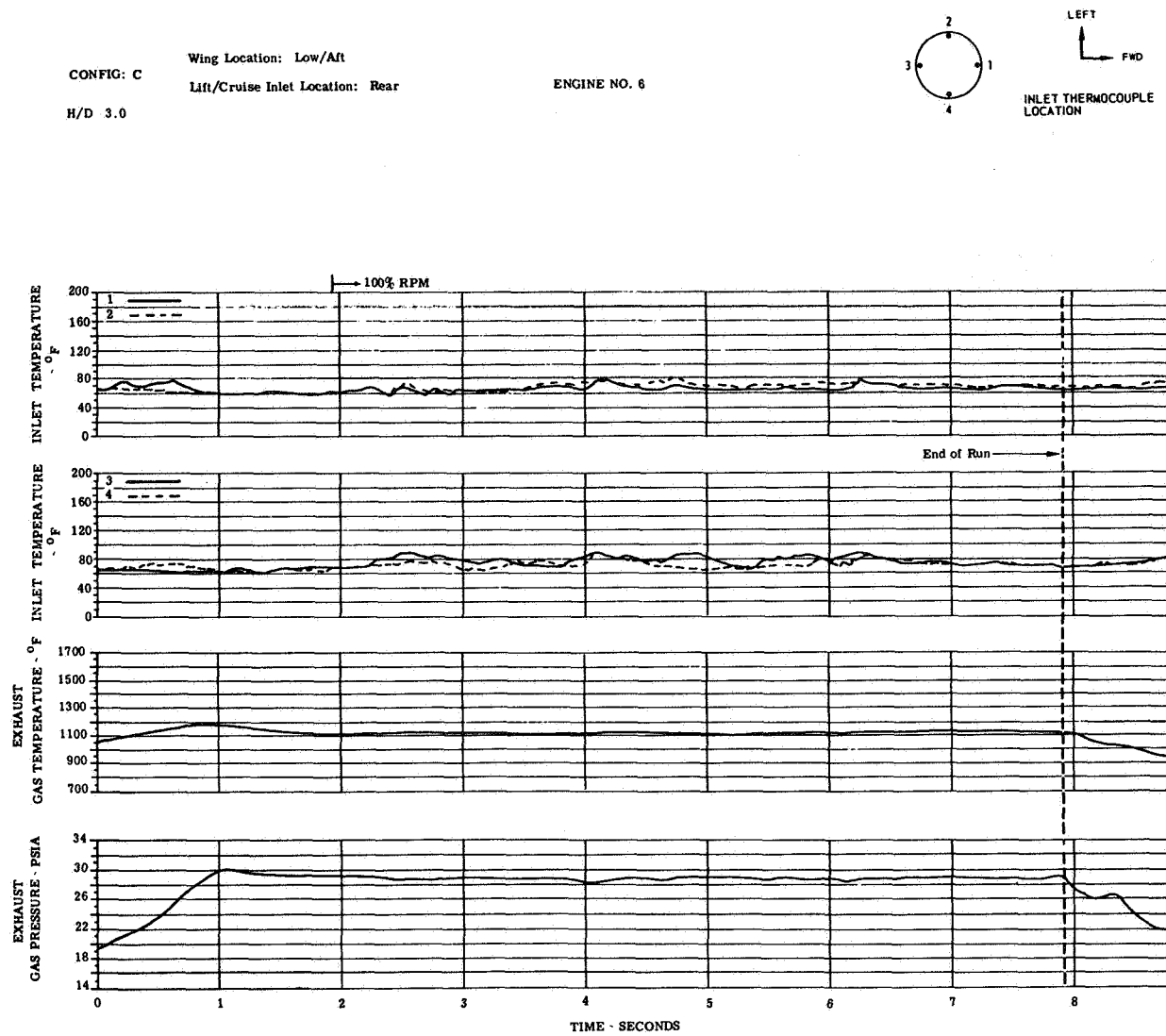

FIGURE 12(e). ENGINE TEMPERATURE AND PRESSURE TRANSIENTS

CONFIG: C

Wing Location: Low/Aft

Lift/Cruise Inlet Location: Rear

ENGINE NO. 7

H/D - 3.0

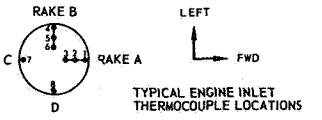

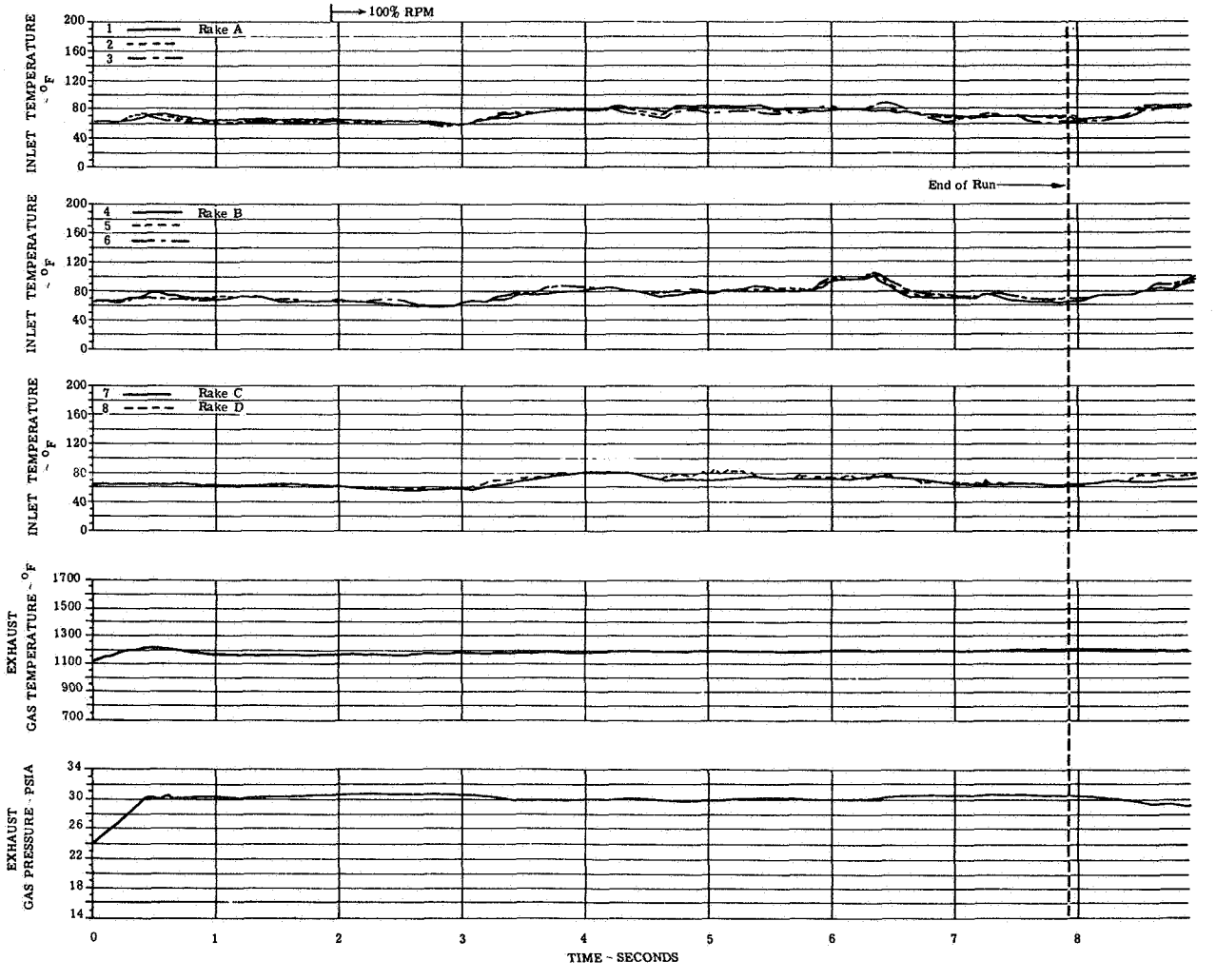

FIGURE 12(f). ENGINE TEMPERATURE AND PRESSURE TRANSIENTS

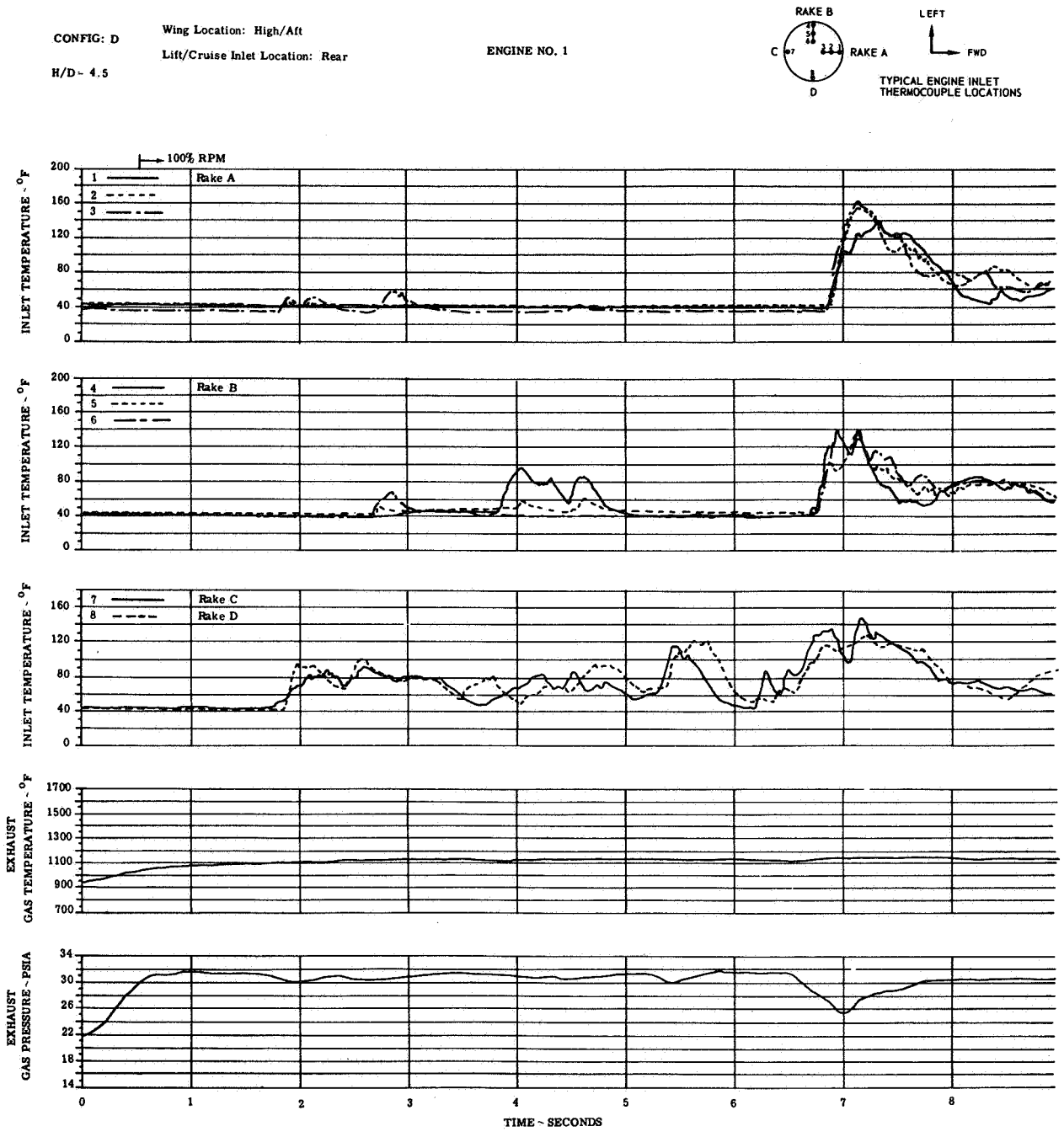

FIGURE 13(a). ENGINE TEMPERATURE AND PRESSURE TRANSIENTS

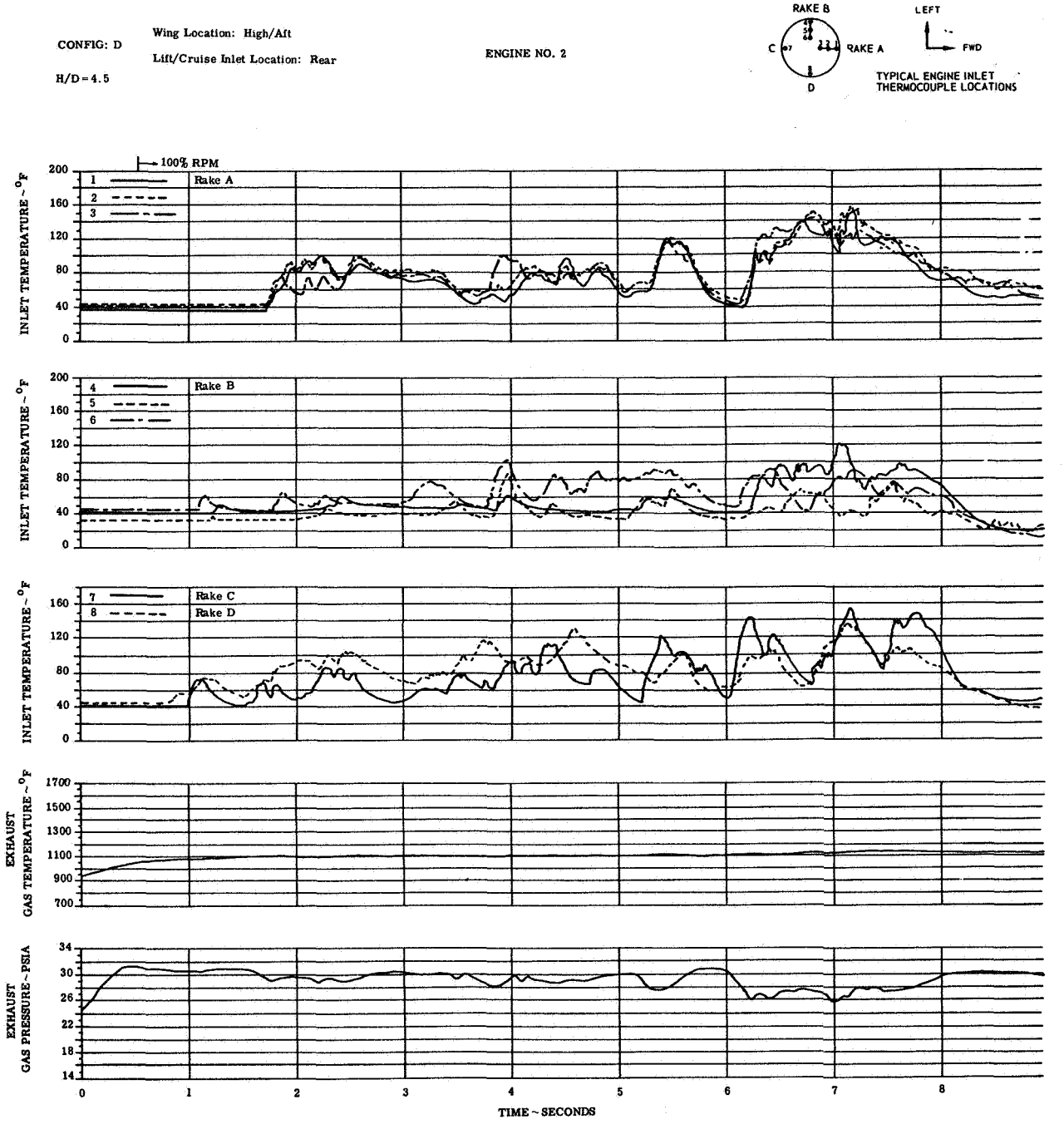

FIGURE 13(b). ENGINE TEMPERATURE AND PRESSURE TRANSIENTS

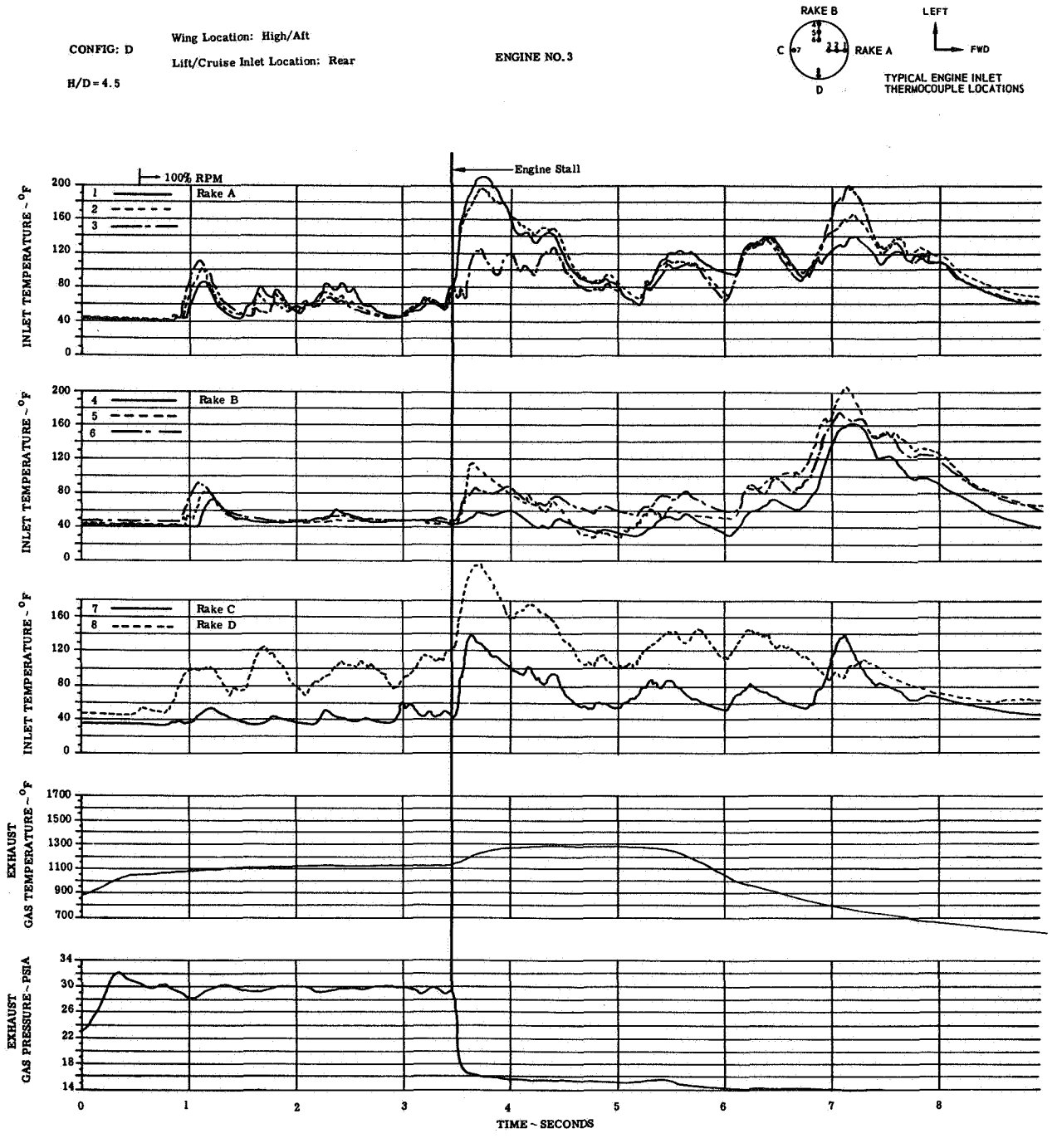

FIGURE 13(c). ENGINE TEMPERATURE AND PRESSURE TRANSIENTS

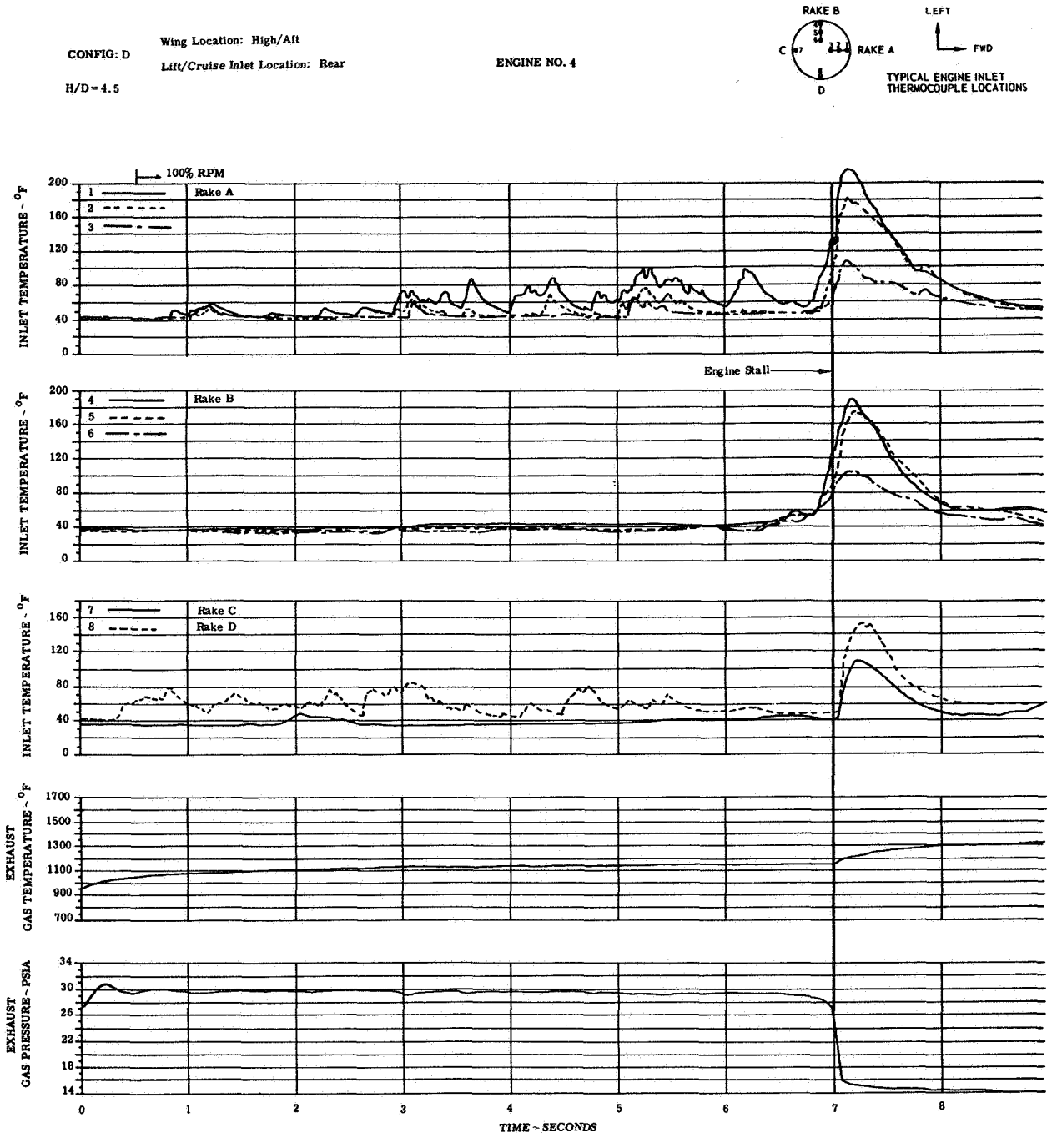

FIGURE 13(d). ENGINE TEMPERATURE AND PRESSURE TRANSIENTS

CONFIG: D

Wing Location: High/Aft

Lift/Cruise Inlet Location: Rear

ENGINE NO. 6

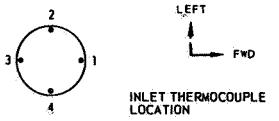

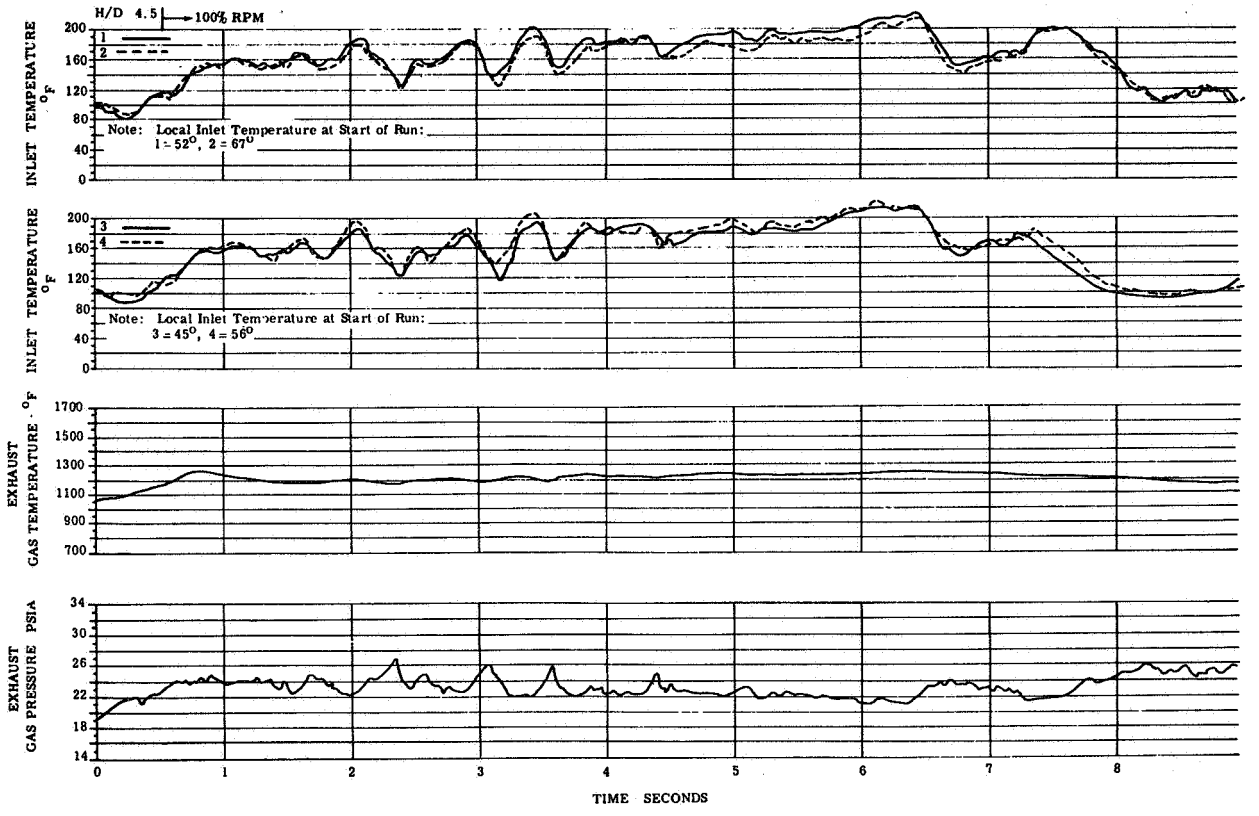

FIGURE 13(e). ENGINE TEMPERATURE AND PRESSURE TRANSIENTS

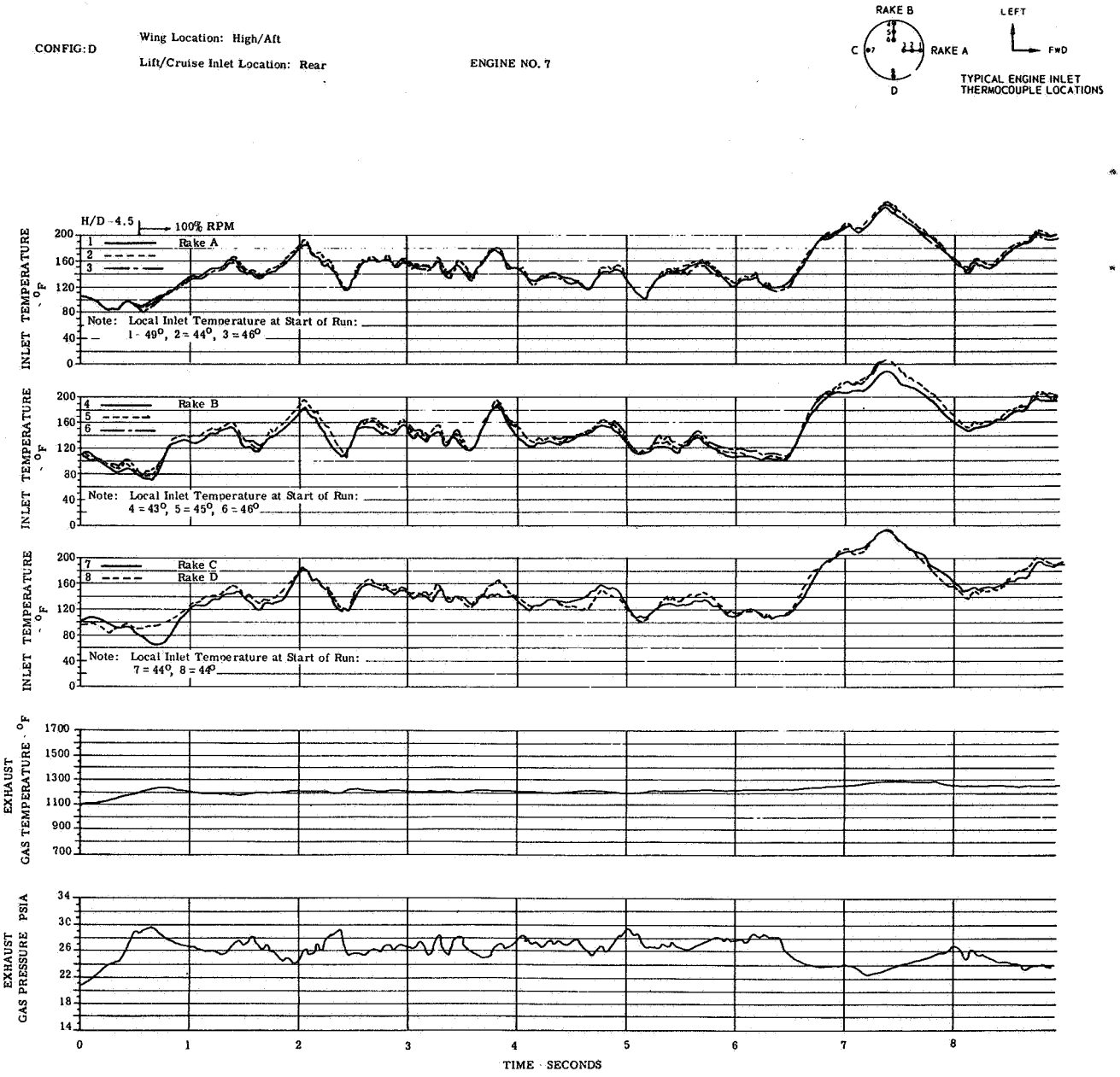

FIGURE 13(f). ENGINE TEMPERATURE AND PRESSURE TRANSIENTS

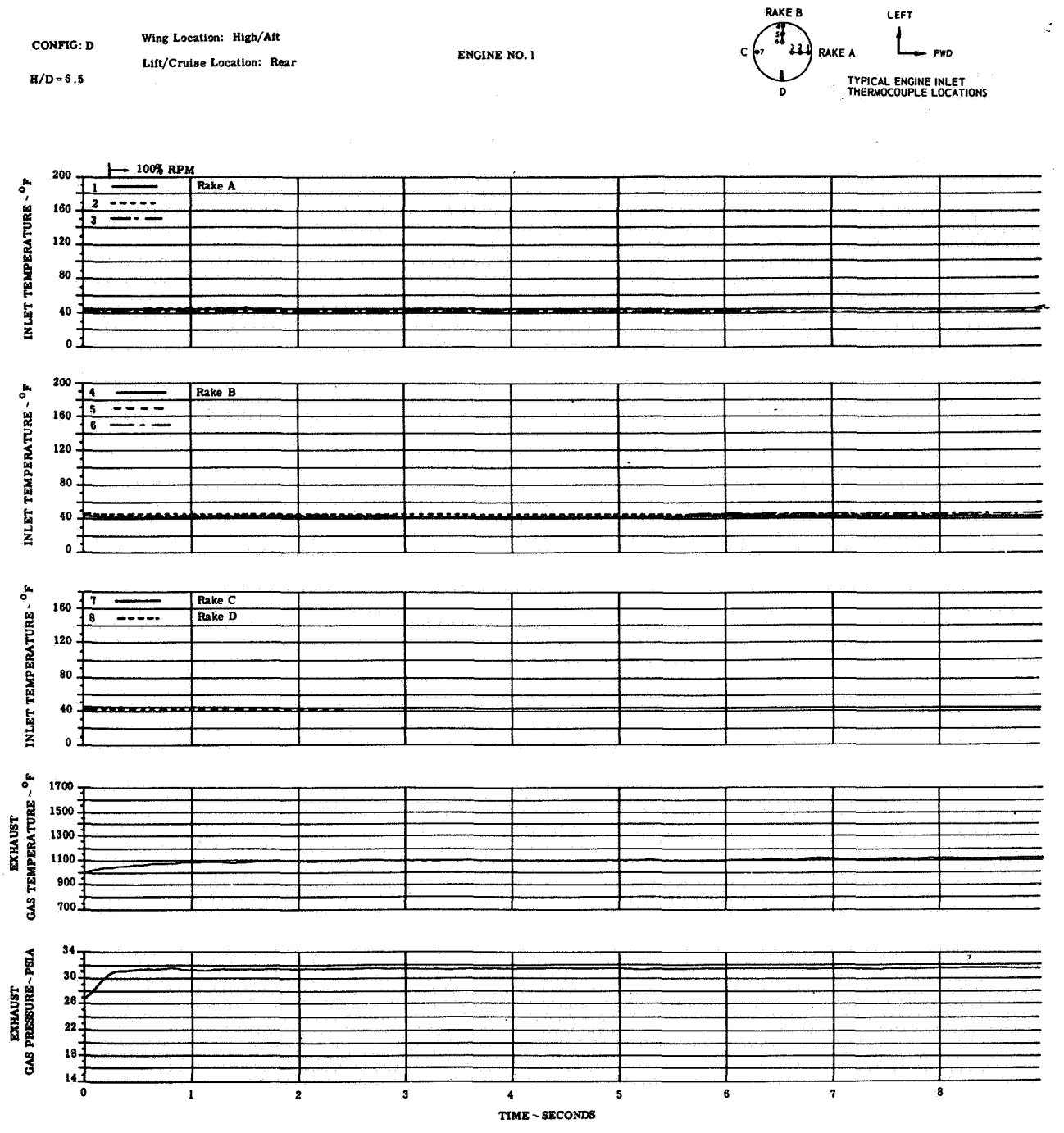

FIGURE 13(g). ENGINE TEMPERATURE AND PRESSURE TRANSIENTS

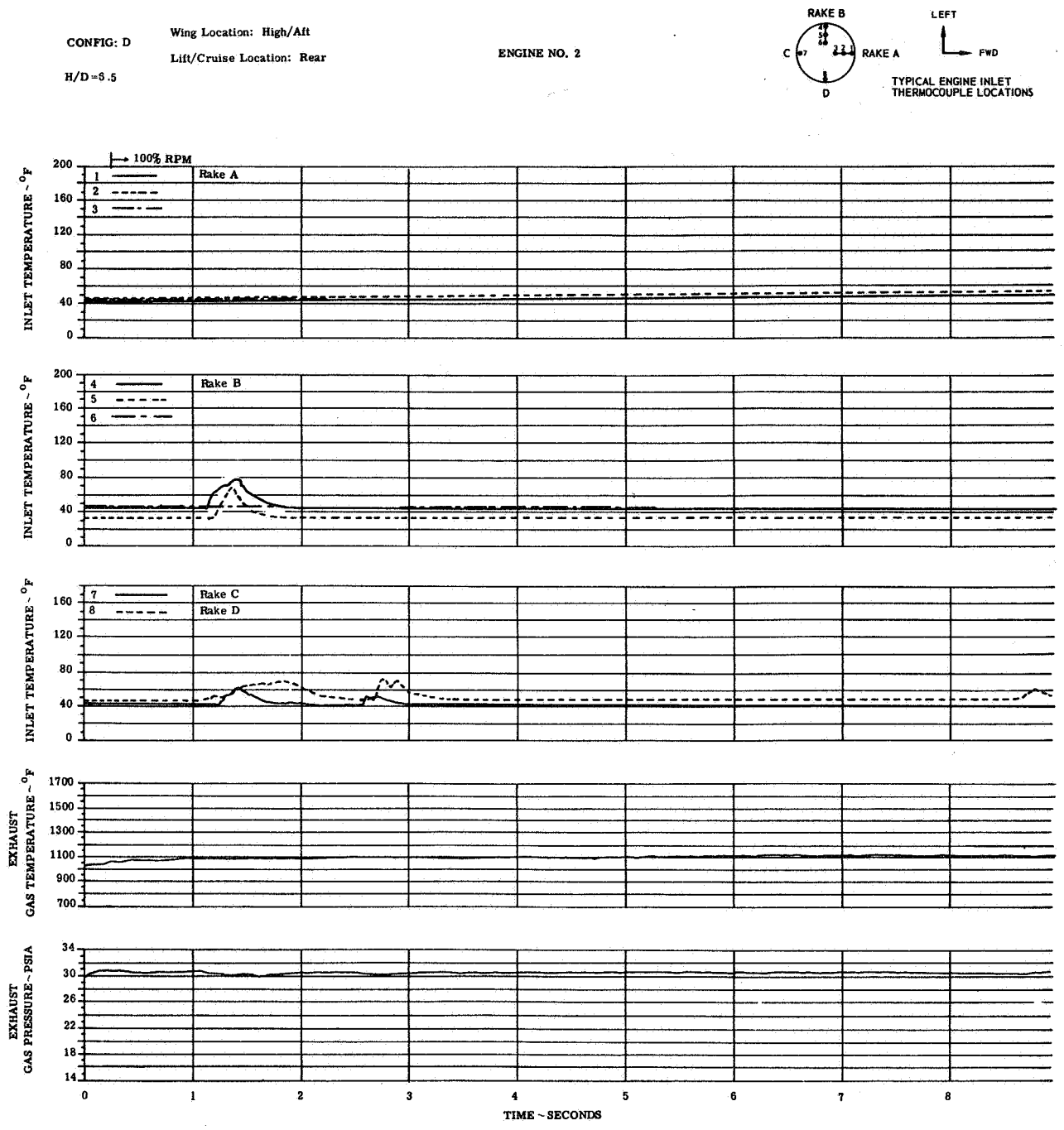

FIGURE 13(h). ENGINE TEMPERATURE AND PRESSURE TRANSIENTS

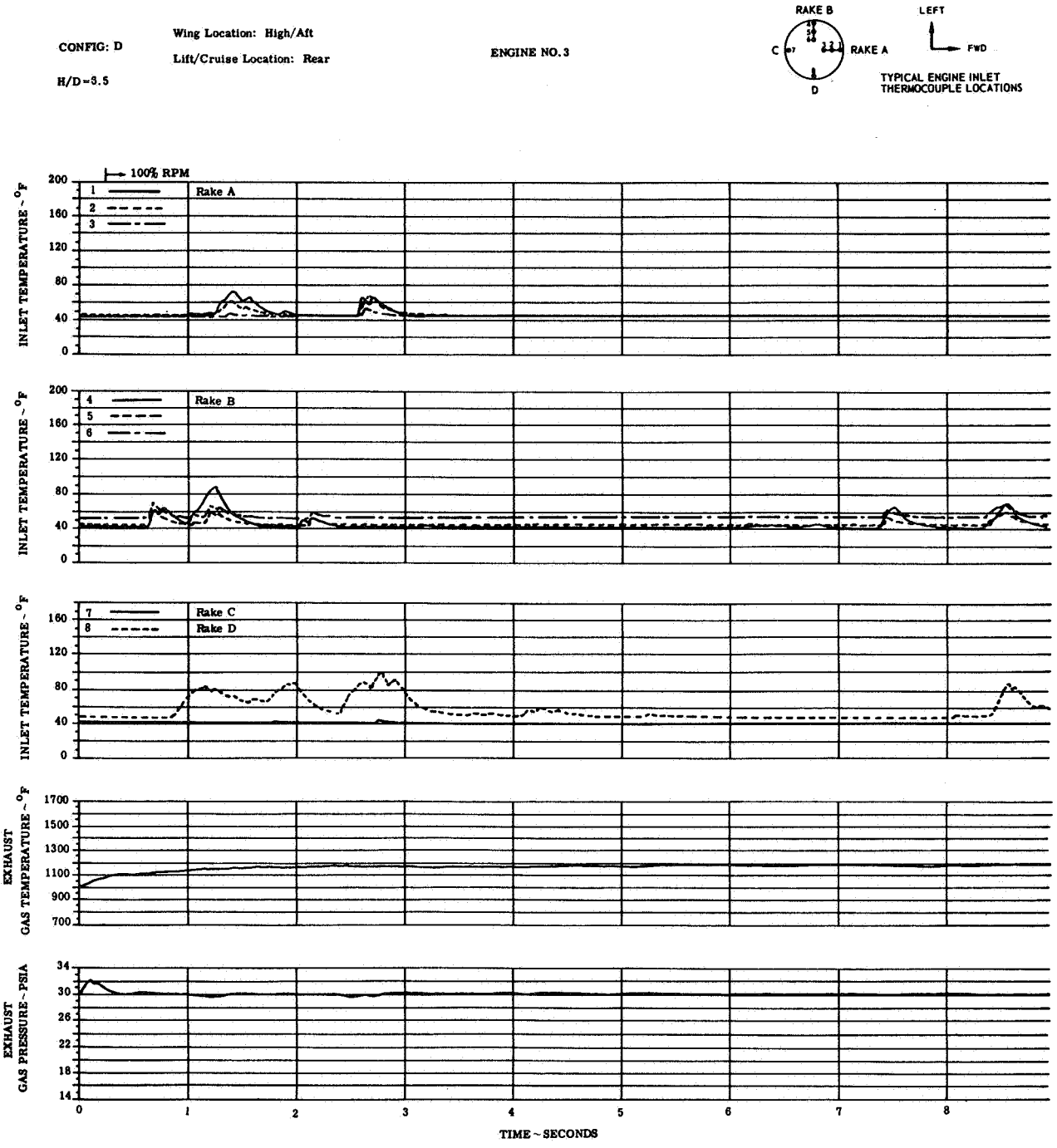

FIGURE 13(i). ENGINE TEMPERATURE AND PRESSURE TRANSIENTS

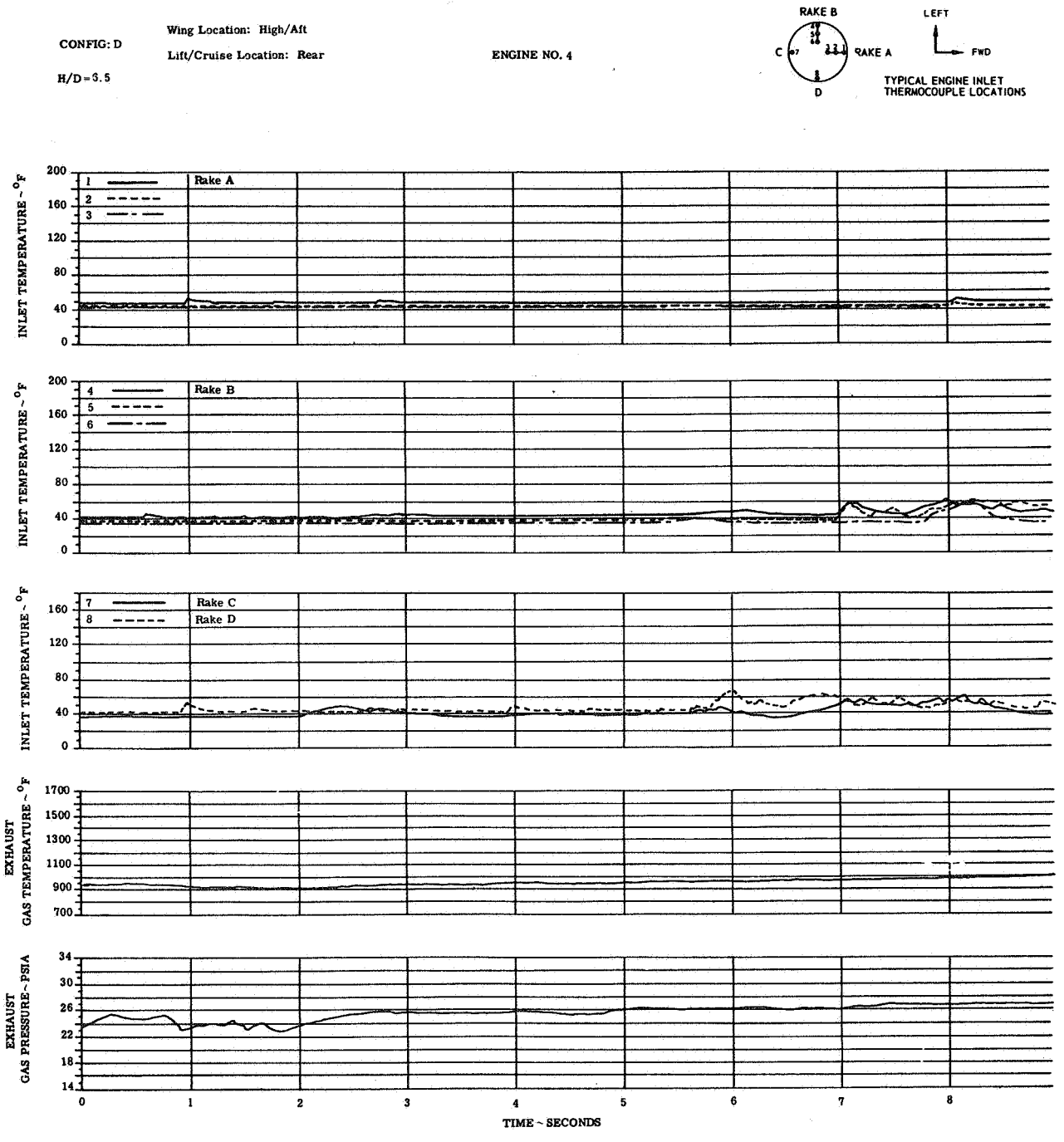

FIGURE 13(j). ENGINE TEMPERATURE AND PRESSURE TRANSIENTS

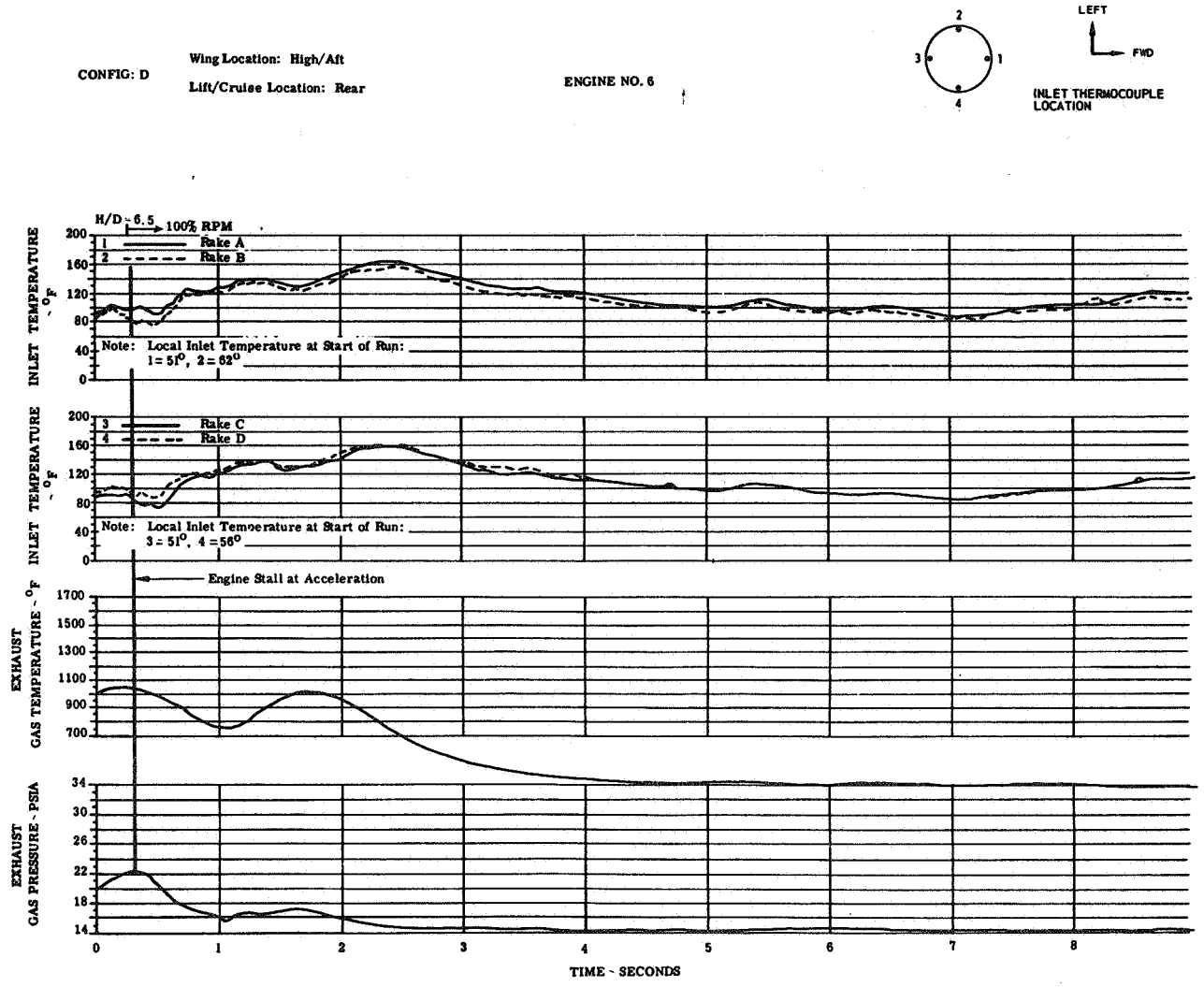

FIGURE 13(k). ENGINE TEMPERATURE AND PRESSURE TRANSIENTS

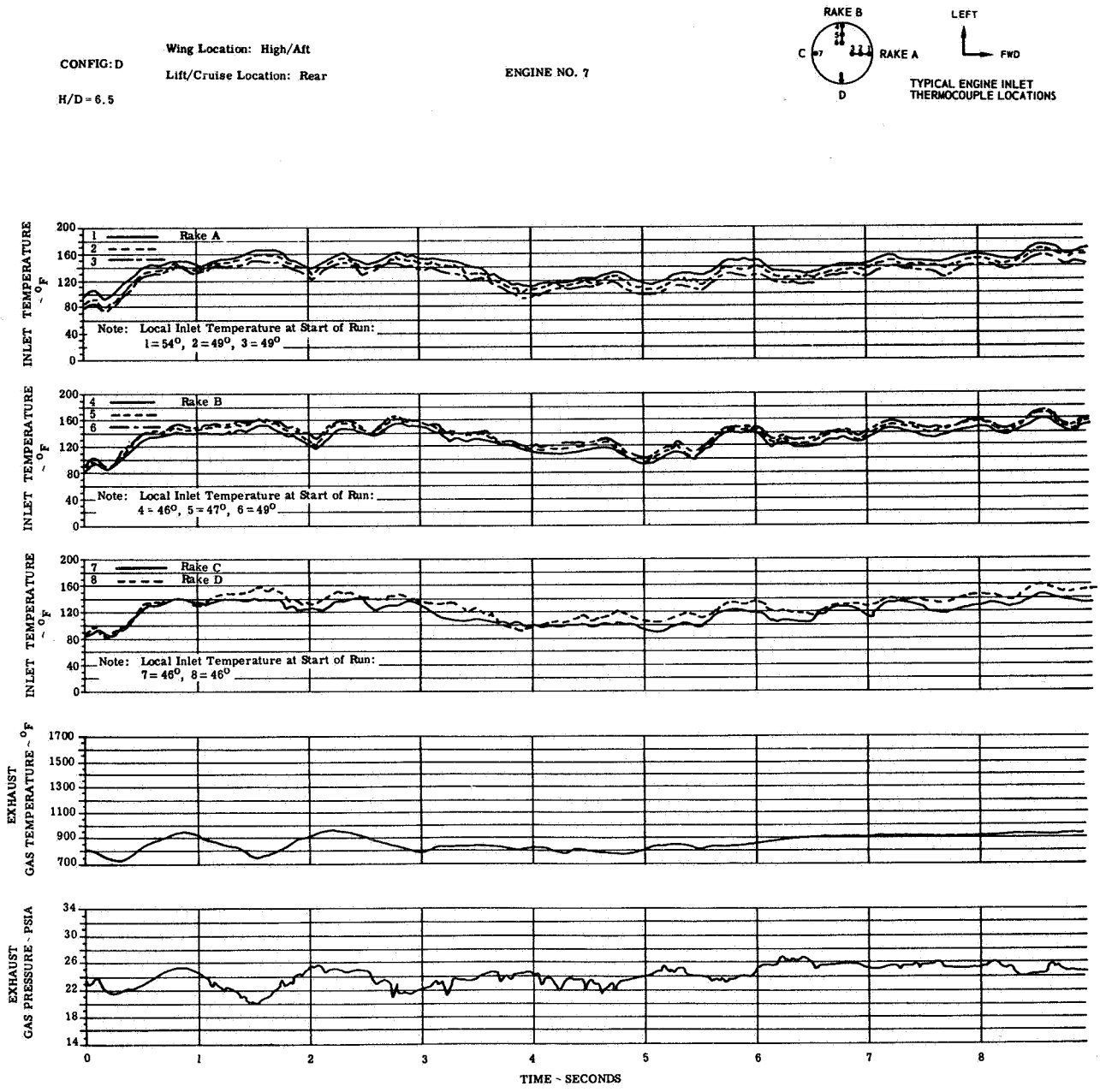

FIGURE 13(l). ENGINE TEMPERATURE AND PRESSURE TRANSIENTS

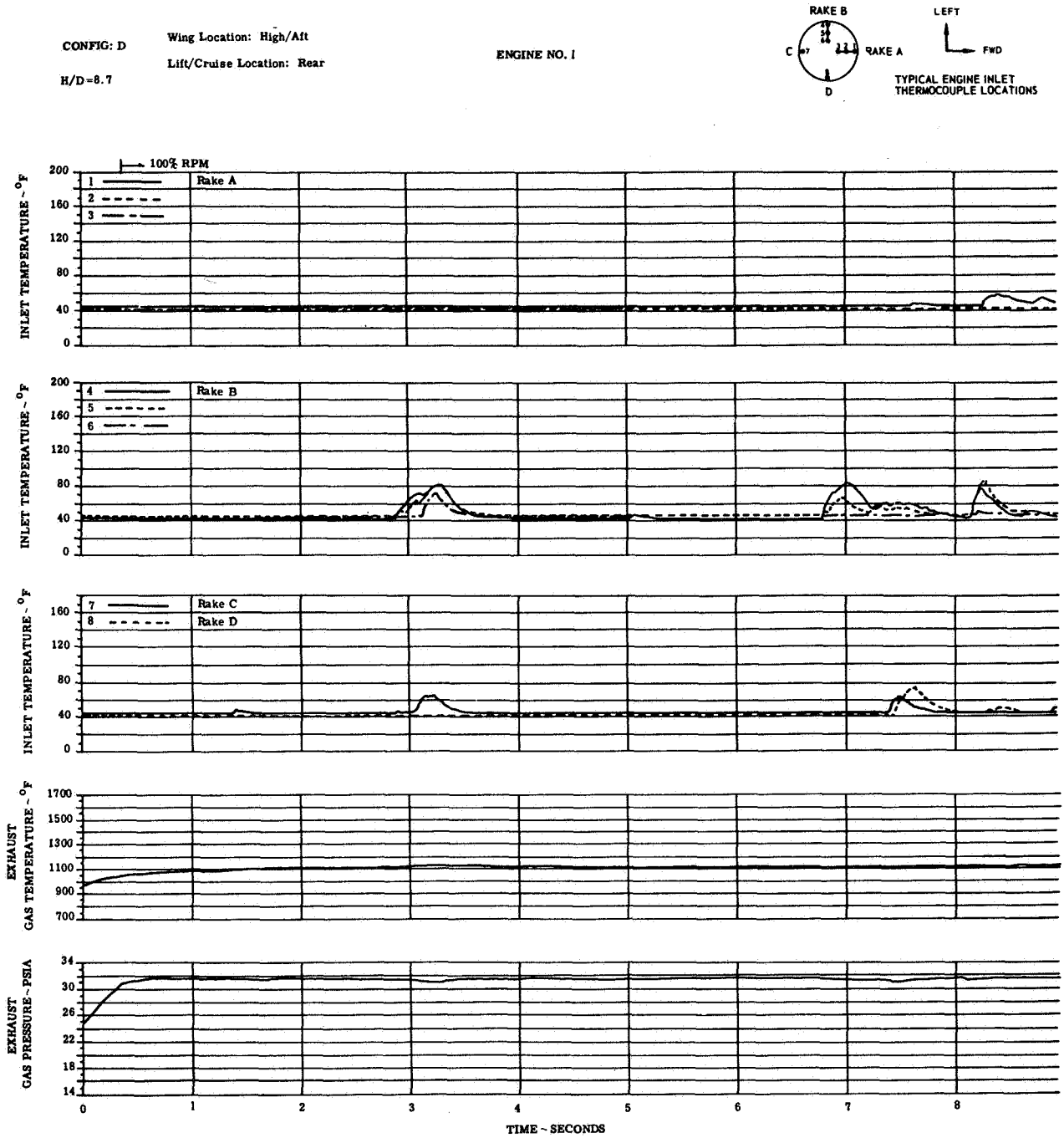

FIGURE 13(m). ENGINE TEMPERATURE AND PRESSURE TRANSIENTS

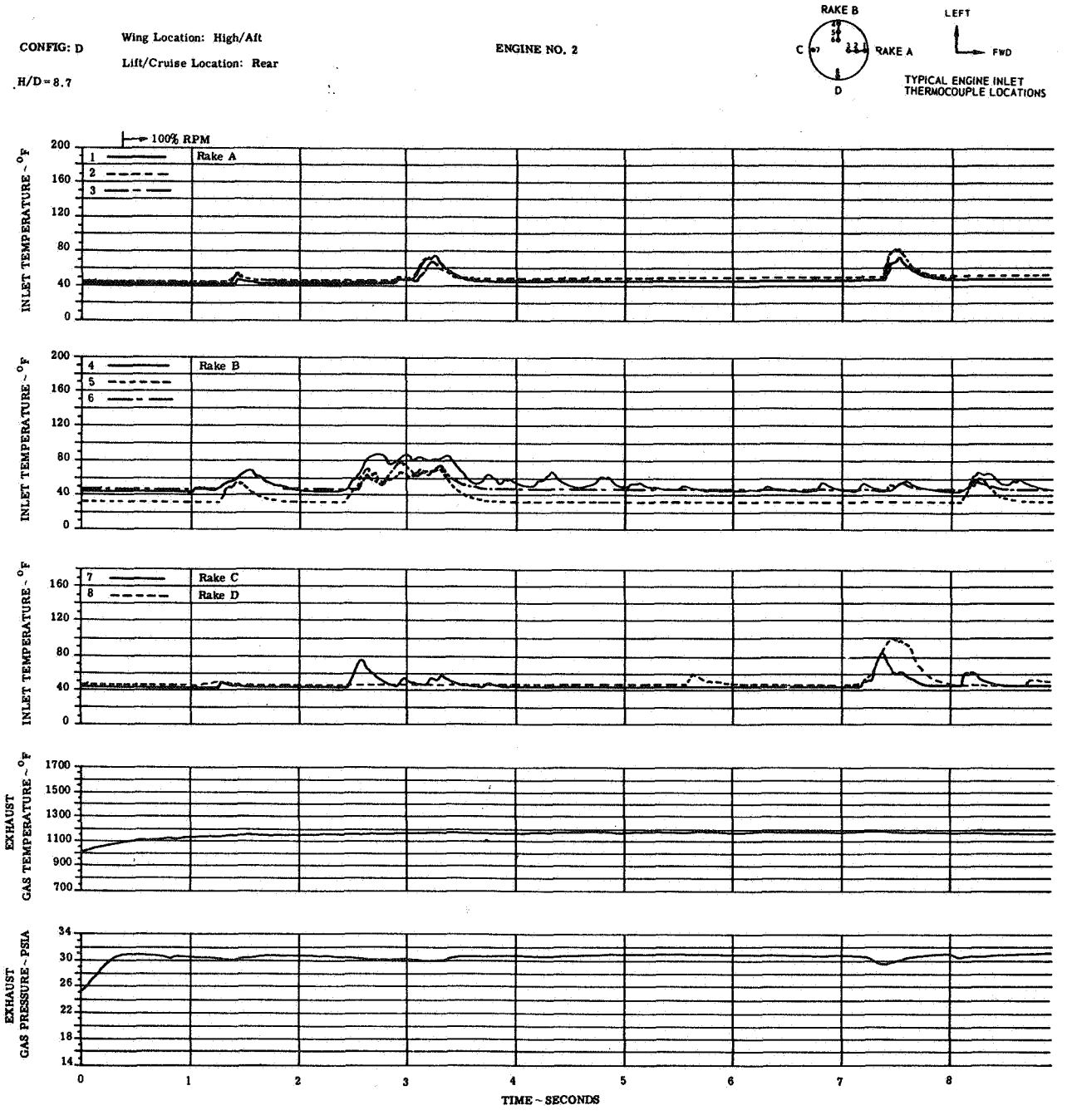

FIGURE 13(n). ENGINE TEMPERATURE AND PRESSURE TRANSIENTS

CONFIG: D

Wing Location: High/Aft

Lift/Cruise Inlet Location: Rear

H/D = 8.7

ENGINE NO. 3

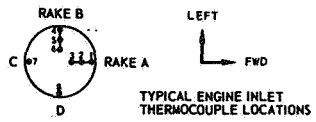

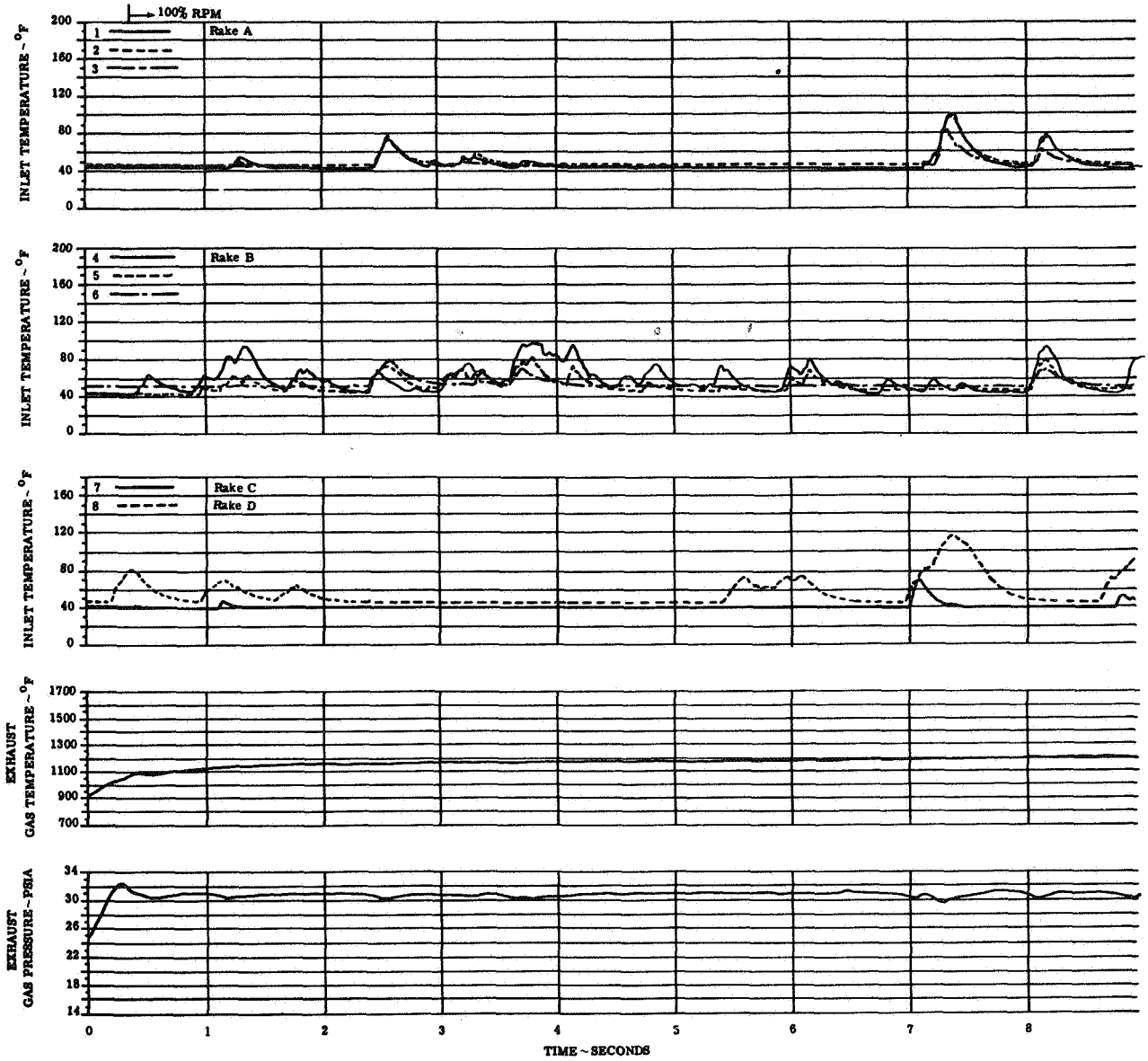

FIGURE 13(o). ENGINE TEMPERATURE AND PRESSURE TRANSIENTS

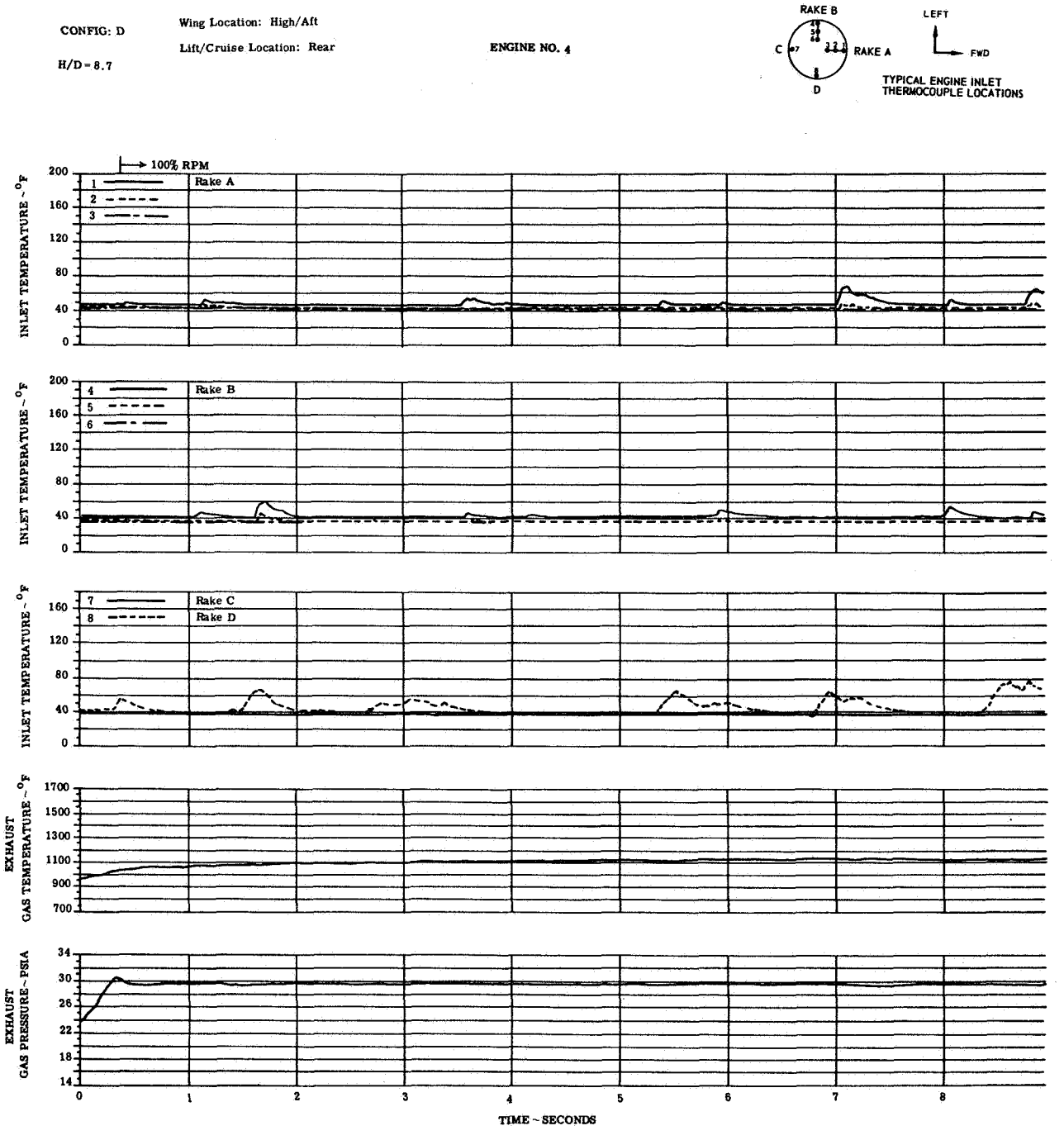

FIGURE 13(p). ENGINE TEMPERATURE AND PRESSURE TRANSIENTS

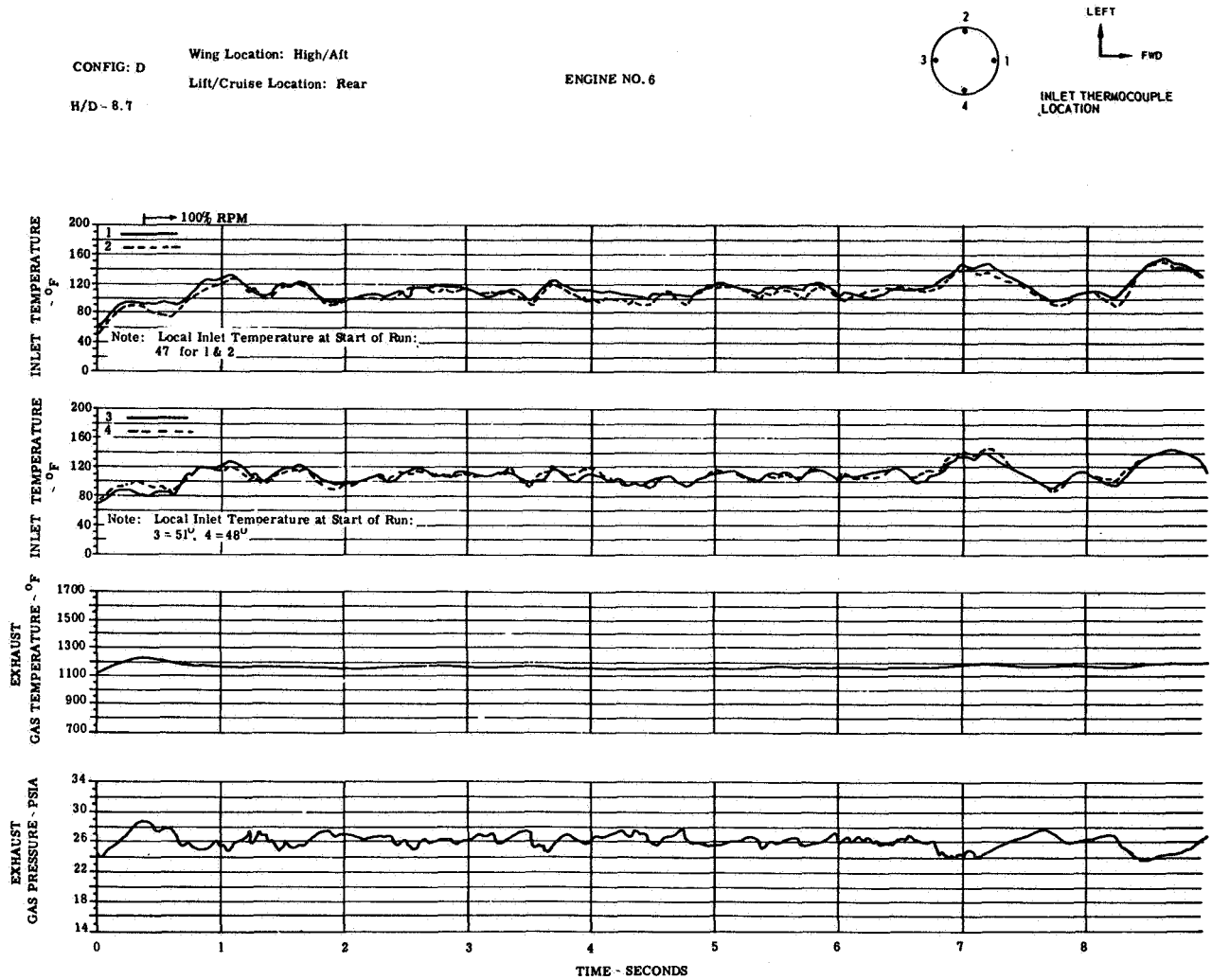

FIGURE 13(q). ENGINE TEMPERATURE AND PRESSURE TRANSIENTS

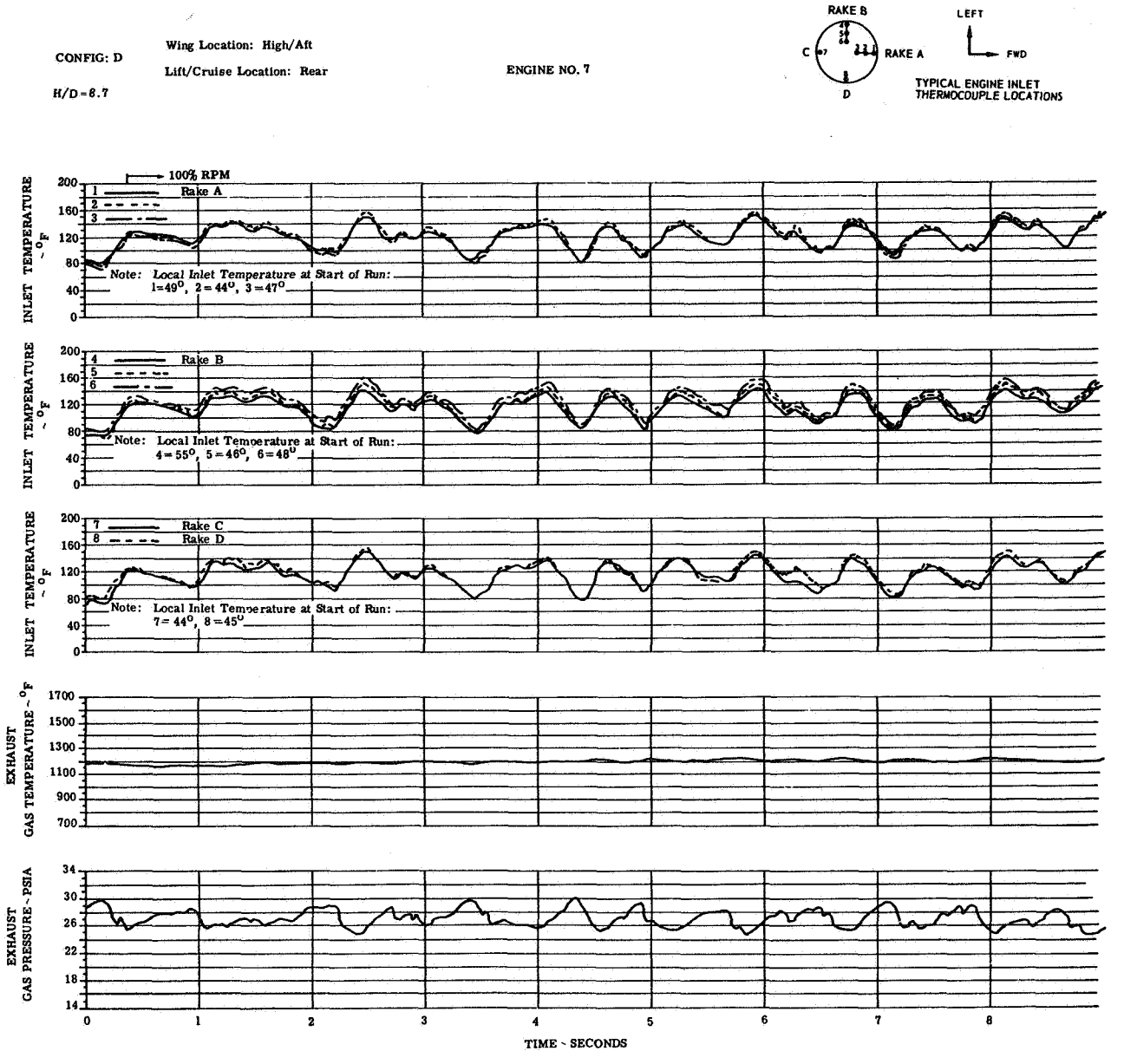

FIGURE 13(r). ENGINE TEMPERATURE AND PRESSURE TRANSIENTS

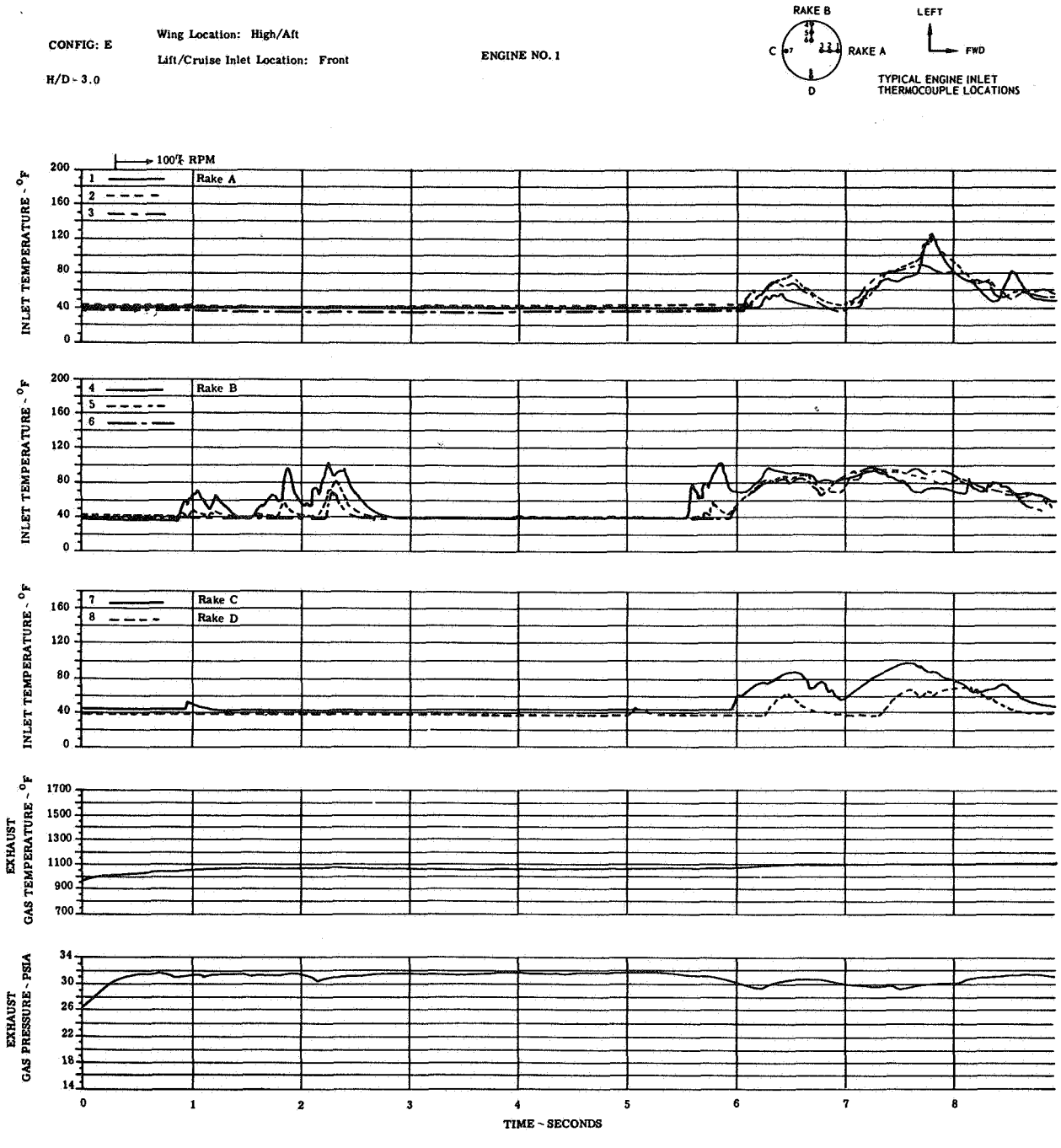

FIGURE 14(a). ENGINE TEMPERATURE AND PRESSURE TRANSIENTS

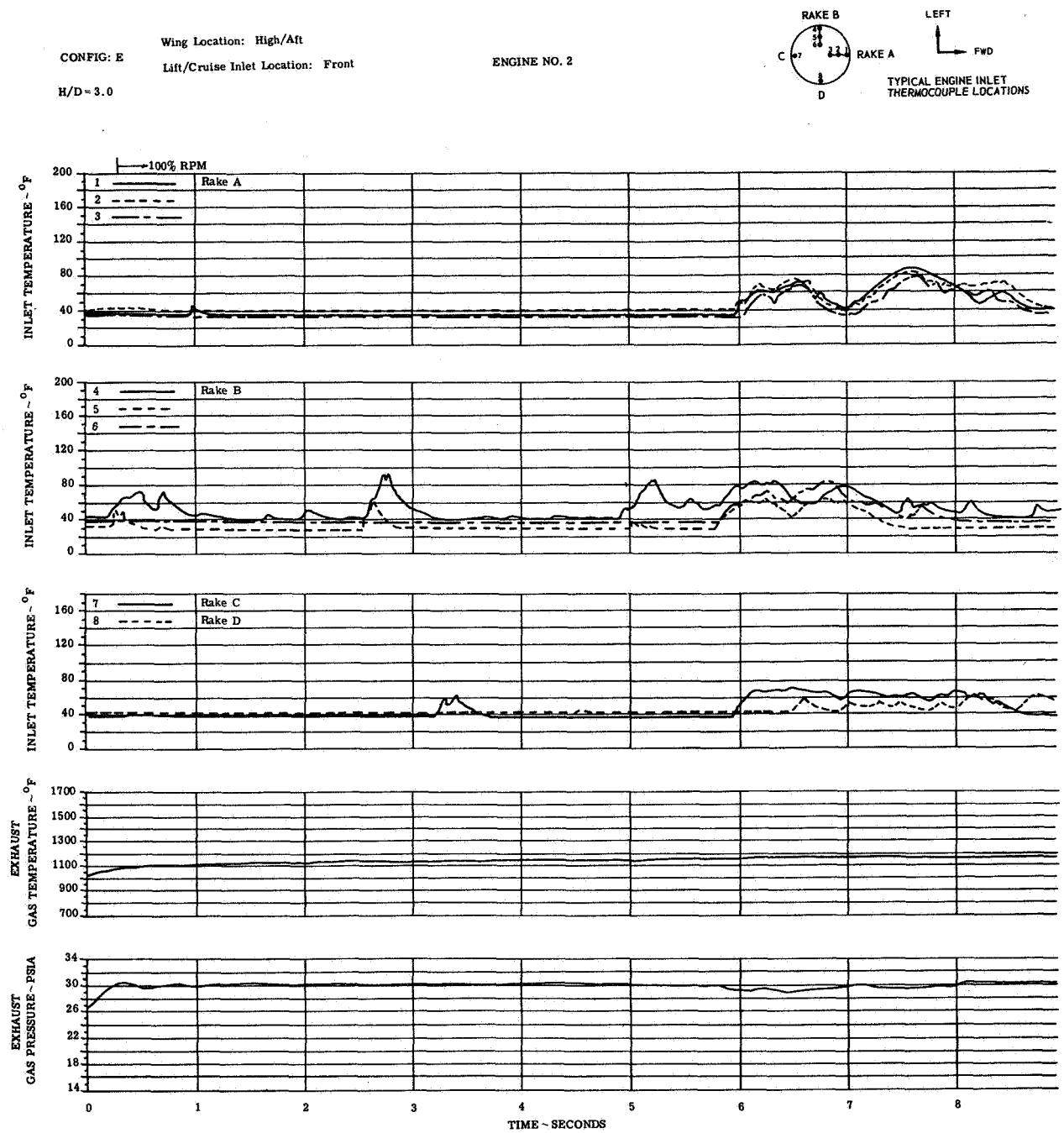

FIGURE 14(b). ENGINE TEMPERATURE AND PRESSURE TRANSIENTS

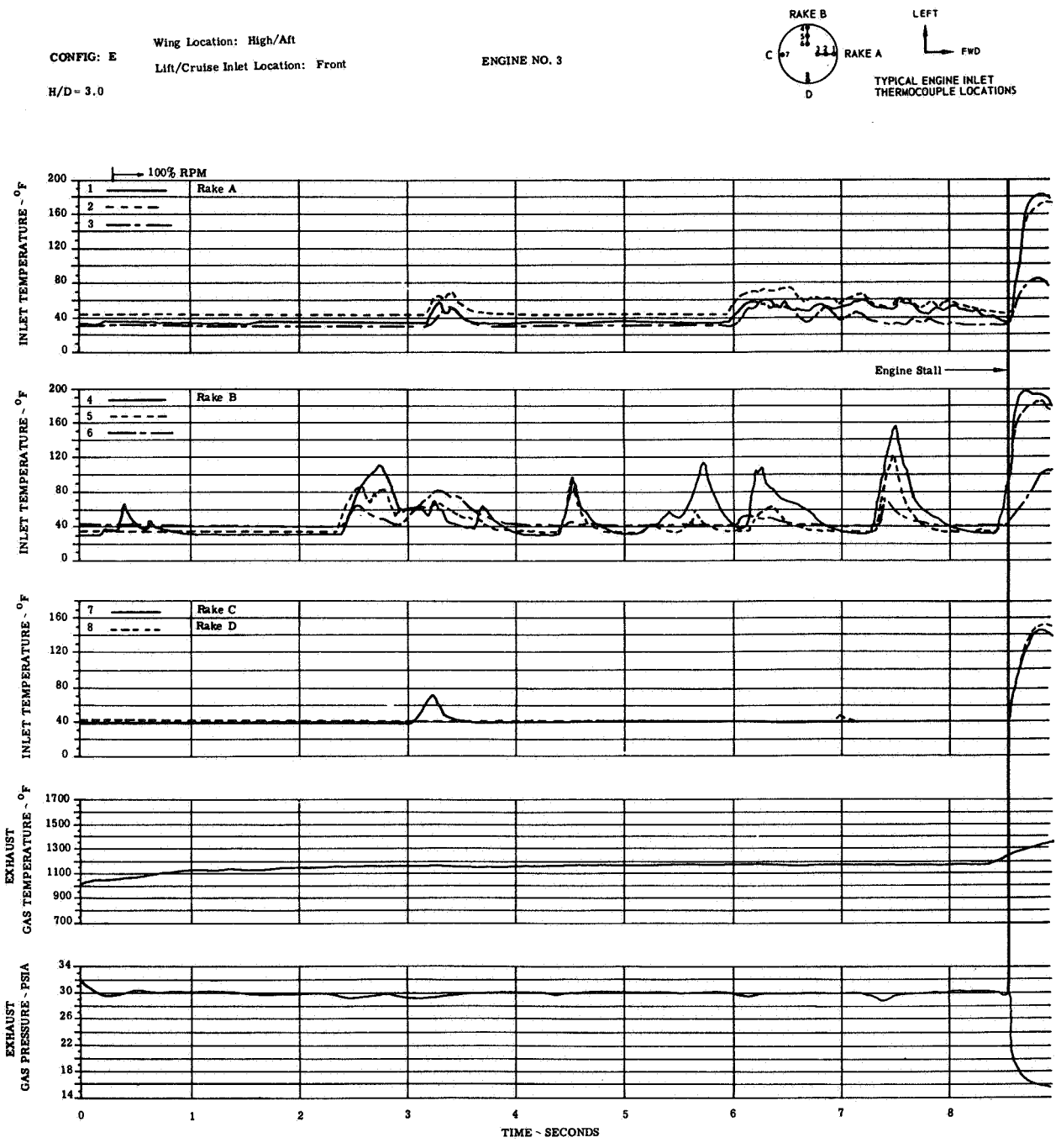

FIGURE 14(c). ENGINE TEMPERATURE AND PRESSURE TRANSIENTS

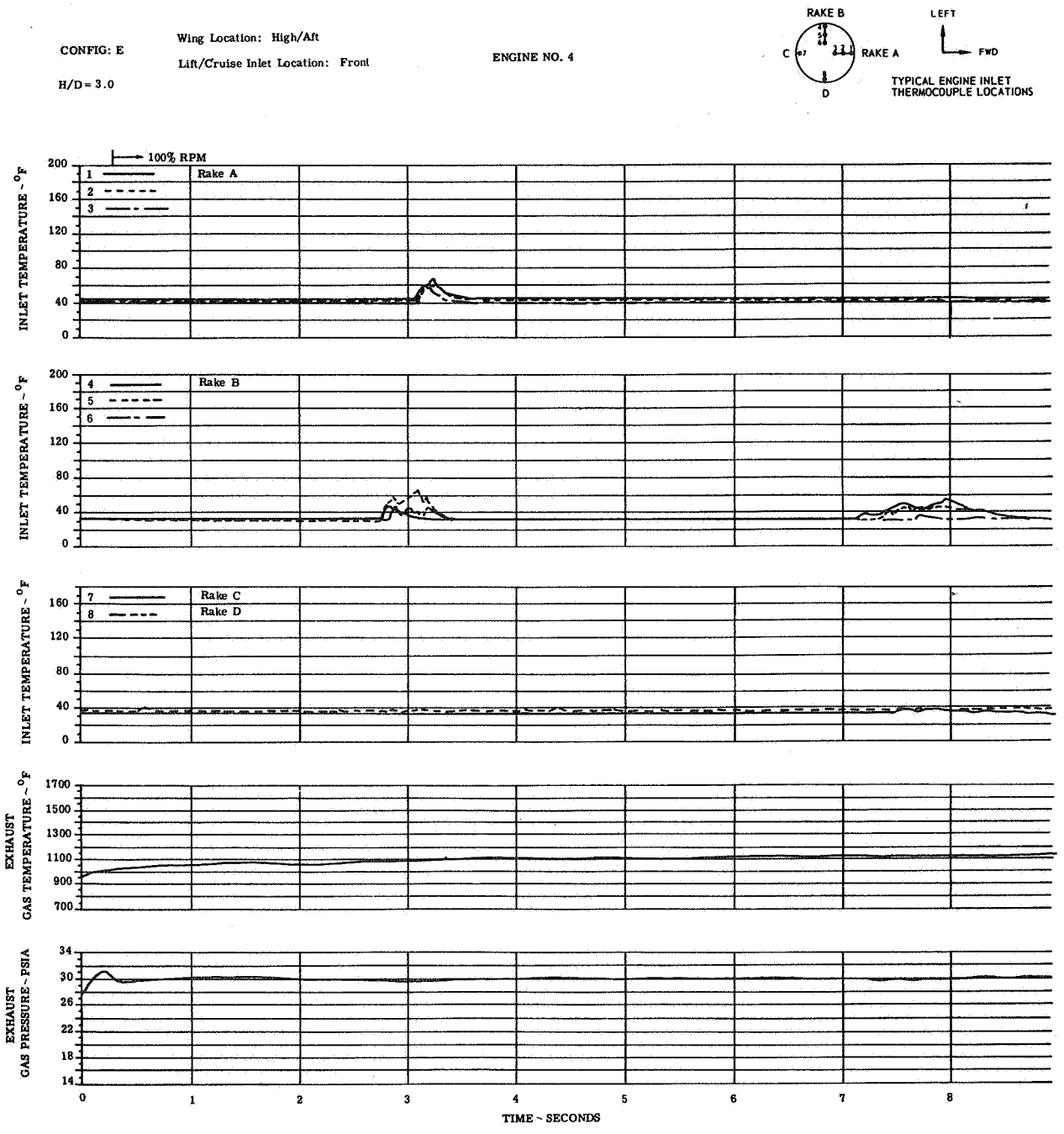

FIGURE 14(d). ENGINE TEMPERATURE AND PRESSURE TRANSIENTS

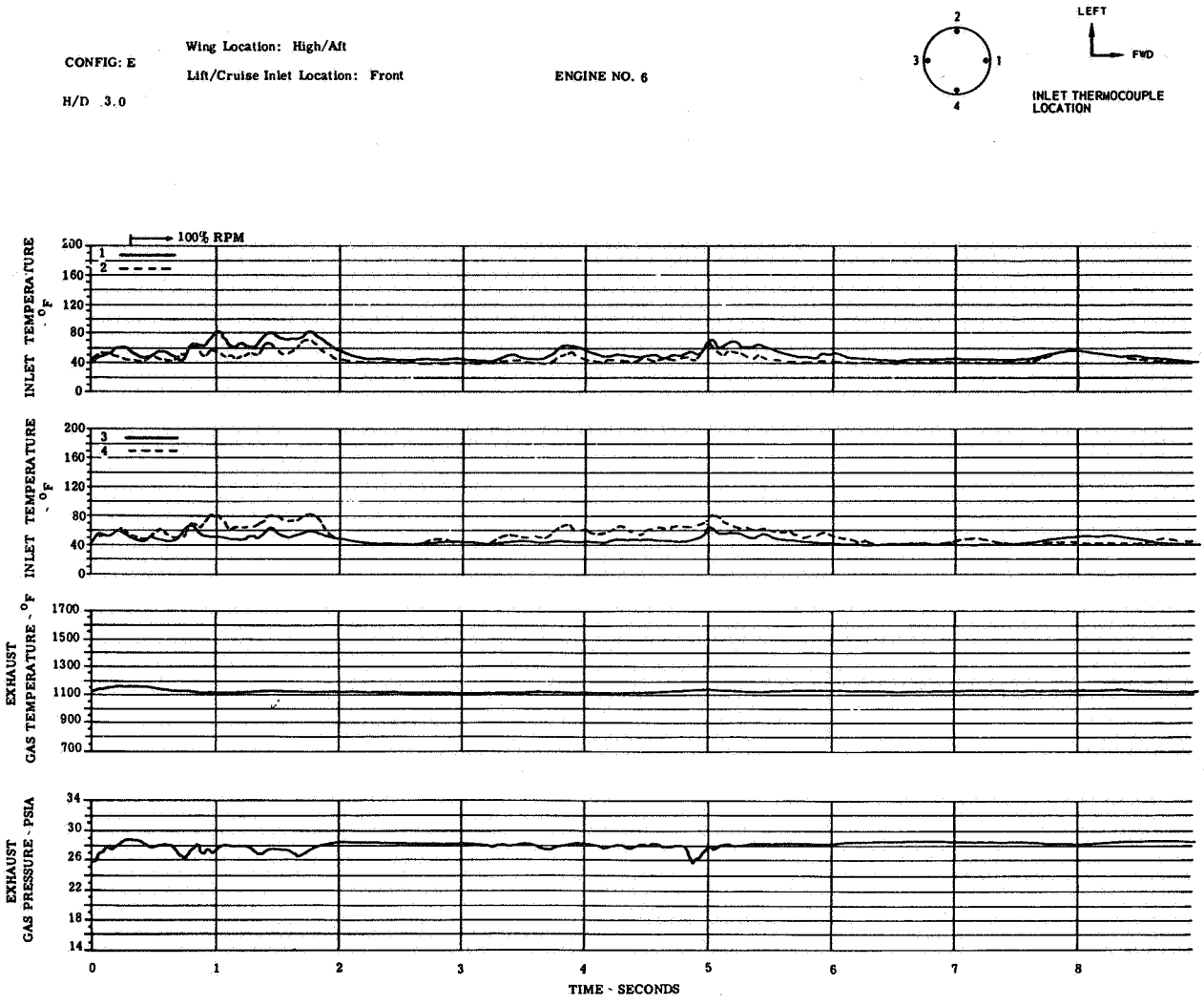

FIGURE 14(e). ENGINE TEMPERATURE AND PRESSURE TRANSIENTS

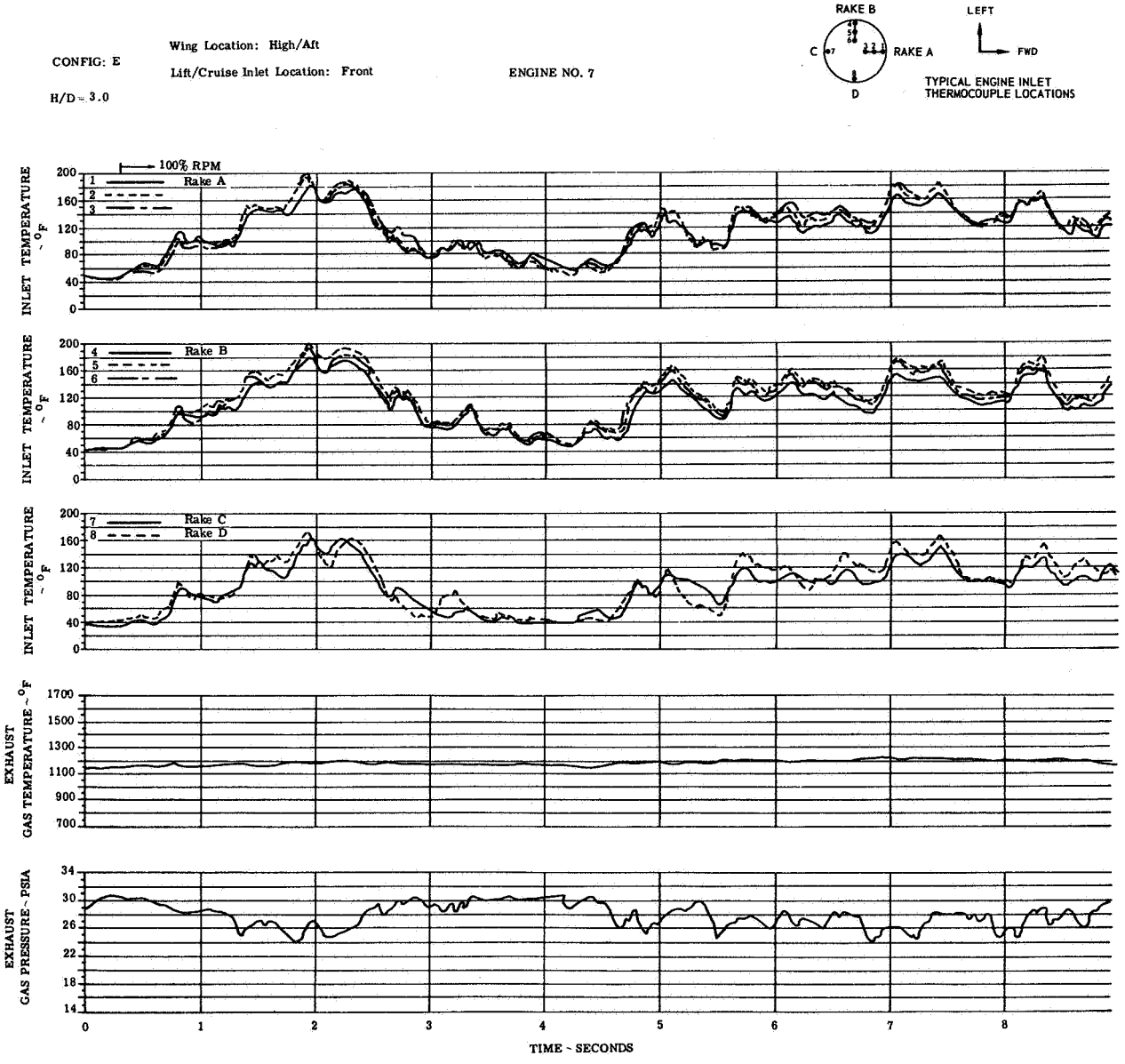

FIGURE 14(f). ENGINE TEMPERATURE AND PRESSURE TRANSIENTS

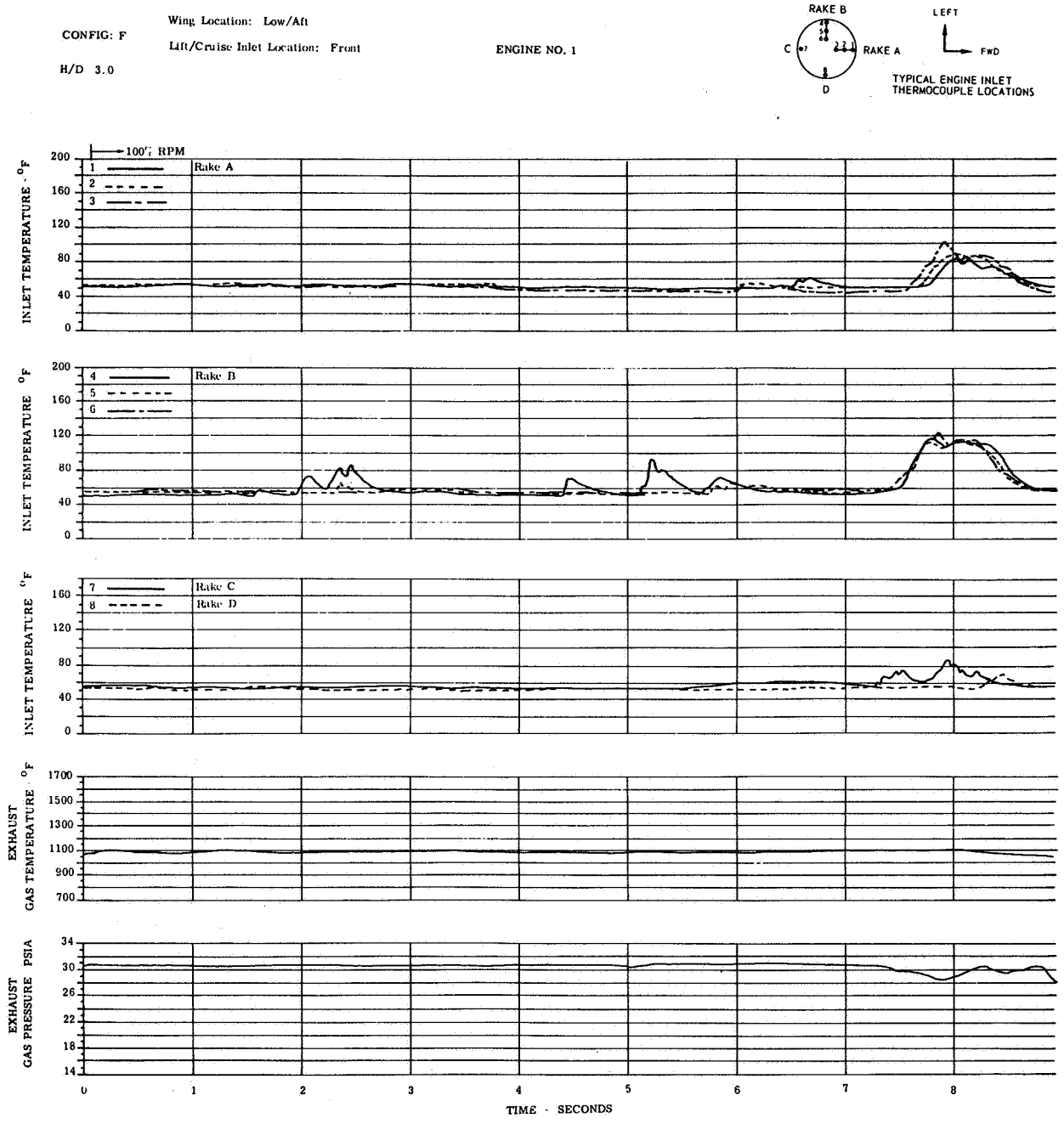

FIGURE 15(a). ENGINE TEMPERATURE AND PRESSURE TRANSIENTS

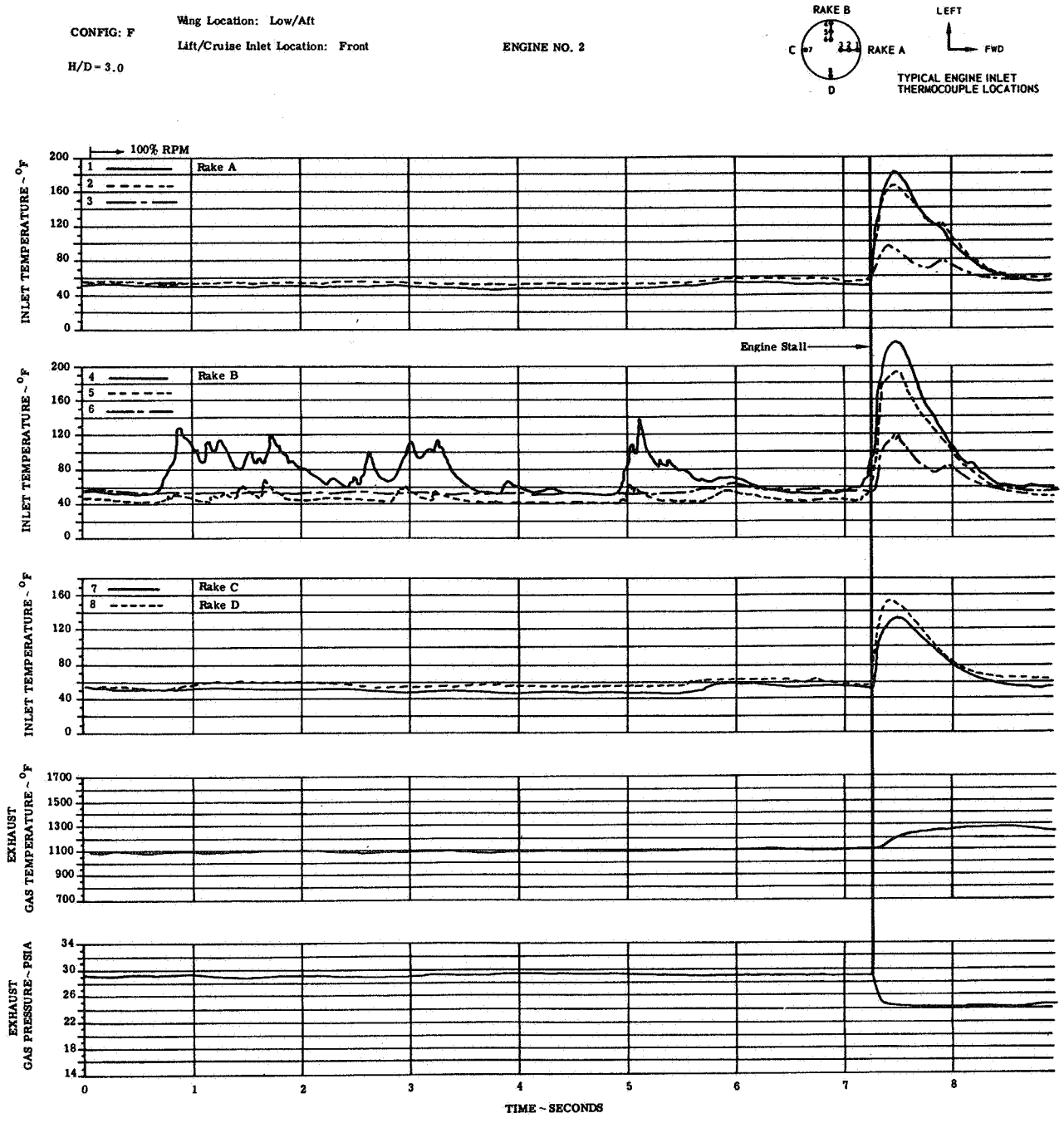

FIGURE 15(b). ENGINE TEMPERATURE AND PRESSURE TRANSIENTS

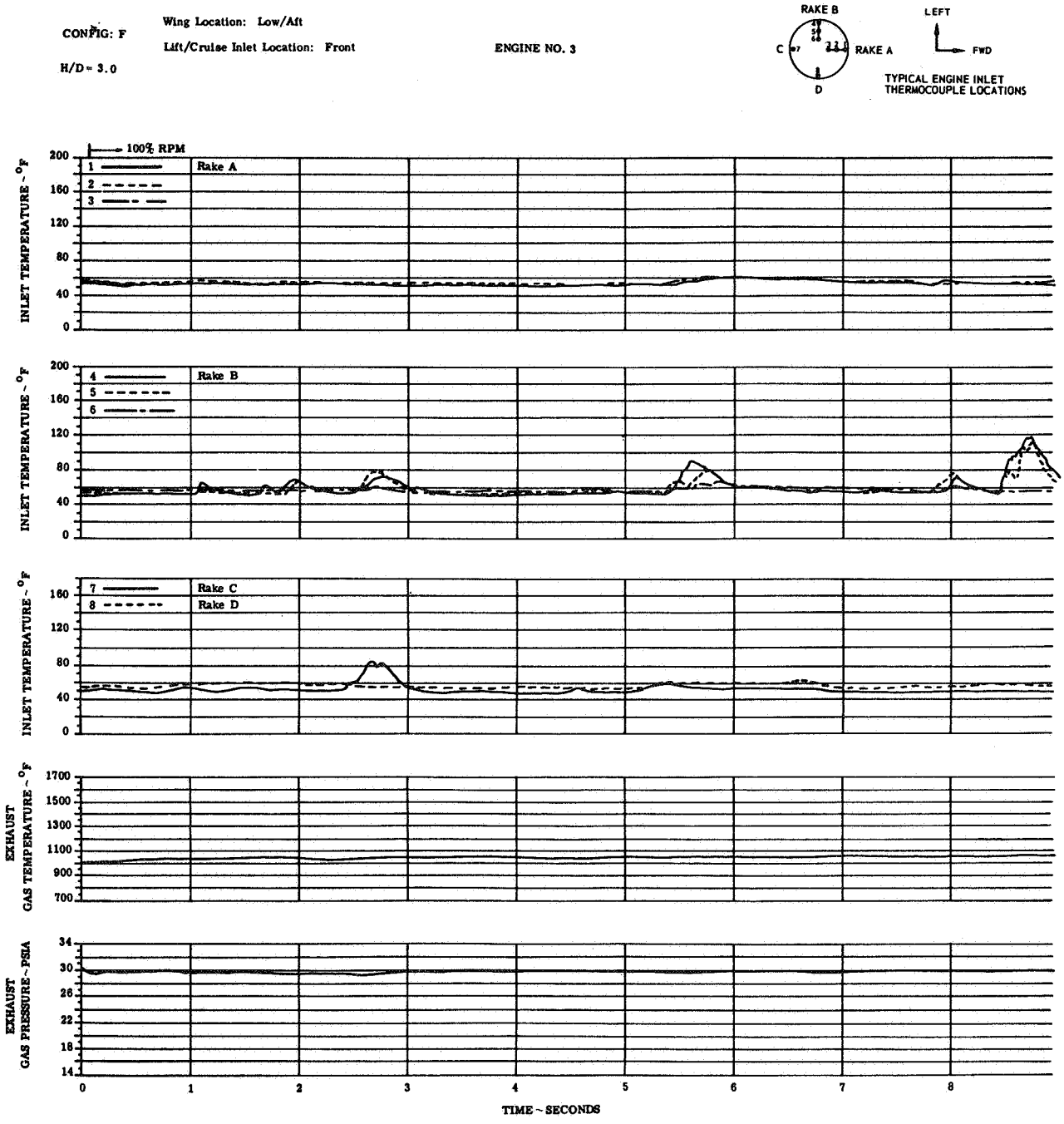

FIGURE 15(c). ENGINE TEMPERATURE AND PRESSURE TRANSIENTS

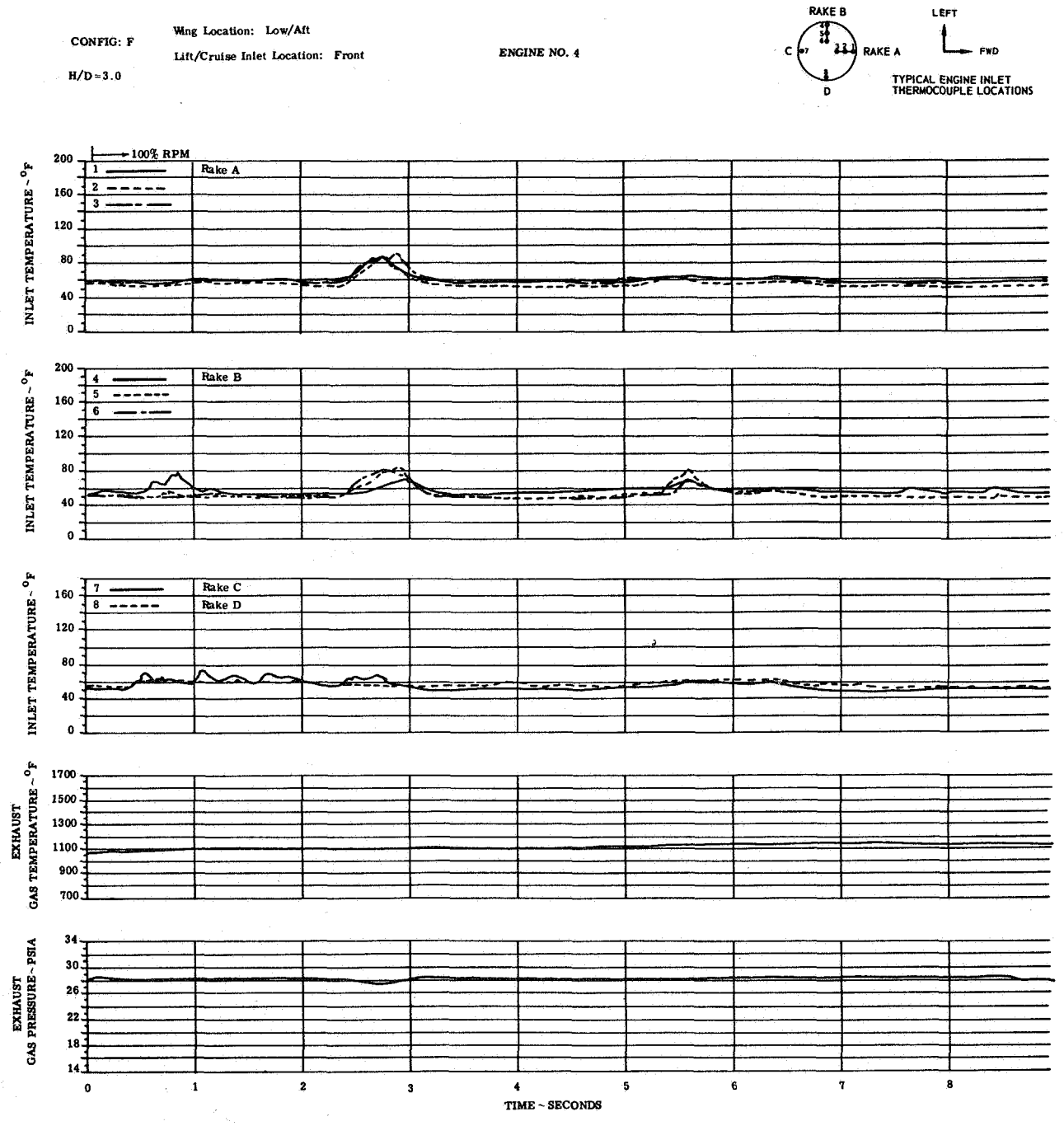

FIGURE 15(d). ENGINE TEMPERATURE AND PRESSURE TRANSIENTS

CONFIG: F

Wing Location: Low/Aft

Lift/Cruise Inlet Location: Front

H/D = 3.0

ENGINE NO. 6

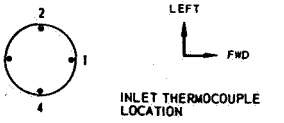

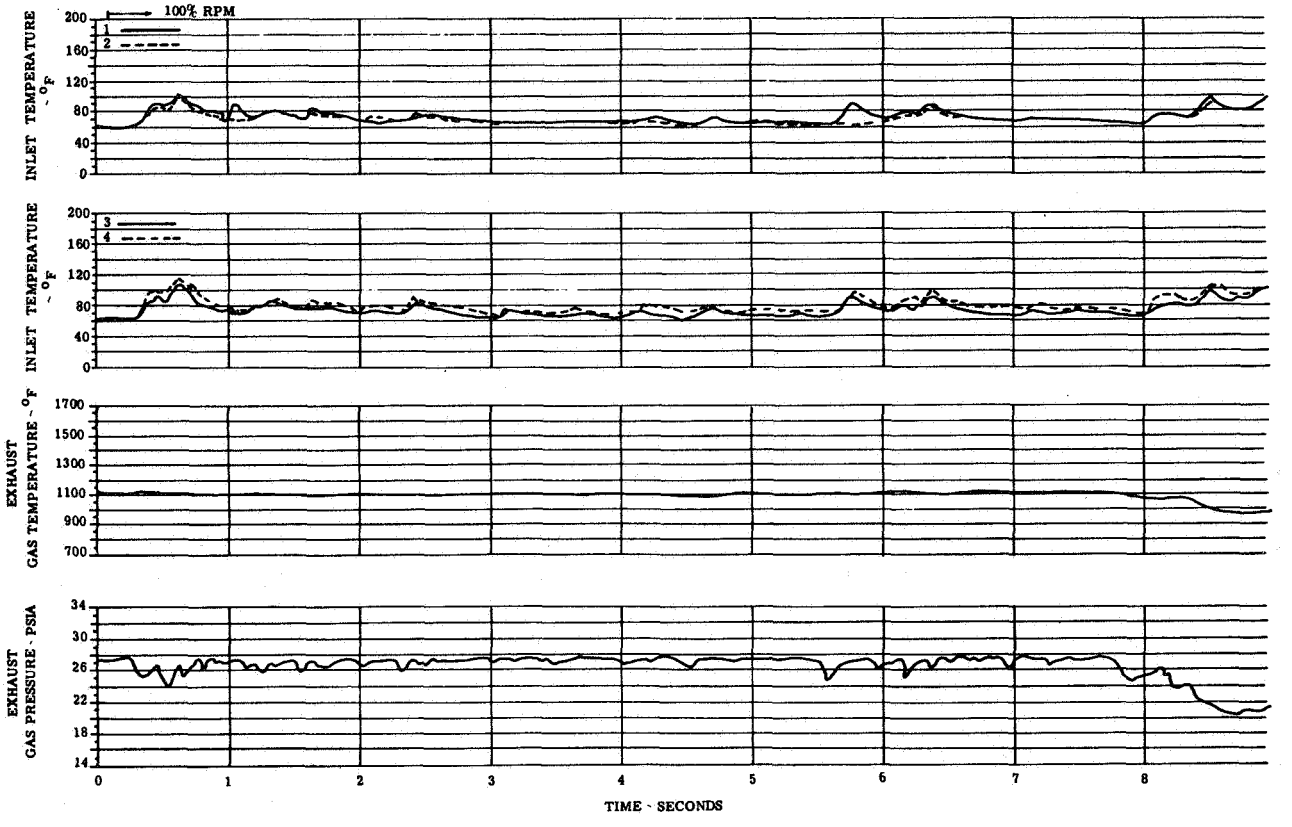

FIGURE 15(e). ENGINE TEMPERATURE AND PRESSURE TRANSIENTS

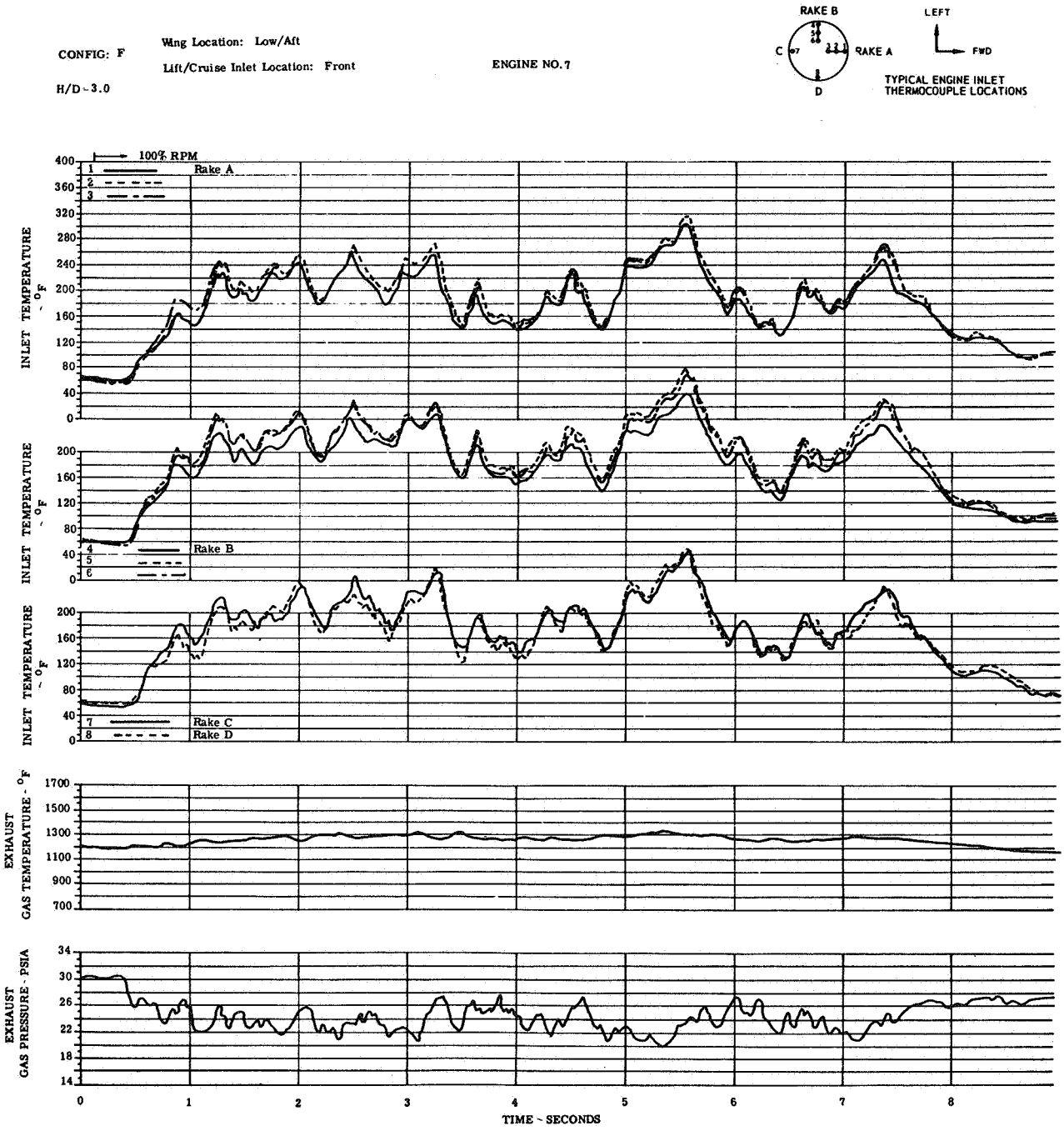

FIGURE 15(f). ENGINE TEMPERATURE AND PRESSURE TRANSIENTS

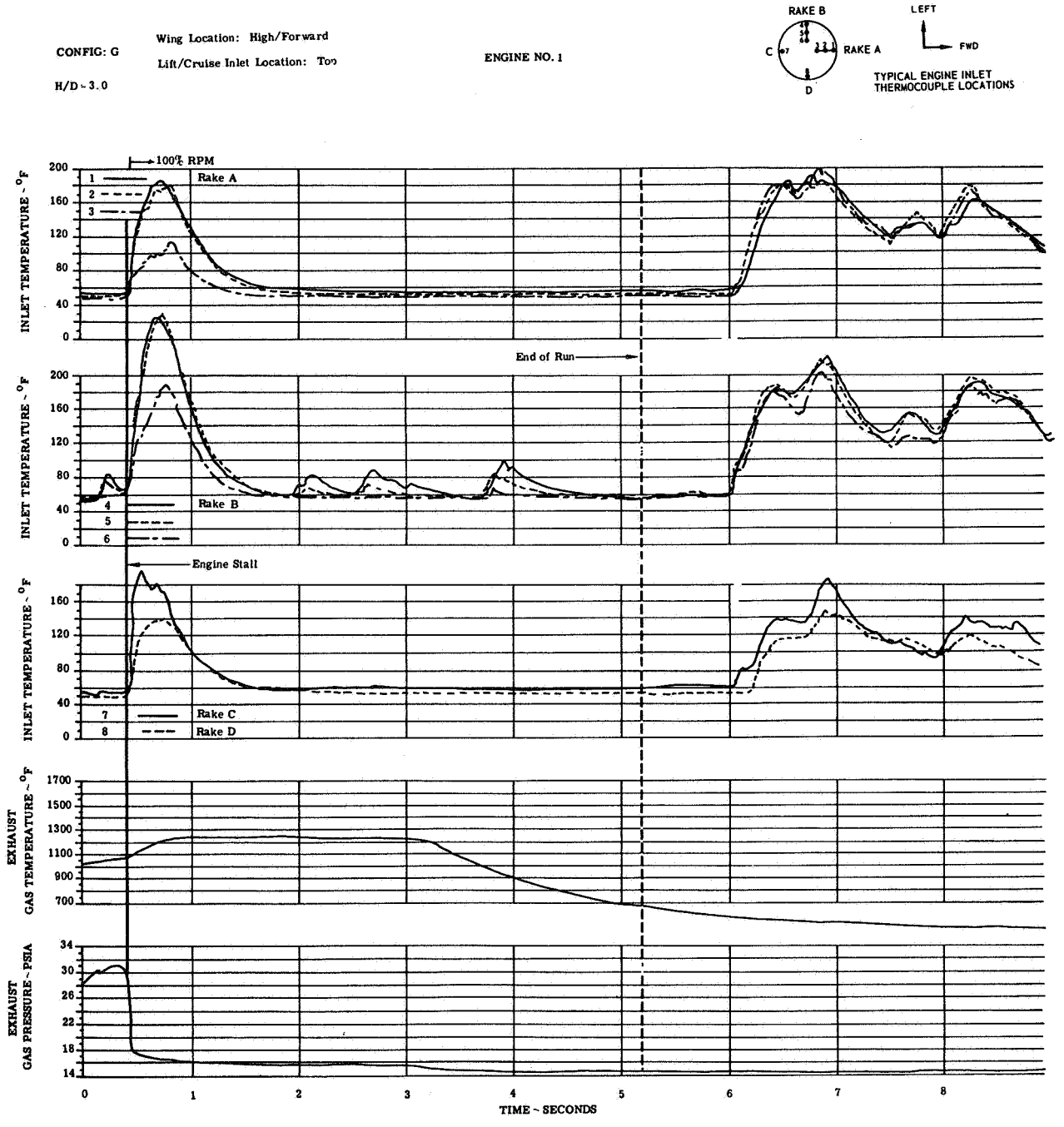

FIGURE 16(a). ENGINE TEMPERATURE AND PRESSURE TRANSIENTS

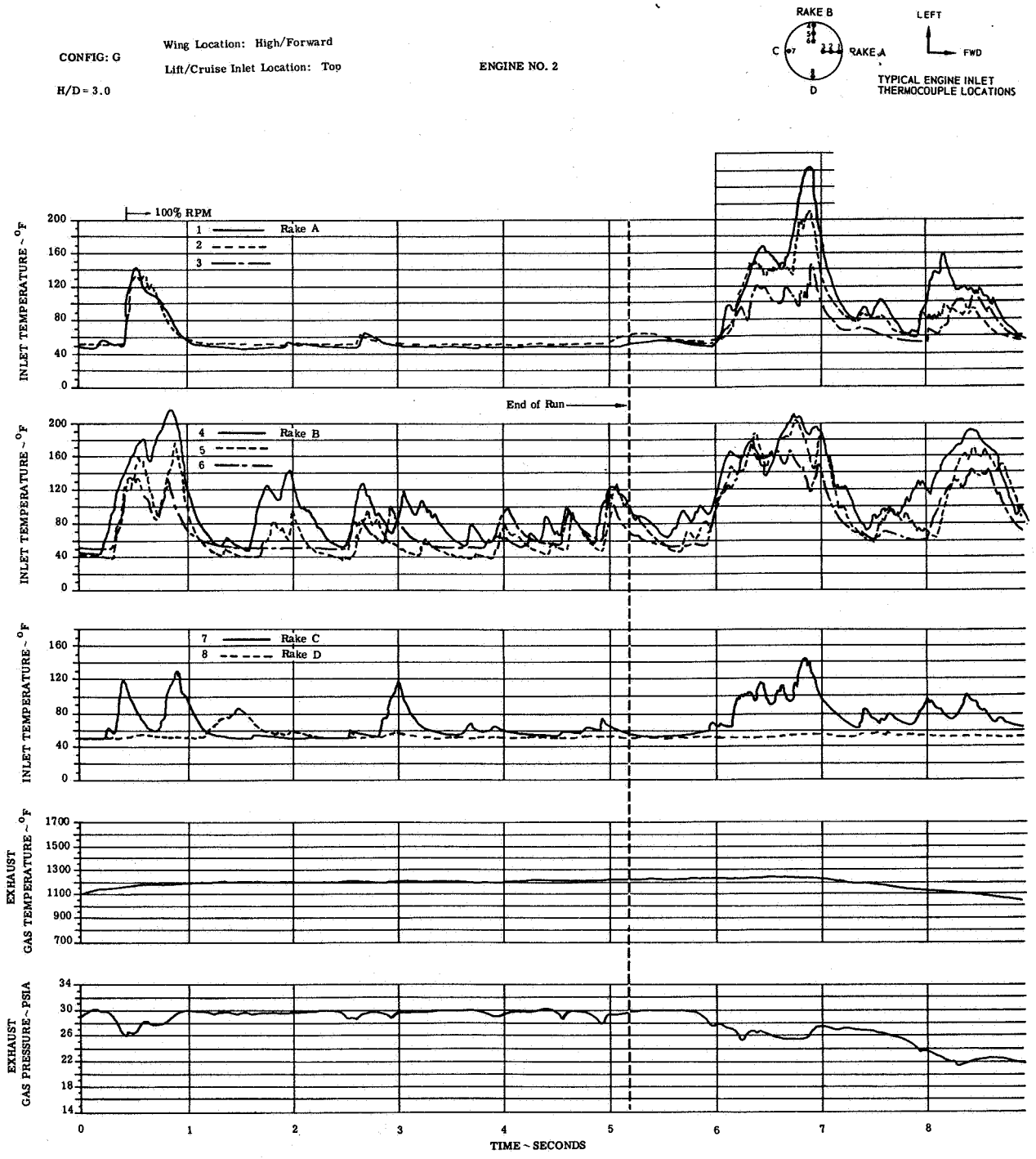

FIGURE 16(b). ENGINE TEMPERATURE AND PRESSURE TRANSIENTS

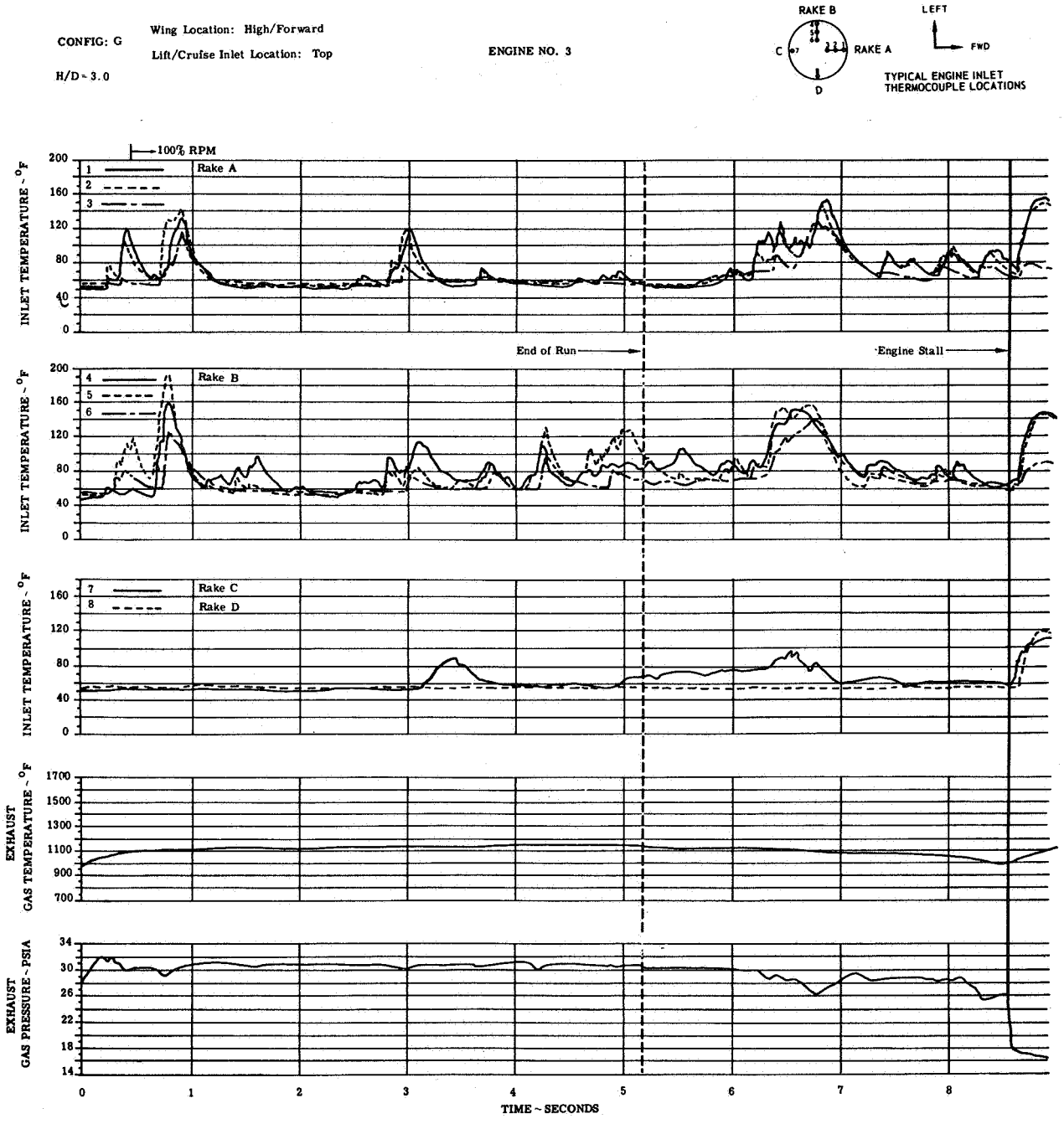

FIGURE 16(c). ENGINE TEMPERATURE AND PRESSURE TRANSIENTS

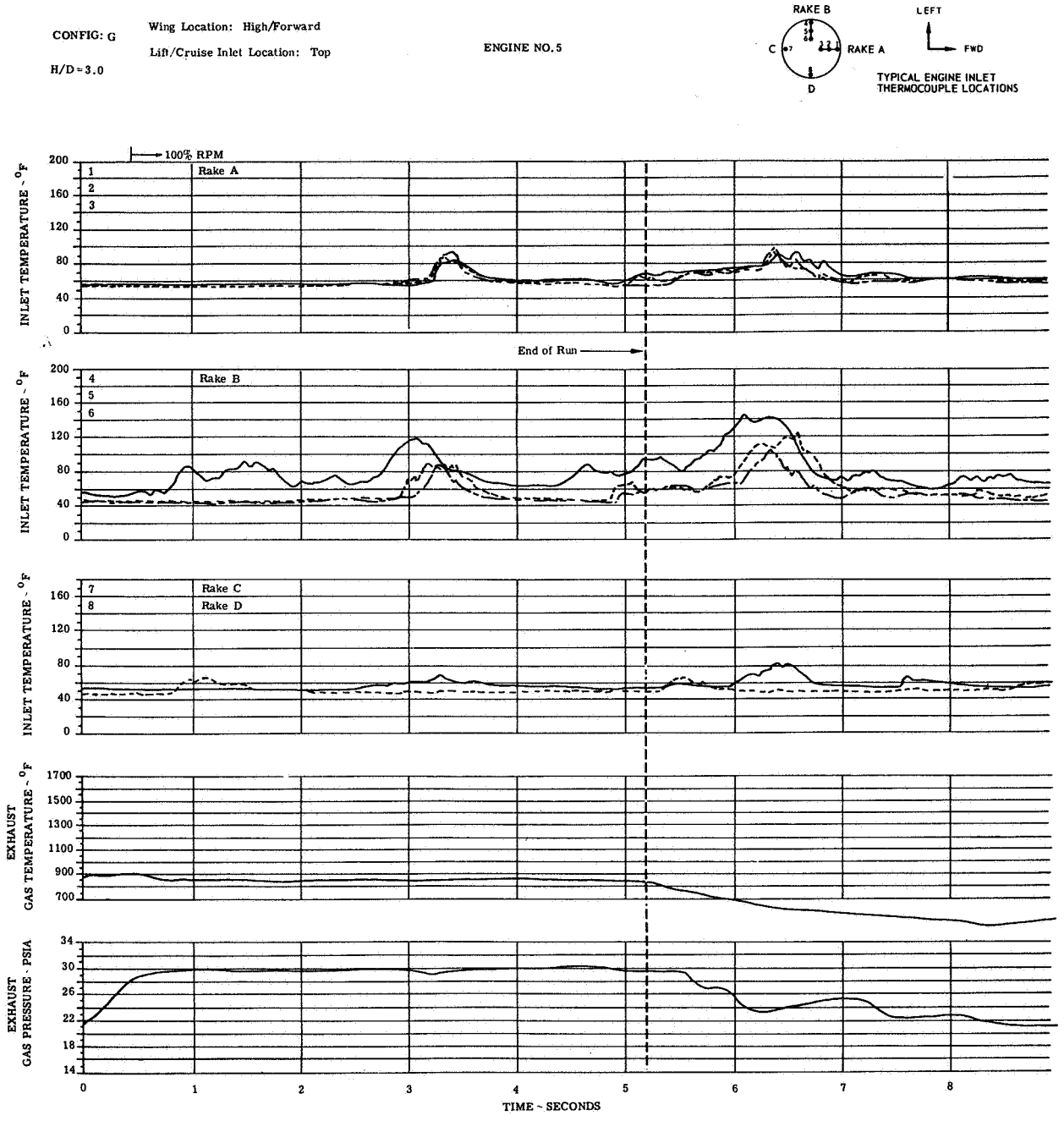

FIGURE 16(d). ENGINE TEMPERATURE AND PRESSURE TRANSIENTS

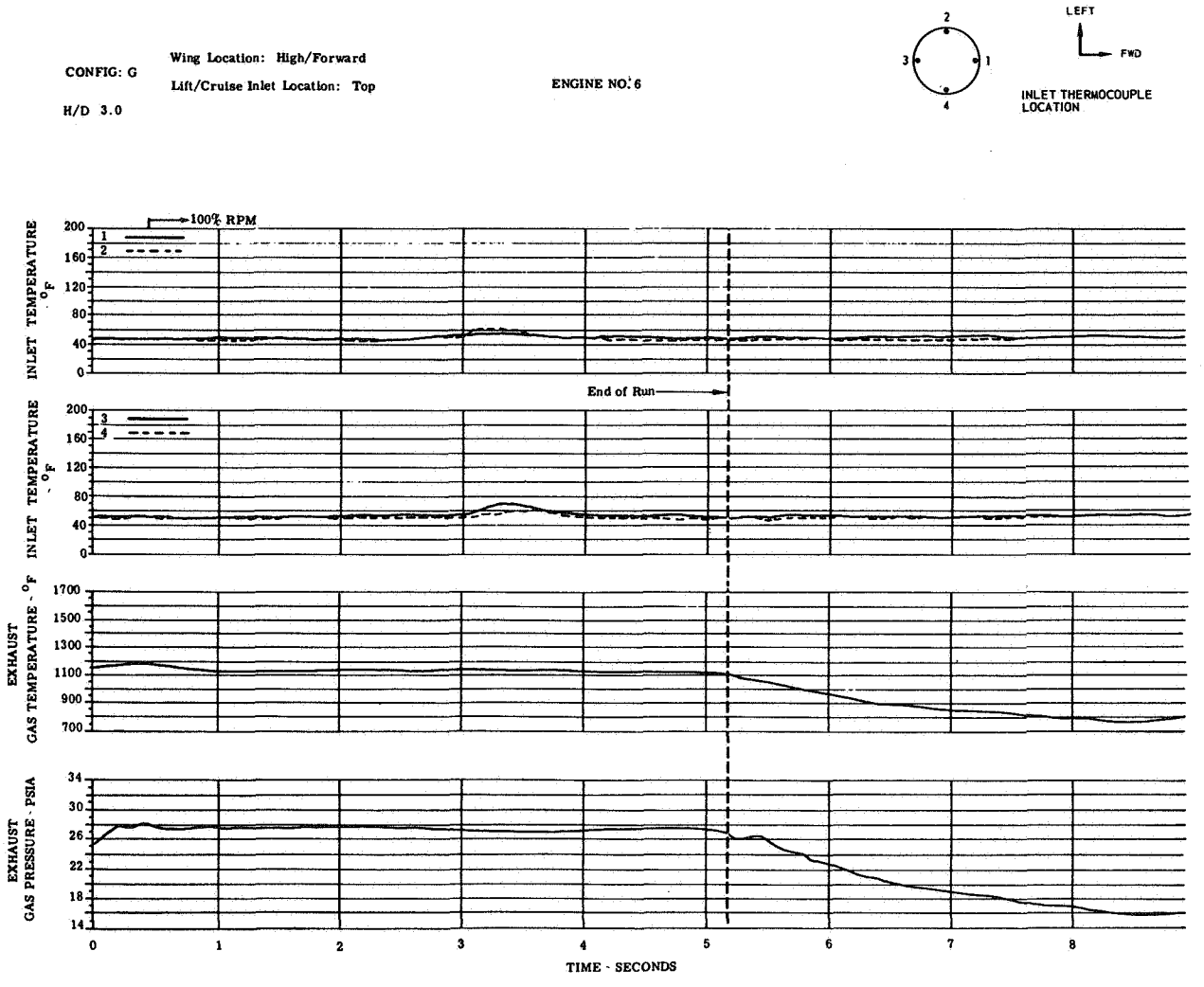

FIGURE 16(e). ENGINE TEMPERATURE AND PRESSURE TRANSIENTS

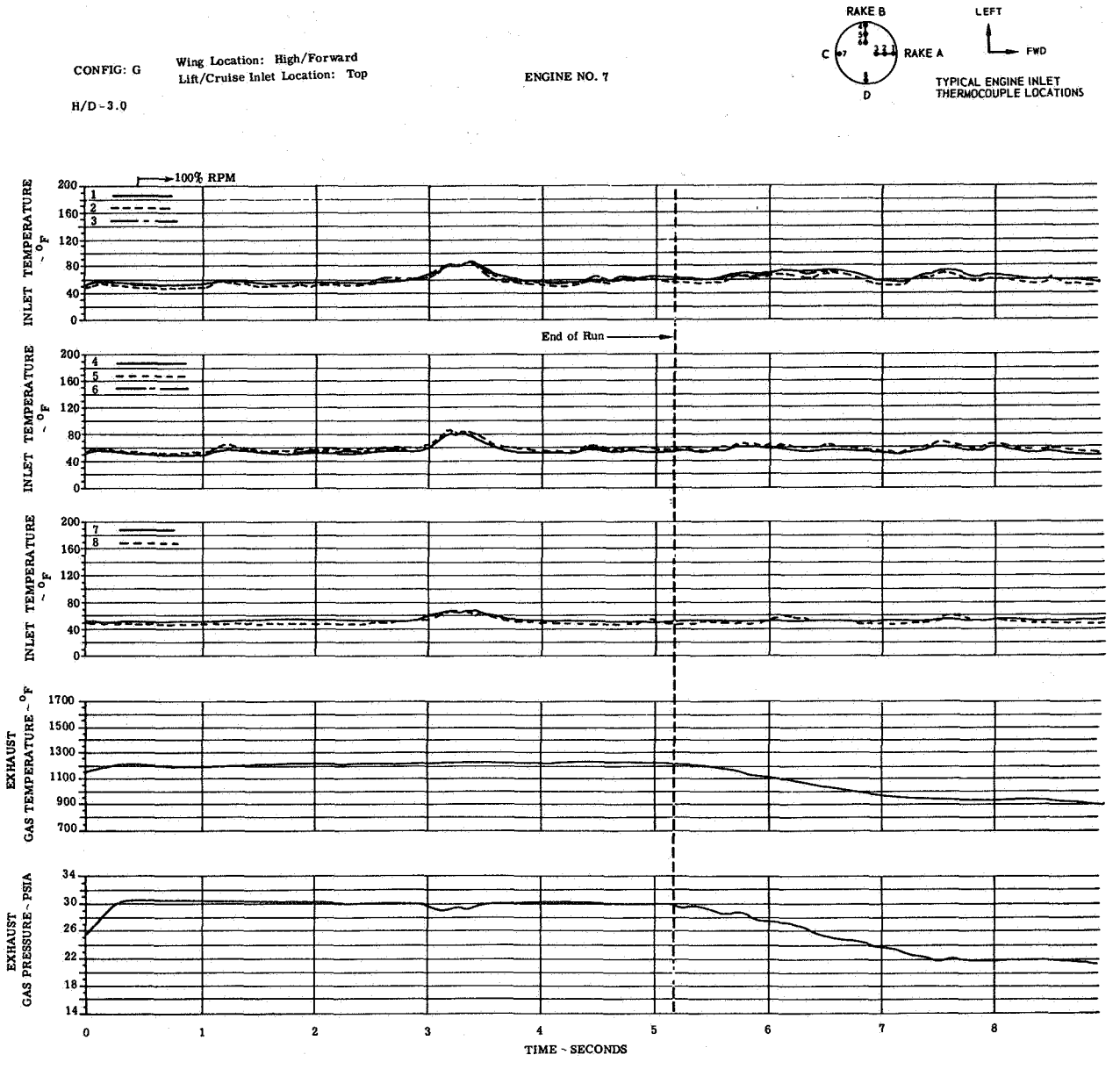

FIGURE 16(f). ENGINE TEMPERATURE AND PRESSURE TRANSIENTS

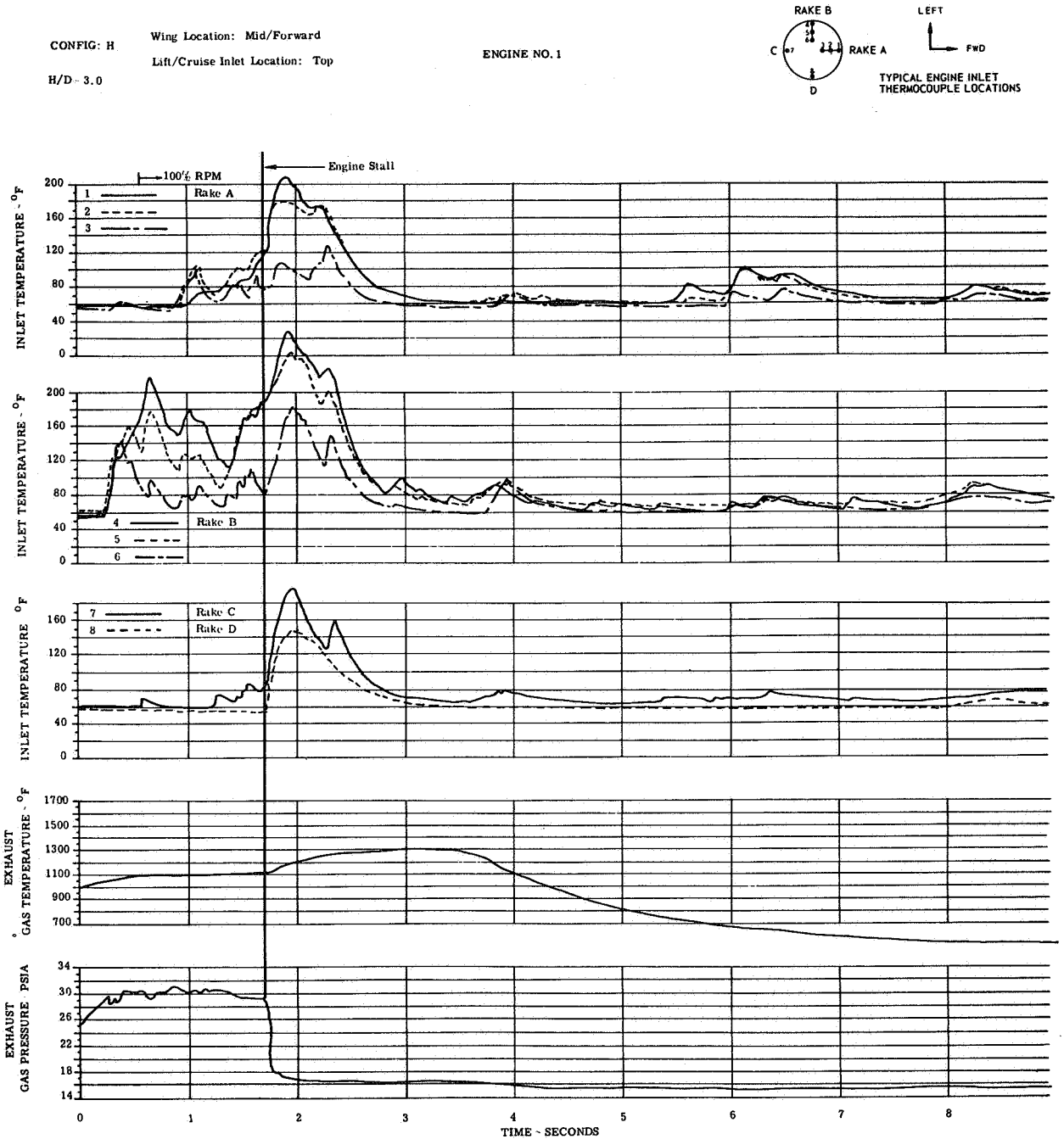

FIGURE 17(a). ENGINE TEMPERATURE AND PRESSURE TRANSIENTS

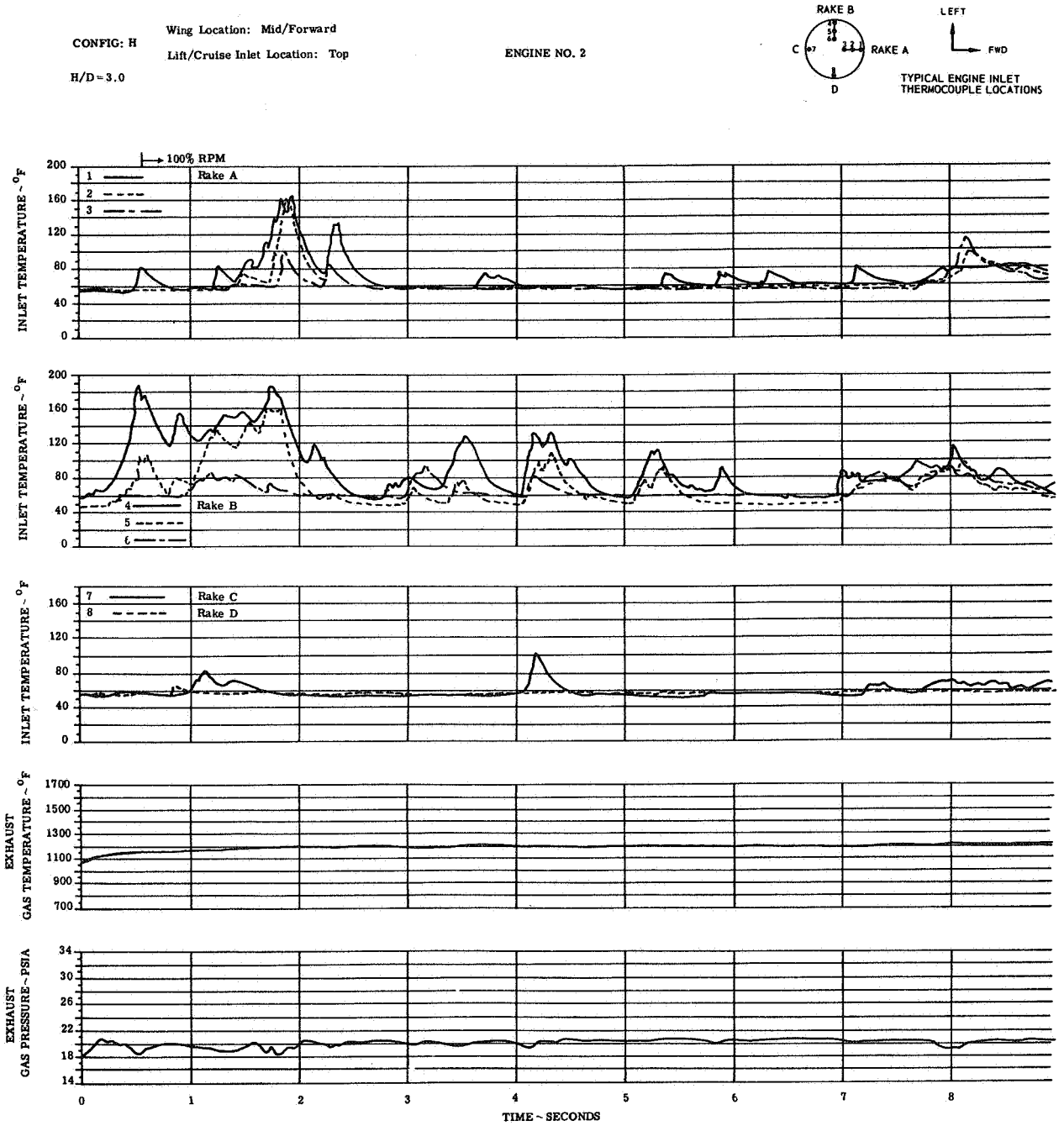

FIGURE 17(b). ENGINE TEMPERATURE AND PRESSURE TRANSIENTS

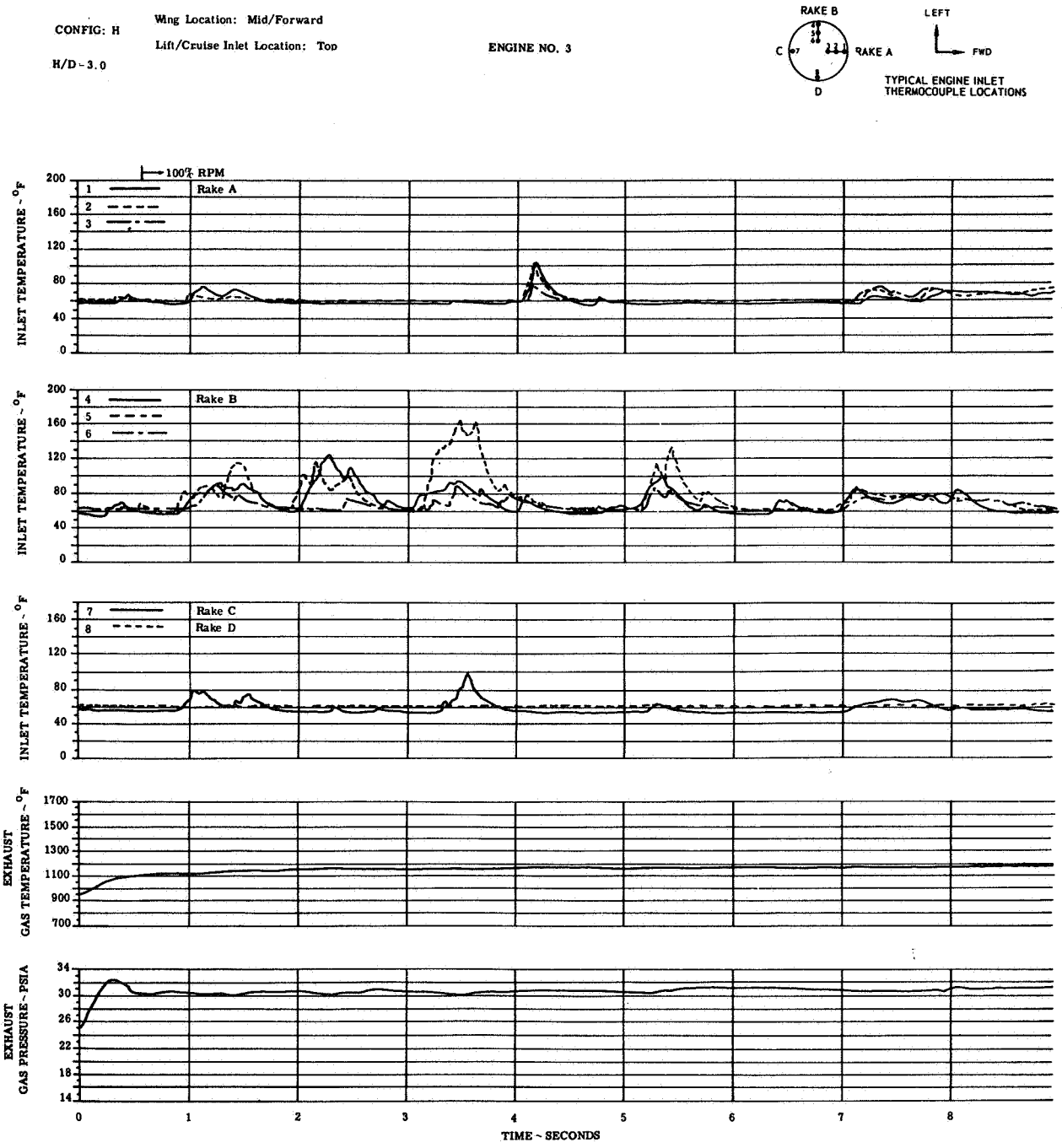

FIGURE 17(c). ENGINE TEMPERATURE AND PRESSURE TRANSIENTS

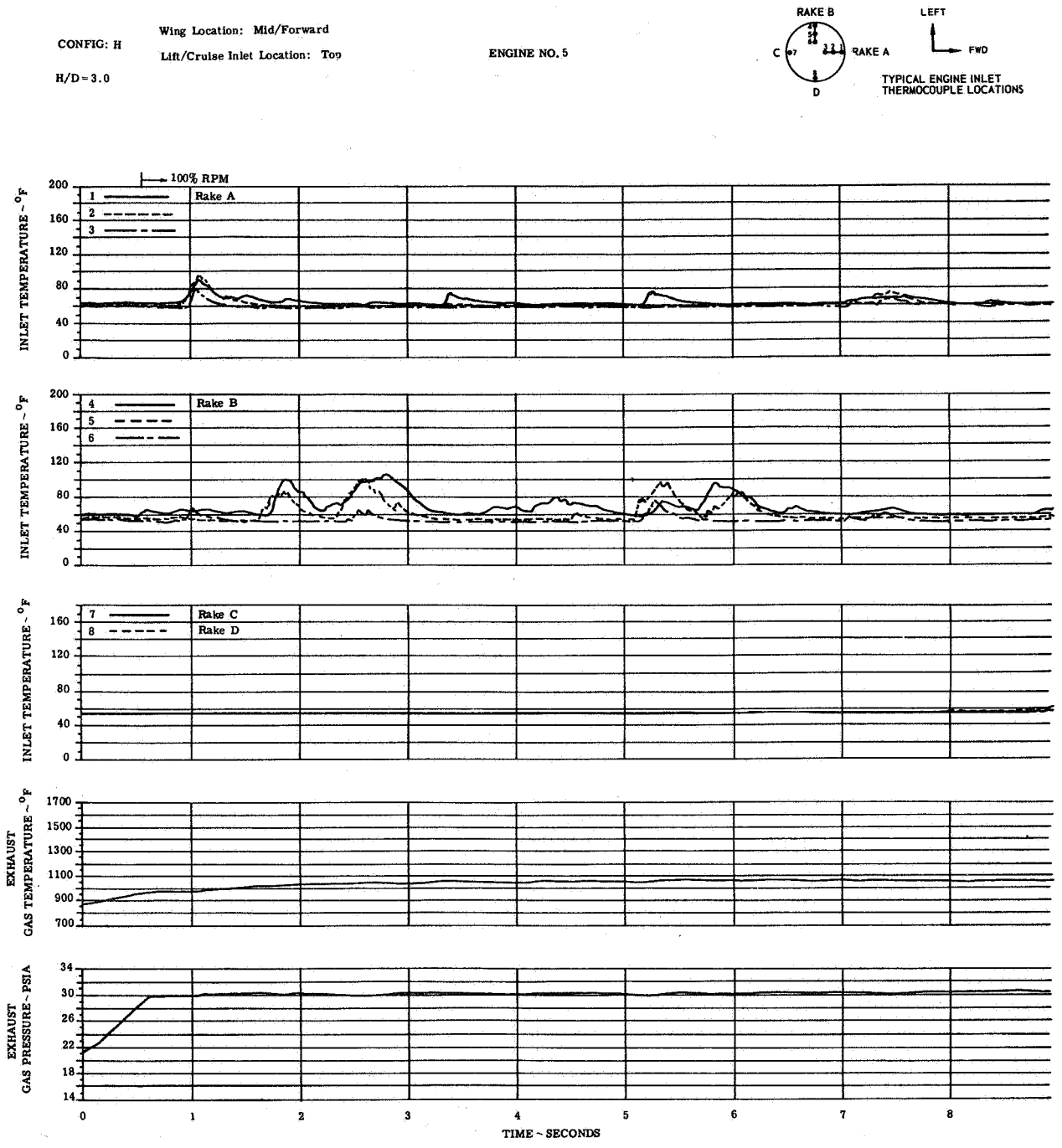

FIGURE 17(d). ENGINE TEMPERATURE AND PRESSURE TRANSIENTS

CONFIG: H

Wing Location: Mid/Forward

Lift/Cruise Inlet Location: Top

H/D - 3.0

ENGINE NO. 6

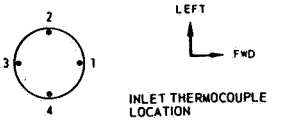

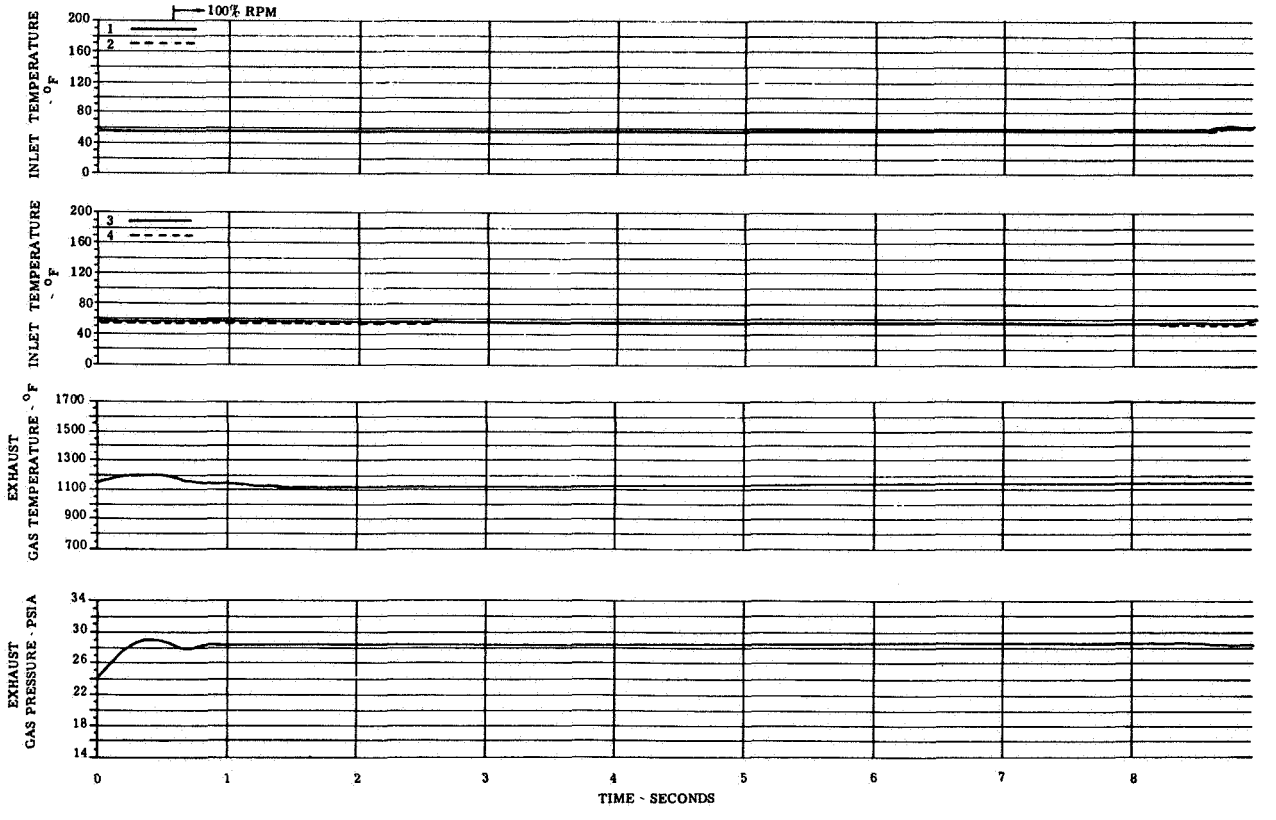

FIGURE 17(e). ENGINE TEMPERATURE AND PRESSURE TRANSIENTS

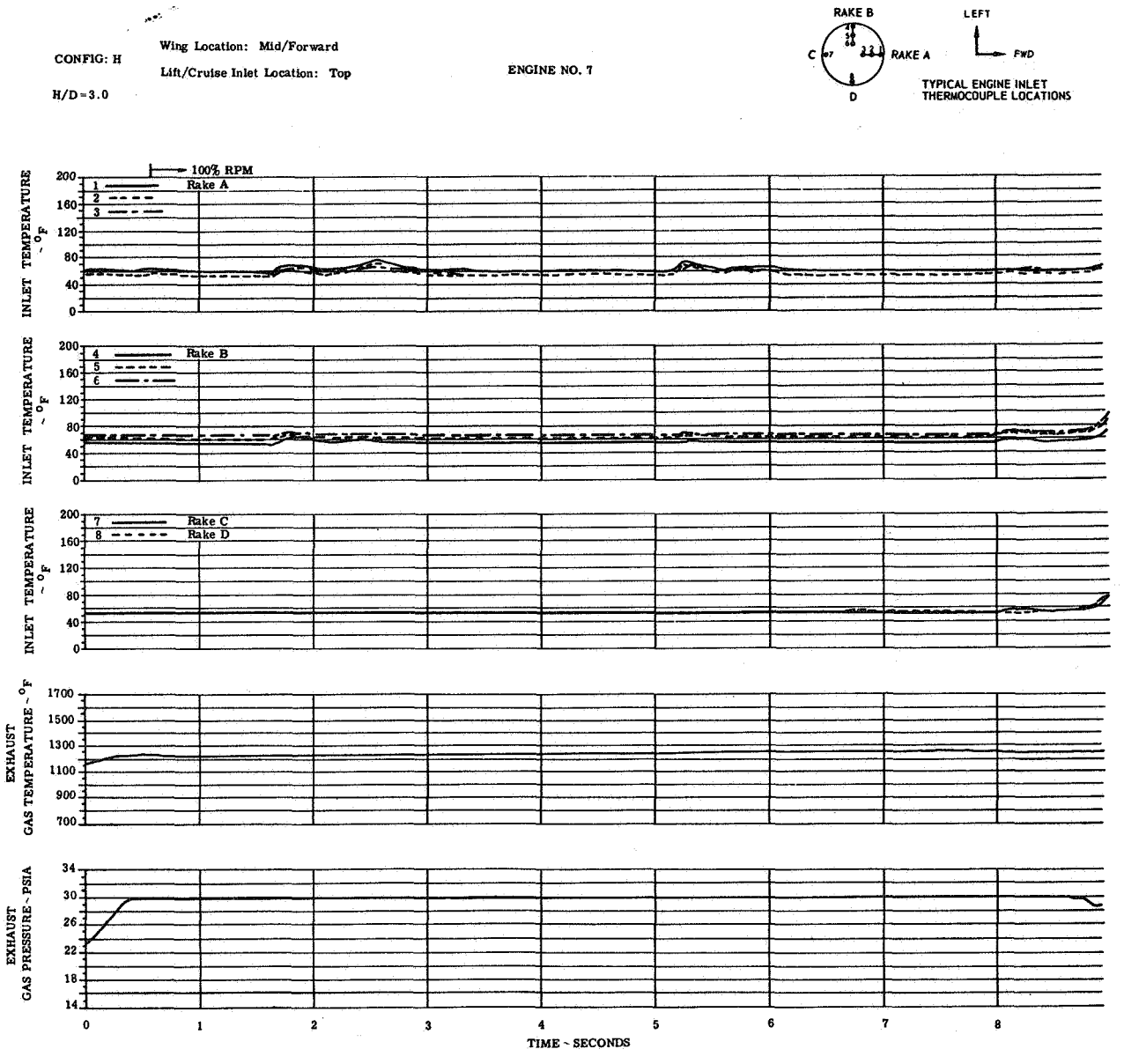

FIGURE 17(f). ENGINE TEMPERATURE AND PRESSURE TRANSIENTS

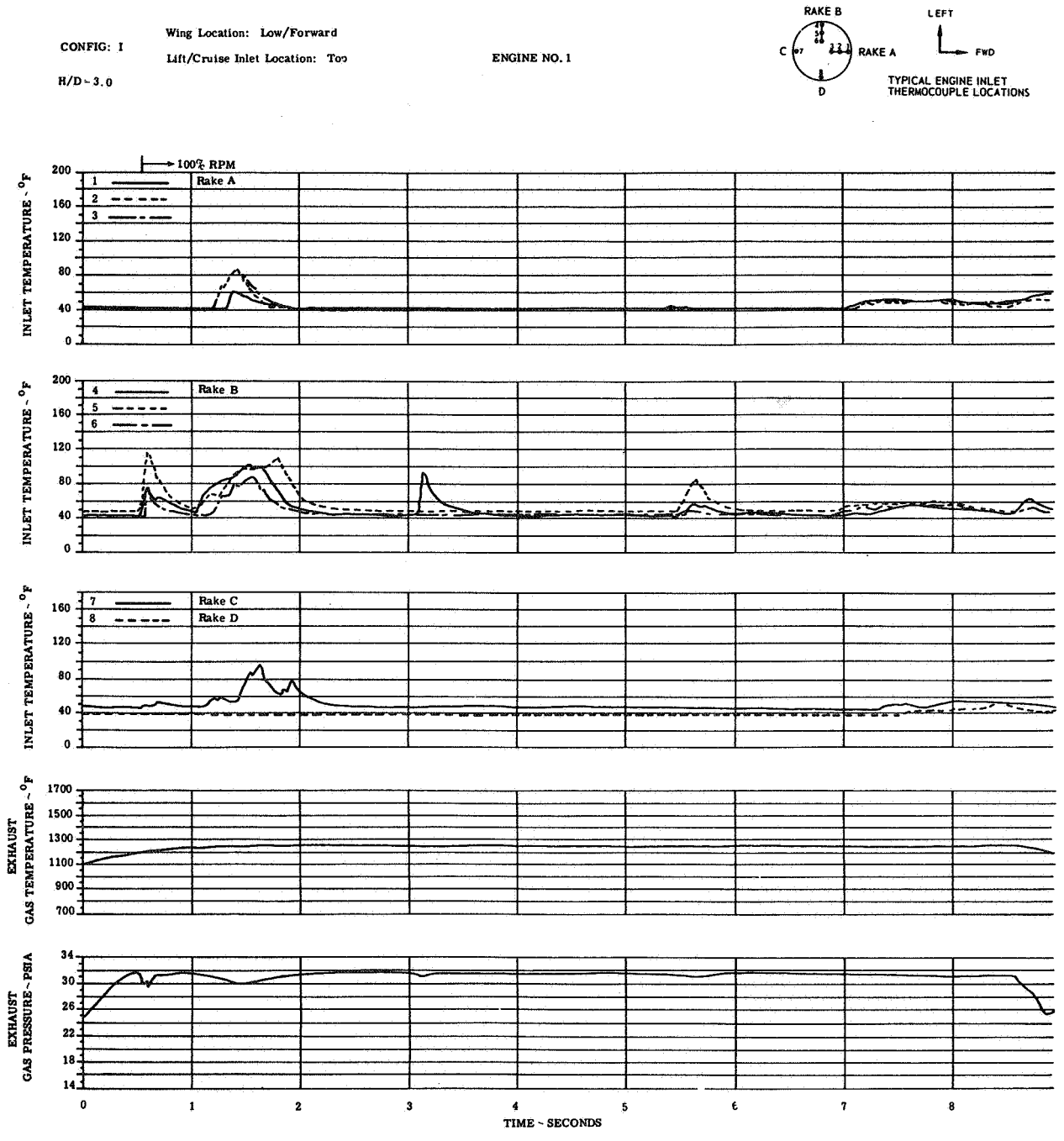

FIGURE 18(a). ENGINE TEMPERATURE AND PRESSURE TRANSIENTS

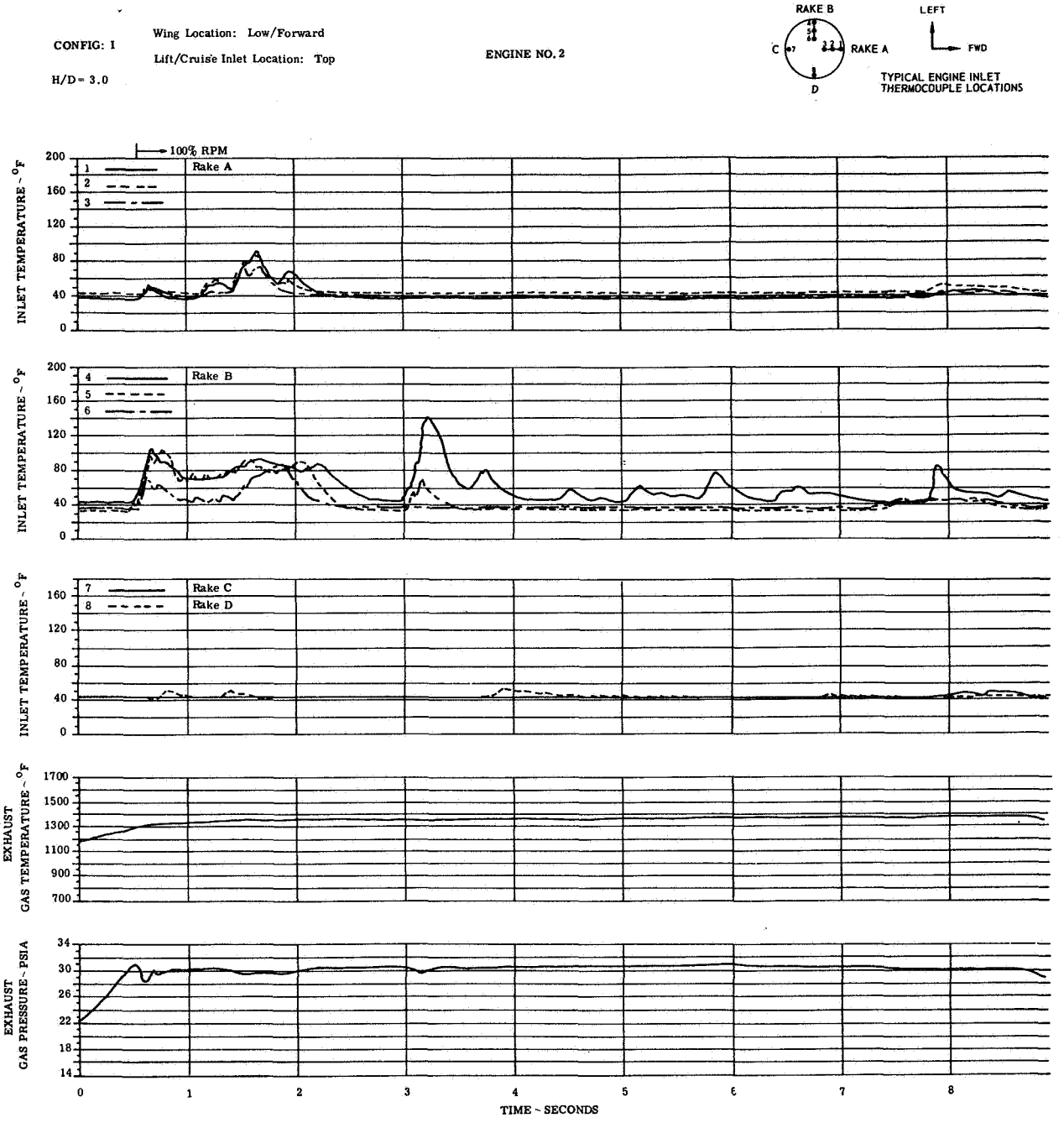

FIGURE 18(b). ENGINE TEMPERATURE AND PRESSURE TRANSIENTS

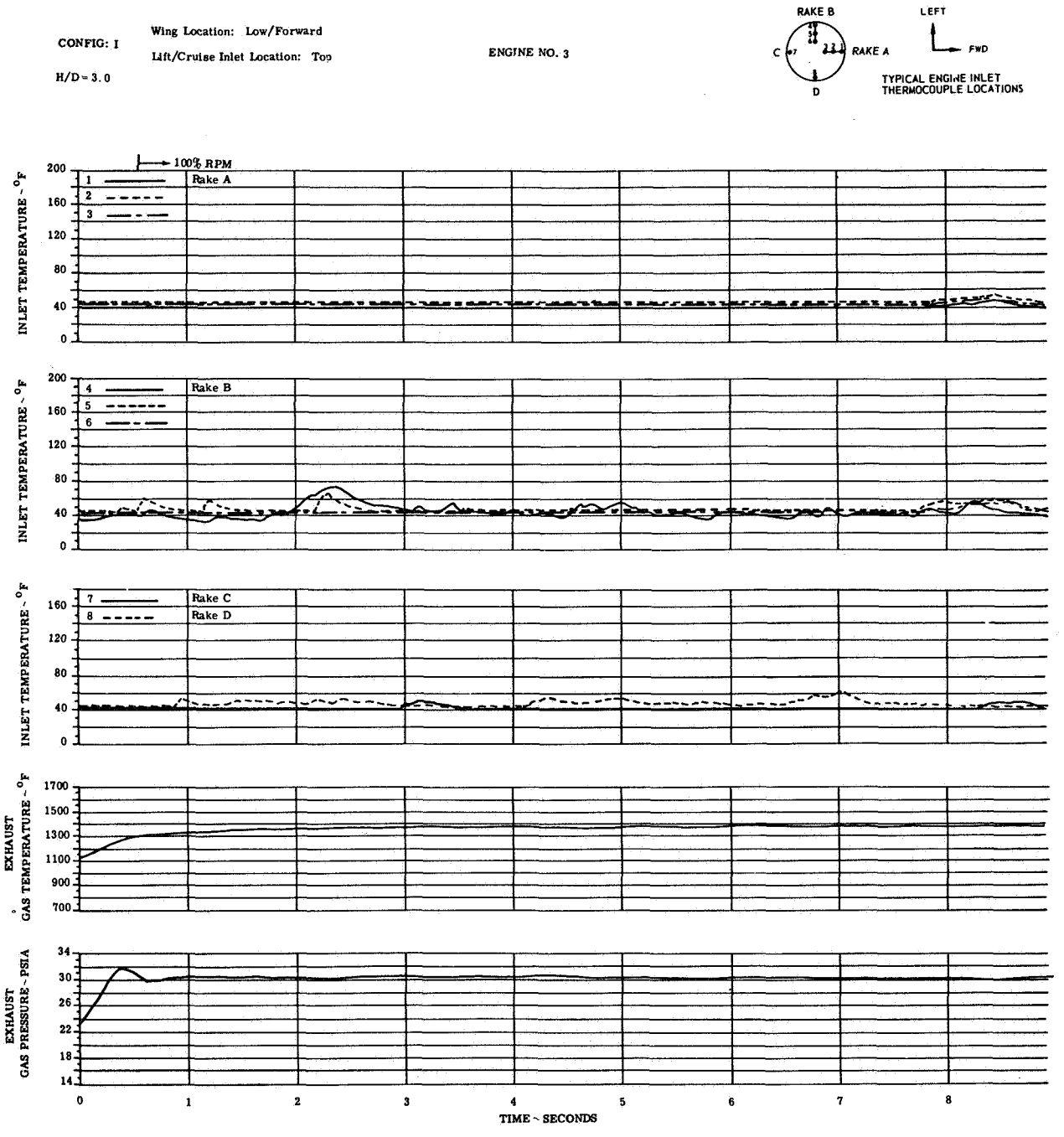

FIGURE 18(c). ENGINE TEMPERATURE AND PRESSURE TRANSIENTS

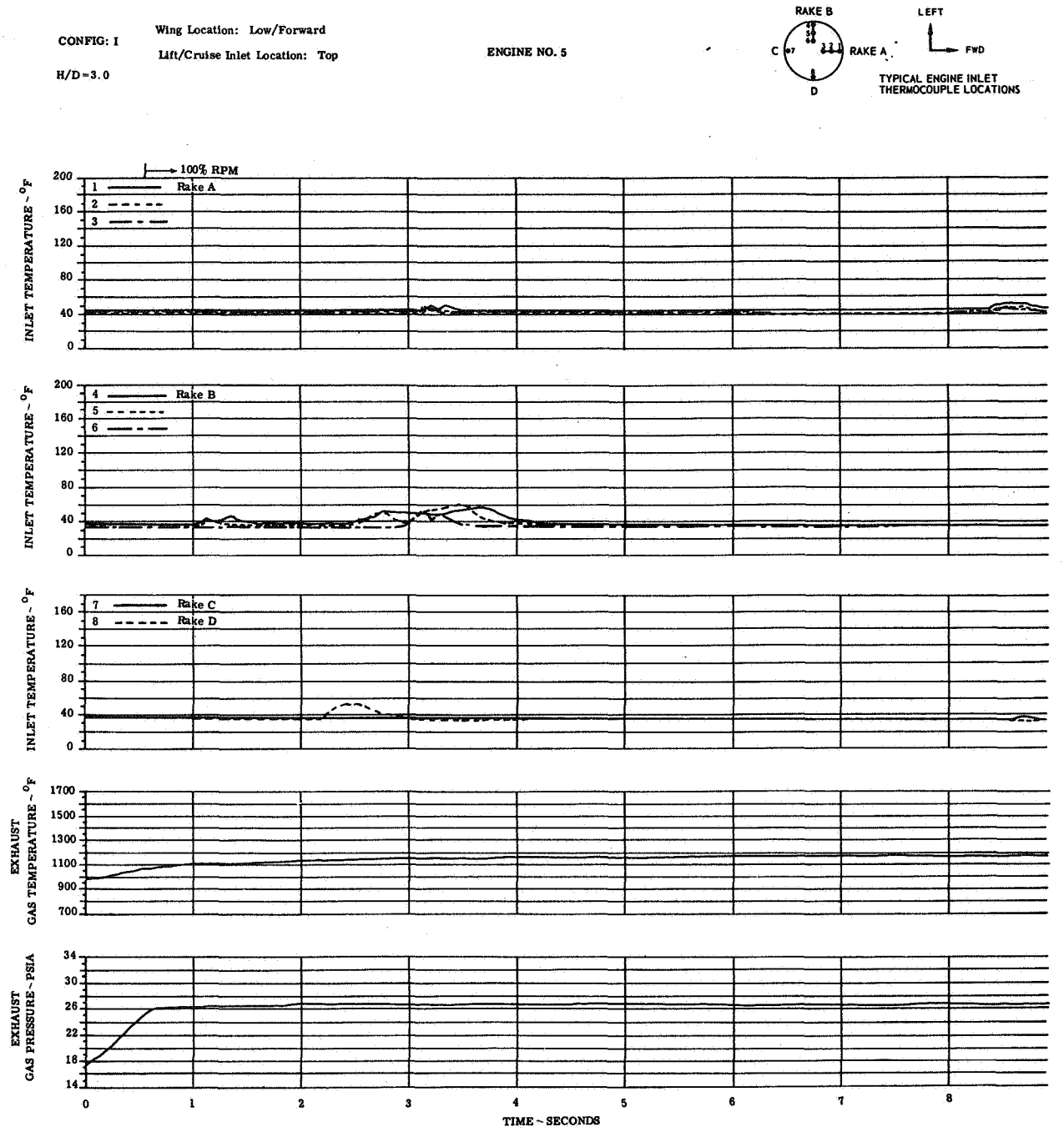

FIGURE 18(d). ENGINE TEMPERATURE AND PRESSURE TRANSIENTS

CONFIG: I

Wing Location: Low/Forward

Lift/Cruise Inlet Location: Top

H/D 3.0

ENGINE NO. 6

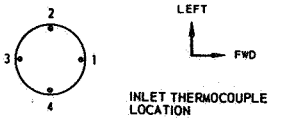

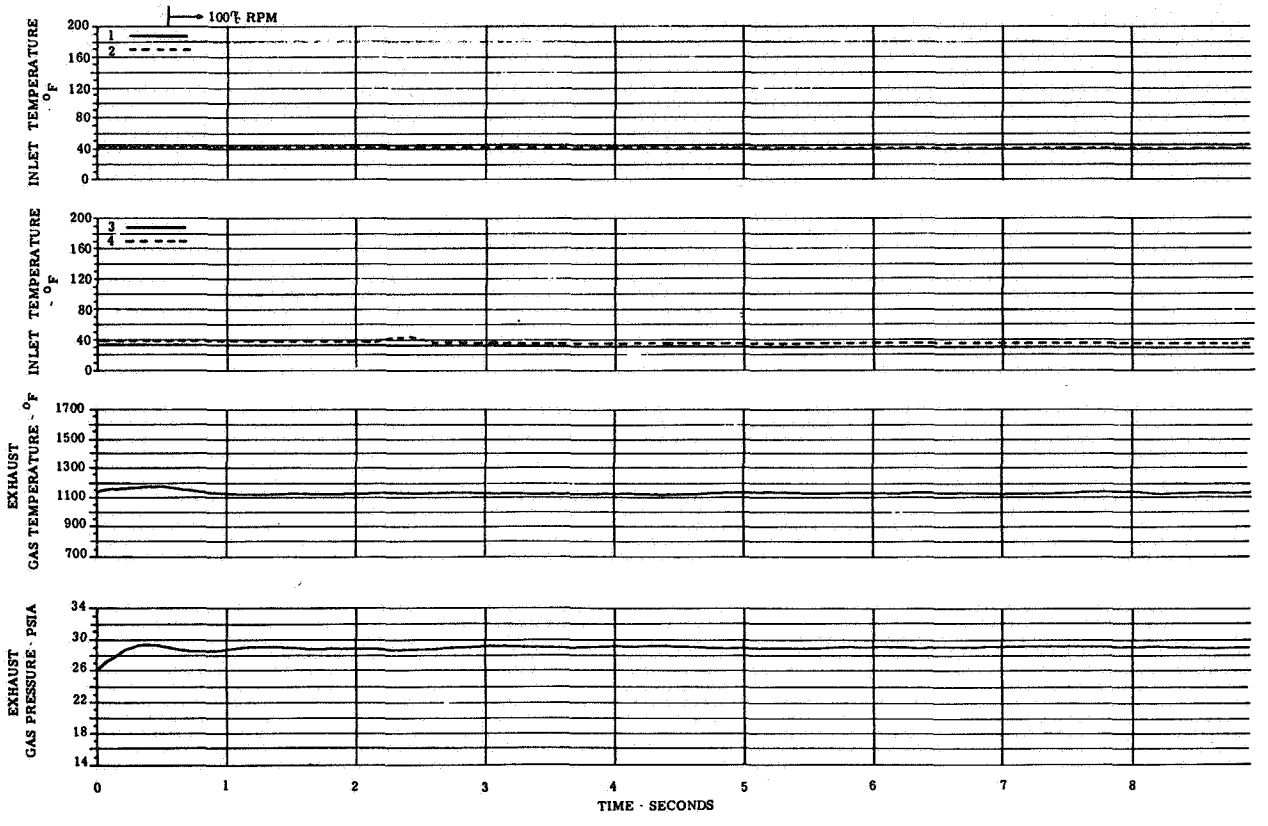

FIGURE 18(e). ENGINE TEMPERATURE AND PRESSURE TRANSIENTS

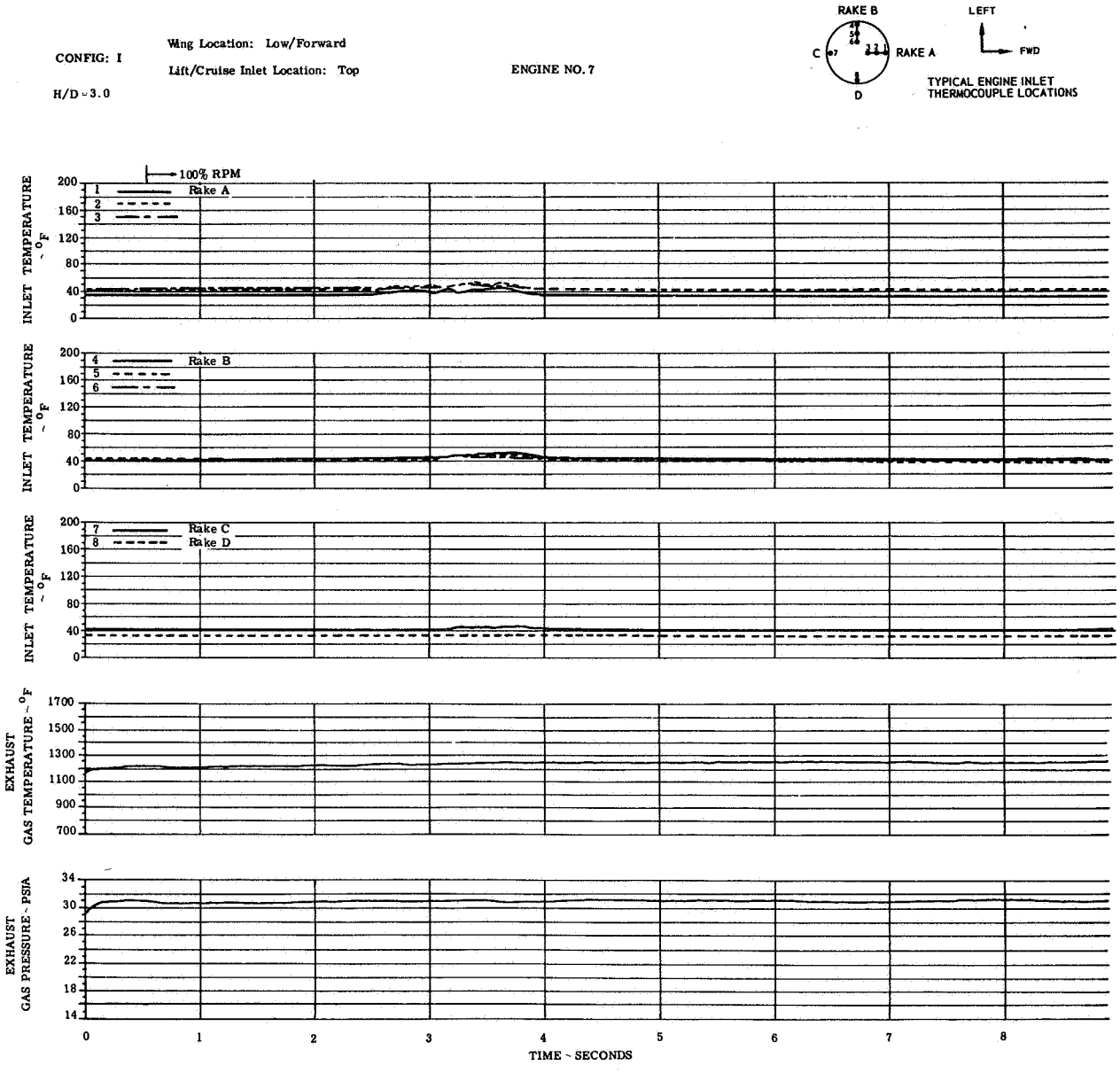

FIGURE 18(f). ENGINE TEMPERATURE AND PRESSURE TRANSIENTS

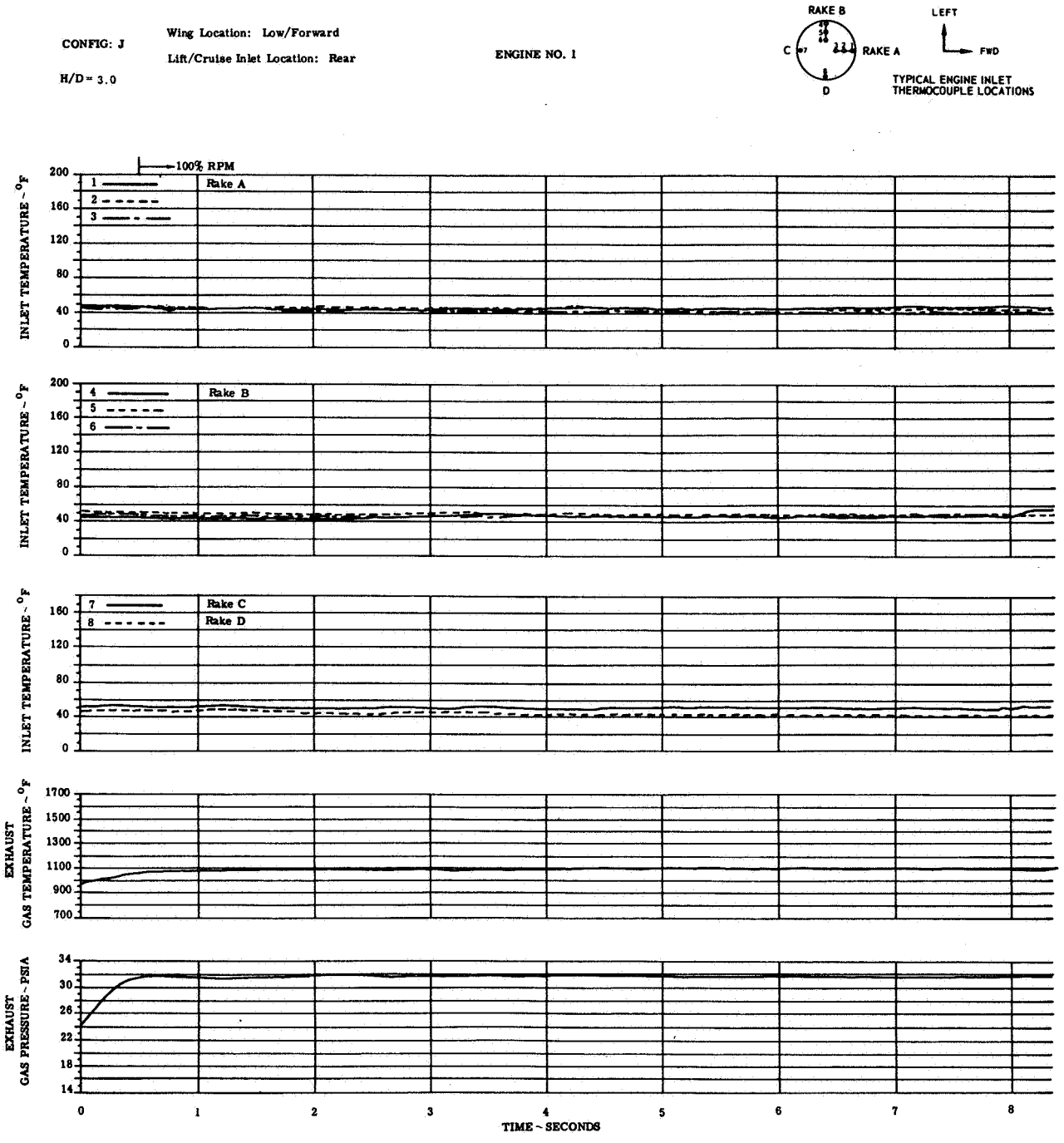

FIGURE 19(a). ENGINE TEMPERATURE AND PRESSURE TRANSIENTS

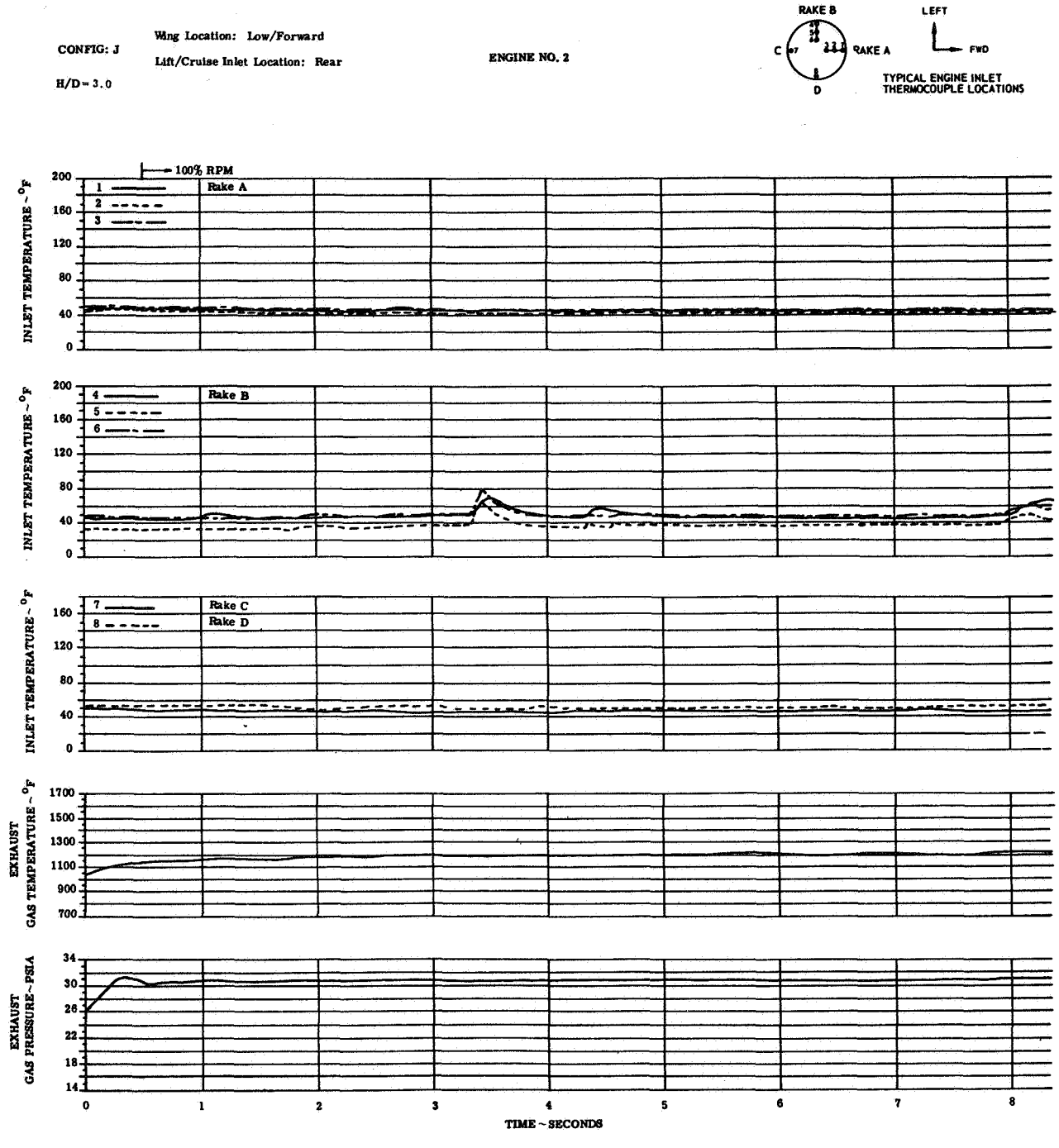

FIGURE 19(b). ENGINE TEMPERATURE AND PRESSURE TRANSIENTS

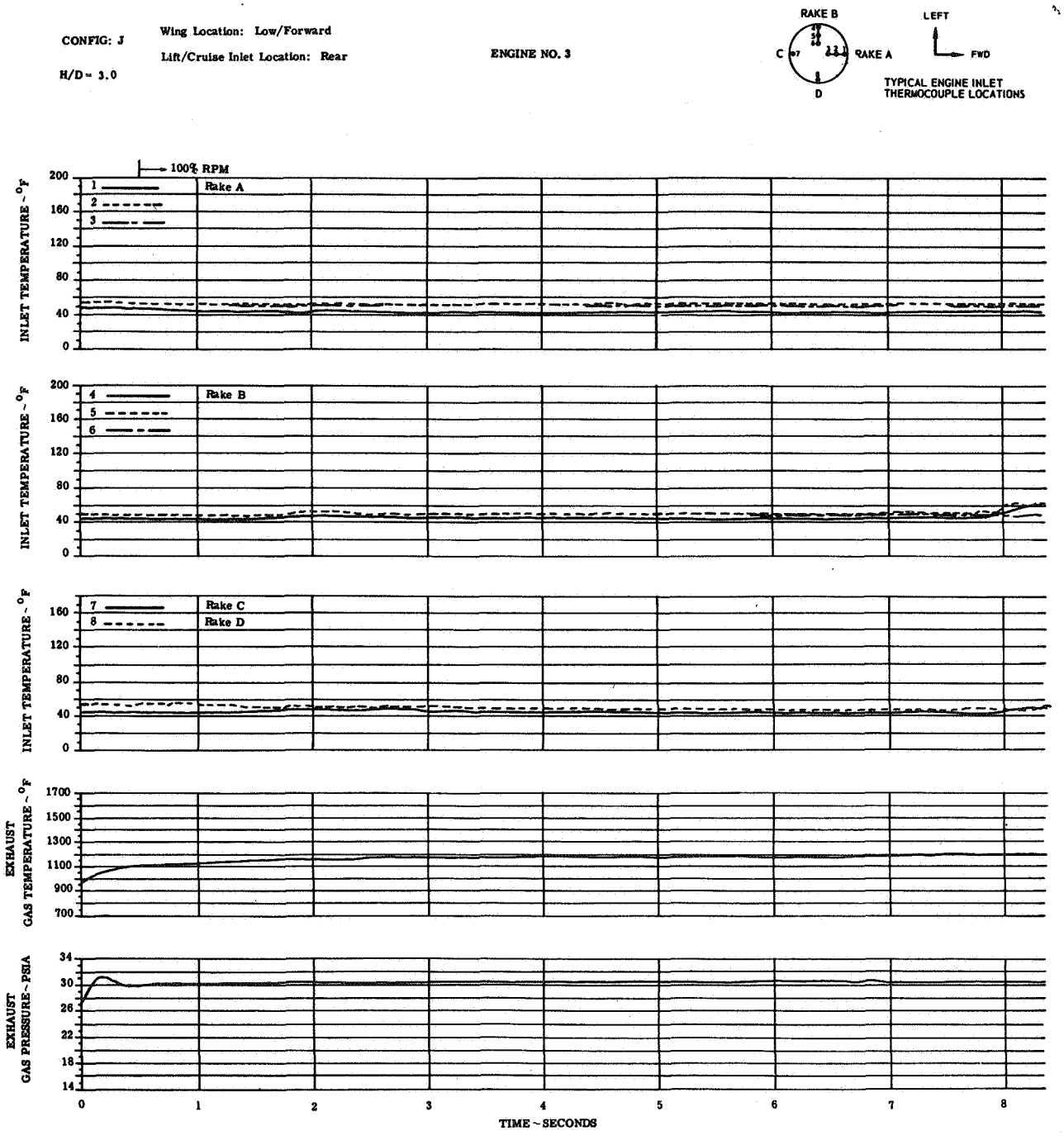

FIGURE 19(c). ENGINE TEMPERATURE AND PRESSURE TRANSIENTS

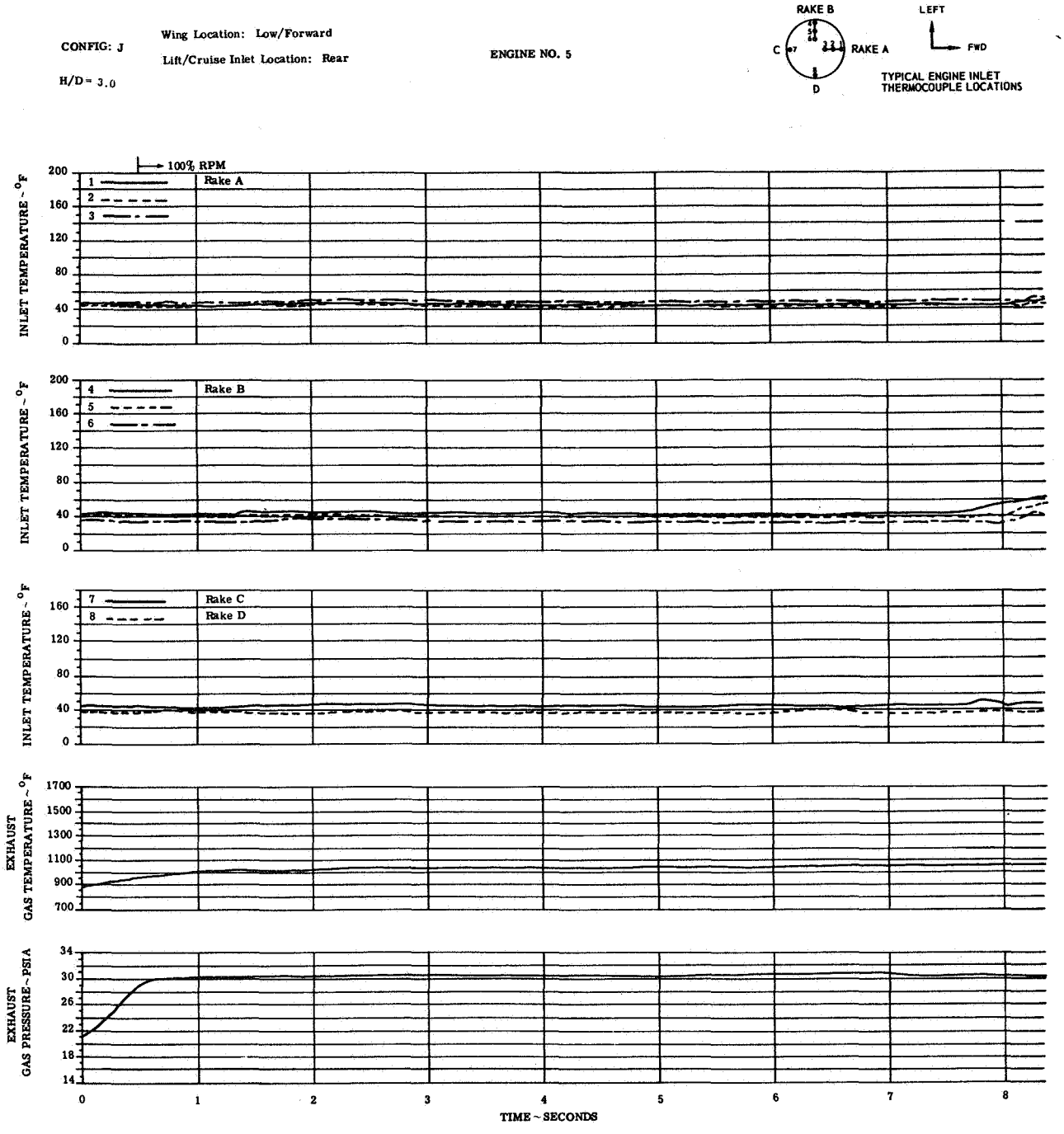

FIGURE 19(d). ENGINE TEMPERATURE AND PRESSURE TRANSIENTS

CONFIG: J

Wing Location: Low/Forward

Lift/Cruise Inlet Location: Rear

H/D = 3.0

ENGINE NO. 6

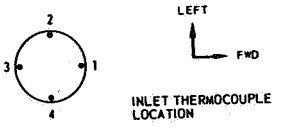

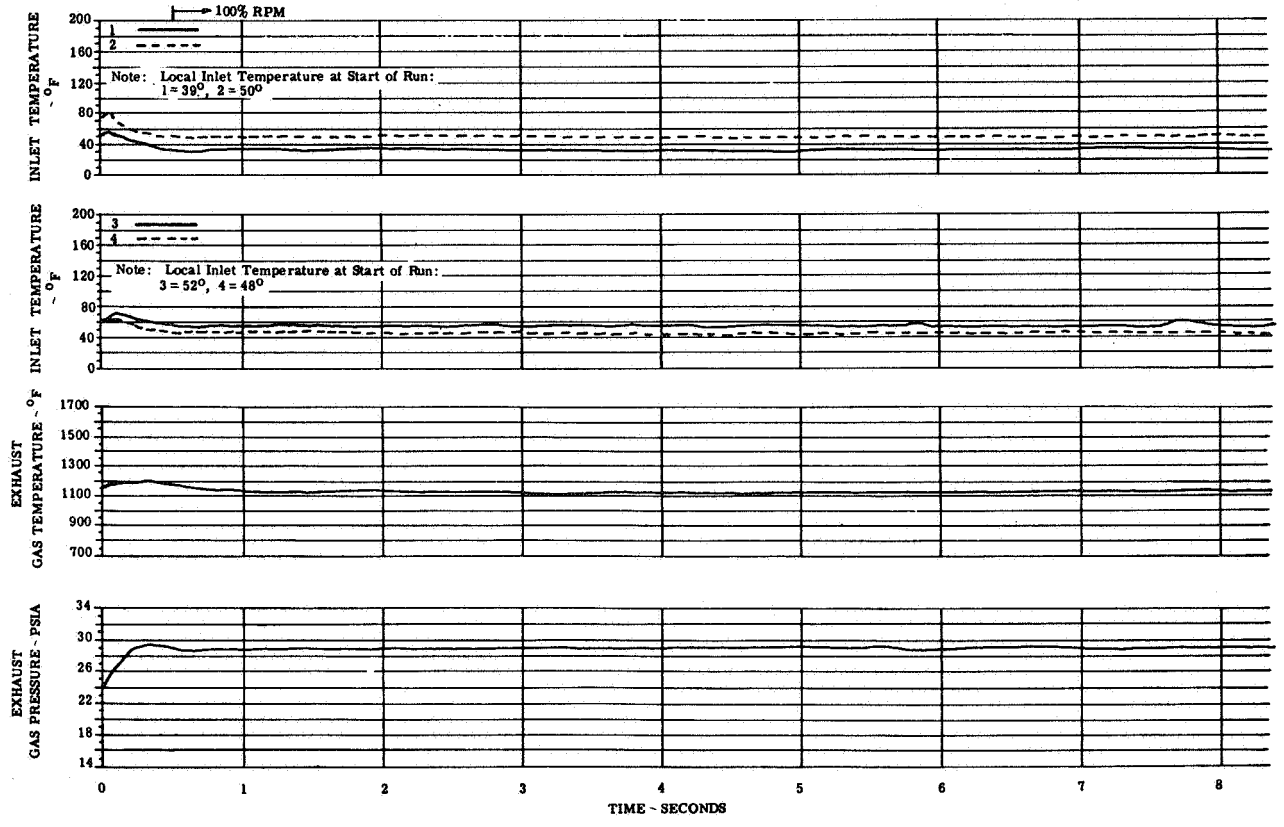

FIGUER 19(e). ENGINE TEMPERATURE AND PRESSURE TRANSIENTS

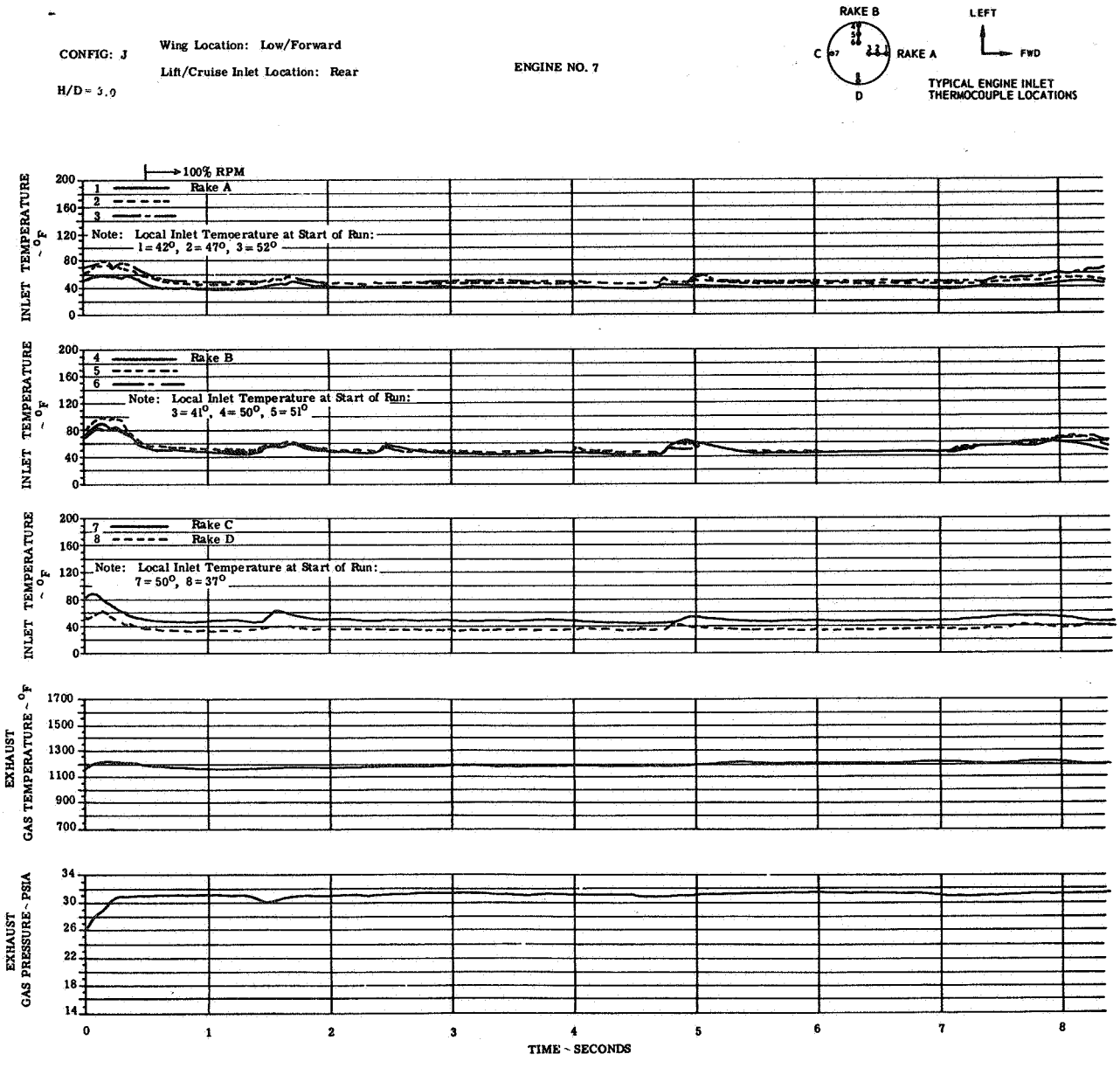

FIGURE 19(f). ENGINE TEMPERATURE AND PRESSURE TRANSIENTS

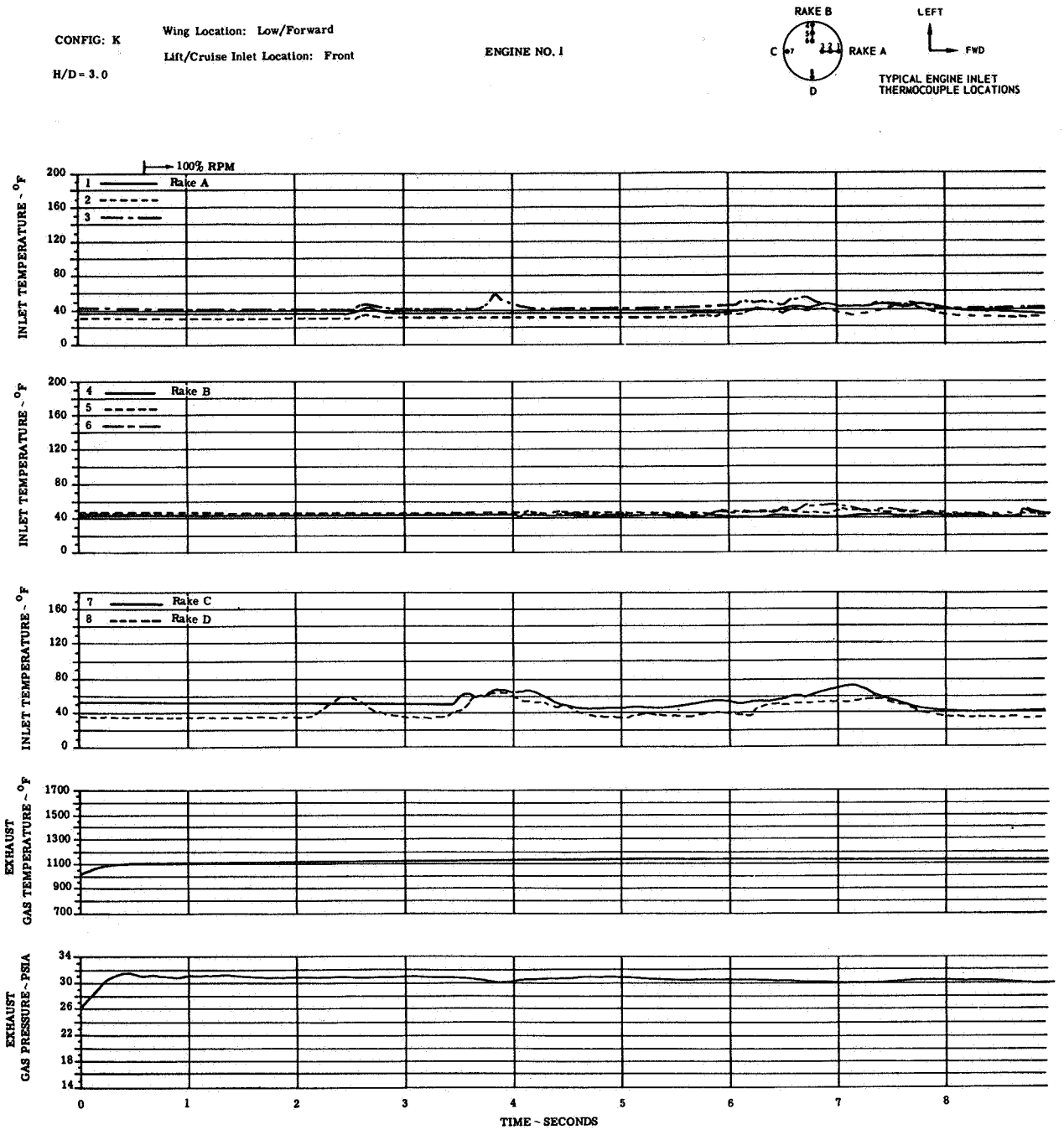

FIGURE 20(a). ENGINE TEMPERATURE AND PRESSURE TRANSIENTS

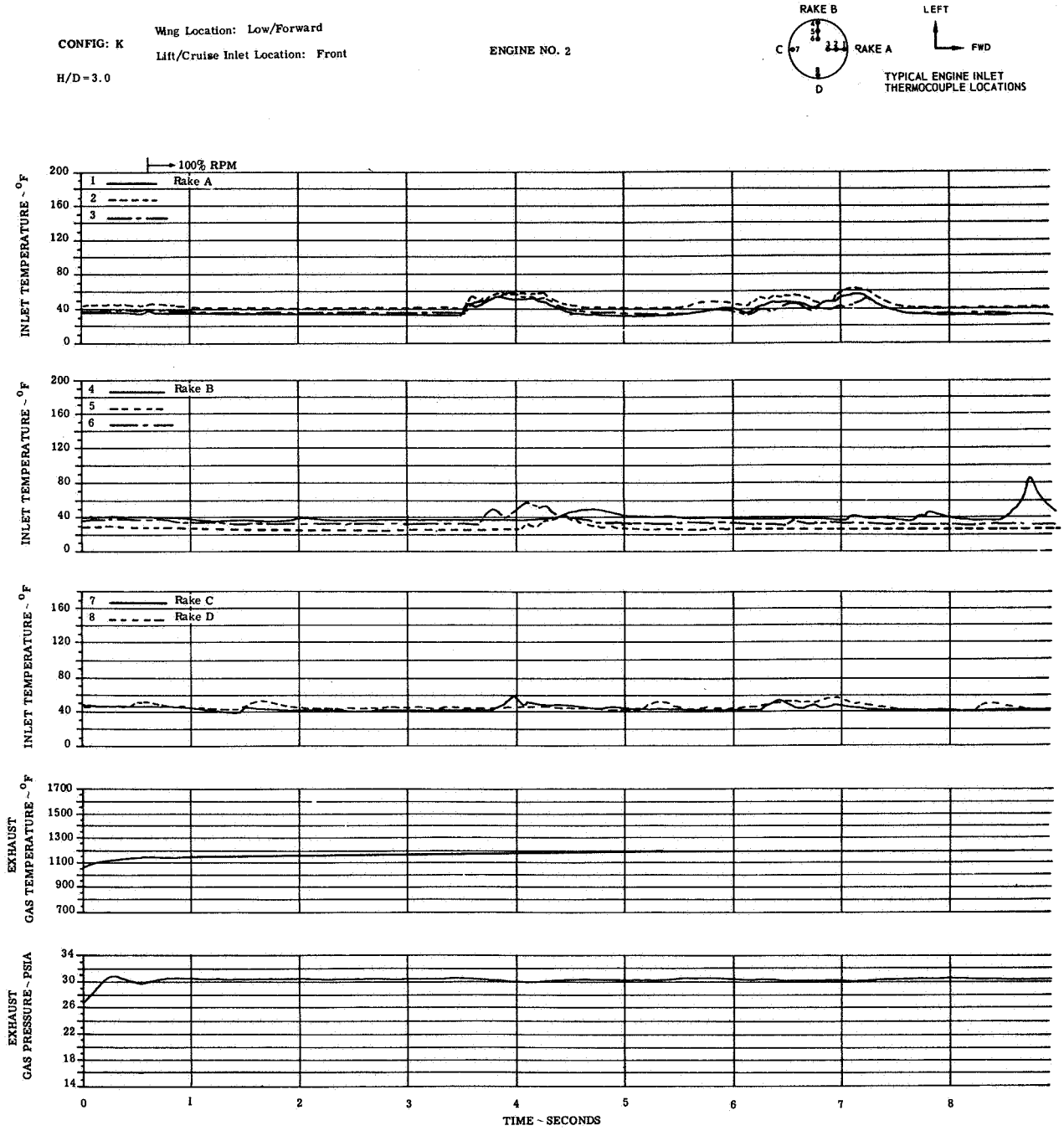

FIGURE 20(b). ENGINE TEMPERATURE AND PRESSURE TRANSIENTS

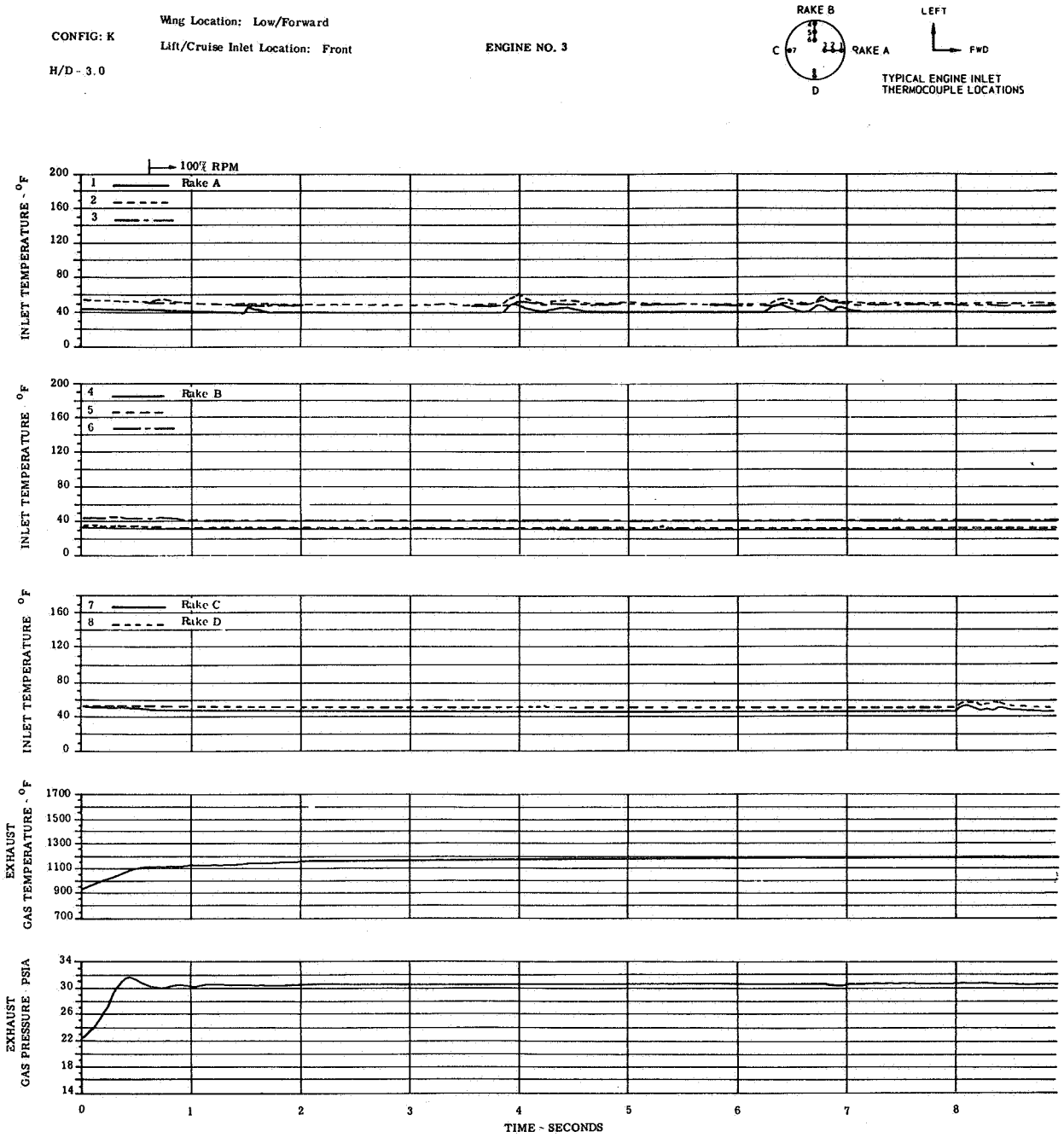

FIGURE 20(c). ENGINE TEMPERATURE AND PRESSURE TRANSIENTS

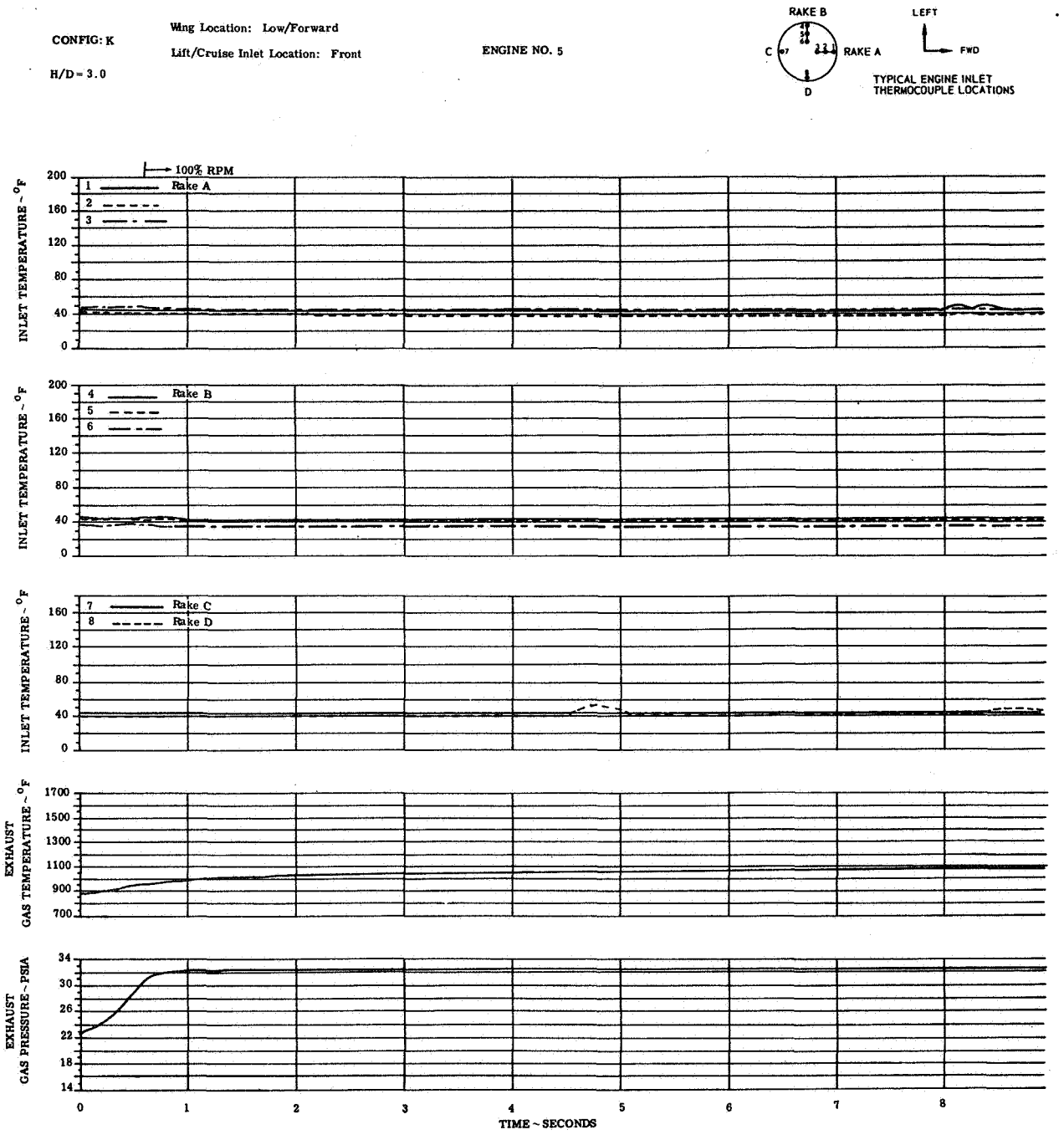

FIGURE 20(d). ENGINE TEMPERATURE AND PRESSURE TRANSIENTS

CONFIG: K

Wing Location: Low/Forward

Lift/Cruise Inlet Location: Front

H/D - 3.0

ENGINE NO. 6

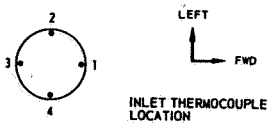

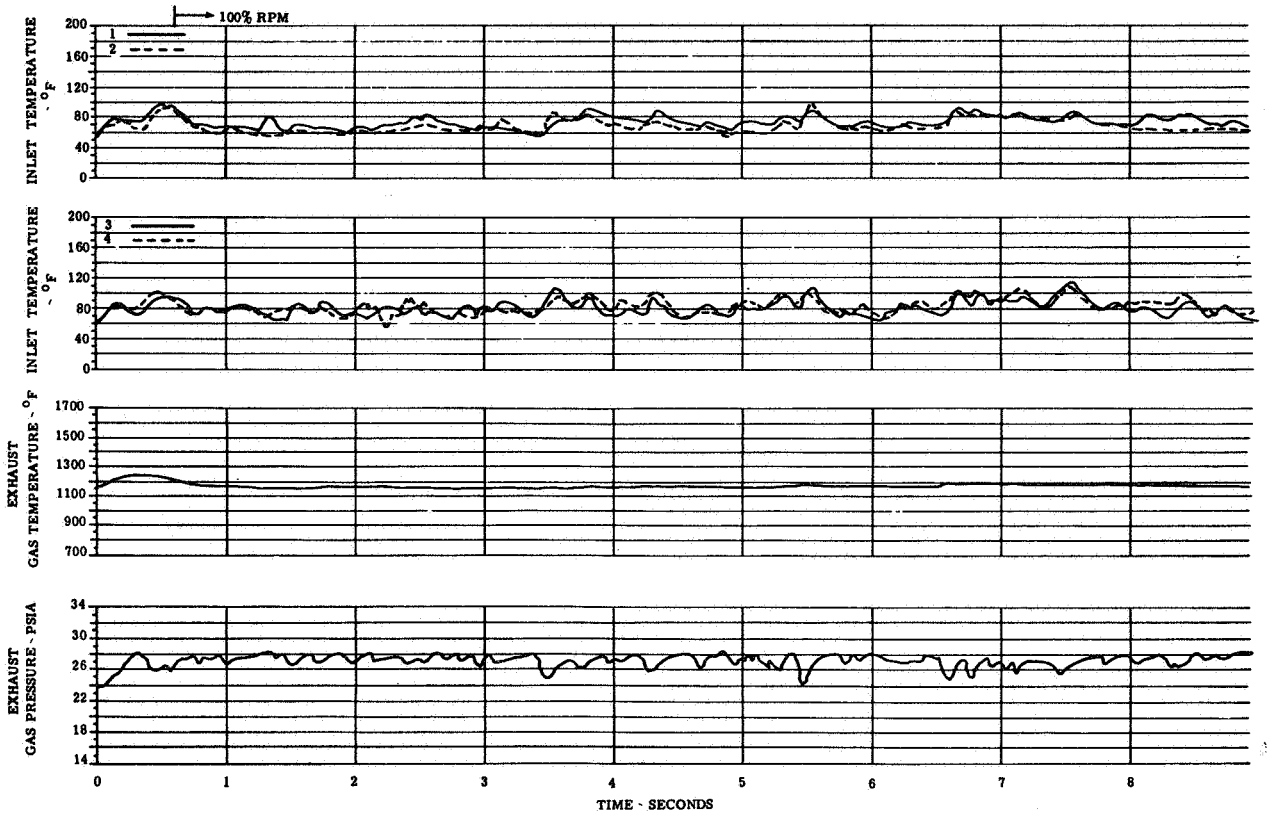

FIGURE 20(e). ENGINE TEMPERATURE AND PRESSURE TRANSIENTS

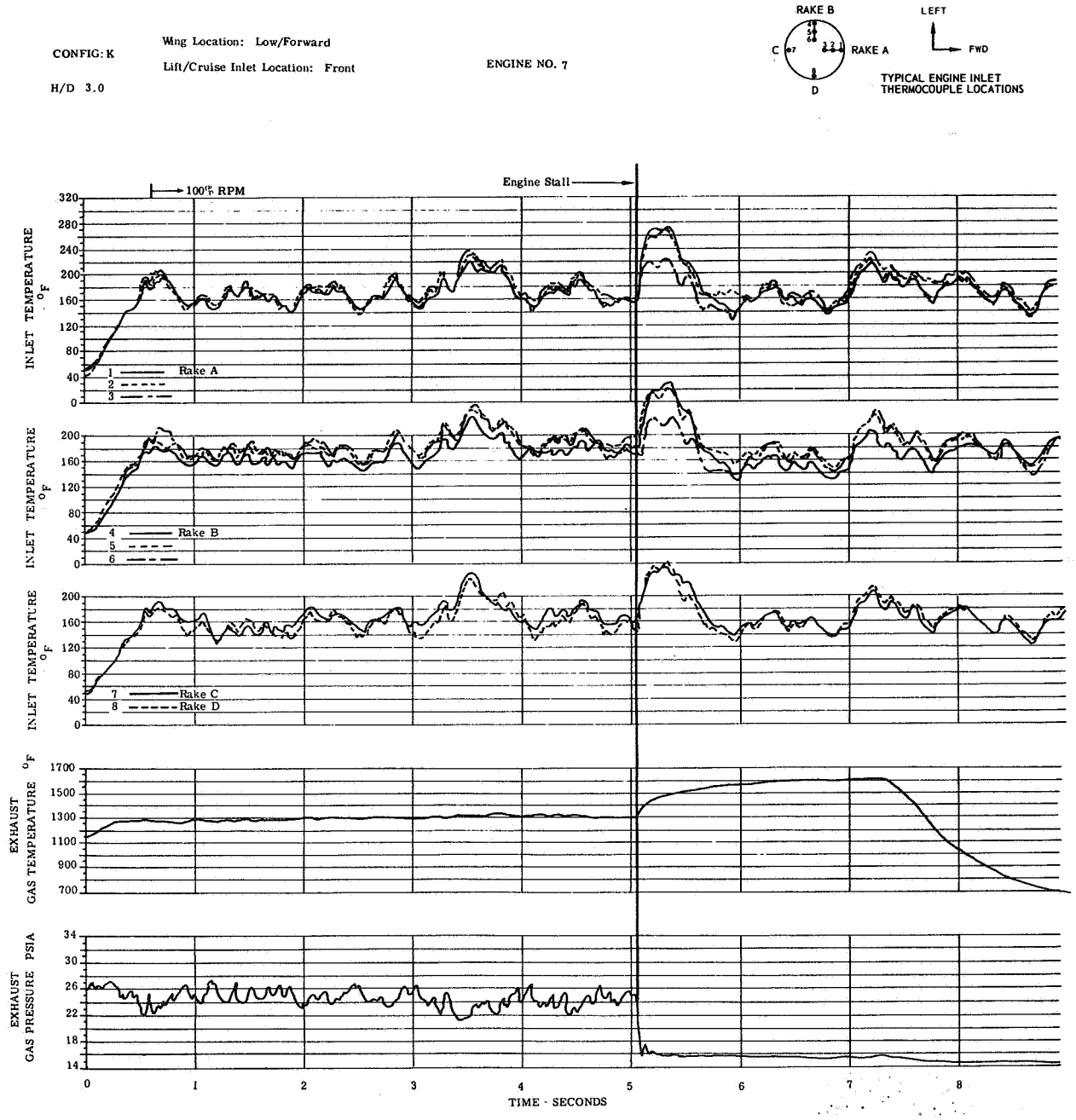

FIGURE 20(f). ENGINE TEMPERATURE AND PRESSURE TRANSIENTS

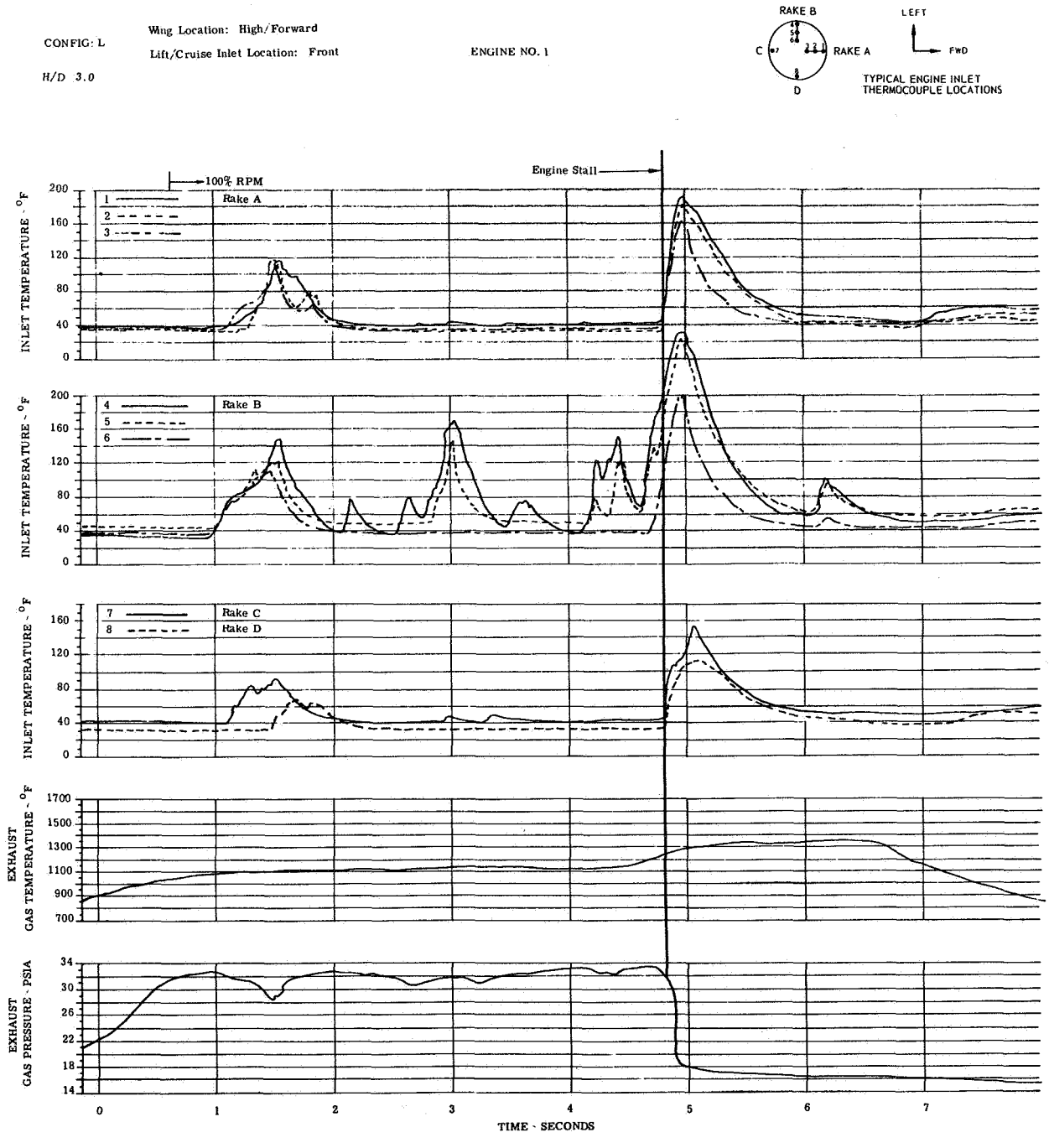

FIGURE 21(a). ENGINE TEMPERATURE AND PRESSURE TRANSIENTS

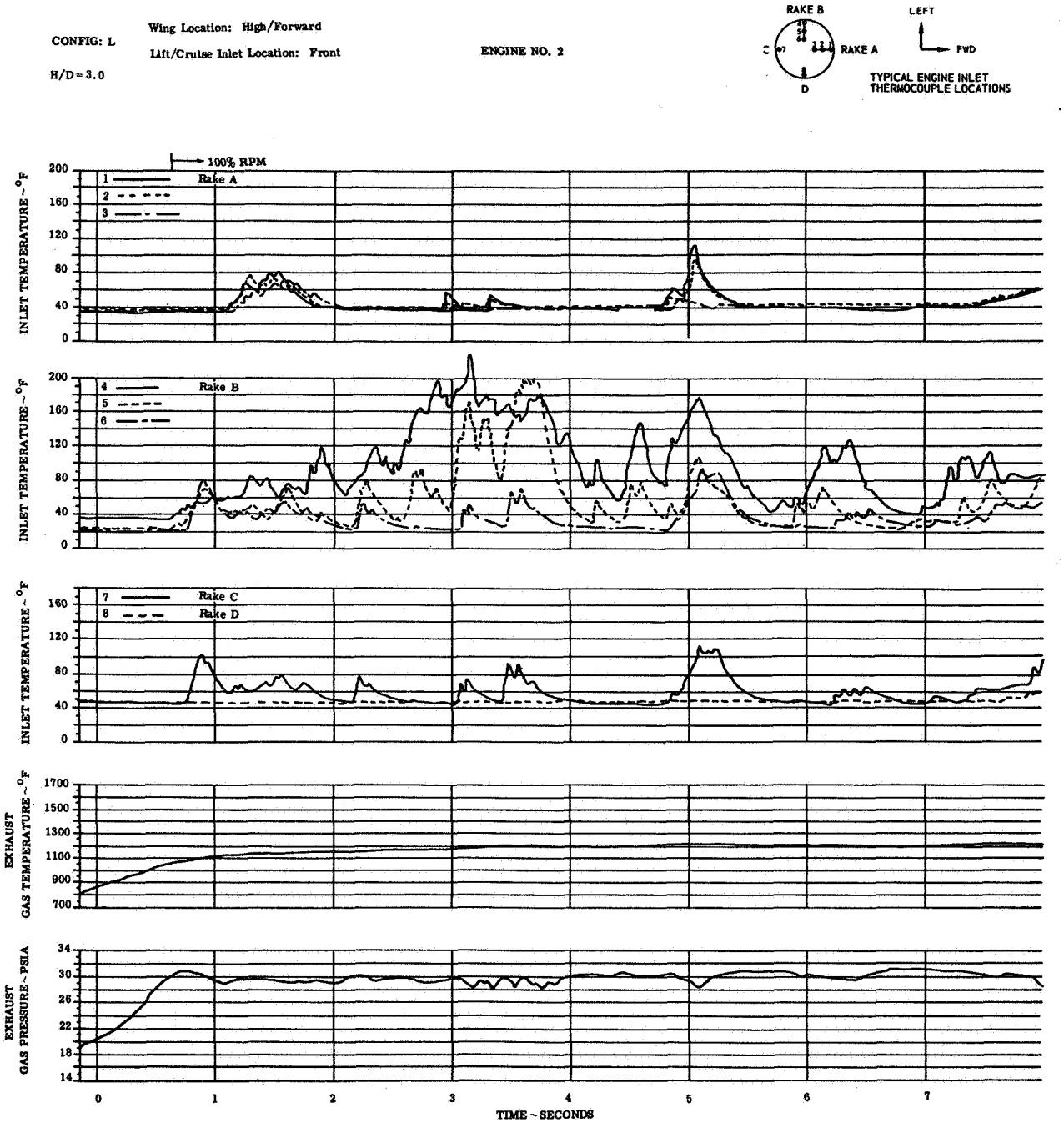

FIGURE 21(b). ENGINE TEMPERATURE AND PRESSURE TRANSIENTS

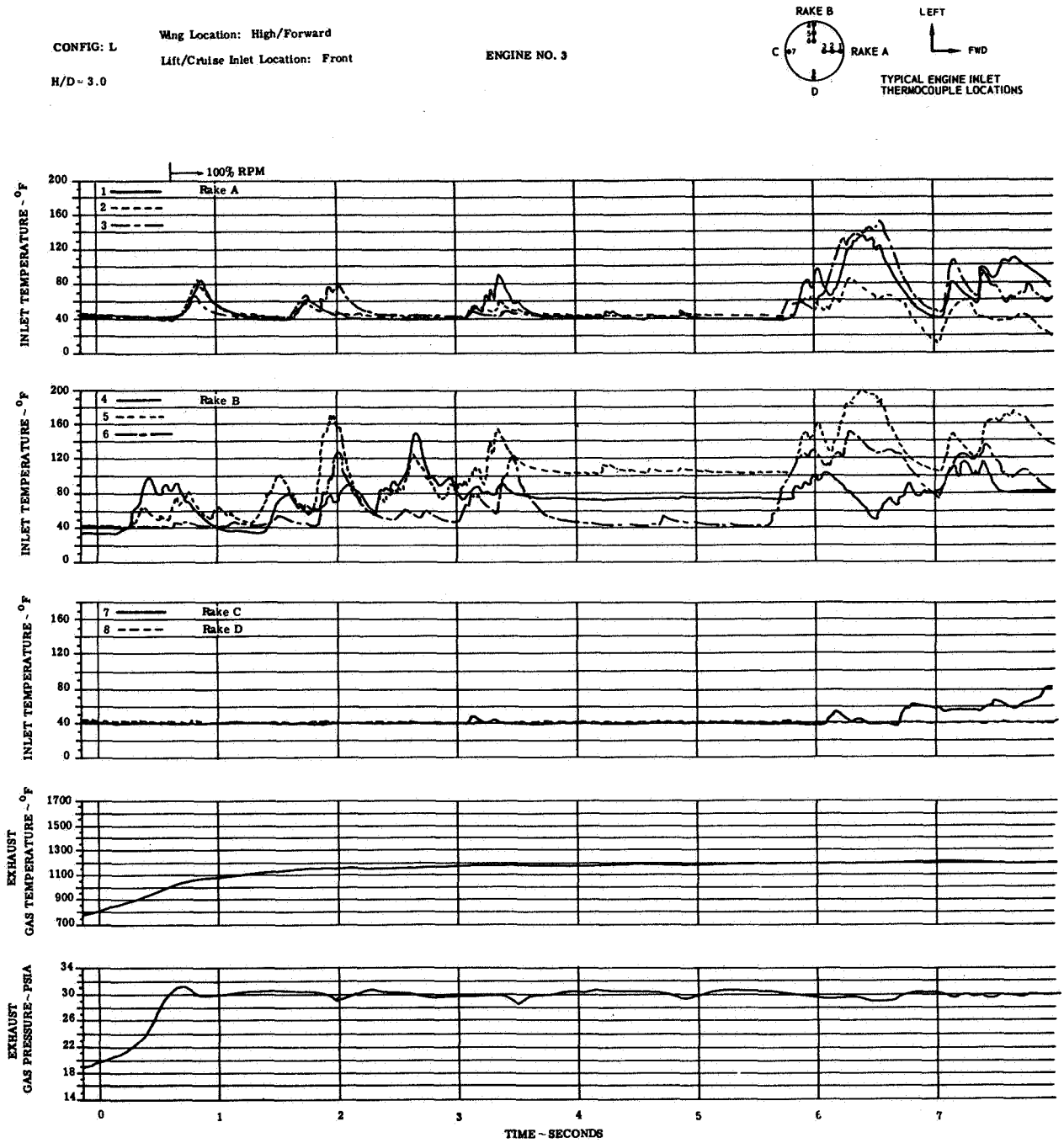

FIGURE 21(c). ENGINE TEMPERATURE AND PRESSURE TRANSIENTS

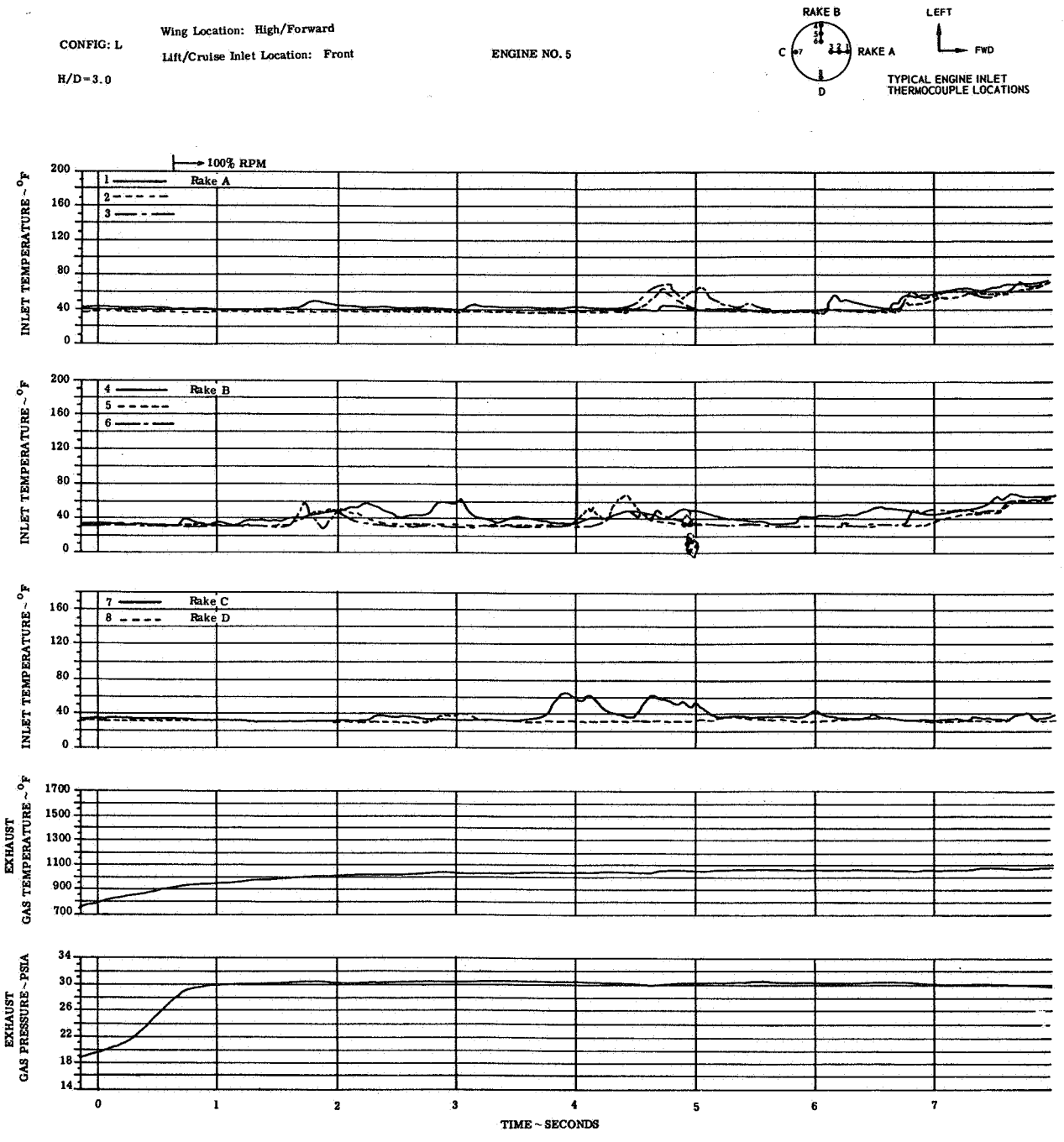

FIGURE 21(d). ENGINE TEMPERATURE AND PRESSURE TRANSIENTS

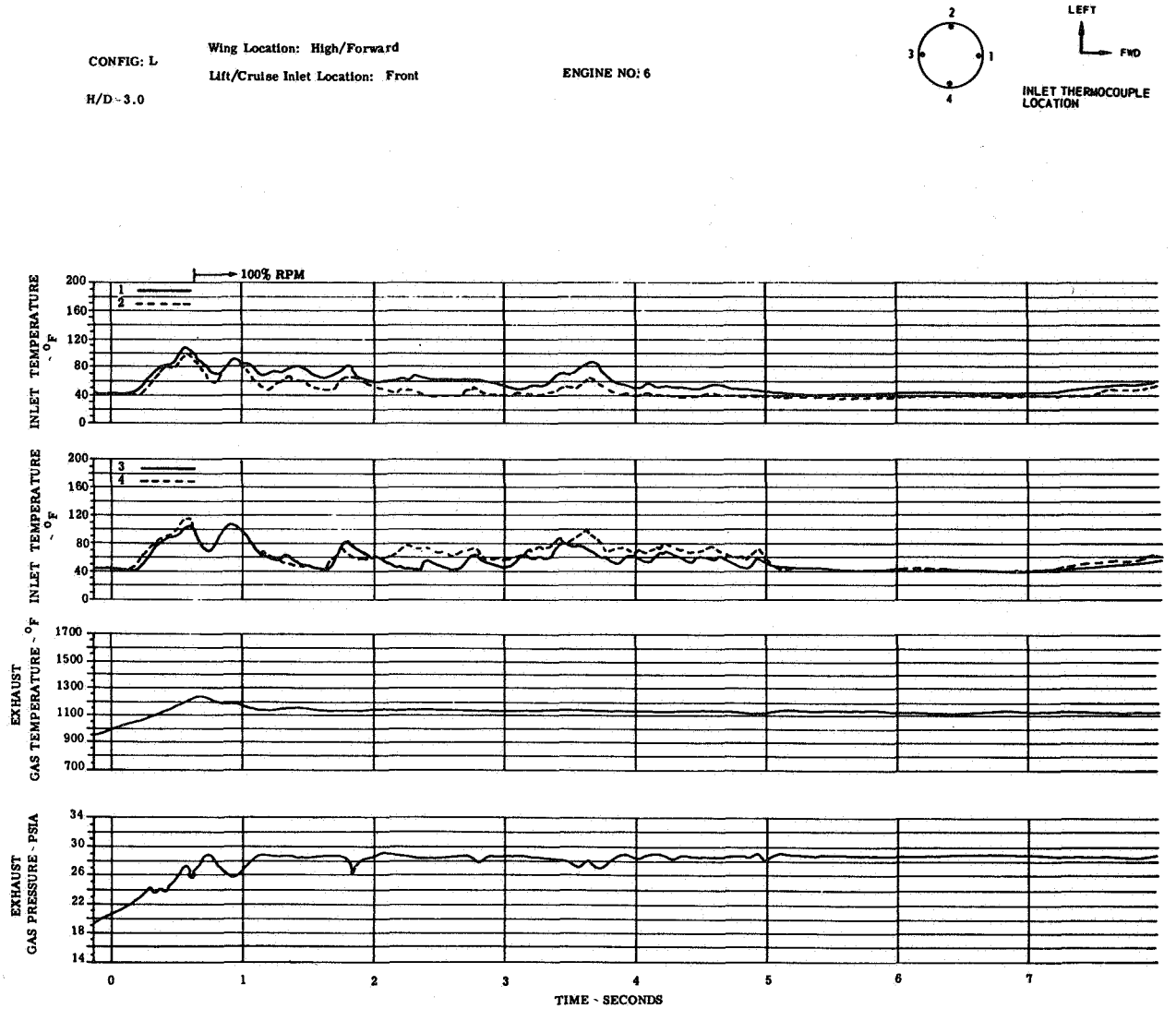

FIGURE 21(e). ENGINE TEMPERATURE AND PRESSURE TRANSIENTS

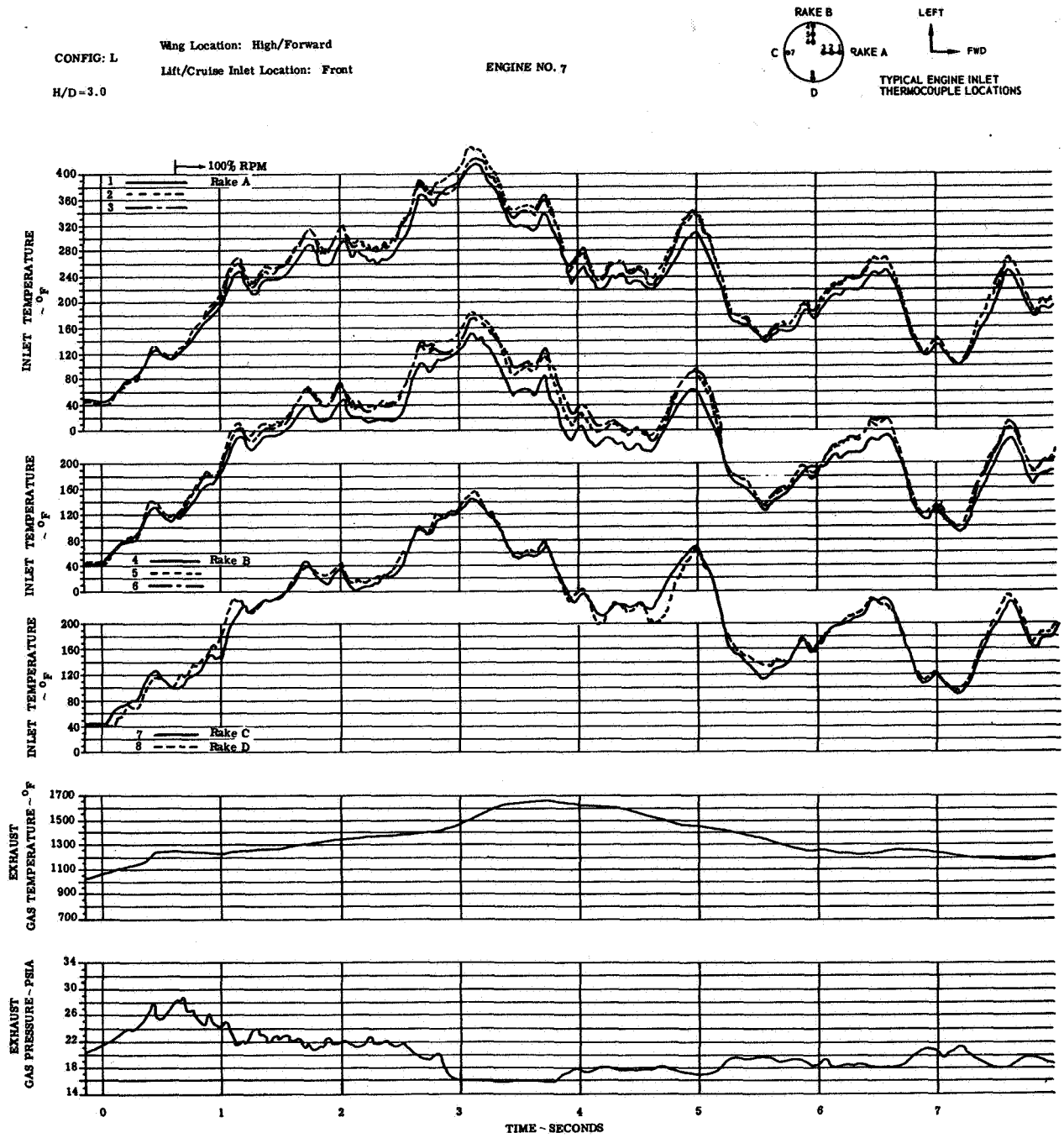

FIGURE 21(f). ENGINE TEMPERATURE AND PRESSURE TRANSIENTS

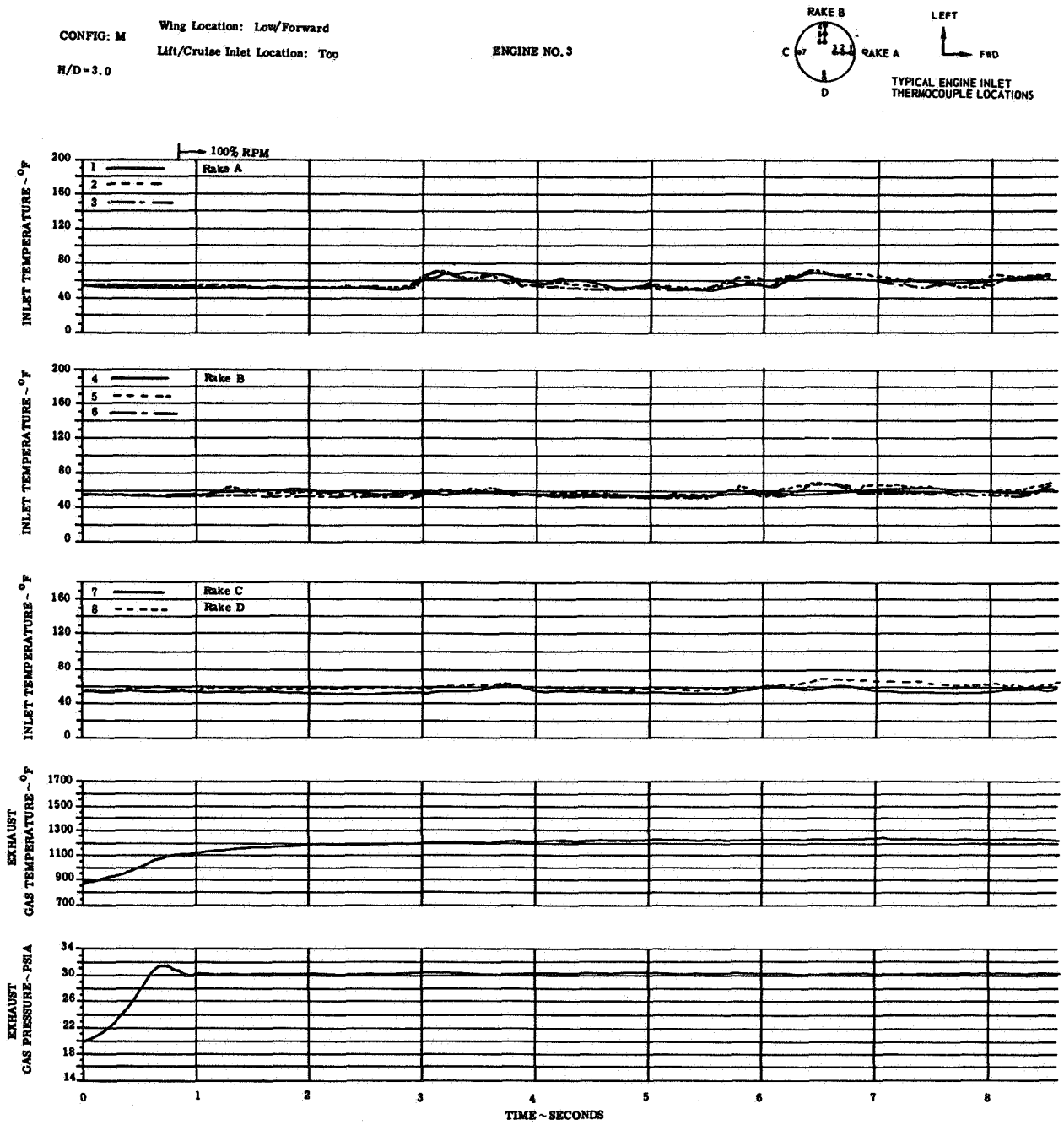

FIGURE 22(a). ENGINE TEMPERATURE AND PRESSURE TRANSIENTS

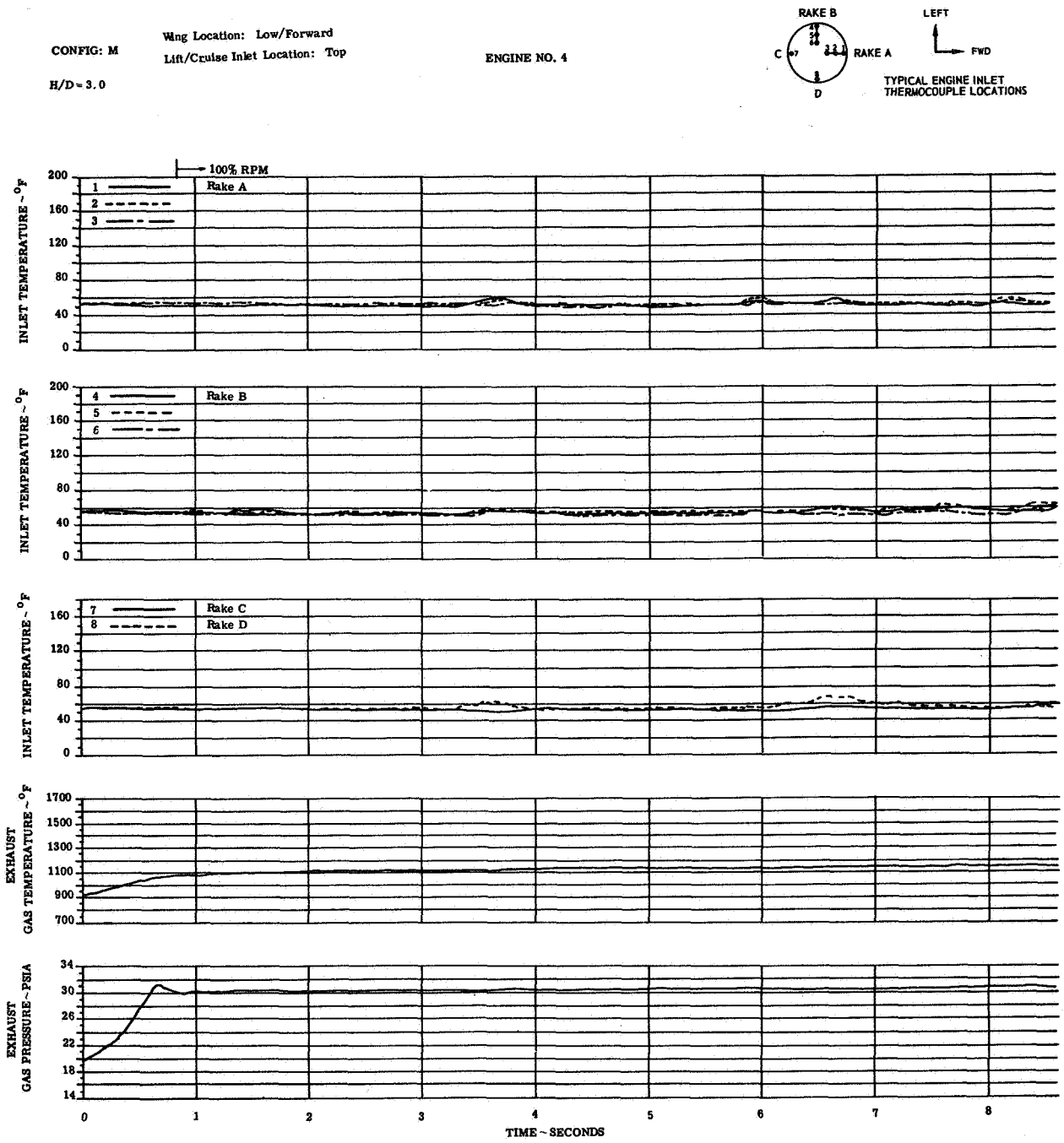

FIGURE 22(b). ENGINE TEMPERATURE AND PRESSURE TRANSIENTS

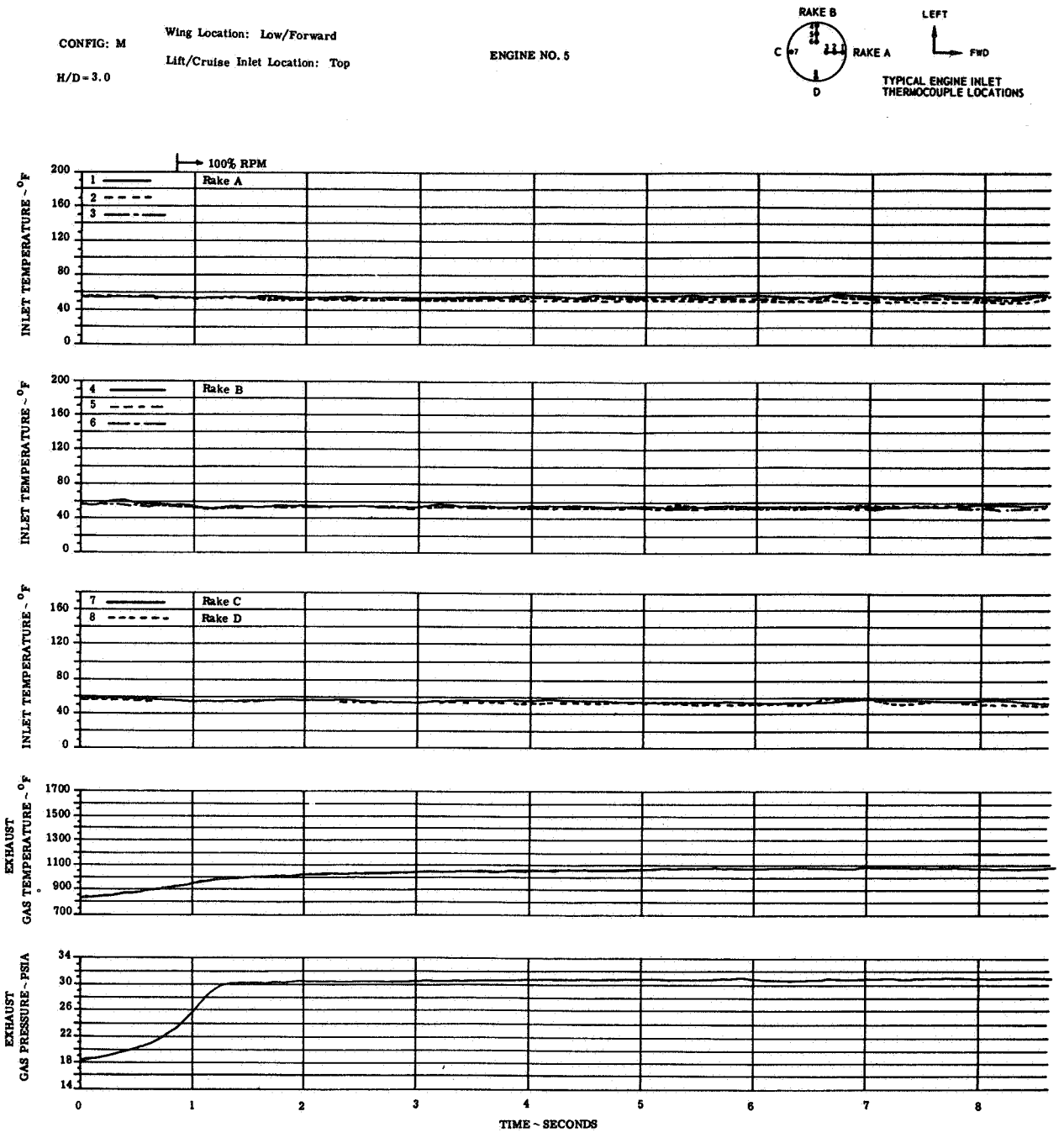

FIGURE 22(c). ENGINE TEMPERATURE AND PRESSURE TRANSIENTS

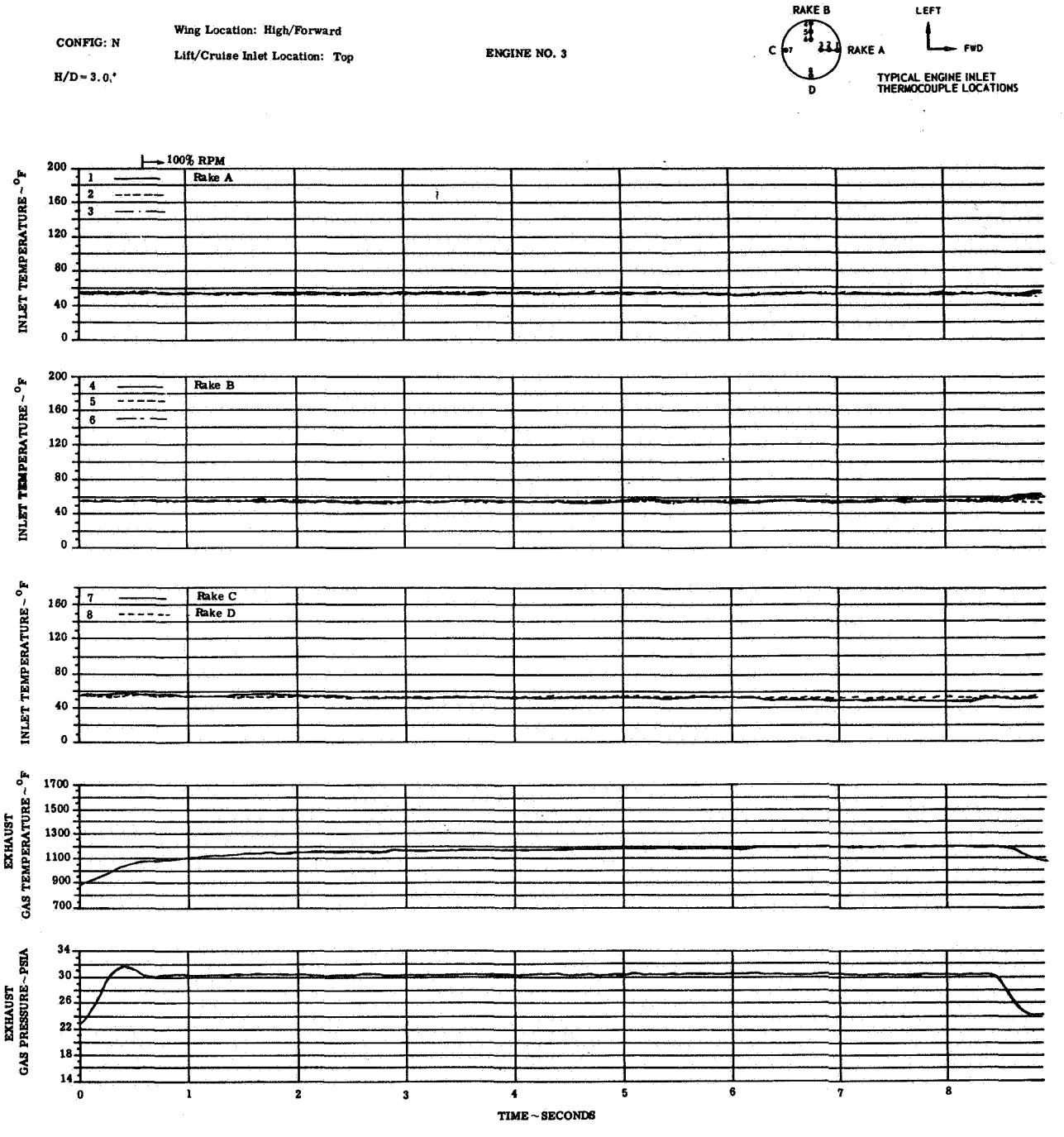

FIGURE 23(a). ENGINE TEMPERATURE AND PRESSURE TRANSIENTS

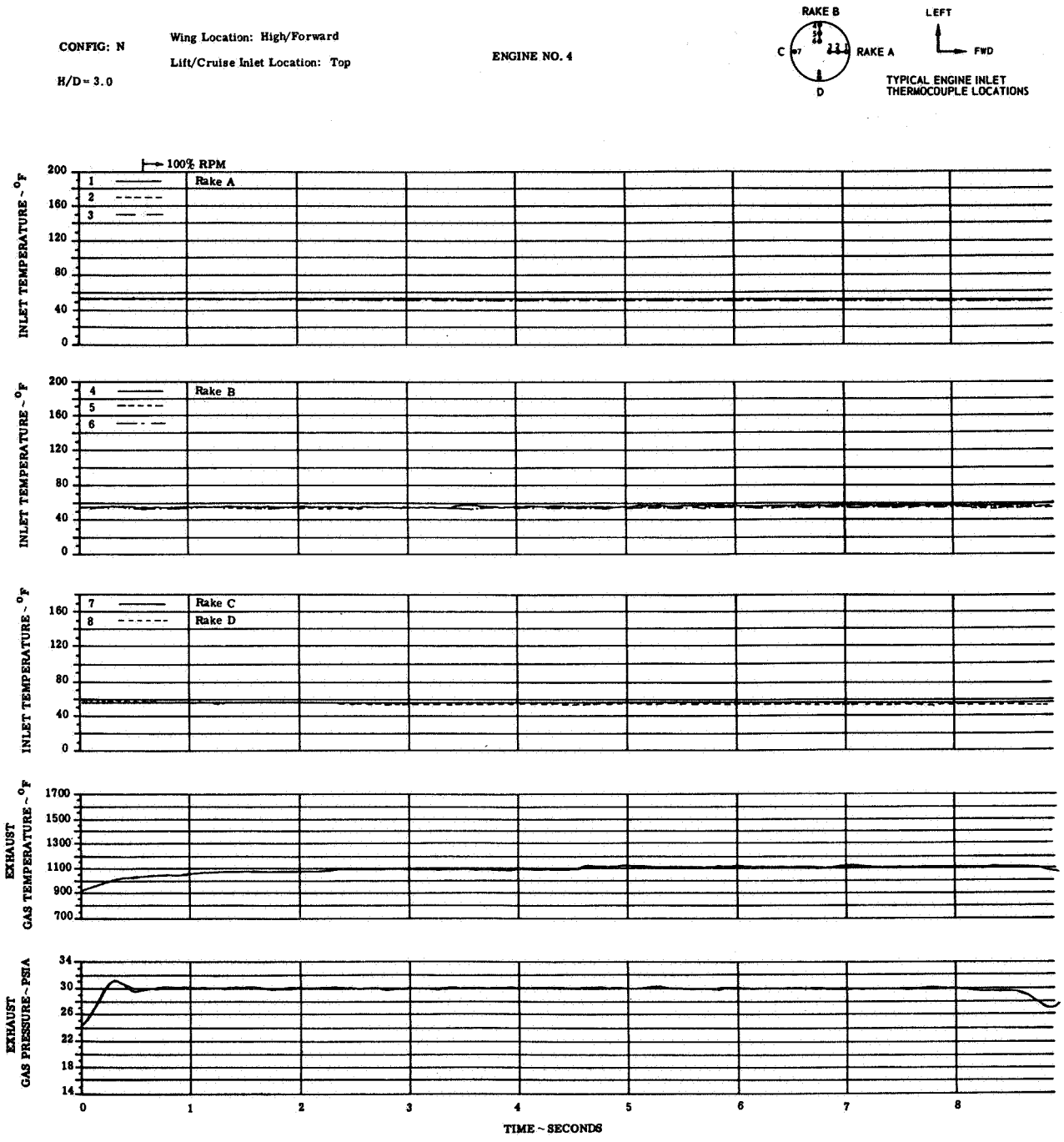

FIGURE 23(b). ENGINE TEMPERATURE AND PRESSURE TRANSIENTS

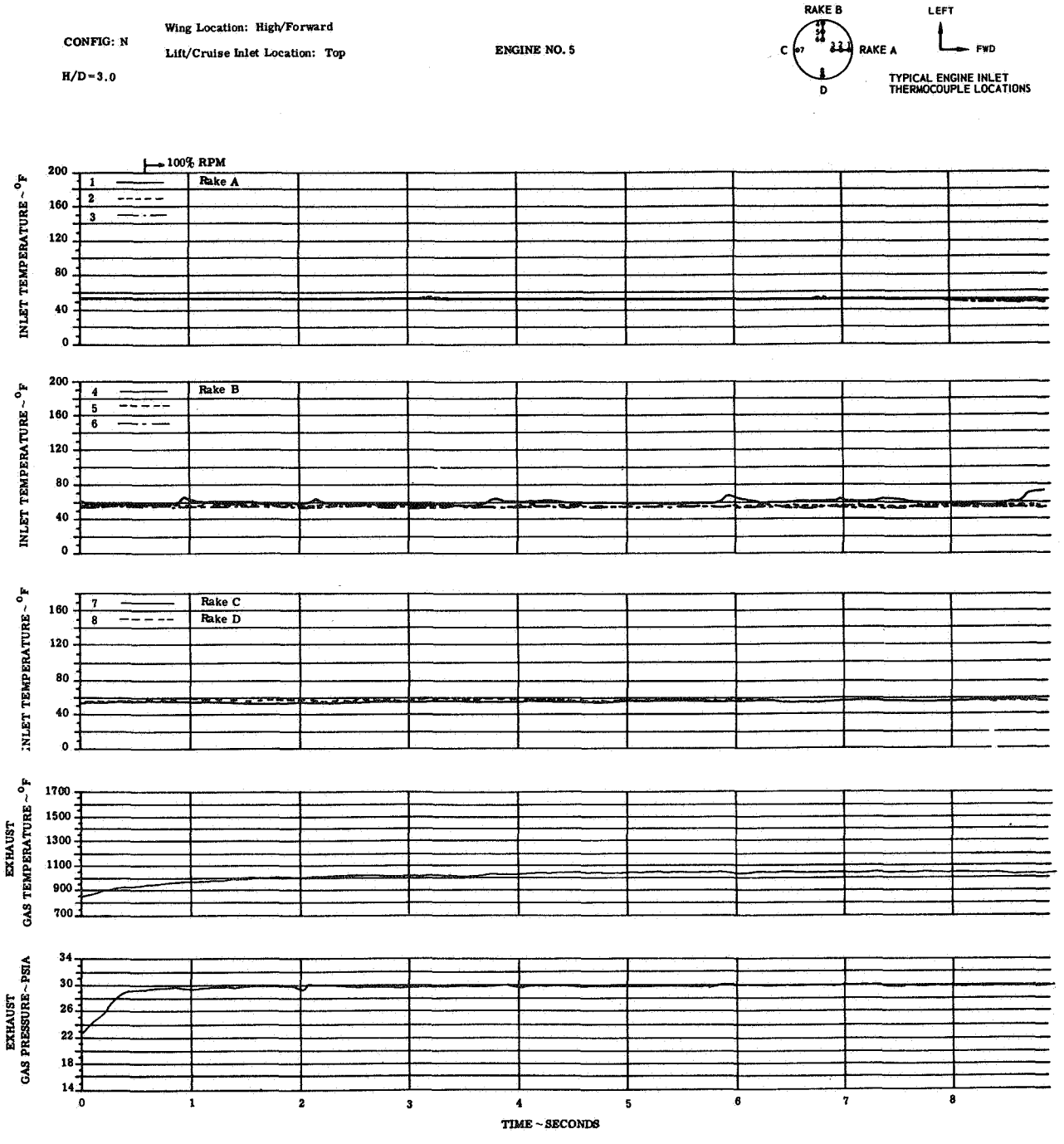

FIGURE 23(c). ENGINE TEMPERATURE AND PRESSURE TRANSIENTS

CONFIGURATION: F

L_∞ = 12,400 LBS

$L_\infty \bar{c}$ = 91,700 FT-LB

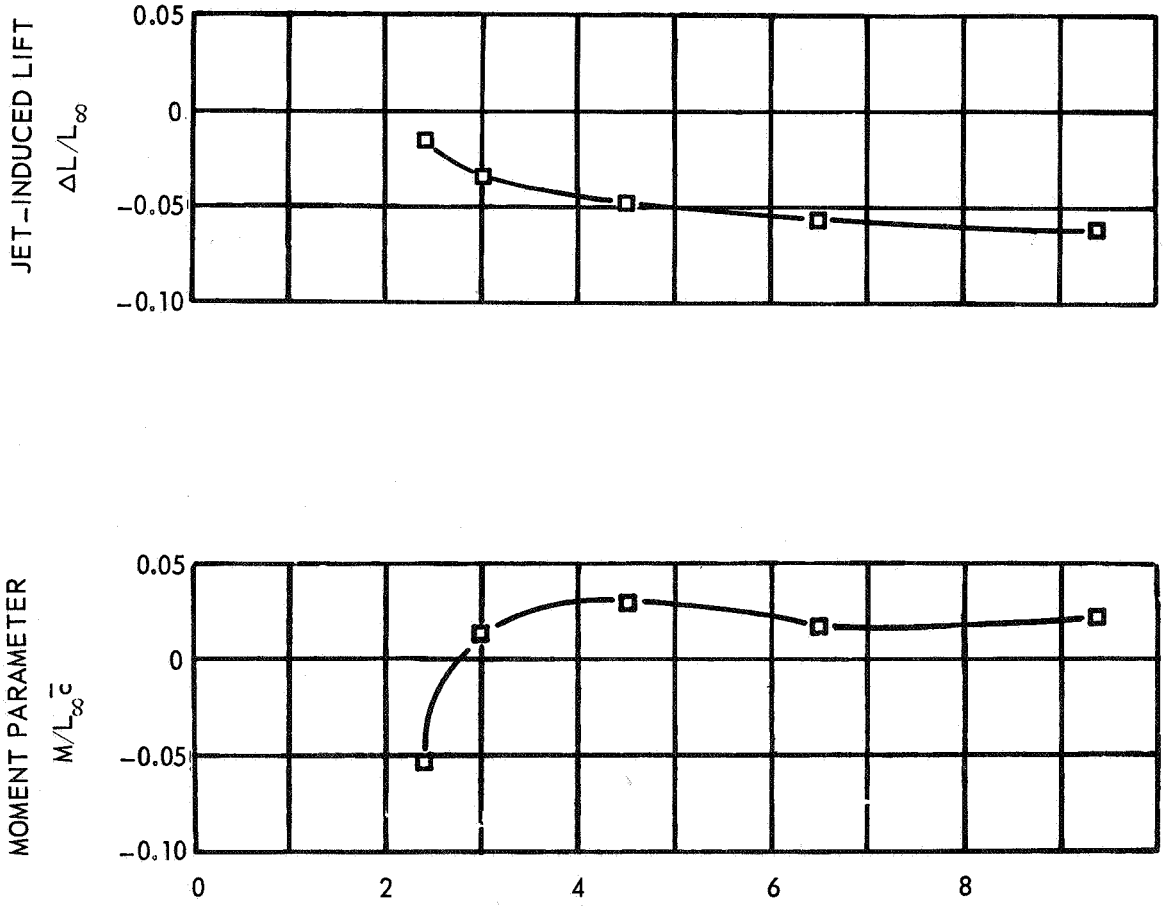

FIGURE 24 – TEST MODEL JET-INDUCED LIFT AND PITCHING MOMENT

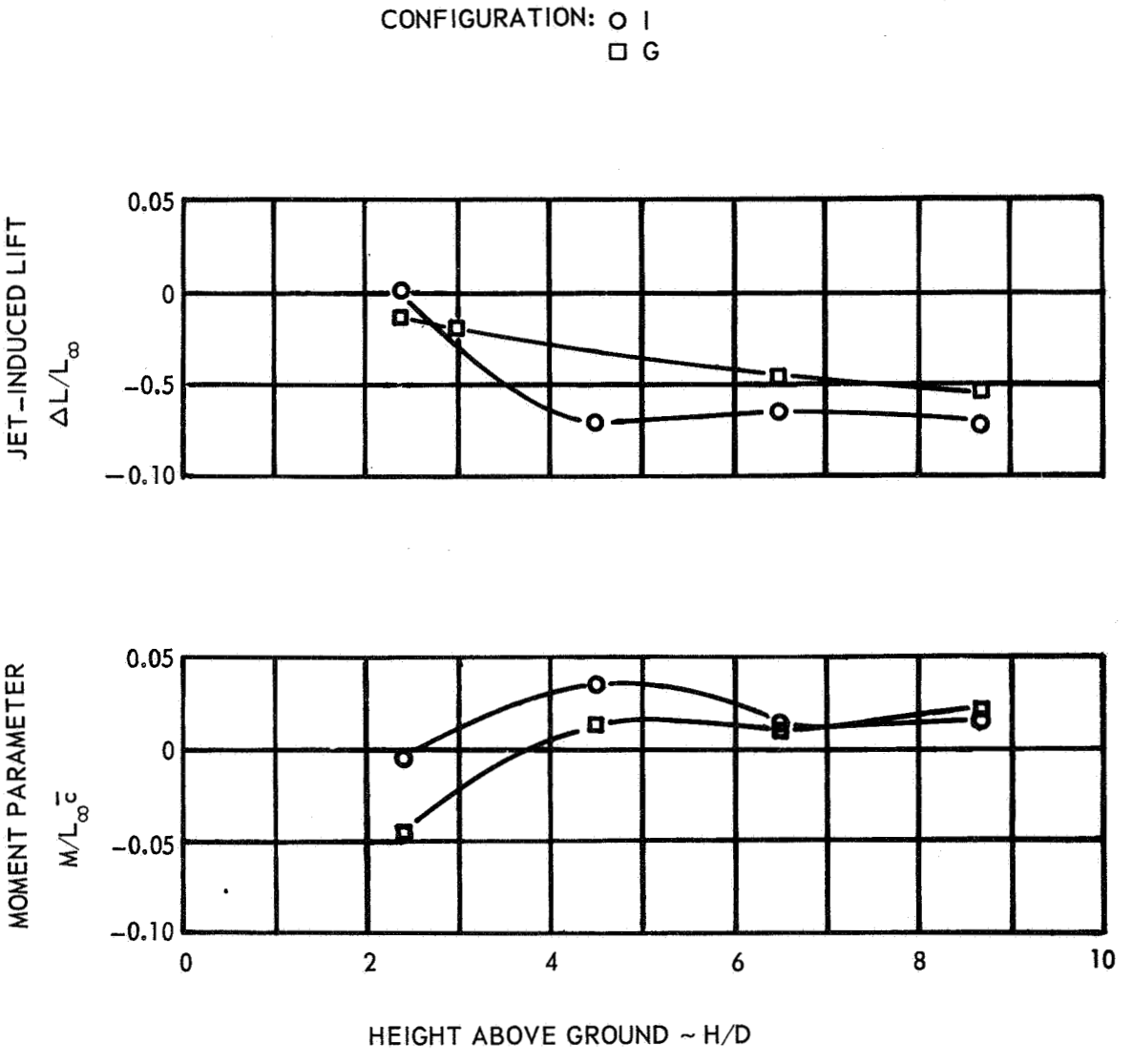

(a) WING + FUSELAGE + HORIZONTAL TAIL

FIGURE 25. VEHICLE JET-INDUCED FORCE AND PITCHING MOMENT

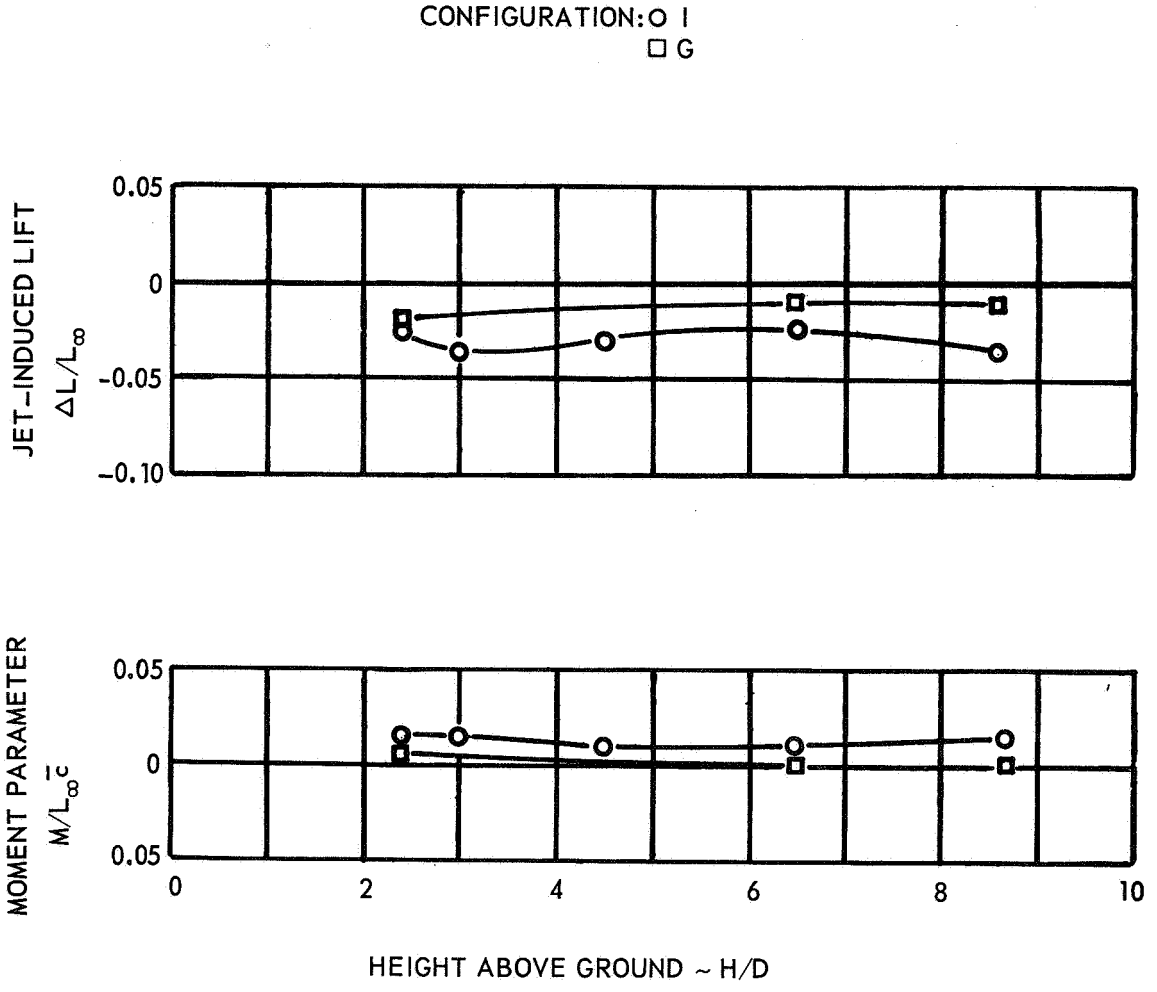

(b) WING ONLY

FIGURE 25 – CONTINUED

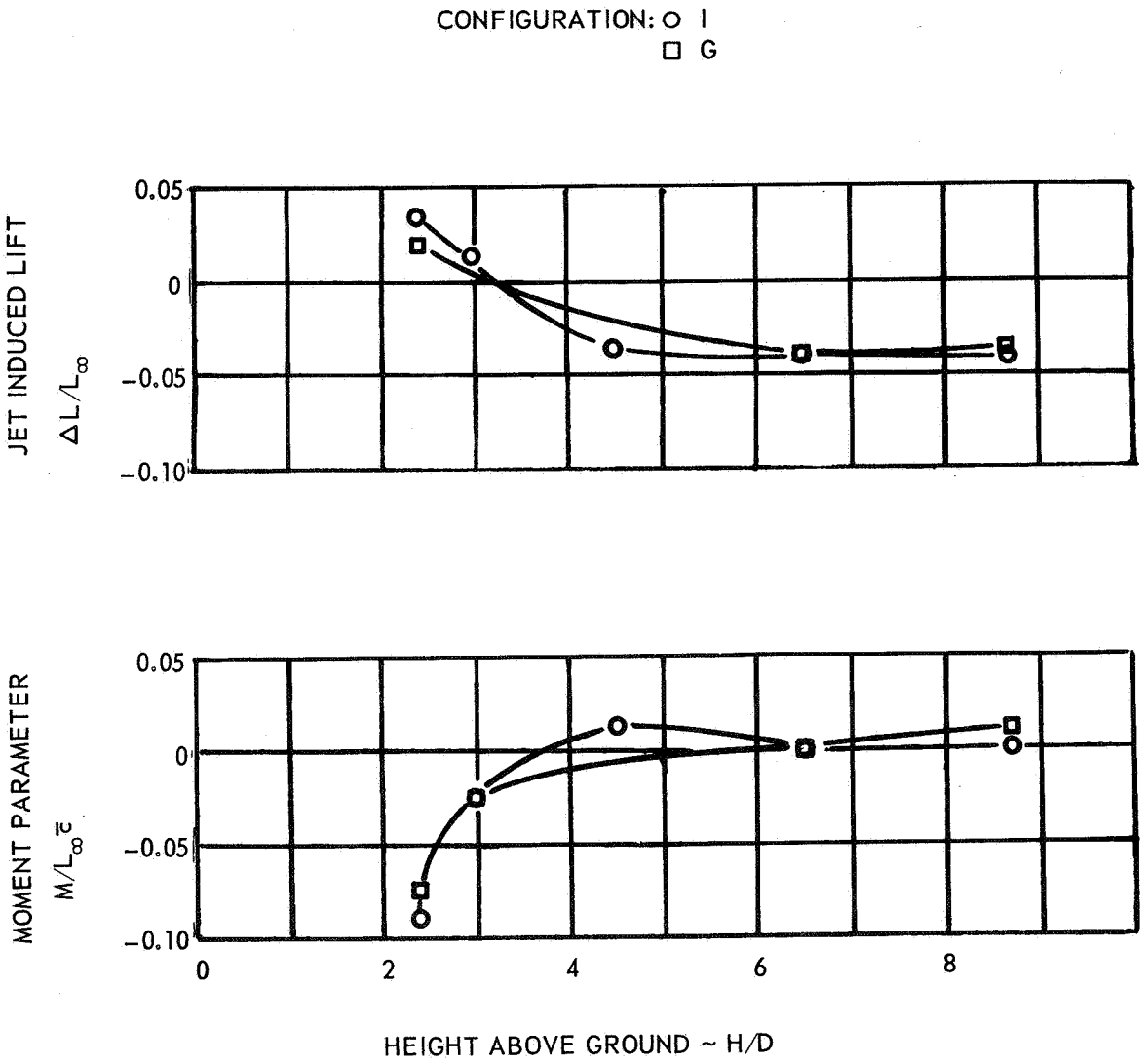

(c) FUSELAGE ONLY

FIGURE 25 – CONCLUDED

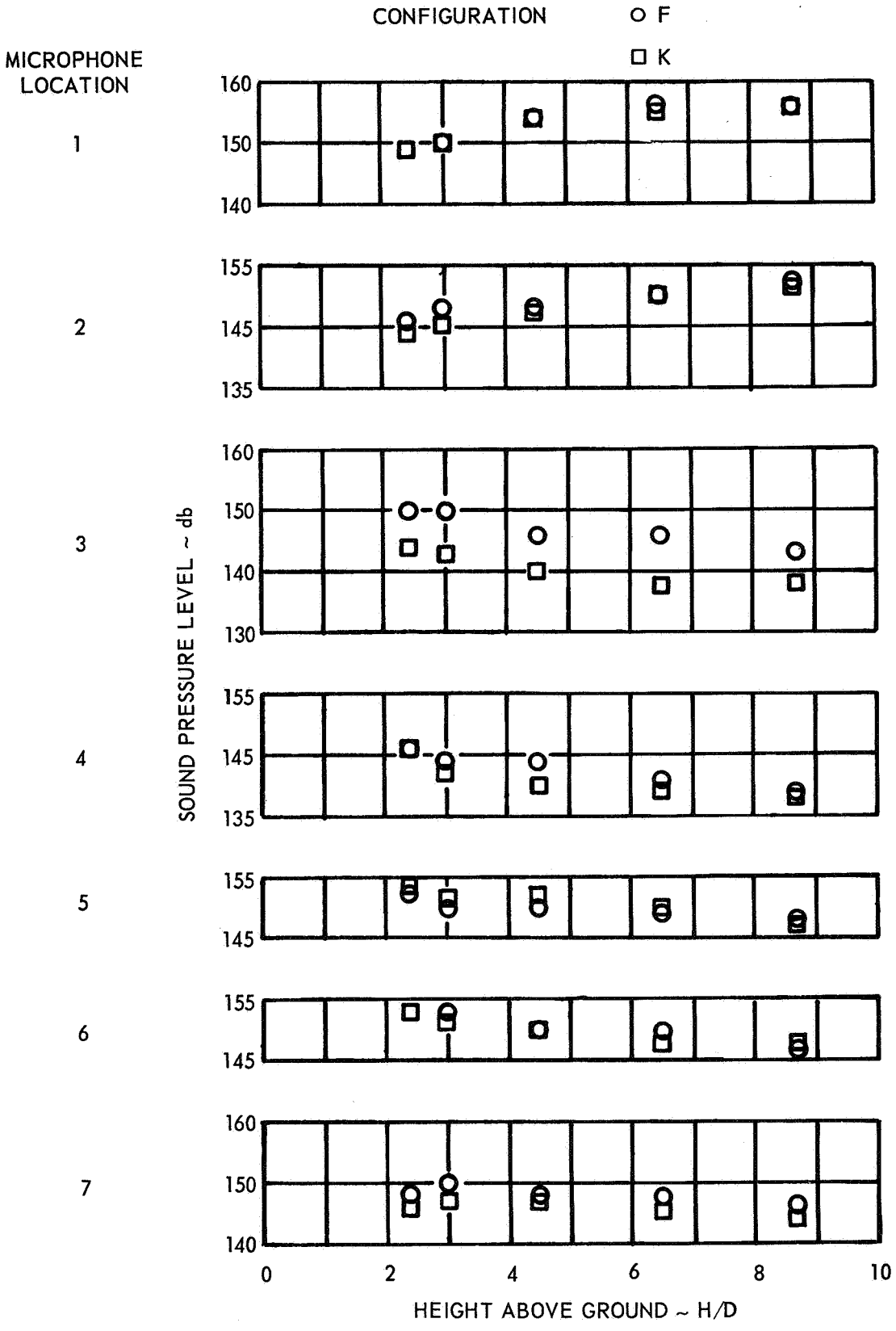

FIGURE 26. NEAR FIELD SOUND PRESSURE

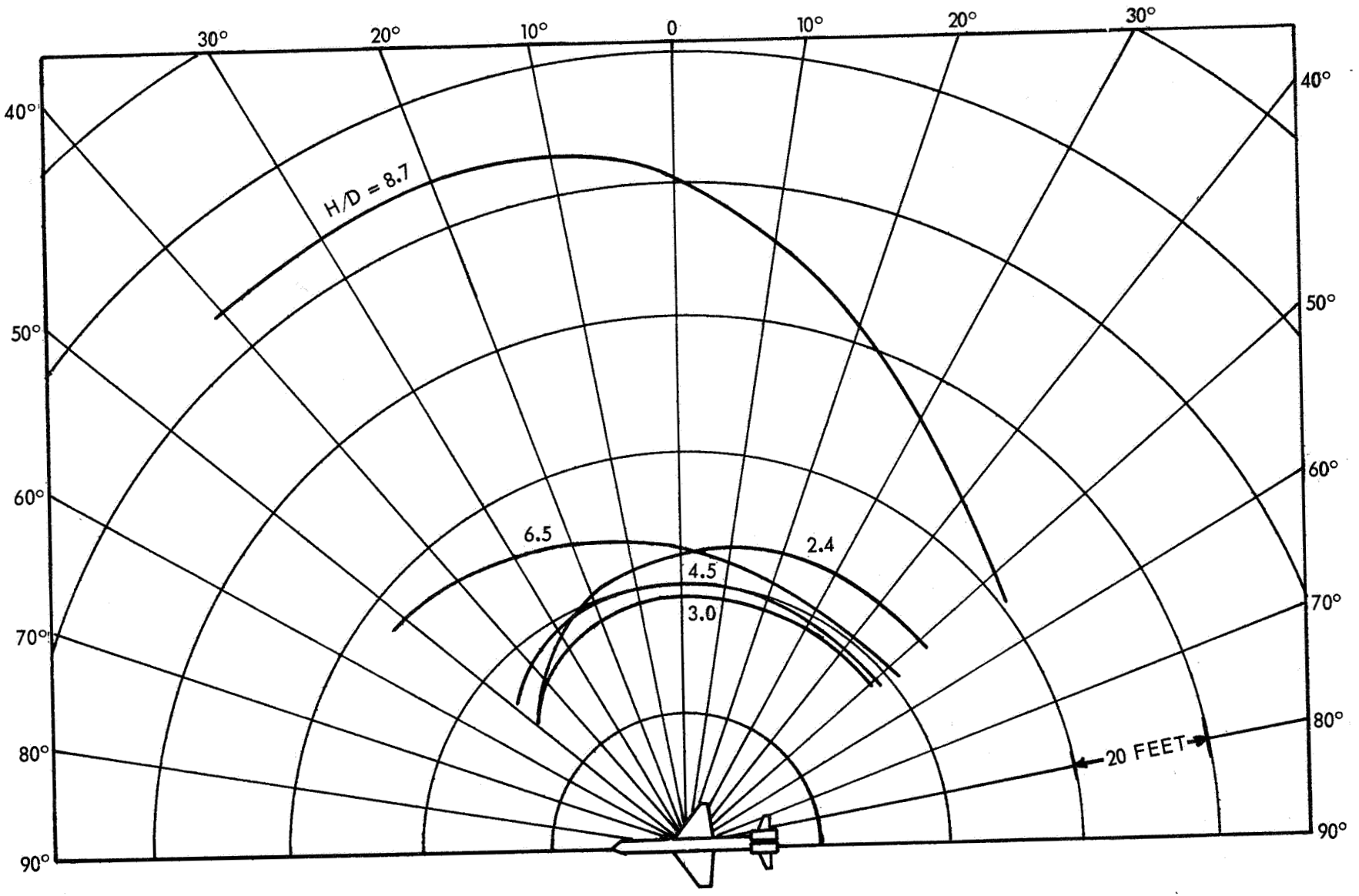

(a) LOW WING

FIGURE 27. 125 db SOUND LEVEL LINES

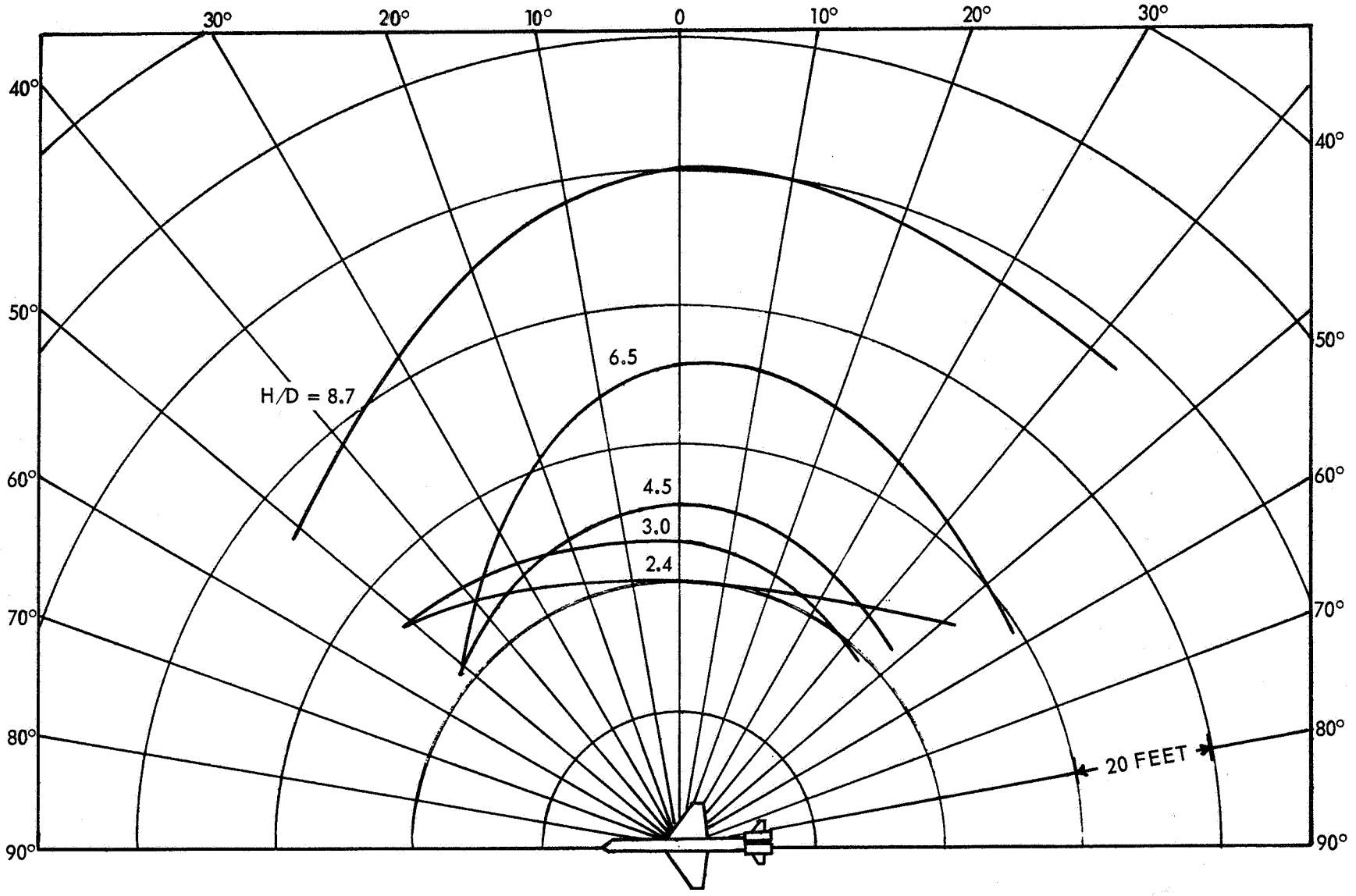

(b) HIGH WING

FIGURE 27. – CONCLUDED

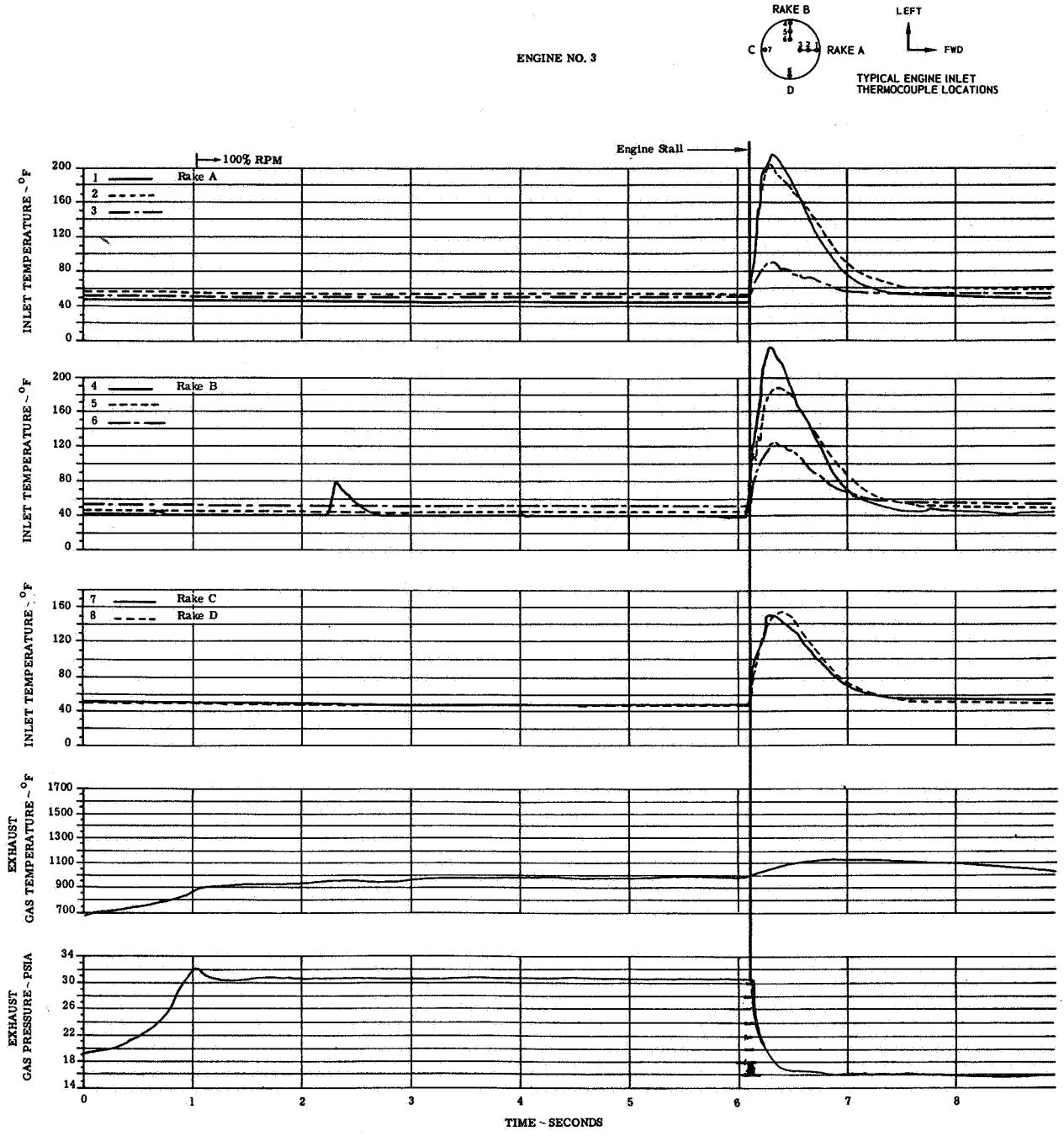

FIGURE 28(a) SELECTED ENGINE TEMPERATURE AND PRESSURE TRANSIENTS USED FOR STALL ANALYSIS

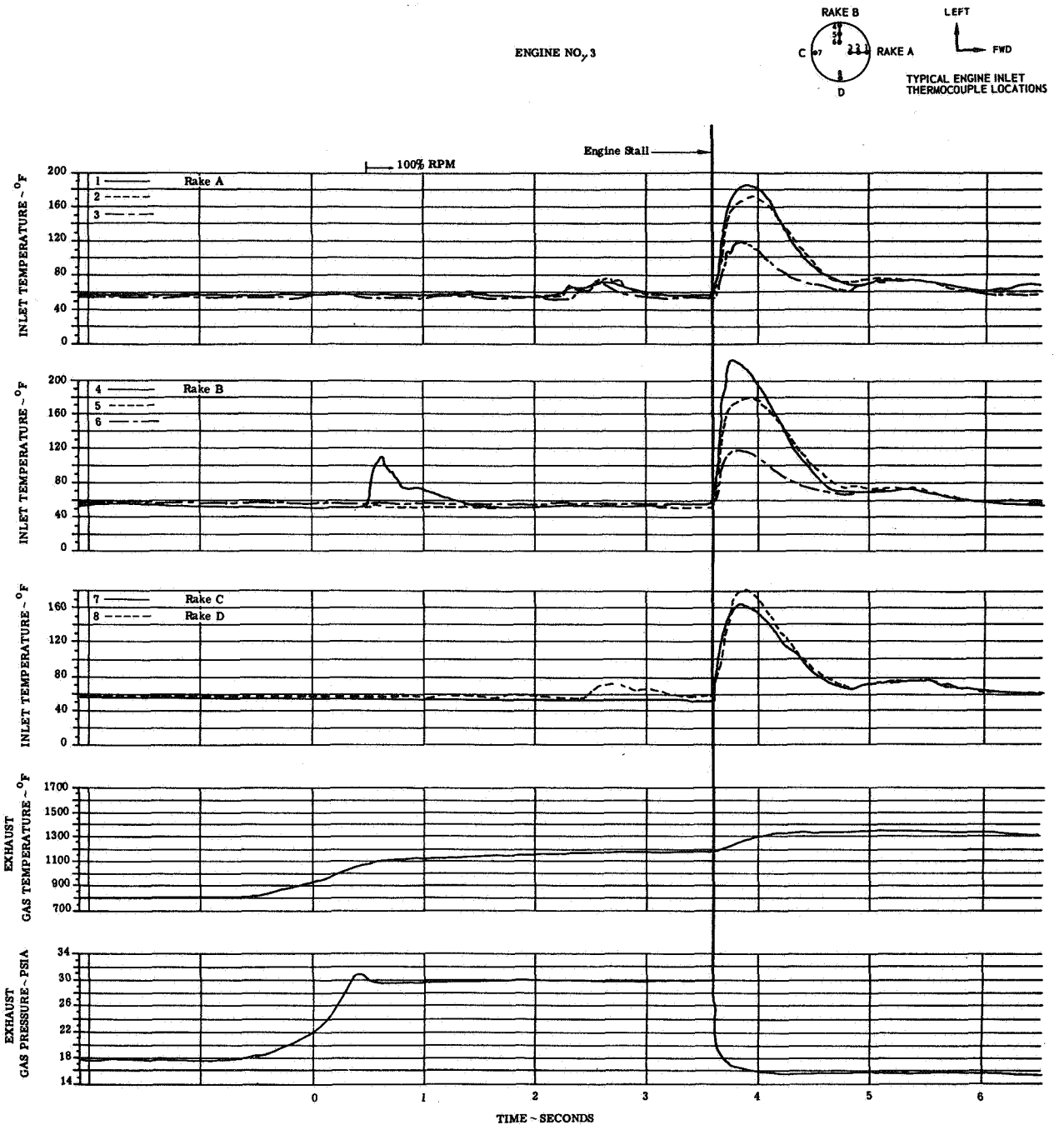

FIGURE 28(b). SELECTED ENGINE TEMPERATURE AND PRESSURE TRANSIENTS USED FOR STALL ANALYSIS

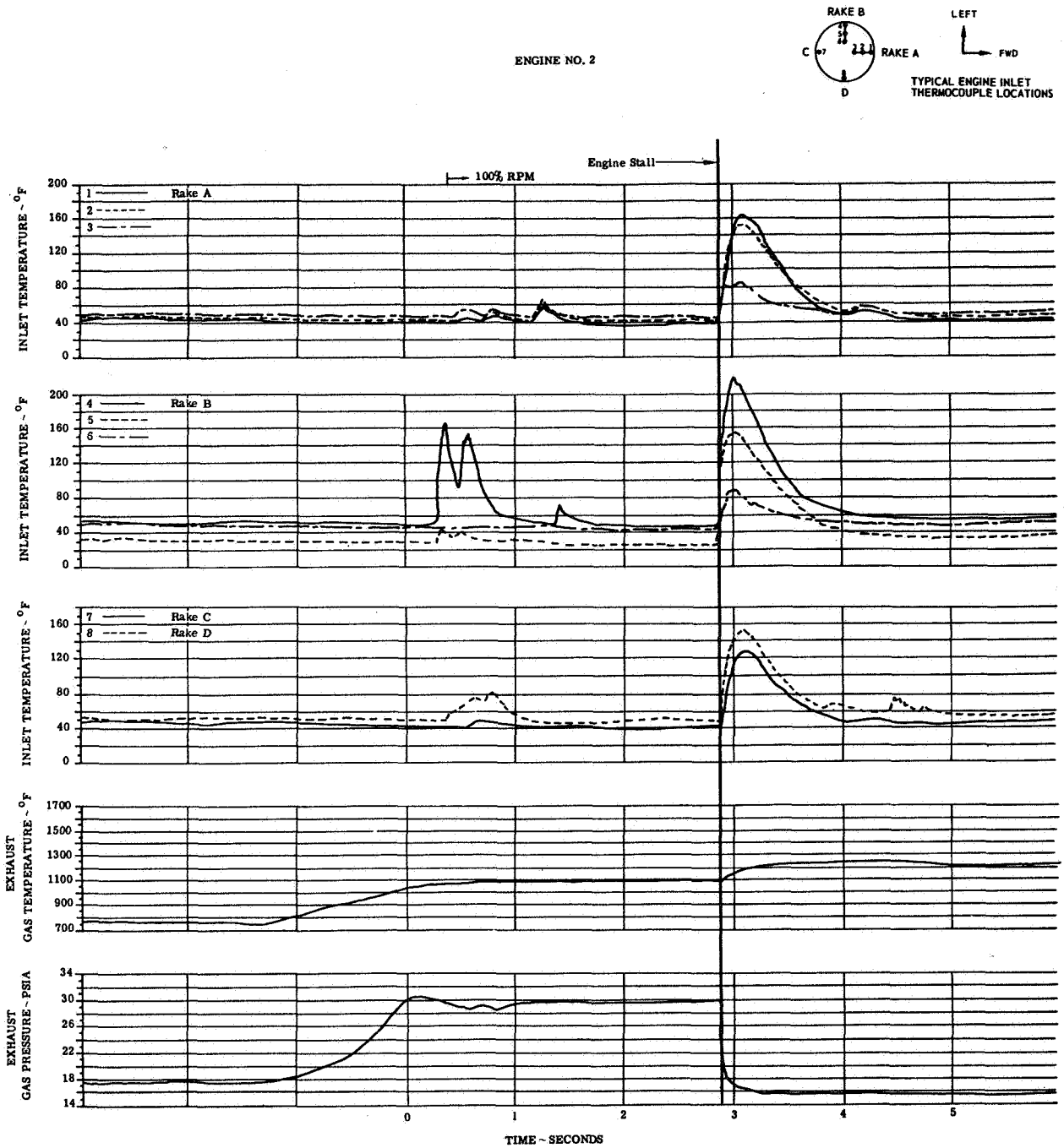

FIGURE 28(c). SELECTED ENGINE TEMPERATURE AND PRESSURE TRANSIENTS USED FOR STALL ANALYSIS

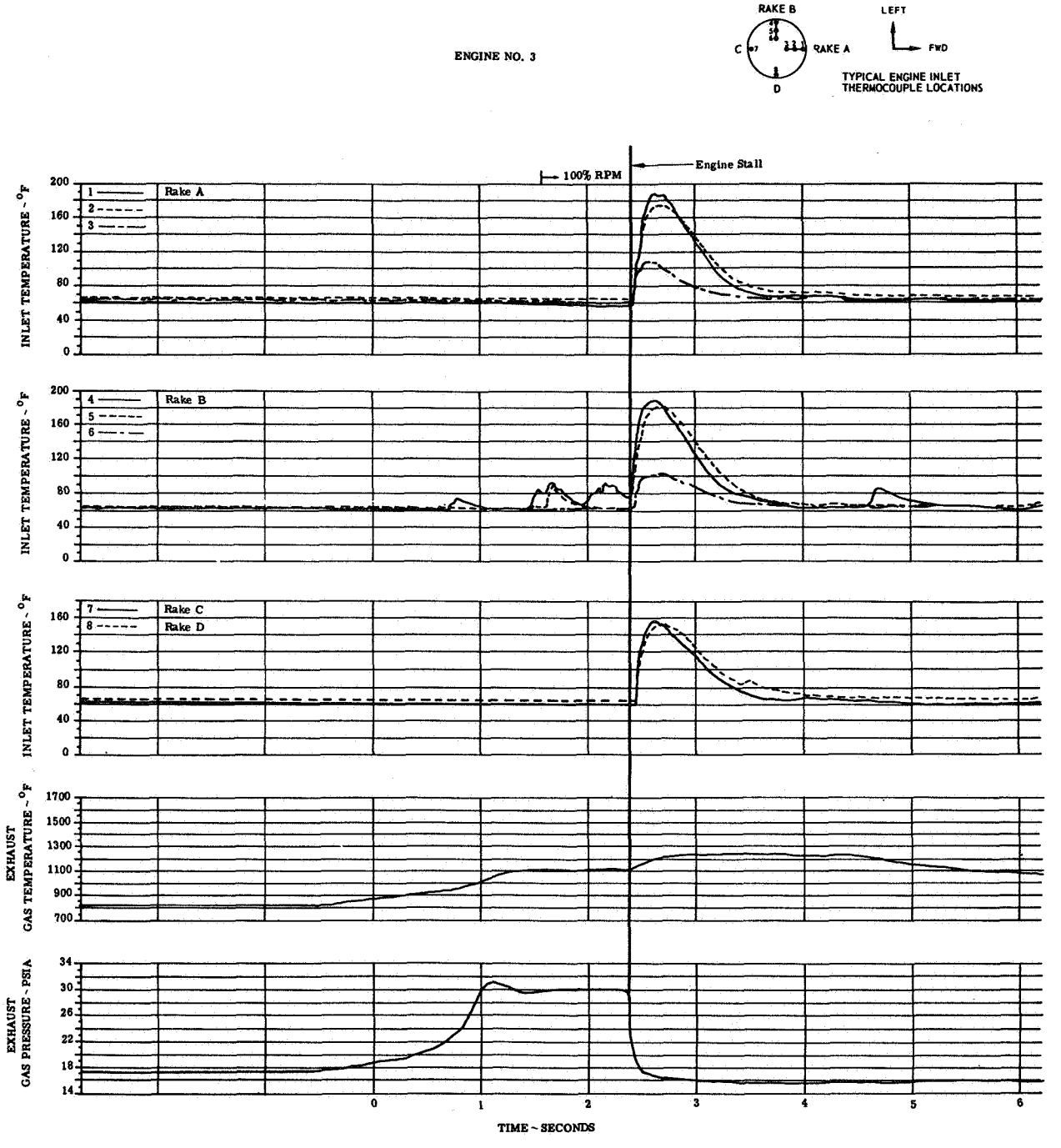

FIGURE 28(d). SELECTED ENGINE TEMPERATURE AND PRESSURE TRANSIENTS USED FOR STALL ANALYSIS

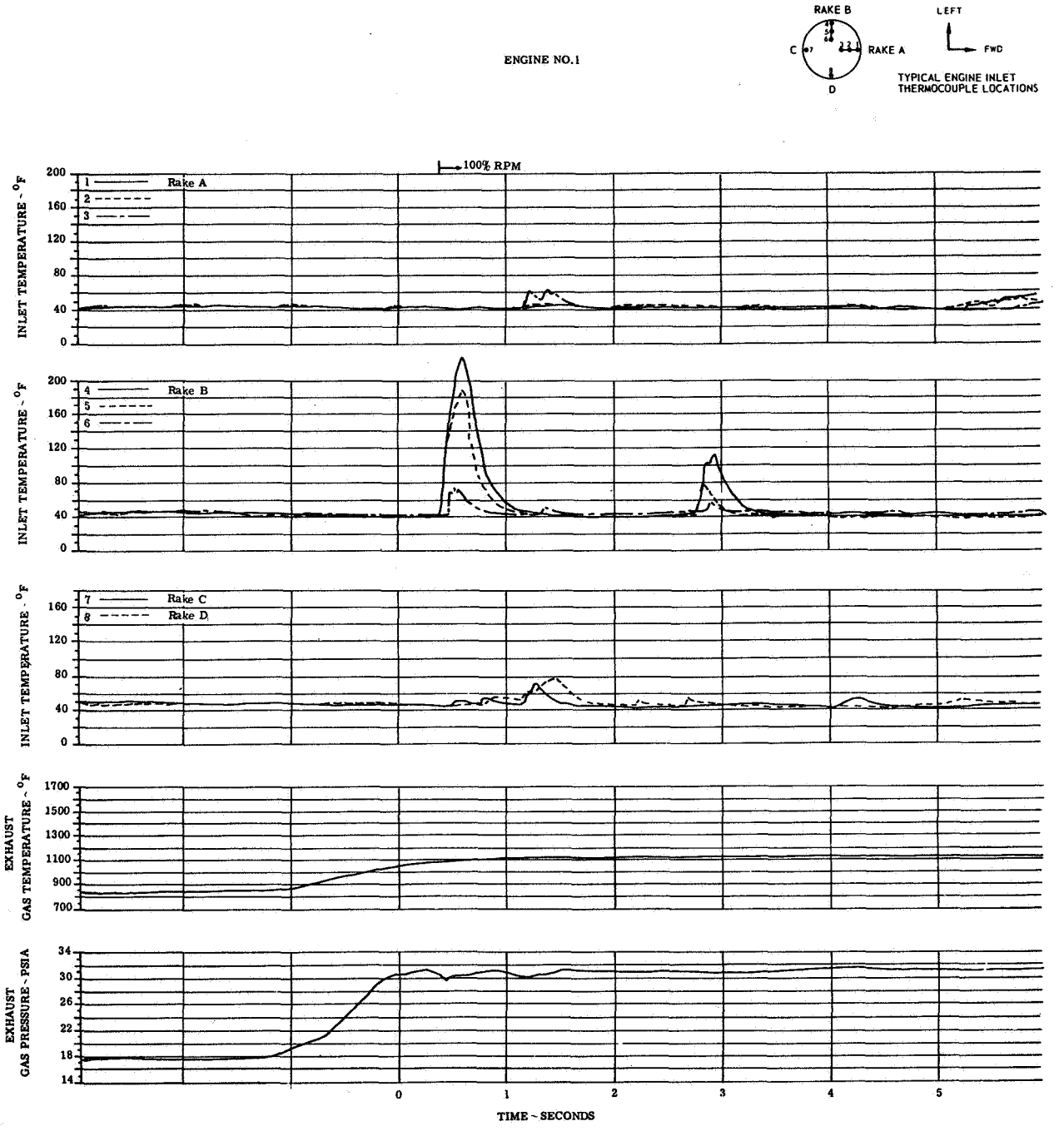

FIGURE 28(e). SELECTED ENGINE TEMPERATURE AND PRESSURE TRANSIENTS USED FOR STALL ANALYSIS

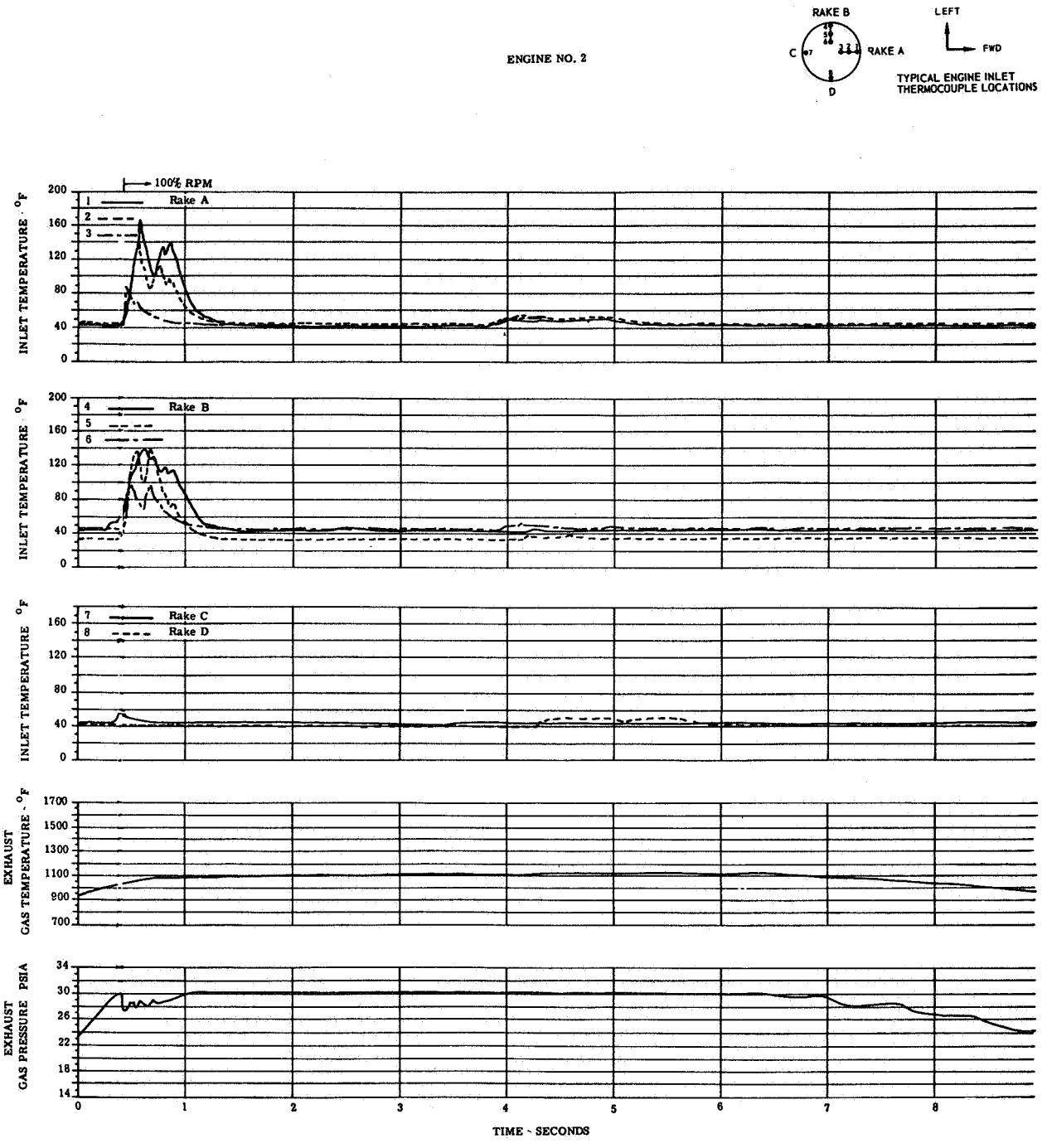

FIGURE 28(f). SELECTED ENGINE TEMPERATURE AND PRESSURE TRANSIENTS USED FOR STALL ANALYSIS

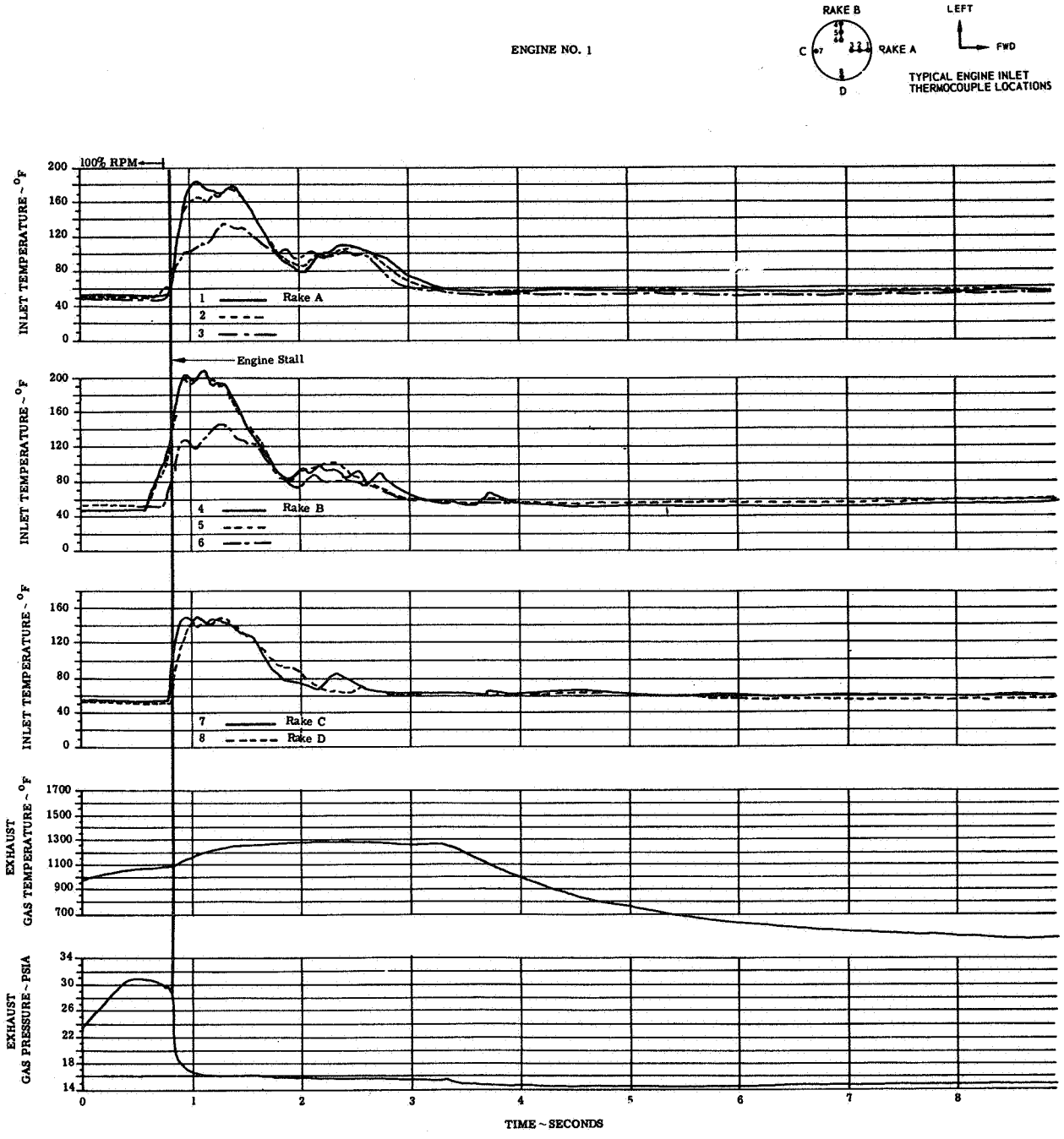

FIGURE 28(g). SELECTED ENGINE TEMPERATURE AND PRESSURE TRANSIENTS USED FOR STALL ANALYSIS

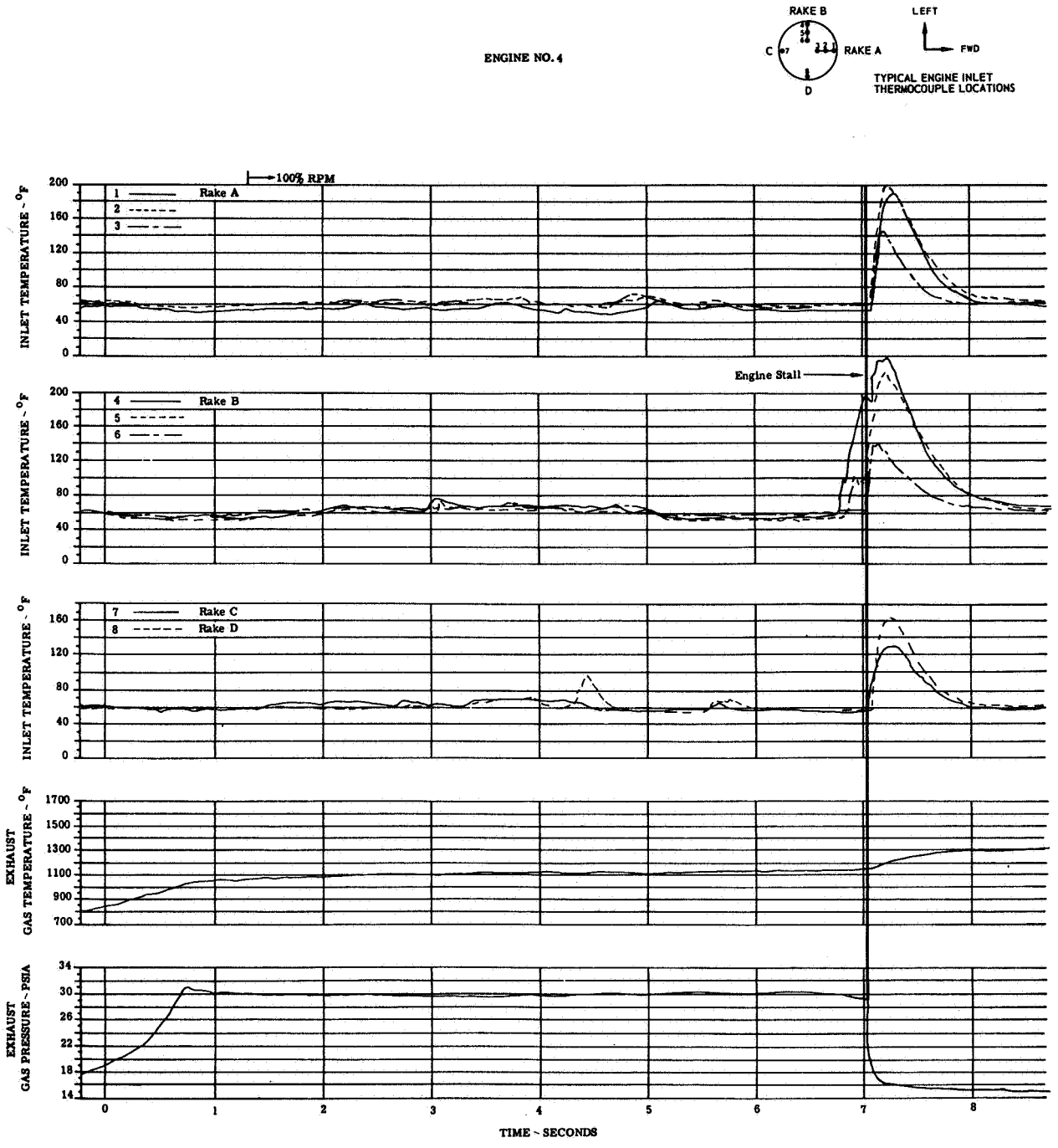

FIGURE 28(h). SELECTED ENGINE TEMPERATURE AND PRESSURE TRANSIENTS USED FOR STALL ANALYSIS

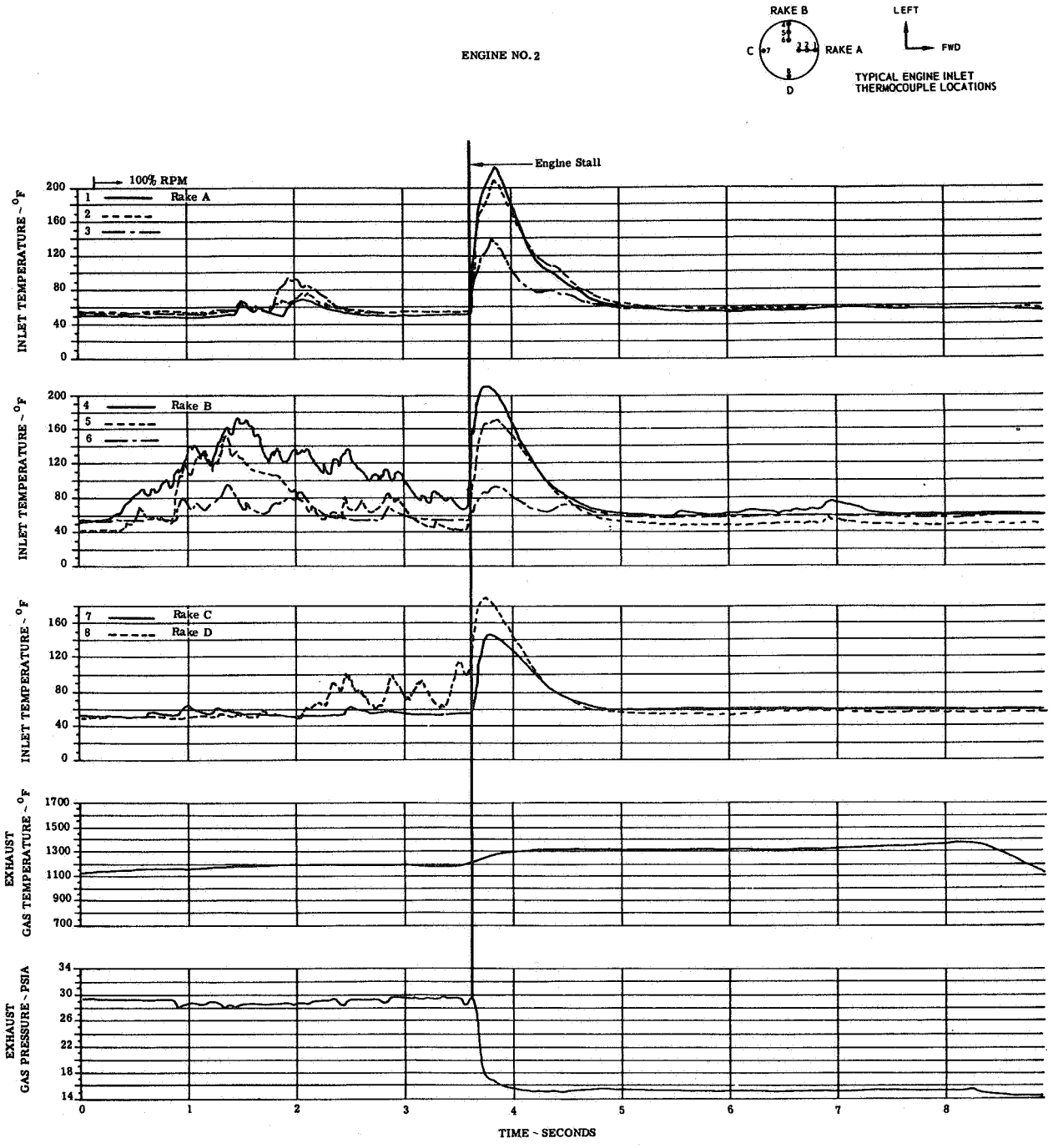

FIGURE 28(i). SELECTED ENGINE TEMPERATURE AND PRESSURE TRANSIENTS USED FOR STALL ANALYSIS

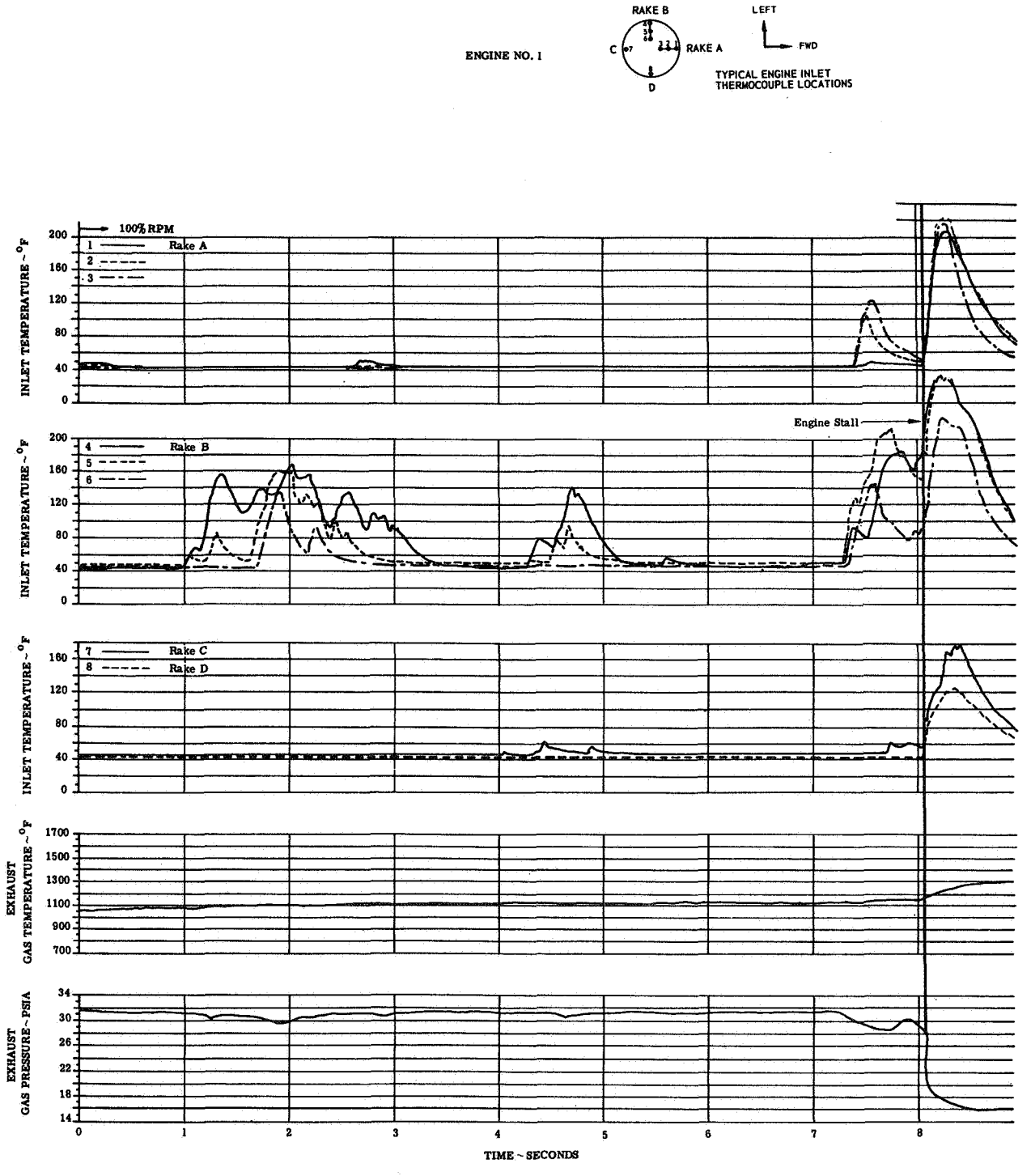

FIGURE 28(j). SELECTED ENGINE TEMPERATURE AND PRESSURE TRANSIENTS USED FOR STALL ANALYSIS

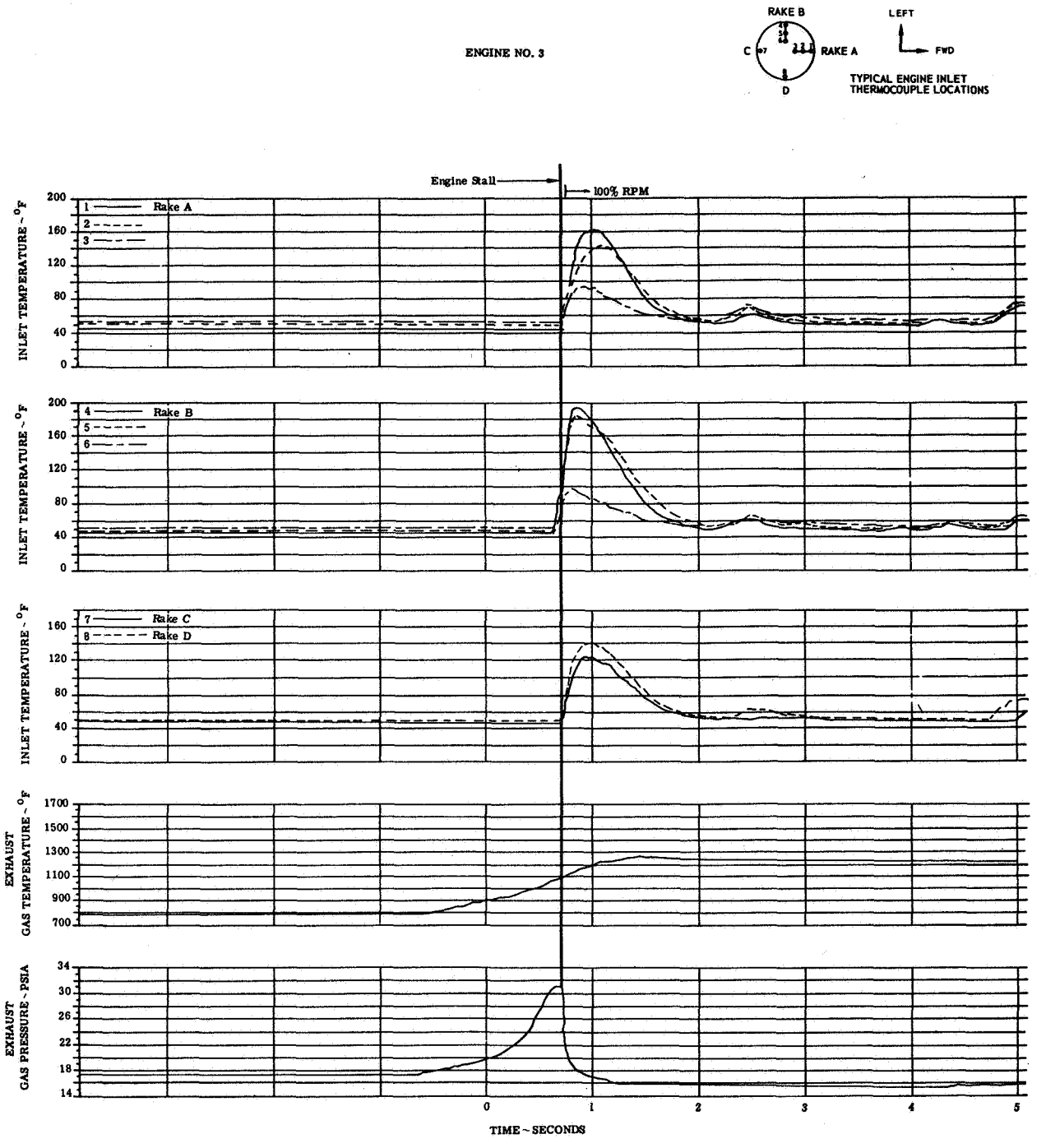

FIGURE 28(k). SELECTED ENGINE TEMPERATURE AND PRESSURE TRANSIENTS USED FOR STALL ANALYSIS

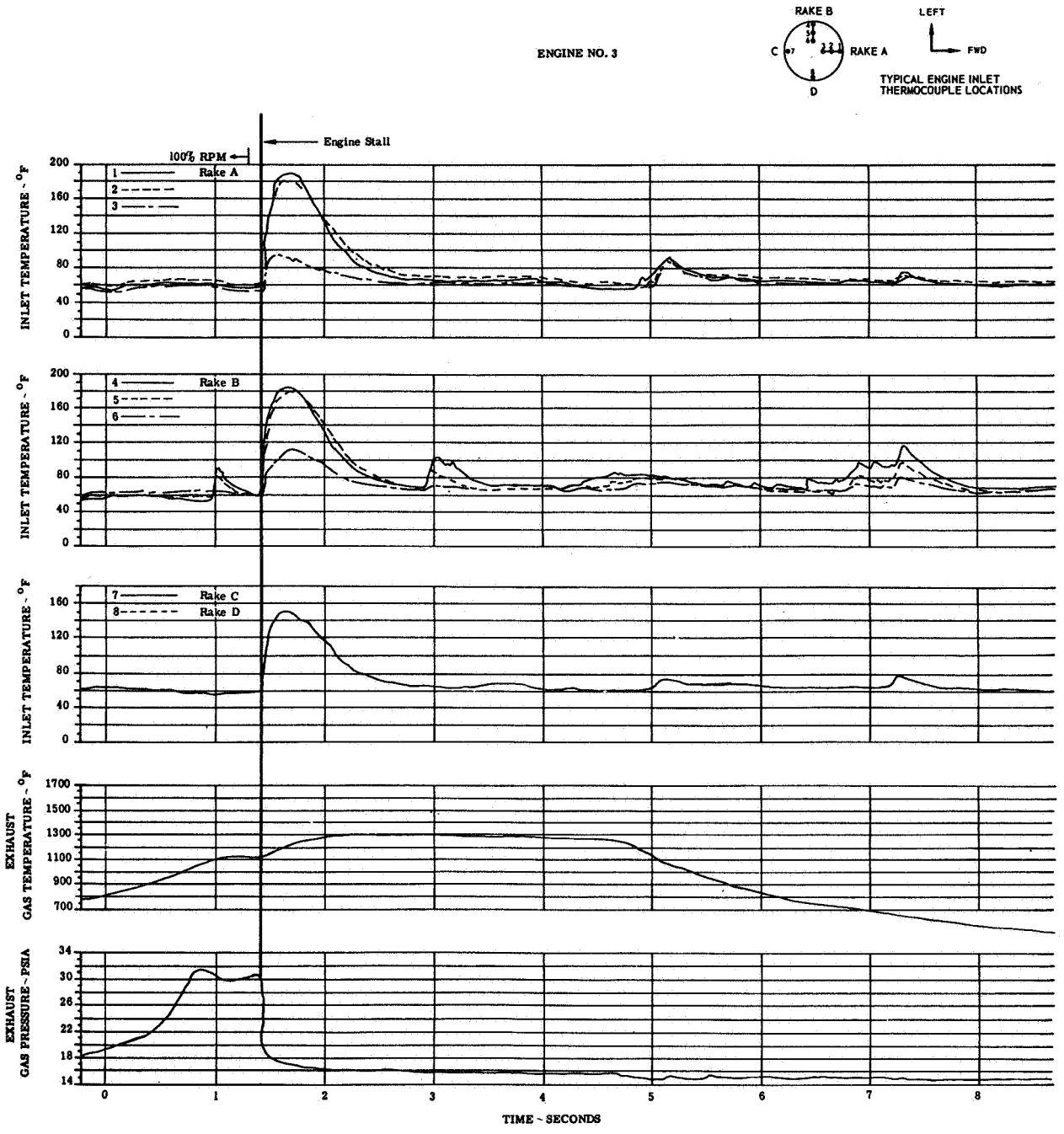

FIGURE 28(1). SELECTED ENGINE TEMPERATURE AND PRESSURE TRANSIENTS USED FOR STALL ANALYSIS

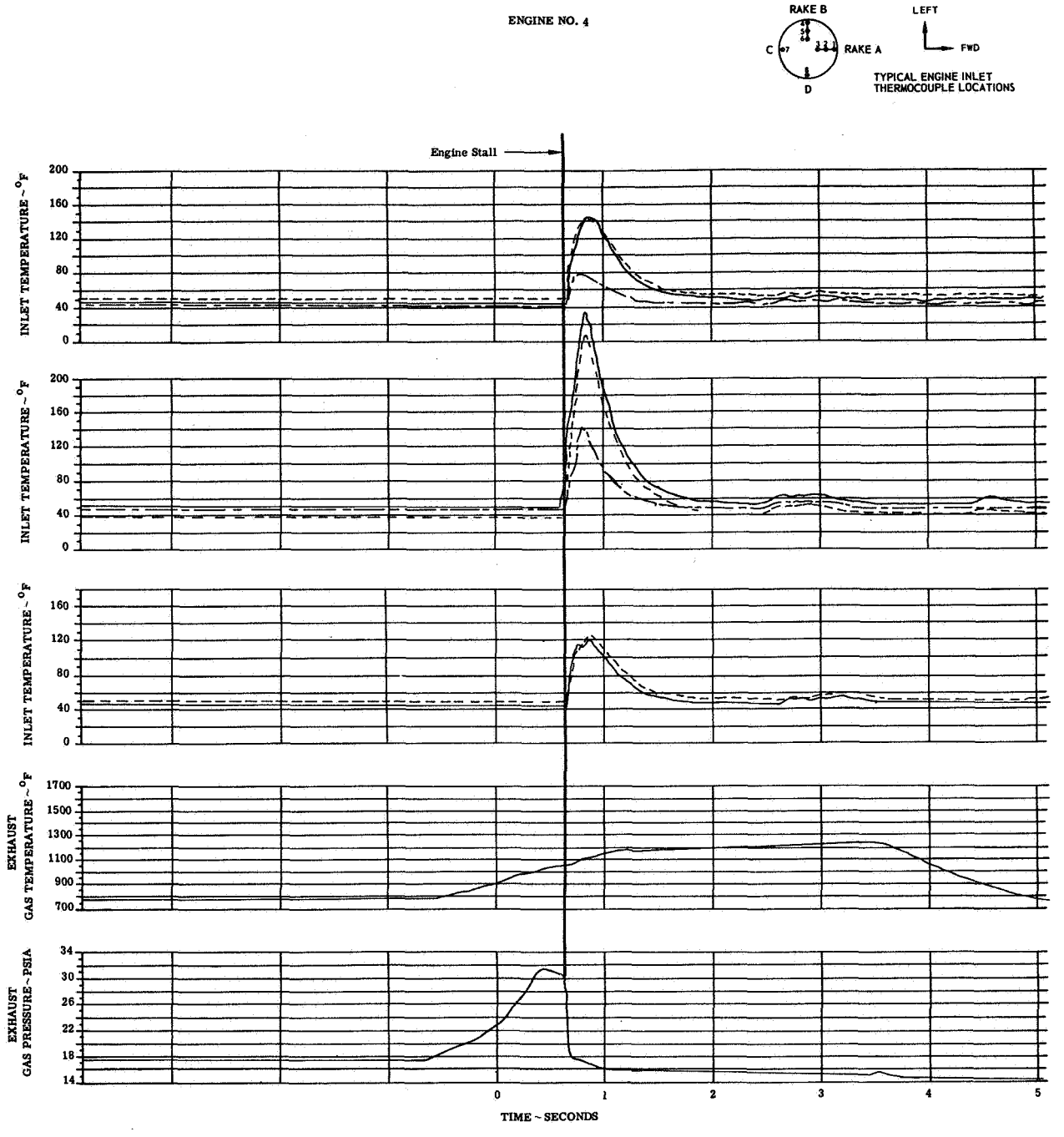

FIGURE 28(m). SELECTED ENGINE TEMPERATURE AND PRESSURE TRANSIENTS USED FOR STALL ANALYSIS

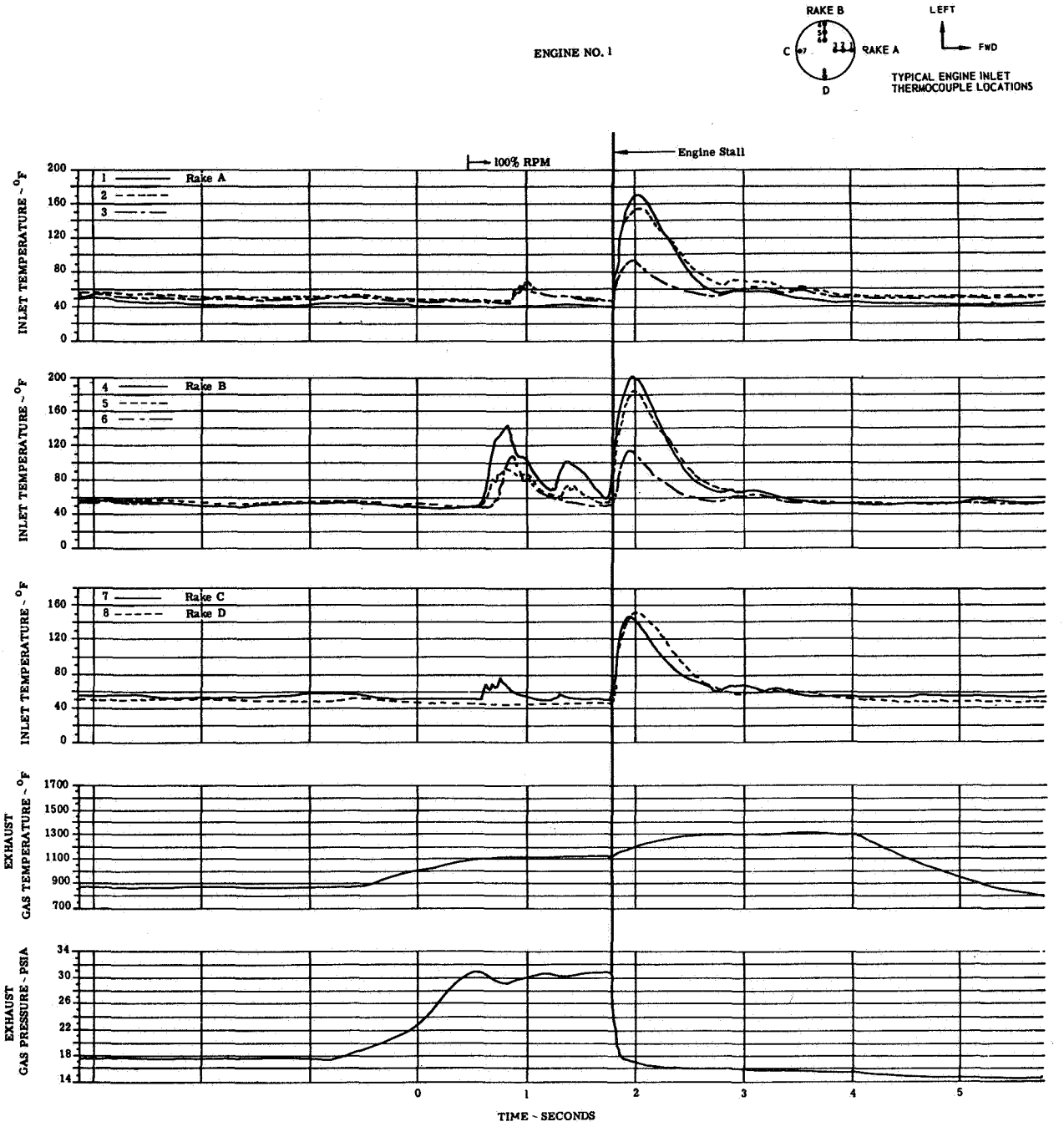

FIGURE 28(n). SELECTED ENGINE TEMPERATURE AND PRESSURE TRANSIENTS USED FOR STALL ANALYSIS

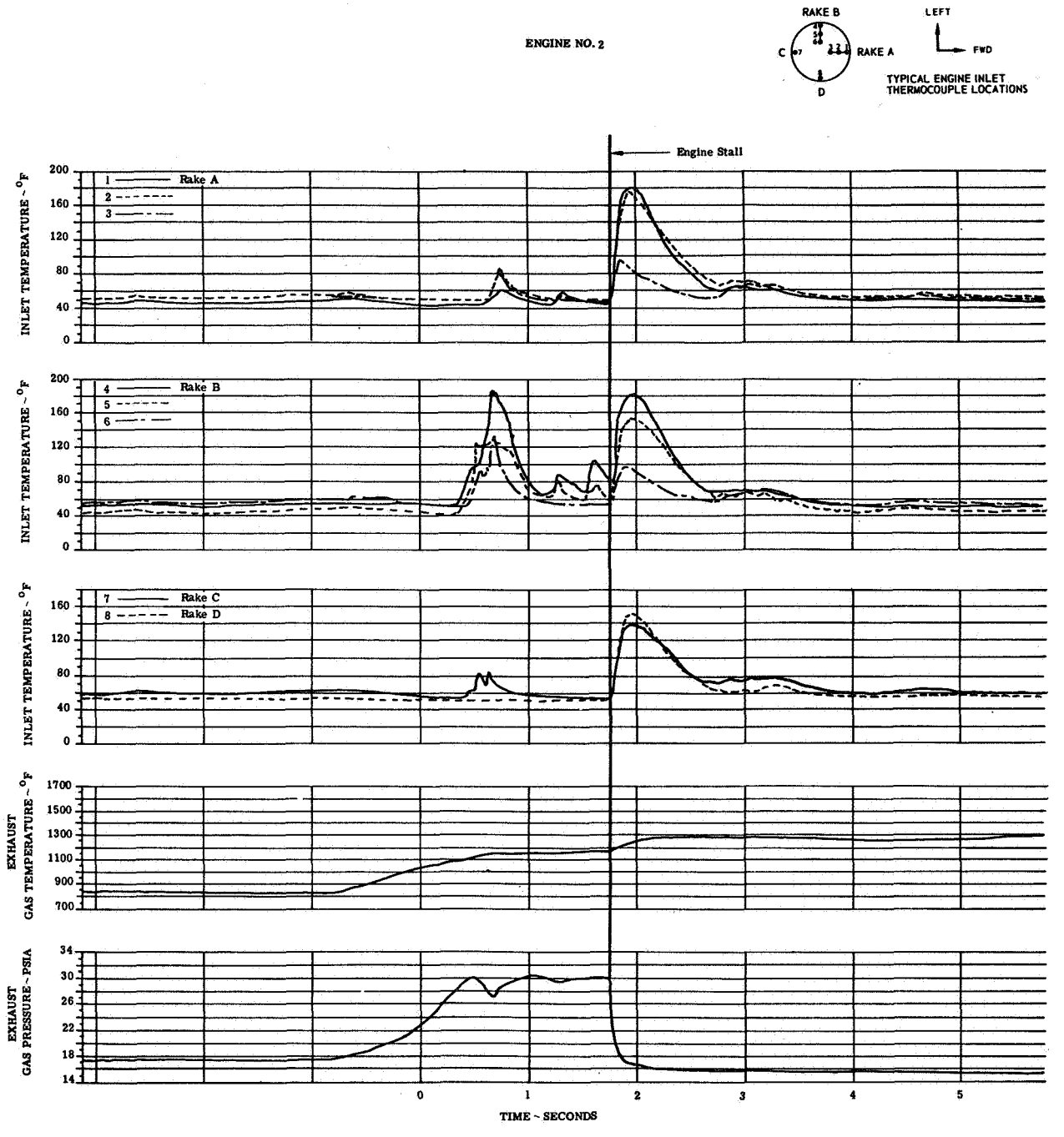

FIGURE 28(o). SELECTED ENGINE TEMPERATURE AND PRESSURE TRANSIENTS USED FOR STALL ANALYSIS

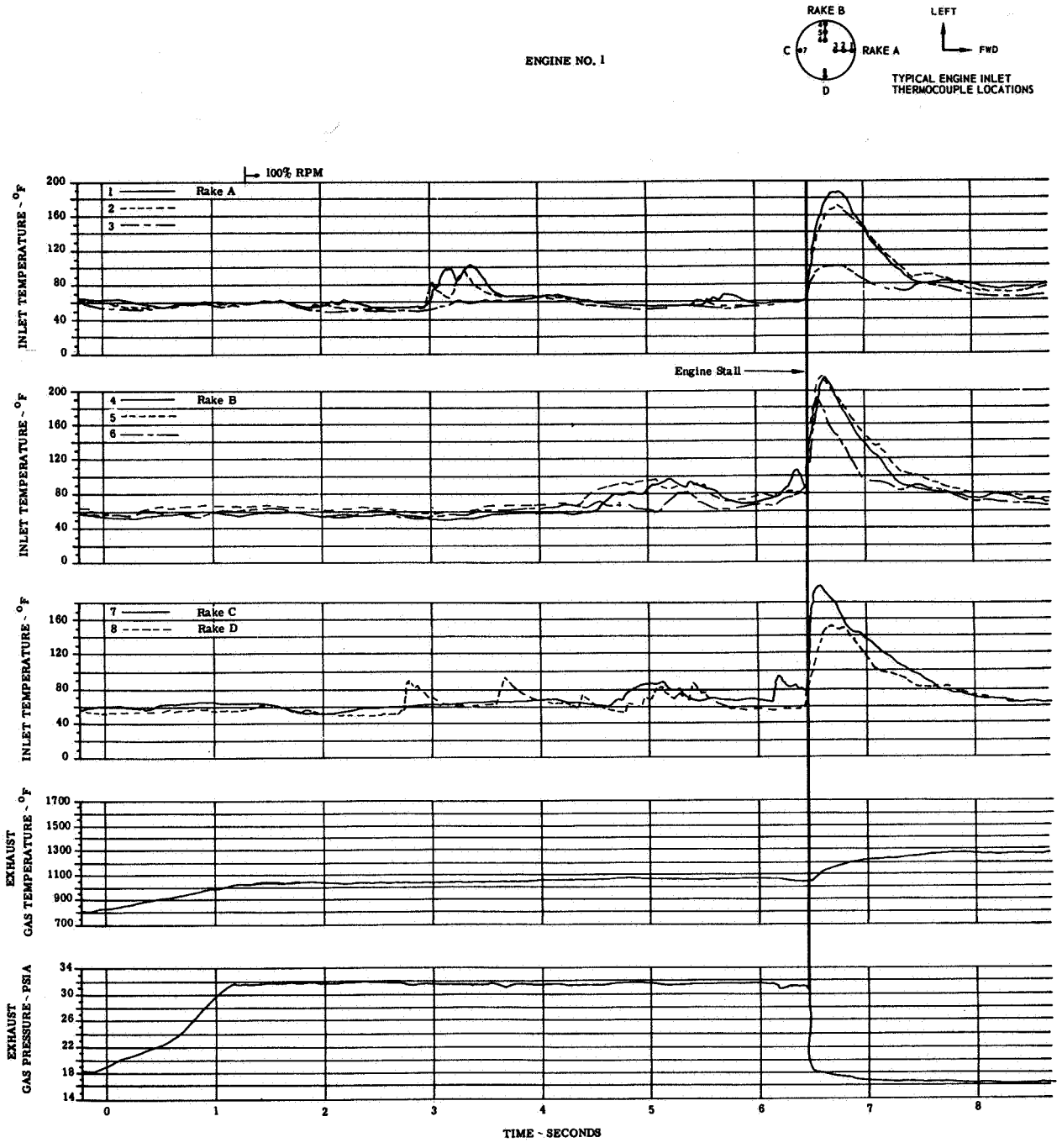

FIGURE 28(p). SELECTED ENGINE TEMPERATURE AND PRESSURE TRANSIENTS USED FOR STALL ANALYSIS

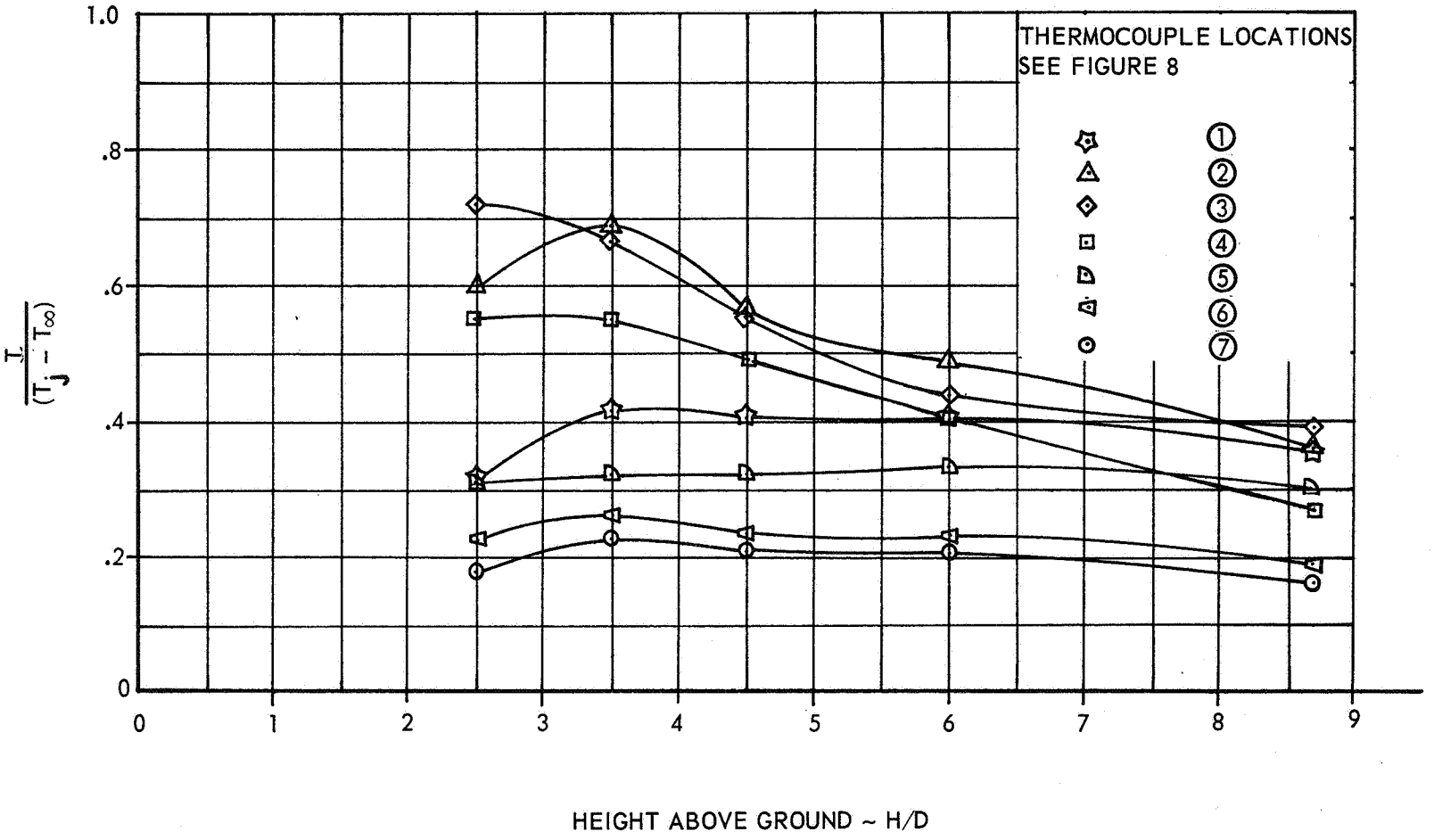

FIGURE 29. GROUND PLANE TEMPERATURES – ALL LIFT ENGINES OPERATING

ENGINES OPERATING

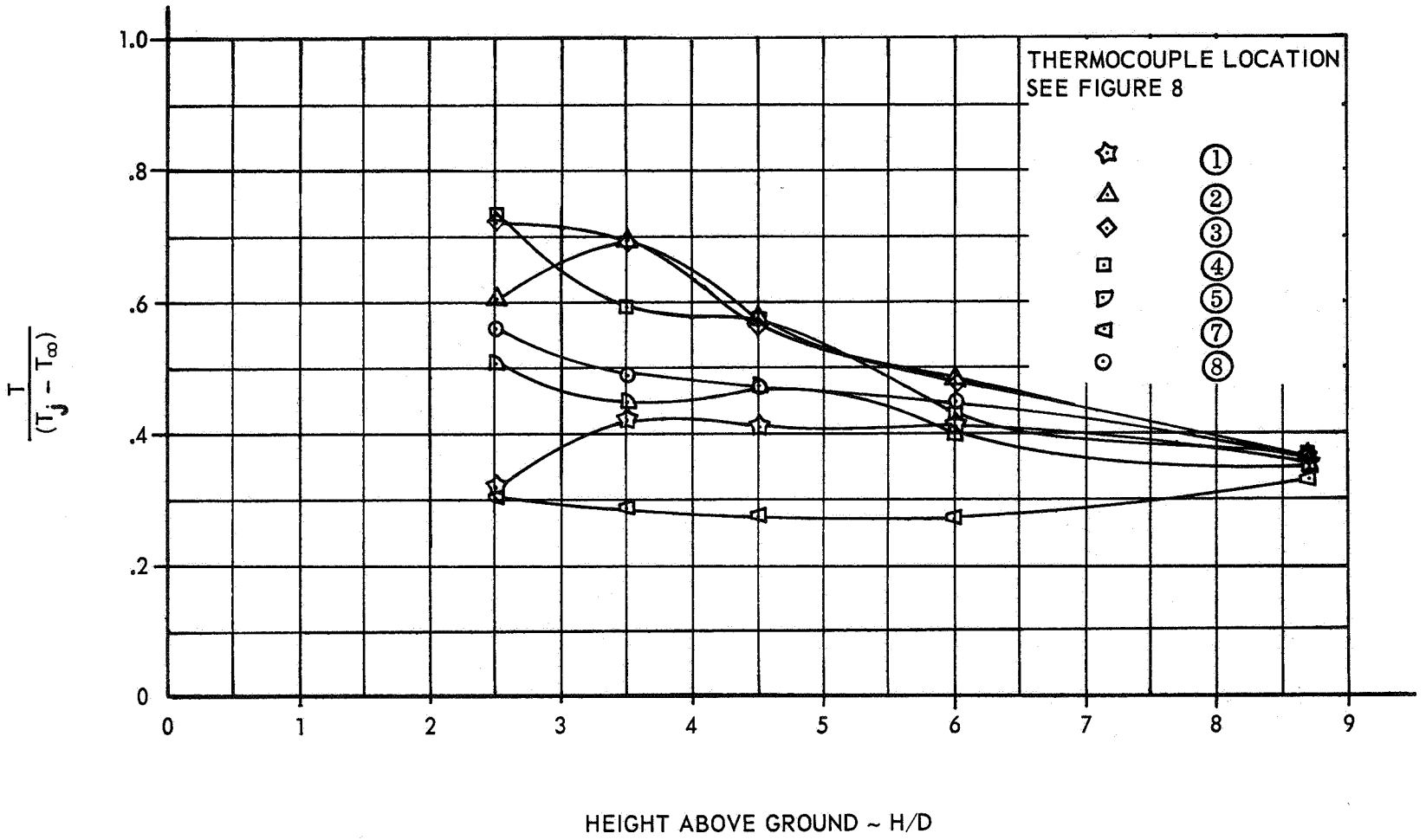

FIGURE 30. GROUND PLANE TEMPERATURES – ALL LIFT AND LIFT/CRUISE ENGINES OPERATING

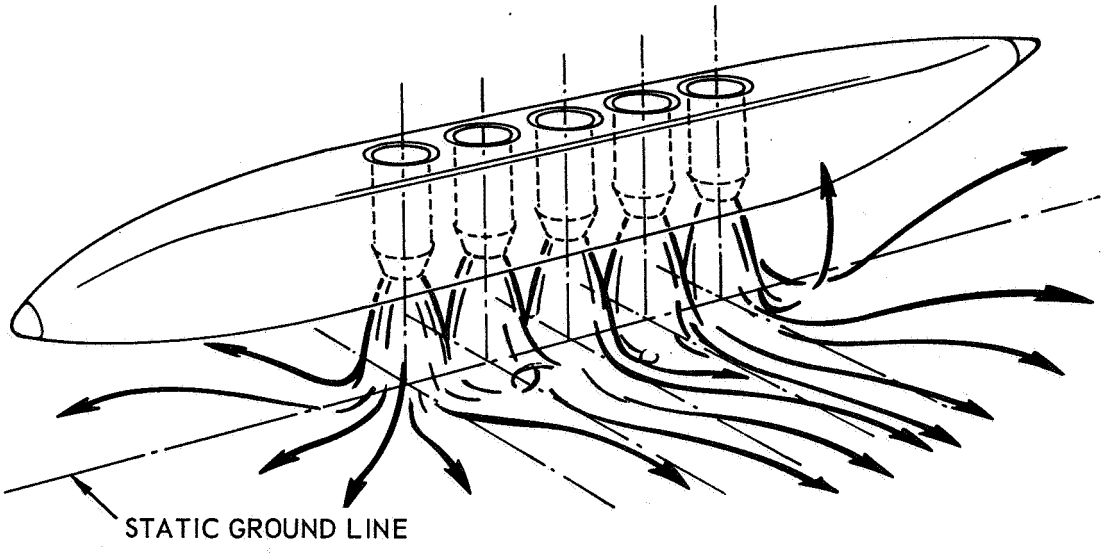

(a) BUOYANCY EFFECT

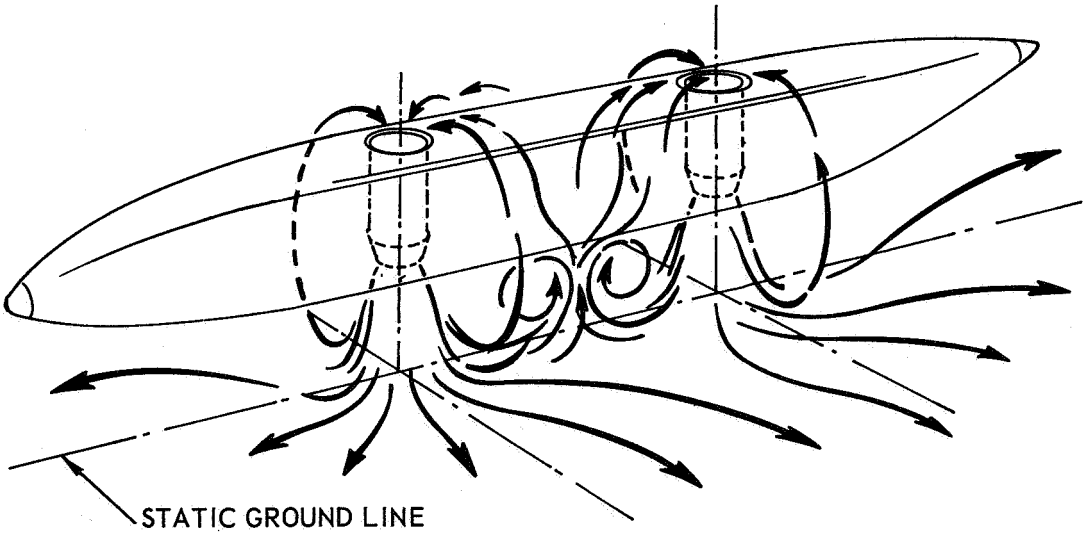

(b) FOUNTAIN EFFECT

FIGURE 31. HOT GAS INGESTION PHENOMENA

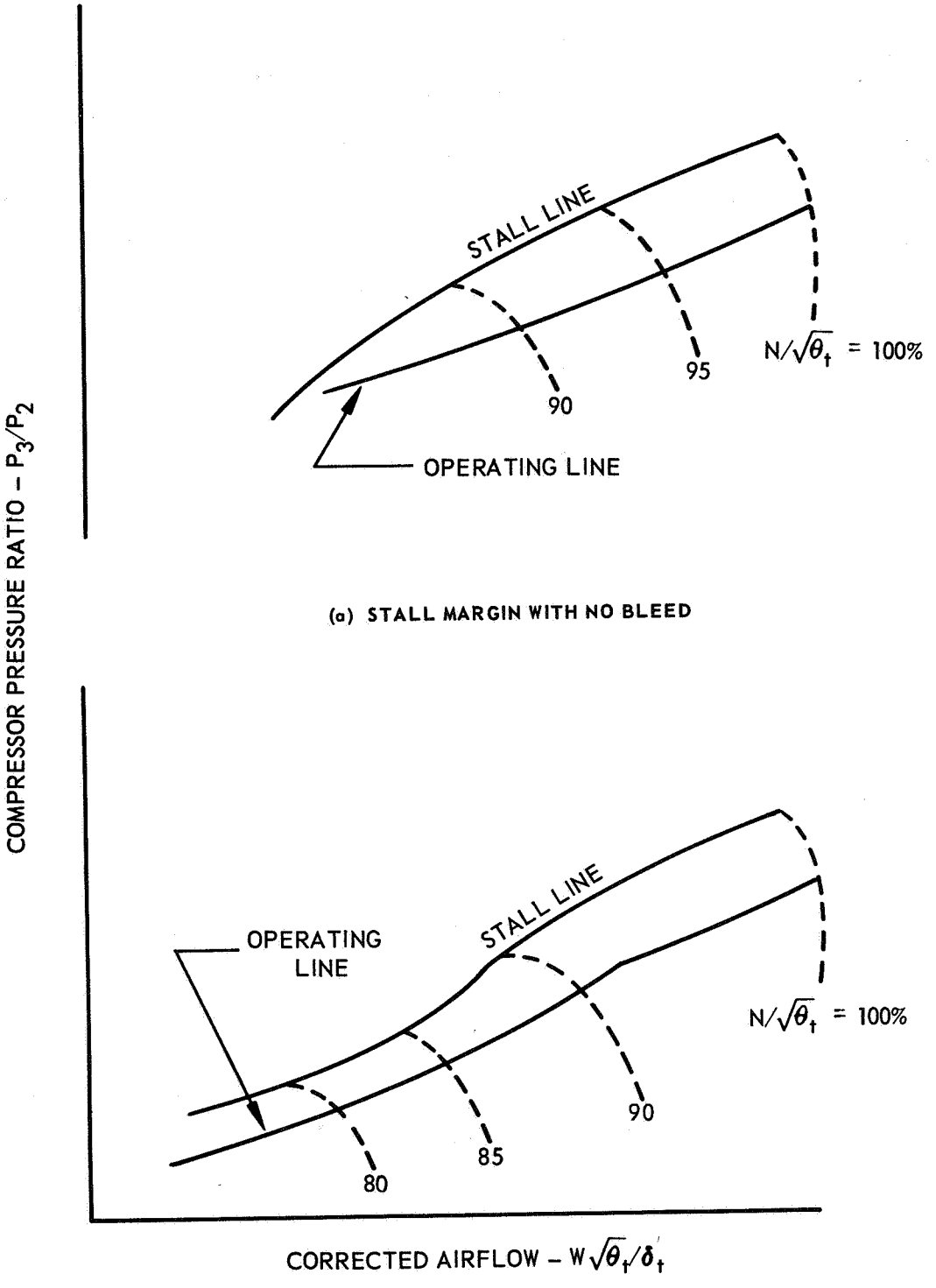

(a) STALL MARGIN WITH NO BLEED

(b) STALL MARGIN WITH SCHEDULED BLEED

FIGURE 32 INFLUENCE OF INTERSTAGE BLEED ON STALL MARGIN

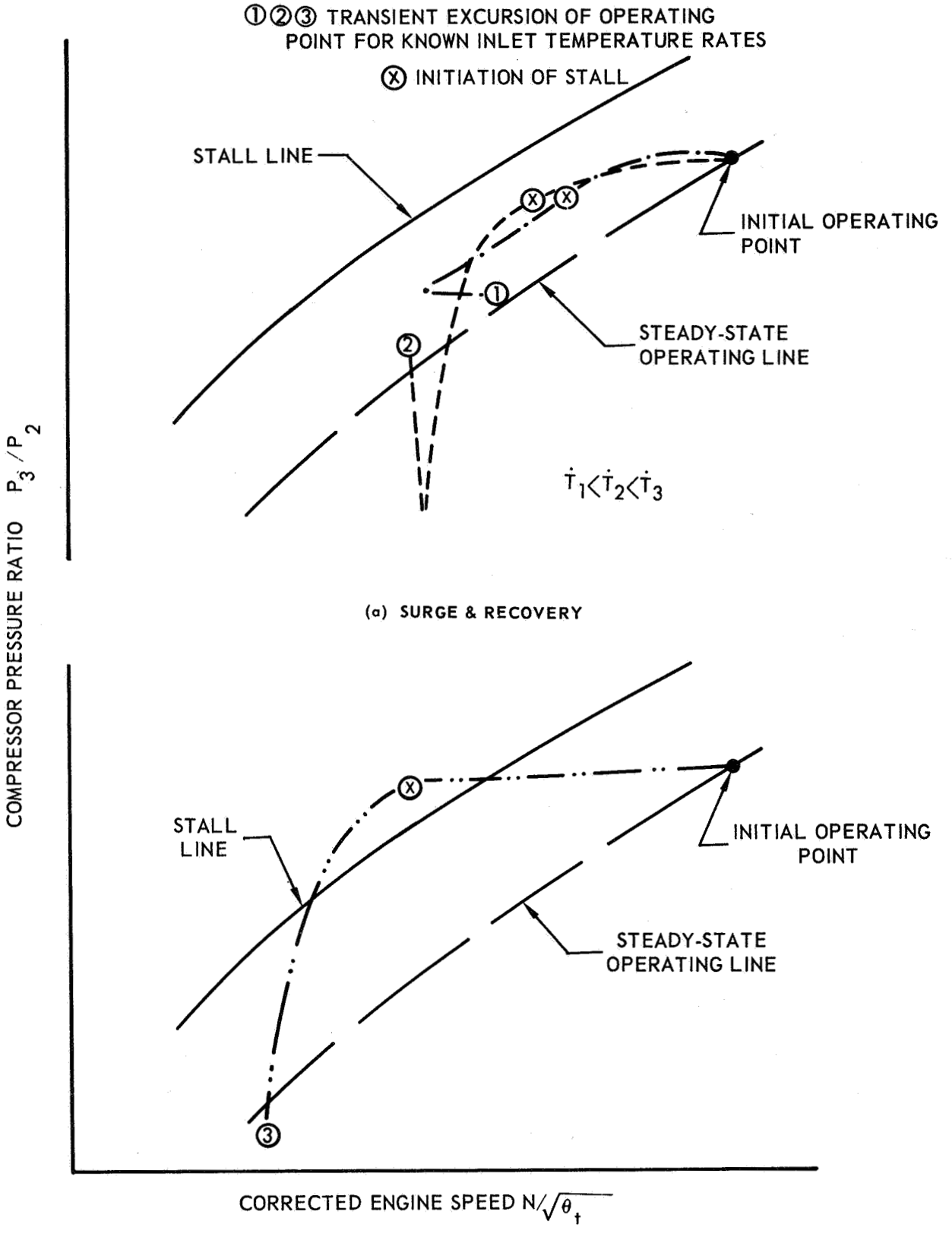

FIGURE 33 EFFECT OF INLET TEMPERATURE RISE ON STALL

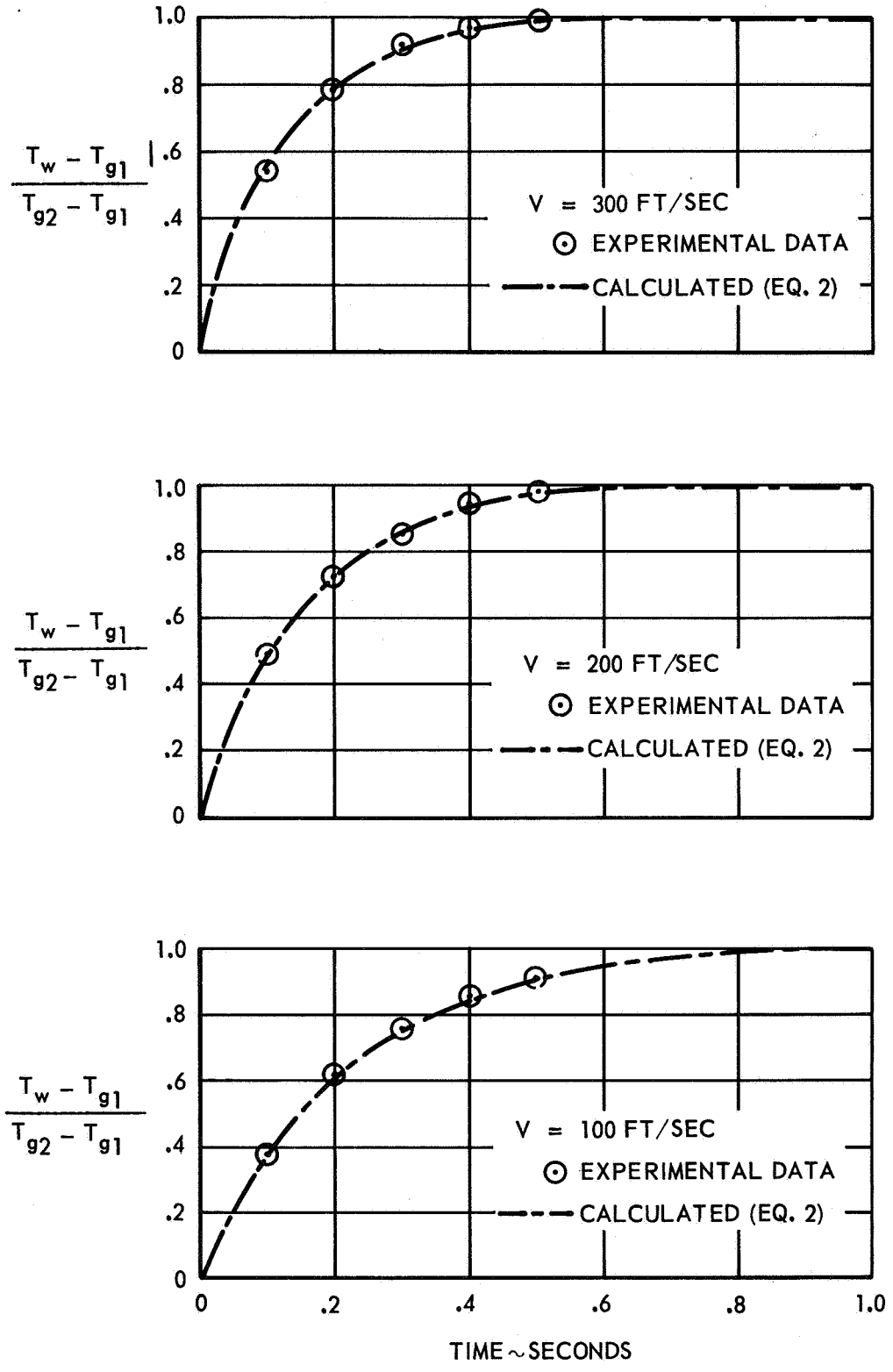

FIGURE 34 COMPARISON OF THEORETICAL RESPONSE TO EXPERIMENTALLY DETERMINED RESPONSE FOR A STEP CHANGE IN GAS TEMPERATURE FROM T_{g1} TO T_{g2}.

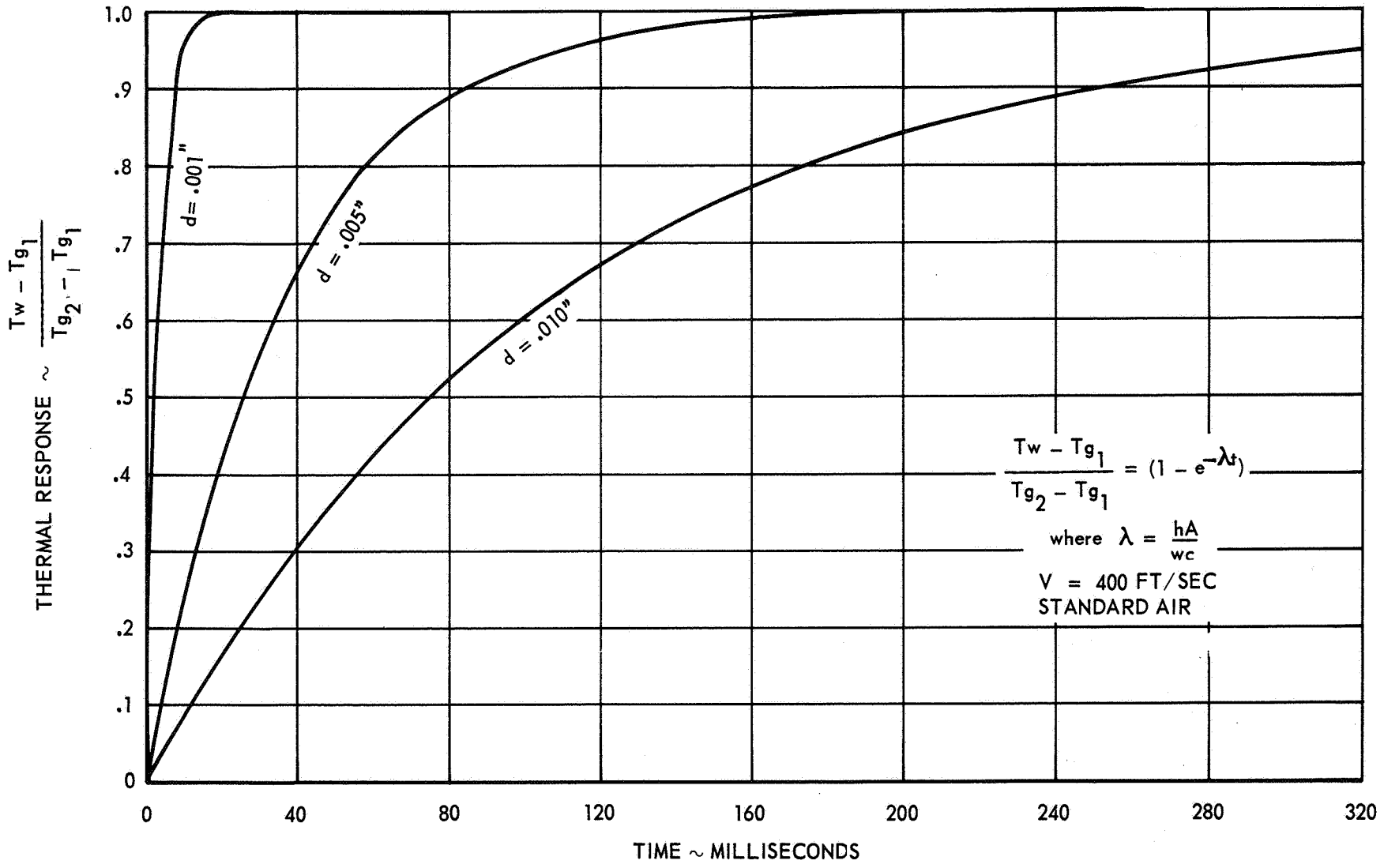

FIGURE 35 RESPONSE OF IRON–CONSTANTAN THERMOCOUPLE TO STEP CHANGE IN GAS TEMPERATURE FROM T_{g_1} TO T_{g_2}.

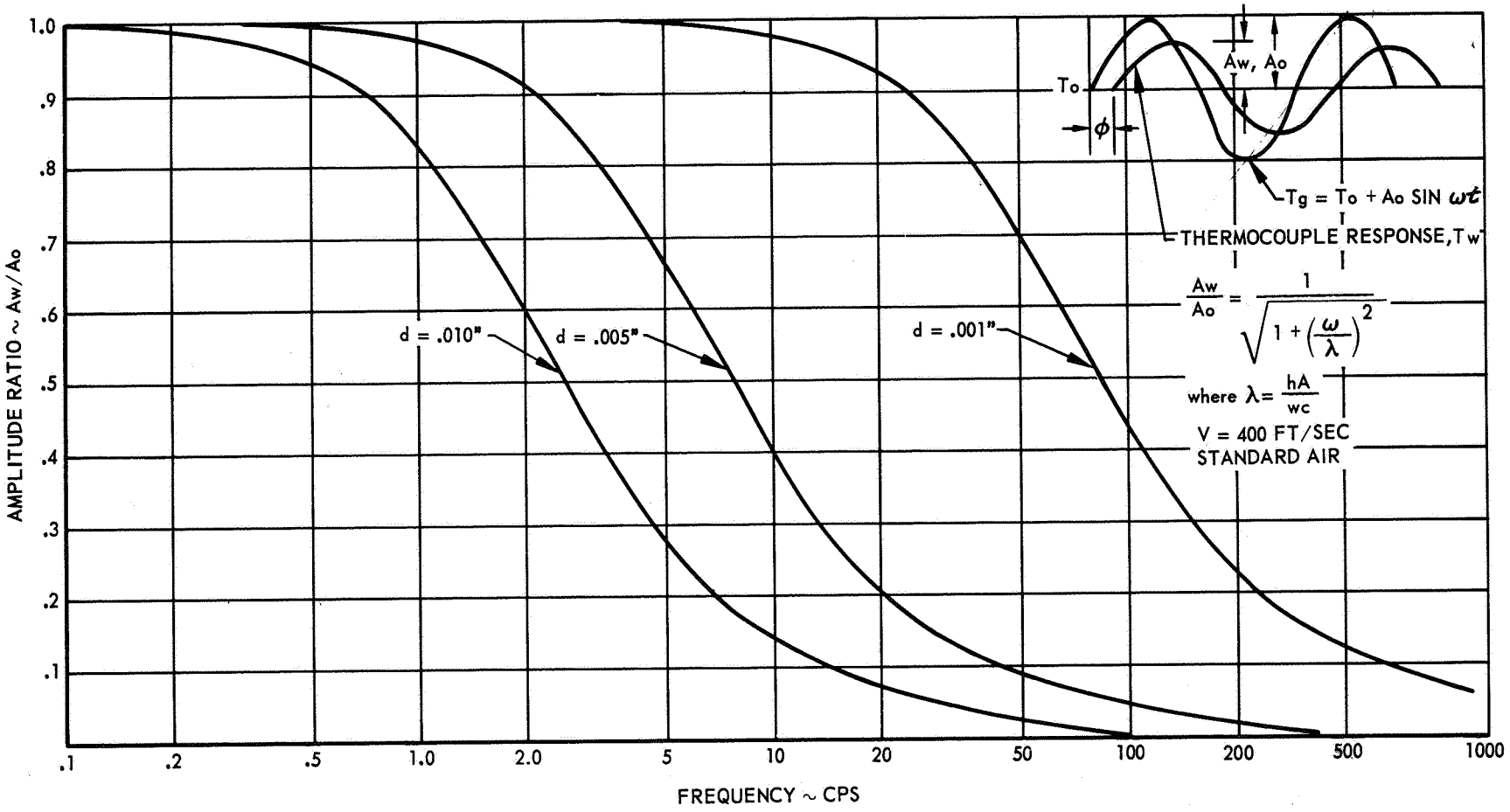

FIGURE 36 RESPONSE CHARACTERISTICS OF IRON–CONSTANTAN THERMOCOUPLE TO A SINUSOIDAL VARIATION OF GAS TEMPERATURE.

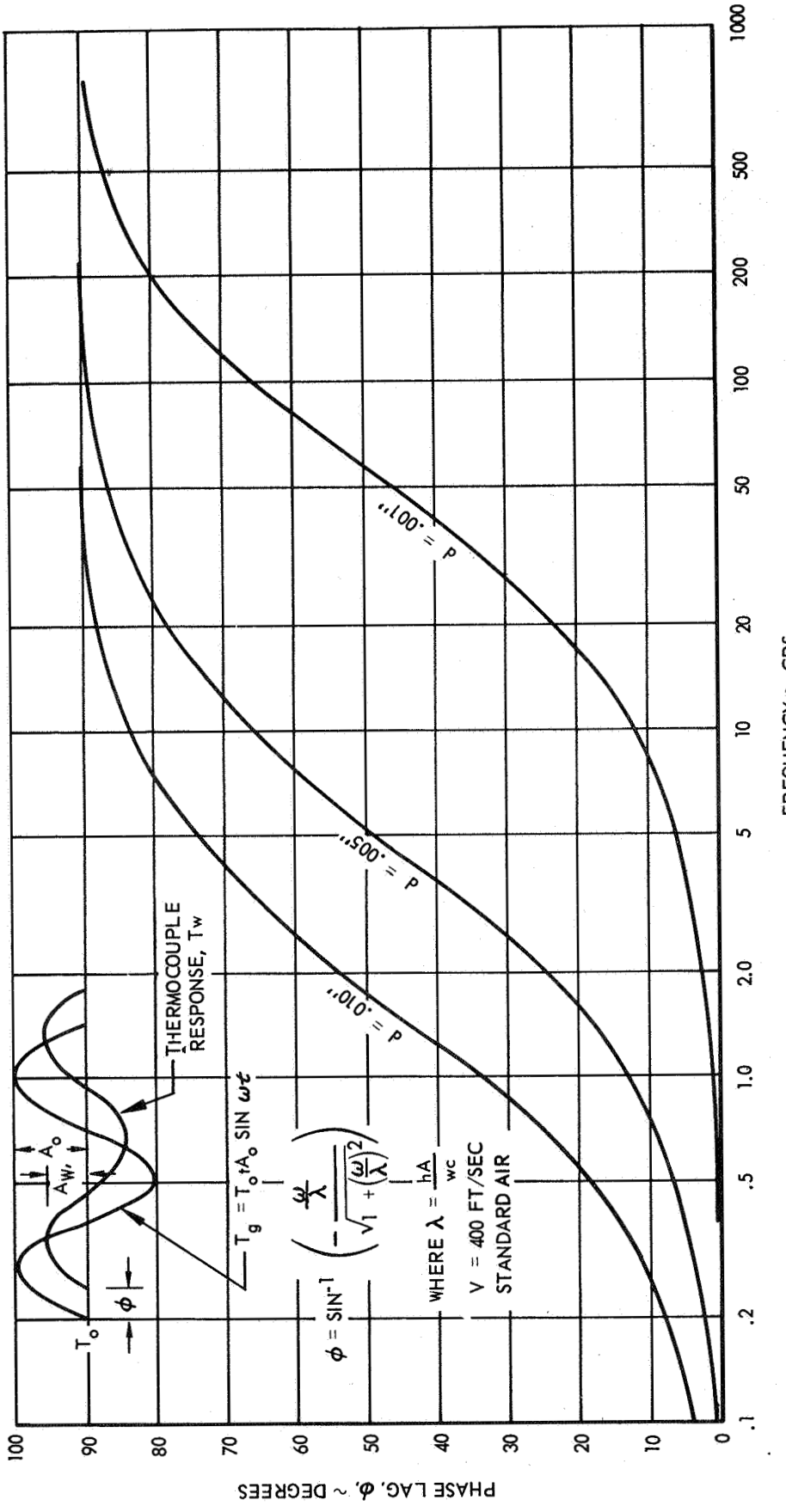

FIGURE 37 PHASE LAG CHARACTERISTICS OF IRON–CONSTANTAN THERMOCOUPLE FOR A SINUSOIDAL VARIATION IN GAS TEMPERATURE

NASA-Langley, 1968 — 2 CR-1098

NATIONAL AERONAUTICS AND SPACE ADMINISTRATION
WASHINGTON, D.C. 20546

OFFICIAL BUSINESS

FIRST CLASS MAIL

POSTAGE AND FEES PAID
NATIONAL AERONAUTICS AND
SPACE ADMINISTRATION

POSTMASTER: If Undeliverable (Section 158
Postal Manual) Do Not Return

"The aeronautical and space activities of the United States shall be conducted so as to contribute . . . to the expansion of human knowledge of phenomena in the atmosphere and space. The Administration shall provide for the widest practicable and appropriate dissemination of information concerning its activities and the results thereof."

— NATIONAL AERONAUTICS AND SPACE ACT OF 1958

NASA SCIENTIFIC AND TECHNICAL PUBLICATIONS

TECHNICAL REPORTS: Scientific and technical information considered important, complete, and a lasting contribution to existing knowledge.

TECHNICAL NOTES: Information less broad in scope but nevertheless of importance as a contribution to existing knowledge.

TECHNICAL MEMORANDUMS: Information receiving limited distribution because of preliminary data, security classification, or other reasons.

CONTRACTOR REPORTS: Scientific and technical information generated under a NASA contract or grant and considered an important contribution to existing knowledge.

TECHNICAL TRANSLATIONS: Information published in a foreign language considered to merit NASA distribution in English.

SPECIAL PUBLICATIONS: Information derived from or of value to NASA activities. Publications include conference proceedings, monographs, data compilations, handbooks, sourcebooks, and special bibliographies.

TECHNOLOGY UTILIZATION PUBLICATIONS: Information on technology used by NASA that may be of particular interest in commercial and other non-aerospace applications. Publications include Tech Briefs, Technology Utilization Reports and Notes, and Technology Surveys.

Details on the availability of these publications may be obtained from:

SCIENTIFIC AND TECHNICAL INFORMATION DIVISION

NATIONAL AERONAUTICS AND SPACE ADMINISTRATION

Washington, D.C. 20546